UNCLASSIFIED

AD NUMBER:	AD0460274

LIMITATION CHANGES

TO:

Approved for public release; distribution is unlimited.

FROM:

Distribution authorized to U.S. Gov't. agencies and their contractors; Administrative/Operational Use; Air Force Materiel Command, Wright-Patterson AFB, OH 45433

AUTHORITY

DNA ltr 25 Sep 1979

Operation Greenhouse

SCIENTIFIC DIRECTOR'S REPORT
ANNEX 3.3

AIR FORCE STRUCTURES TEST
VOLUME IV

46 0 2 7 4

INTERIM REPORT

THE AIR FORCE STRUCTURES PROGRAM

PROJECT 3.3.

OPERATION GREENHOUSE.

by

ROBERT E. PETTITT

INTERIM REPORT.

Approved:

SHERWOOD B. SMITH
Director, Program 3

Approved:

ALVIN C. GRAVES
Commander, TG 3.1

Headquarters, Air Materiel Command

Wright-Patterson Air Force Base

Dayton, Ohio

August, 1951.

RESTRICTED DATA
ATOMIC ENERGY ACT 1946

ARMOUR RESEARCH FOUNDATION OF ILLINOIS INSTITUTE OF TECHNOLOGY

- 1 -

(upper case)

(6) # THE AIR FORCE STRUCTURES PROGRAM.

APPENDIX E.

BLAST LOADING AND STRUCTURAL RESPONSE.

VOLUME III.

BLAST LOADING AND RESPONSE OF PROTOTYPE STRUCTURES AND QUARTER SCALE MODEL.

(9) Interim rept.

(11) aug 51,   by

(12) 411 p.

~~ARMOUR RESEARCH FOUNDATION~~

of

~~ILLINOIS INSTITUTE OF TECHNOLOGY~~
~~Technology Center~~
~~Chicago 16, Illinois~~

(5) IIT Research Inst.,
Chicago, Ill.

(15) Contract ● AF 33(038)-9761

(21) Report on OPERATION GREENHOUSE—
Project 3.3.

August 30, 1951

This is Volume III of the three-volume Appendix E to
"The Air Force Structures Program, Project 3.3, Operation Green-
house" prepared under Contract No. AF 33(038)-9761 at the request
of Air Materiel Command, Air Installations Division, and under
subcontract to Howard T. Fisher and Associates, Inc.

Respectfully submitted,

ARMOUR RESEARCH FOUNDATION OF
ILLINOIS INSTITUTE OF TECHNOLOGY

J. Edmund Fitzgerald, Project Engineer

Robert J. O'Brien, Supervisor

Stephen J. Fraenkel, Assistant Chairman
Department of Structural Research

Division of Engineering Mechanics Research

ARMOUR RESEARCH FOUNDATION OF ILLINOIS INSTITUTE OF TECHNOLOGY
- 3 -

CONTENTS

ARMOUR RESEARCH FOUNDATION OF ILLINOIS INSTITUTE OF TECHNOLOGY

PART II   THE RESPONSE OF STRUCTURES TO BLAST LOADING

ILLUSTRATIONS

TABLES

CHAPTER E.2   BUILDING 3.3.3

ABSTRACT

The purpose of this report is to predict the blast loading and response of buildings 3.3.3, 3.3.8h, 3.3.4, 3.3.5a, and 3.3.5b. These buildings are industrial types (3.3.3 and 3.3.4), a linear quarter-scale model of the 3.3.3 structure (3.3.8h), and load bearing brick dwelling type (3.3.5a and 3.3.5b).

The fundamentals developed in Vol I of this appendix and applied to the six idealized models (3.3.8a-e and 3.3.8g) in Vol II ar' applied herein to the aforementioned structures. Because of the comparative complexity of these structures the methods, in particular the loading methods, must be somewhat modified. Since the fundamental information, derived from shock tube tests and compressible flow theory on one hand, and from fundamental dynamics and basic knowledge of structures and materials on the other hand, is the same for this work as for the analysis of the idealized models, the additional complexities must be accounted for in the analysis largely by means of intuitive reasoning.

Perhaps the most important difference between these analyses and the previous work is the consideration of the behavior of components, in particular, windows and masonry panels. The interrelation of panel loading, panel response, and loading of the main frame (where "panel" refers to both window glass and masonry) results in a sort of iterative procedure between the loading and response phases.

ARMOUR RESEARCH FOUNDATION OF ILLINOIS INSTITUTE OF TECHNOLOGY

The assumed behavior of masonry panels divides the motion of the panel into three phases: elastic panel, flat arch, and rigid body.

Using the aforementioned methods and considerations, this report obtains the loading and response of the subject buildings. An exception to this statement is the case of the dwelling type structures (3.3.5a and 3.3.5b). The nature of these particular structures is such that little or no analytical analysis can be performed in this respect, especially in the consideration of response.

It can be concluded from this work that considerable shock tube and model test work must be performed with increased emphasis on duplicating the prototype situation and extending the knowledge for a greater range of overpressures. Further, an experimentally verified method of treating component panels is surely needed, as well as information on the effects of variations in structural parameters and changes in orientation.

APPENDIX E

BLAST LOADING AND STRUCTURAL RESPONSE

VOLUME III

BLAST LOADING AND RESPONSE OF PROTOTYPE STRUCTURES

AND QUARTER SCALE MODEL

PART I   BLAST LOADING OF STRUCTURES

CHAPTER E.1

GENERAL

E.1.1   INTRODUCTORY REMARKS

This part of Volume III of Appendix E to the Operation Green-house report on the Air Force Structures Program consists of a discussion and prediction of the blast loadings on five buildings under Greenhouse test conditions. These are buildings 3.3.3, 3.3.8h, 3.3.4, 3.3.5a, and 3.3.5b. In the following chapters loadings are determined for the first three; loadings are only partially determined on the latter two structures. This work is based on general material and methods developed in Part I of Vol I to this appendix, to which frequent reference will be made; a few references will be made to Vol II. For reasons given in Chapters E.5 and E.6, the calculations given for the

3.3.5 type buildings are only illustrative, showing the mode of approach to be used when genuine predictions can be made.

As noted in Chapter E.9, Vol I, predictions of blast loading can best be based, for the present, on shock tube tests (see references 1-9)[1] and on wind tunnel tests (see references 10-14). The shock tube results can be used (with rather extensive modifications) to predict loadings during the early periods after the shock front strikes the building, while wind tunnel tests are necessary to determine wind forces in the later period of flow past the structure (the "pseudo steady state period" of Vol I). In general, predictions for a specific building can be made only by a series of speculations from the relatively few shapes of obstacles tested in shock tubes. Since such speculation tends to be a function of personal preference, and since the mode of approach used has already been illustrated in Vol II, Chapter E.3, predictions herein are presented without extensive discussion of the speculative process.

The five buildings are shown in Figs. E.1.1-E.1.3. Wing walls, which act as horizontal extensions of the front walls, are omitted from the first two of these drawings. Building 3.3.3 and its approximately scaled model, building 3.3.8h, are steel-framed industrial type buildings with large roof monitors; building 3.3.4 is an industrial type structure of reinforced-concrete framing equipped with roof monitors.

---

1. Unless otherwise noted, all references are to the Bibliography, Vol I. The same list of references is included at the end of this volume.
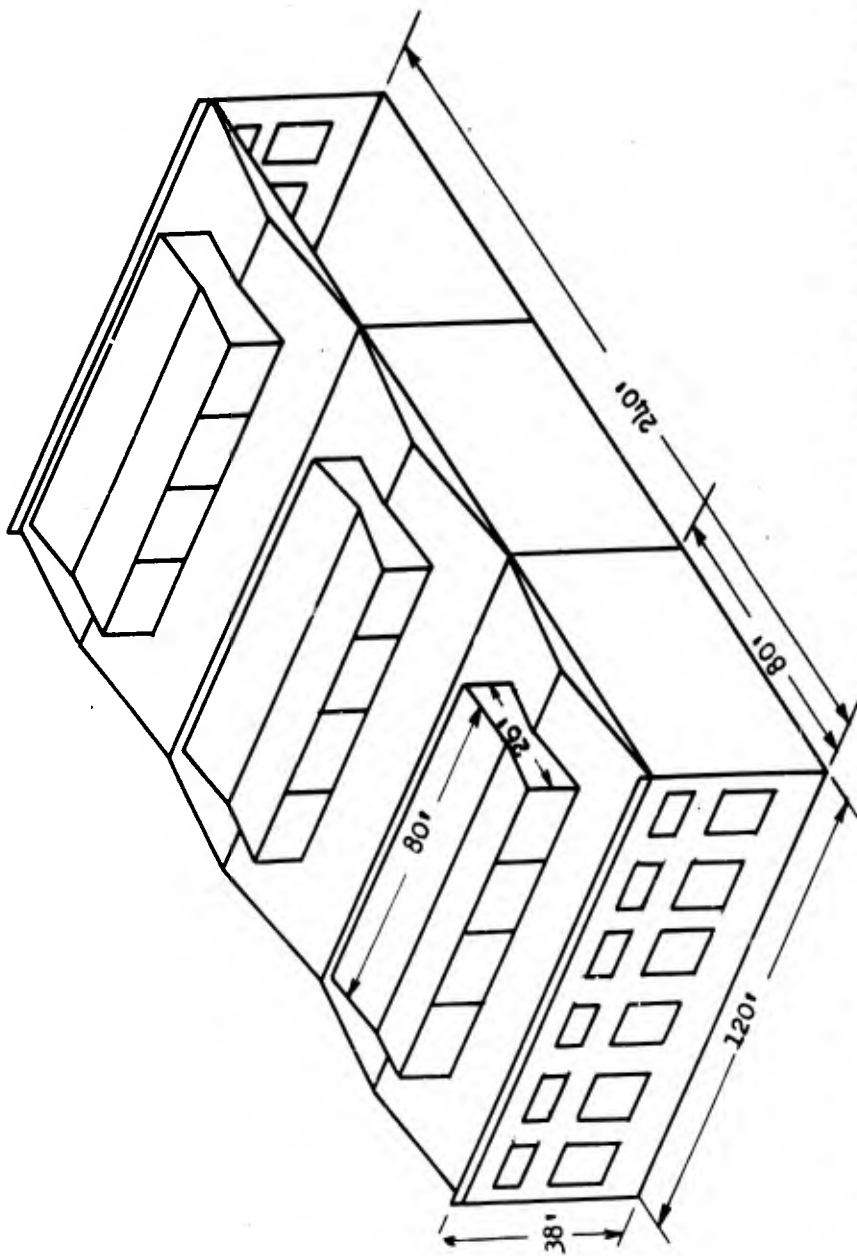
Fig. E.1.1   Approximate Dimensions of Building 3.3.3 (Wing Walls Omitted), and
of Building 3.3.3h (1/4 Scale of Building 3.3.3)
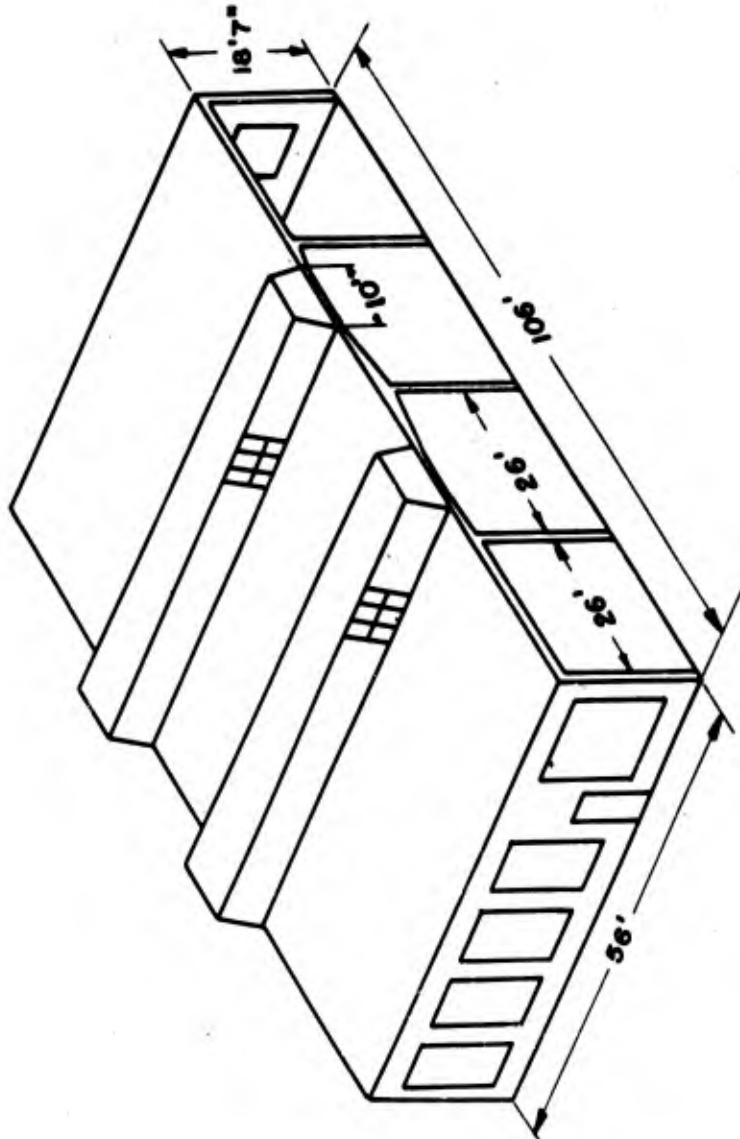
Fig. E.1.2   Building 3.3.4 (Wing Walls Omitted)
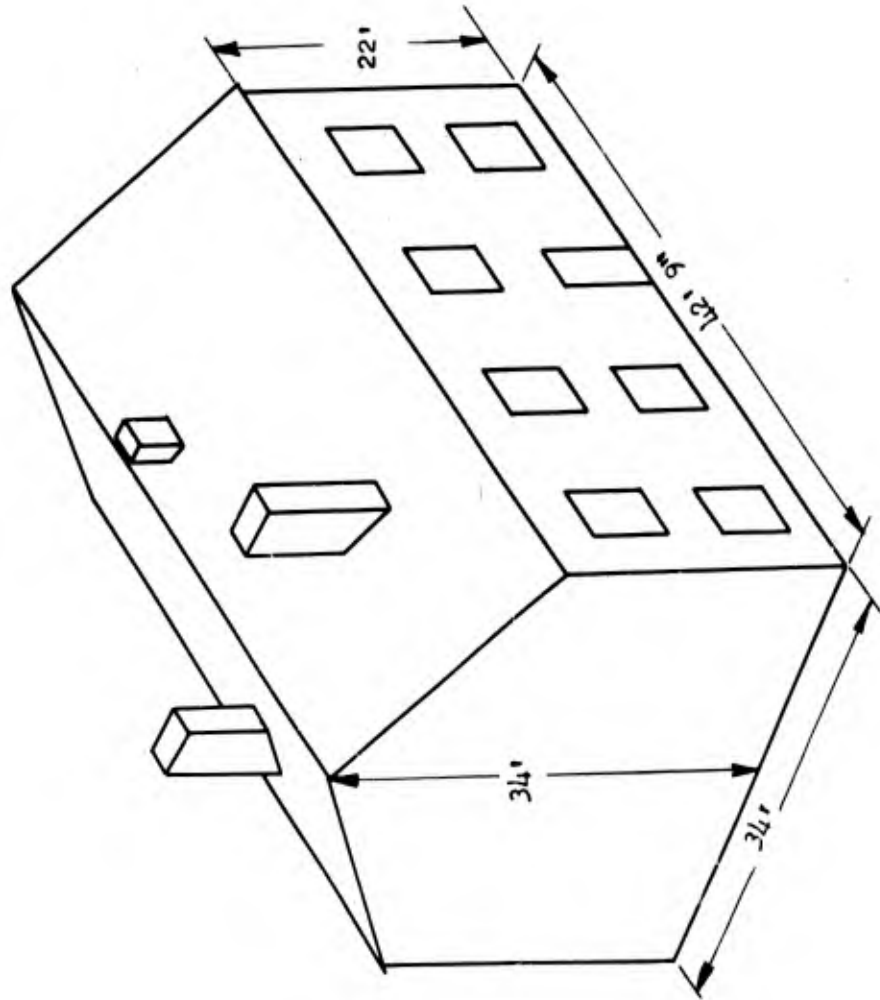
Fig. E.1.3 Buildings 3.3.5a and 3.3.5b

These three structures were built to represent portions of
larger structures whose damage could be studied from the testing of
these sections. Hence these Greenhouse structures have no side walls
and are provided with "wing walls" which are intended to cause loadings
approximately equal to those which would occur on the prototype structures.
The wing walls affect the air flow, but are not connected structurally
to the building; hence they do not transmit their loads to the building.
A discussion concerning the predicted effectiveness of the wing walls
in attaining this goal appears in Section E.1.3.1. These first three
structures are located at distances where the peak side-on pressure is
expected to be between 3 and 4 psi overpressure.

Fig. E.1.3 shows buildings 3.3.5a and 3.3.5b, which differ only
in their location relative to ground zero. These buildings are wood-framed
brick-walled structures typical of small apartment houses. Therefore,
their interiors are broken up into a number of rooms with numerous doors
and closets (see Fig. E.5.1). The peak side-on pressure expected at these
buildings is about 9 and 4 psi, respectively. Clearly, the behavior of
the blast wave in the interiors will be extremely complex.

The five buildings treated in this volume differ from those con-
sidered in Vol II by virtue of the complexity caused by windows, doors,
walls and, in some cases, interior partitions which may collapse, per-
mitting the path of shocks and air flow to be altered considerably.
Hence, it is necessary to compute which structural elements will fail
and approximately when they will fail in order that the loadings on the

ARMOUR RESEARCH FOUNDATION OF ILLINOIS INSTITUTE OF TECHNOLOGY

entire structure can be predicted.

In Chapters E.2-E.4 preliminary computations are made for loadings on any elements which may be expected to fail. These loadings are used in Part II to test for failure. The results of such calculations (that is, whether or not collapse occurs and the approximate time of failure) are included in Part I in order that this information may be used in considering the effects of such failures on the flow around and hence on the loading of the remaining components of the building.

Each of these buildings is oriented so that one wall (called the "front wall" here) directly faces ground zero. The shock front is assumed to be approximately plane in the vicinity of any single building.

An estimate of the accuracy of predictions in this volume cannot be made because of the considerable amount of intuitive thinking involved in their development. As in Vol I and II, wherever approximations of known accuracy have been made, it has been attempted to remain within 20 per cent of the correct values if the deflections of the structures will be affected appreciably by such approximations.

Because of the approximate nature of predictions, computations in Part I of this volume are slide rule calculations. In each number listed the third figure has no significance. Since the final predictions are not to be considered accurate to even two figures, higher accuracy in calculations is not warranted.

E.1.2 QUALITATIVE DISCUSSION OF LOADINGS

In Vol I, Section E.2.3, an introductory discussion of blast

loadings described some of the more prominent phenomena which occur when a shock wave strikes a simple structure. The following material describes the important features of shock diffraction and air flow which can be expected on the more complex buildings treated in this volume (see Figs. E.1.1-E.1.3).

This discussion assumes a general familiarity with the corresponding section of Vol I and is applicable, as was that section, when the peak overpressure is not too high (see Section E.1.3.3). Many statements are given without proof; later sections of Part I supply the justification for such statements. Furthermore, the discussion assumes that the main frames of the buildings do not suffer substantial deflections or velocities (see Section E.1.3.3).

In this section, "pressure" will mean overpressure (i.e., gage pressure) and, when referred to a wall or roof surface, will mean the average pressure across that surface. These conventions will be adherred to throughout this report, except where the context clearly indicates otherwise. The terminology used below follows the list given in Vol I, Section E.3.1.

Briefly, the sequence of phenomena is as follows. When the shock front strikes the front wall it reflects to a high pressure and the windows soon break, allowing flow into the interior, causing the formation of an inside shock. Meantime, the pressure on the outside of the front wall drops off and the primary shock moves down the length of the building. On sloped roofs some reflection occurs. On those buildings with monitors,

the monitor glass breaks and more air flows into the interior, strengthening the inside shock. While this is happening the inside shock has raised the pressure on the back of the front wall and on the underside of the roof to some fraction of side-on pressure. In the buildings with trusswork diffraction of the shock occurs around most steel members, followed by drag forces for the duration of the wave. Concurrently, pressures on the front wall have stabilized so that only drag forces act there.

The interior shock has an extremely complex history in the 3.3.5 type buildings and will not be discussed until later. In the other buildings, the interior shock is strengthened by flow through the monitor openings in the roof and through the open sides. This interior shock builds up to almost the strength of the outside shock, strikes and reflects from the back wall and then moves back upstream over part of the length of the building before it dissipates its strength. In moving upstream it imposes upward forces on the rearmost parts of the roof. During this period the back wall windows have broken and the wall has been swept by the outside shock and by air flowing through the rear windows. Finally the pressures on the back wall stabilize to drag pressure.

Now only drag acts on the various parts of the structure, decreasing to zero as the later portions of the main shock wave (with lower pressure and flow velocity) pass the structure. These brief remarks are extended in the following paragraphs.

When the shock front strikes and reflects from the front wall, the

pressure on the upstream side of that wall rises instantaneously to more than double the side-on pressure. Rarefaction waves immediately move in from the outside edges of the wall, starting the "clearing" (or "relief") process. As the rarefaction waves move inward, the high pressure air flows outward, over the edges of the wall, and into the free stream. This clearing process reduces the reflected pressure to pseudo steady state pressure.[2] This pressure is equal to the instantaneous value of side-on pressure plus the drag pressure which is expected for the particular side of the wall under consideration. It is always considerably less than reflected pressure for an outside front wall. As the shock wave passes, the side-on and drag pressure (and hence, the pseudo steady state pressure) drop off until they reach zero at the beginning of the negative phase.

On those buildings which have wing walls, little "clearing" of the front wall proper can take place around the side edges, since it is the function of the wing walls to prevent just that. It is assumed that the wing walls stand and perform their function through the early period of shock diffraction.

Windows and doors in the front wall will probably break under the reflected pressure, though not instantaneously. However, they generally will break before the clearing of reflected pressure is

---

2 "Pseudo", because no true steady state can exist in a continually changing flow such as occurs behind the blast wave.

complete; hence, part of the clearing will occur through the window openings, allowing high pressure air to flow into the interior. This sudden release of high pressure air will cause shocks to form in the interior, just as the bursting of a diaphragm in a shock tube generates a shock. These inside shocks, formed at each opening, will spread downstream from each opening and will tend to combine into a single shock front followed by a few weaker shocks. This interior shock is, at least for a time, considerably weaker than the incident (outside) shock.

With the breaking of the windows, pressure on the rear side of the front wall begins to build up towards its pseudo steady state value (side-on pressure plus a certain drag pressure).[3]

Meantime the incident shock front has moved past the front wall and is sweeping across the roof. On the flat-roofed building (3.3.4) pressure on the outside of the roof is raised to approximately side-on pressure at this time. All the remaining buildings have a sloped roof, and an oblique reflection of the shock takes place on the slopes which "face" the blast. The 3.3.5 type buildings have rather steep roof slopes compared with the 3.3.3 structure and its model, and have higher reflected pressures. ~~pressures.~~ The pressure then falls off to the pseudo steady state value for these surfaces.

At this point it is necessary to discuss the buildings in two different groups: the industrial-type buildings (3.3.3,3.3.8h and 3.3.4),

---

3 On this surface, the drag pressure is suction and hence has a negative value.

which possess monitors, wing walls, and have no side walls; and the dwelling units (3.3.5a and 3.3.5b), which have side walls and considerable interior obstructions. The industrial type buildings are treated first.

E.1.2.1   Buildings 3.3.3, 3.3.8h and 3.3.4

The foregoing discussion of front walls (outside and inside) applies to these buildings. However, the description of the interior shock and the initial outside pressure on the roof is applicable only up to the first monitor. In the following paragraph inside roof pressures up to the first monitor are discussed; then the effects of the monitor and of the absence of side walls are considered.

As the outside shock moves across the roof exterior the interior shock which formed at the front wall openings moves across the underside of the roof (lagging the outside shock slightly) imposing on that surface pressures above atmospheric pressure, but considerably below side-on pressure. Thus the roof section in front of the first monitor is initially exposed to a net downward force (outside roof pressures being side-on or higher, depending on the building).

Up to the first monitor the interior shock obtains its strength almost wholly through the front wall openings. However, as the primary outside shock sweeps down the length of the building it tends to extend itself into the interior from the sides and from around the outside edges of the roof. Such spreading of a shock transverse to the flow direction can be seen in references 7 and 6 where the shock curls down

the rear faces of the models. These parts of the outside shock which spread into the interior through the sides combine with the interior shock, strengthening it. This effect and the strengthening which occurs at the monitors (discussed below) build up the interior shock in strength until it carries almost the same pressure as the outside shock when these shocks are perhaps one-half or two-thirds of the way down the length of the building.

The outside shock wave reflects from the (mainly glass) upstream wall of the first monitor creating high reflected pressures as on the front wall. A clearing process begins immediately, the glass breaks, and a shock of nearly the strength of the incident shock is created inside the monitor (since almost the entire area of the monitor wall breaks out).

Meanwhile the outside shock moves over the top and around the sides of the monitor and then expands around the rear monitor wall. This wall is struck at about the same time by the strong shock which formed inside the monitor and all the glass can be assumed to break out.

The shock inside the monitor, in addition to striking the rear monitor wall, also spreads downward into the building to some extent, reinforcing the shock in the interior of the building as mentioned earlier.

The roof behind the first monitor may receive pressures on the outside surface which are below side-on because of the local weakening of the shock in flowing around and through the monitor, and

(in the case of buildings 3.3.3 and 3.3.8h) because of sloping of the roof towards the rear.

On buildings 3.3.3 and 3.3.8h the outside surfaces of the *second & third* bays (monitors and roof areas) are loaded approximately the same as the first bay, except that the outside shock probably does not re-form rapidly enough to have a well defined reflection on the sloped sections upstream of each monitor.

On building 3.3.4 the outside surfaces of second monitor and the remaining roof area have about the same loading as the first monitor and the roof area in front of it. As already suggested, slightly smaller loadings may occur behind both monitors due to local weakening of the primary shock.

On all three of these structures the undersides of the roof are loaded with pressures close to the pressure of the interior shock (which has risen as the shock is reinforced from the monitors and from the sides). However, on the 3.3.3 and 3.3.8h structures the underside of the roof does not present a smooth boundary for flow because purlins, supporting the roof surface, run transverse to flow across the underside. Some further lowering of pressure is induced by these purlins.

Interior trusswork which is present in these same two buildings is not believed to "cut up" the interior shock severely, although rather considerable forces are exerted on this steelwork. Most of the trusswork members will be exposed to the shock front and will experience reflection, diffraction, etc. However, since the time for these phenomena to give way to pseudo steady state forces is proportional to the width

and depth of the member involved, these forces will be of extremely short duration on the narrow steel members. The pseudo steady state forces, which are simply drag forces here, provide a much larger impulse than the diffraction forces on these members because drag forces continue for the duration of the wave, no matter how small the dimensions of the member in cross section.

The shock which reflects from the back wall, and the loadings on the back wall itself, remain to be considered for the industrial type buildings. This reflection occurs when the interior shock, strengthened to nearly the pressure of the incident shock wave reaches the inside face of the back wall. After this reflection the phenomena follow closely the sequence described on the front wall after reflection there. But here, however, the roof prevents relief of reflected pressures from occurring over the top of the wall; further, the absence of wing walls at the rear of the building allows relief to occur around the sides of the back wall. The windows break and clearing of the high pressures brings the upstream face of the back wall to its pseudo steady state pressure as described for the front wall reflection.

This reflected shock exerts some influence on the roof before it dissipates. It travels upstream against the flow, just as does the reflected shock from the front wall (which can be observed in any of references 1-4 or 6-8), weakening as it spreads outward beyond the line of outside columns. When this reflected shock reaches the rearmost monitor it may be presumed to lose any appreciable remaining strength in spreading upward through the monitor opening. During its

brief lifetime it has exerted an upward force of short duration on the rearmost section of the roof. The force is upward since approximately side-on pressure exists on the outside of the roof, whereas this reflected shock initially imposes pressures above side-on on the underside (since it originates from reflection of a shock carrying approximately side-on pressure).

The sequence of events on the front face of the back wall (until pseudo steady state) has already been described. On the rear face the pressure simply builds up gradually to its pseudo steady state value after the outside shock sweeps in from the edges and part of the inside pressures escape through the broken windows to cover the rear surface.

E.1.2.2   Buildings 3.3.5a and 3.3.5b

The clearing of the front wall, breaking of the front windows, and loading of the front slope of the roof by reflection have been discussed. As the outside shock moves over the roof peak it expands across the rearward facing slope with some weakening. Hence, pressures rather below side-on (and below pseudo steady state) are felt as the shock crosses this surface. After a relatively long period of time, pressure on the rear slopes rises to the pseudo steady state pressure for that surface. For less sharply sloped roofs the time to reach pseudo steady state (i.e., side-on pressure plus drag pressure)[4] would

---

4   In this case, drag pressure has a negative value.

be considerably earlier.

The primary shock moves across the back wall of the buildings from the sides and from above and imposes some faction of side-on pressure on the outside of that wall. This pressure is probably great enough to break out the rear wall windows (even for the 3.3.5b structure at the lower pressure region). It is possible that the interior shock(s) reach some of these windows first; in any case the windows may be expected to break. Those openings at which the interior shocks have not yet arrived will then admit air flow at relatively low pressure (i.e., slightly above atmospheric pressure) to the interior.

During this period, the air flow through the front wall window and door openings has produced interior shocks which move through the various rooms. Depending on the values of pressure involved, doors and interior partitions may or may not collapse. In any case reflections, clearing, and interaction between different interior shocks will occur for a period of time. Gradually the pressure in each room will rise towards the side-on pressure (or a value close to it) which exists outside at this time. Then pressure will fall off as the side-on pressure drops to zero at the end of the positive pressure phase. A more exact tracing of the time history of inside pressures must be made in such detail, and is so tentative compared with other predictions of this volume, that such discussions are best left for the specialized chapters devoted to the 3.3.5 type structures.

E.1.3   COMMENTS APPLICABLE TO ALL STRUCTURES

E.1.3.1   Brief Topics on Loadings

E.1.3.1.1   Negative Pressure Phase of Blast Wave

As a typical blast wave passes a given point, the gage pressure at that point drops from the peak overpressure towards zero. Concurrently, the air velocity decreases, reaching zero at the same time as the pressure (Section E.4.2.2, Vol. I). Following this time there is a period of pressures below atmospheric and expected of air flow back toward ground zero. These two periods are called the positive (pressure) phase and negative (pressure) phase, respectively. Peak pressures in the negative phase are believed to be much less than in the positive phase. Since the form of the negative phase is not known and since the effects are not believed to be large compared with those during the positive phase, the entire period of negative pressures is neglected in these calculations.

It is anticipated that pressure variation in the negative phase is no more rapid than in the latter part of the positive phase. If this is correct, then predictions of loadings can be obtained readily for the negative phase when data on its form become available. Applying the notions used in the predictions of these volumes and under the above assumption concerning rate of pressure variation, only drag forces will act during the negative phase on the buildings treated in this volume. Since the drag pressure increases approximately with the square of the instantaneous side-on pressure for moderate

pressures (see Eq. E.4.19, Vol. I), and since peak side-on pressure in the negative phase is believed to be considerably less than in the positive phase, the forces in the negative phase may be expected to be relatively small compared with the early drag forces in the positive phase.

E.1.3.1.2 Atmospheric Conditions

The temperature and pressure of the atmosphere in front of the shock are necessary in computing the velocity of the shock front. In Vol. I standard atmospheric conditions were used in evaluating the shock velocity; the results (Fig. E.4.2, Vol. I) will be used in this volume. From Eq. E.4.8, in Vol. I it is seen that correction of the shock velocity to other atmospheric conditions leads to small changes: e.g., for air temperatures of 100°F, shock velocities from Vol. I must be multiplied by 1.04. If such allowance were made for temperature, no changes in forces in the loading predictions would occur, but the early portion of the time axis would be compressed by 1.04 for the above example. Such changes are not deemed to be large enough to be included.

E.1.3.1.3 Changes in Shock with Distance

As the shock wave from a blast propagates outward, the peak pressure and shock front velocity gradually decrease while the duration of positive pressures increases. For the buildings treated in this volume, changes in these quantities as the shock moves

down the length of each individual structure have been disregarded. The greatest changes for these buildings occur on the 3.3.3 structure, which is 240 ft. long. Peak pressure at the front wall is anticipated as 3.4 psi; this would drop to about 3.3 psi at the rear wall if a 20-KT weapon were used. The associated change in the shock front velocity at the rear wall would change the time scale for the rear wall by a fraction of one per cent; changes in the wave duration would probably be imperceptible in inducing changes in loadings. Even the changes in pressure noted above are believed to be small compared with the uncertainties which are present in the loading predictions developed herein.

E.1.3.1.4 Wing Walls and Open Sides on Industrial Type Buildings

Buildings 3.3.3, 3.3.6h, and 3.3.4 represent sections of larger buildings. For example, the prototype (the larger building) corresponding to building 3.3.3 would be composed of a series of sections similar to it placed side by side with side walls only on the end sections. It is believed that the behavior of these sections would be similar to the action of the prototypes under blast loadings. Side walls are not present in the 3.3.3, presumably because that would give a structural resistance against transverse loadings which is not present in any but the end sections of the prototype. Wing walls slow the clearing of reflected pressures along the outside vertical edges, just as the front walls of adjacent sections would tend to prevent clearing in the prototype structure.

It is predicted that the absence of side walls allows heavy reinforcement of the interior shock wave in these buildings, thus increasing the loading on the underside of the roof and the front of the back wall. Such an effect would not occur in the prototype structure.

The absence of some type of side wall is considered (with due regard for the difficulties of their inclusion) to be a fairly serious departure from reproducing the behavior of the prototype. The wing walls tend to improve this situation slightly, however, in addition to the fact that they probably fulfill their function satisfactorily if they do not fail (or do not fail before the front wall clearing process is completed).

However, had the wing walls been left off entirely, the clearing rate would probably be increased at most by 10 per cent over the rate for the prototype buildings. This can be checked by making an obvious change in the calculation of clearing time for the front wall in Section E.2.2.1.7. This would probably lead to a very small difference in the behavior of the buildings, unless the loadings bring the buildings or walls to the threshold of collapse, at which point slight changes in loading produce gross differences in the behavior of the structure. Therefore, as far as front wall clearing is concerned, the wing walls probably could have been omitted on these three buildings without great differences in structural response.

E.1.3.1.5   Centers of Pressure on Walls and Roofs

The forces which are predicted in Part I of this volume are assumed to act at the center of each surface for the purpose of computing structural response in Part II. Such a procedure is not believed to lead to serious inaccuracies.

Pressure profiles shown in Fig. E.5.6-E.5.20 in Vol. I show that after the early diffraction period the center of pressure is close to the geometric center of each surface. Hence, it appears that no improvement in choosing the line of action of forces could be made unless a point of force application which changes with time were included in the structural calculation. This would render the calculations of Part II much more complex and would, it is believed, be so slight a refinement as to be unwarranted in the present work.

E.1.3.1.6   "Maximum" and "Minimum Turbulence"

In Vol. II alternate predictions were presented for the loadings on some surfaces. The alternate loadings, termed "maximum turbulence" and "minimum turbulence", might also be called "direct scaling" (from shock tube tests) and "nondirect scaling". The alternatives reflect an uncertainty, at the present time, as to whether or not vortices (and the turbulent regions which they create) will scale in size and in intensity from small model tests to full size structures. These two approaches are discussed more fully in Vol. I, Sections E.2.3, E.3.1, E.8.1 and E.8.2, and in Vol. II, Section E.2.1.

In this volume alternate predictions do not appear except to a slight extent in the 3.3.5 type buildings. This does not imply that the questions of scaling have been settled. Rather, the two predictions happen to coincide numerically for the industrial type buildings. This situation is elaborated on in the chapters which discuss those buildings. Essentially, there are two factors involved: first, the differences between "maximum" and "minimum turbulence" cannot be readily divined for these structures and, second, these differences are felt to be smaller, percentagewise, than on the buildings of Vol. II. Furthermore, differences between "maximum" and "minimum turbulence" predictions frequently tend to cancel when the net pressures (pressure on the outside of a surface minus that on the inside) are computed.

E.1.3.2 Pseudo Steady State and Drag Pressures

During the positive (pressure) phase of the blast wave, relatively complicated diffraction phenomena around a structure gradually die out until the structure is loaded only by wind (drag) forces. For the buildings treated in this appendix, this period of drag forces, called the "pseudo steady state period," begins rather early in the positive phase and continues until the blast loading ceases. Thus when the entire building has reached pseudo steady state, equations of the following form are used for predictions:

$$f(t) = C_{df} \, p_d(t)$$
$$b(t) = C_{db} \, p_d(t)$$
$$r(t) = C_{dr} \, p_d(t)$$

where f, b, and r are the average pressures on the front wall, back wall, and roof, respectively, t is time,[5] C_d is the drag coefficient (with the appropriate subscripts), and p_d is the "basic" drag pressure. (See Section E.1.4.3 for a more detailed identification of symbols.)

In the predictions of this appendix some surfaces are estimated to reach pseudo steady state before the remainder of the structure. Thus, if the downstream side of a wall is subject to diffraction forces after the upstream side of the wall has reached pseudo steady state, a pseudo steady state equation is needed for this upstream surface. For one side of a wall, pseudo steady state pressure is not simply drag pressure, but equals the sum of side-on pressure and drag pressure. Thus, when pseudo steady state exists on the outside front wall,

$$f_o(t) = p_\sigma(t) + C_{fo} \, p_d(t)$$

where f_o represents the average pressure on the outside of the front wall, p_σ is side-on pressure, and C_{fo} equals the drag coefficient for the outside of the front wall. Similarly, when pseudo steady state exists on the inside front wall,

$$f_i(t) = p_\sigma(t) + C_{fi} \, p_d(t)$$

with the subscript i denoting the inside surface of the wall.

-----

5 With symbols which appear as function of time, t may be dropped from the notation whenever ambiguity will not result.

It is useful to introduce the notations $f_{os}(t)$ and $f_{is}(t)$ to represent the right-hand members of two above expressions. After pseudo steady state is reached on the outside front wall, $f_o(t) = f_{os}(t)$; after pseudo steady state is reached on the inside of the front wall, $f_1(t) = f_{is}(t)$.

Corresponding expressions may be defined for pseudo steady state pressures on the roof and back wall. However, since t is measured from the time the shock strikes the front wall, a time shift must be introduced in the expressions for $p_\sigma (t)$ and $p_d (t)$ when applying them to the back wall or roofs. These timeshifts are shown in Eqs. E.1.2 and E.1.3.

These time shifts are equal to the time taken by the shock front (velocity, U) to travel from the front of the building, length ℓ, to the back of the building (for back walls) or to the middle of the roof (for roofs). The time shift used for the roof, $\ell/2U$, assumes that the average side-on pressure in the free stream above the roof is equal to the side-on pressure above the middle of the roof. This amounts to the requirement that side-on pressure and drag curves vary approximately linearly with time over any interval of time equal to ℓ/U.

The pseudo steady state equations are as follows:

$$f_{os}(t) = p_\sigma (t) + C_{fo} p_d(t),$$

$$f_{is}(t) = p_\sigma (t) + C_{fi} p_d(t), \qquad (E.1.1)$$

and $\qquad f_s(t) = f_{os}(t) - f_{is}(t) = C_{df} p_d(t)$

since $C_{df} = C_{fo} - C_{fi}$ by their definitions (Section E.1.4.3).

Likewise,

$$b_{os}(t) = p_\sigma(\tau) + C_{bo}\, p_d(\tau) \quad \text{with } \tau = t - \ell/U. \tag{E.1.2}$$

Equations for $b_{is}(t)$ and $b_s(t)$, analogous to the second and third equations of Eq. E.1.1, can be written.

Similarly,

$$r_{os}(t) = p_\sigma(\tau) + C_{ro}\, p_d(\tau) \quad \text{with } \tau = t - \ell/2U. \tag{E.1.3}$$

Equations for $r_{is}(t)$ and $r_s(t)$, analogous to the second and third equations of Eq. E.1.1, can also be written. For sloped roofs, which may be made up of a number of sections, several sets of pseudo steady state equations may be used. Each such set may have a different time shift and a different drag coefficient.

E.1.3.2.1   Drag Coefficients for Front and Back Walls

The drag coefficients for the front wall, C_{fo} and C_{fi}, and for the back wall, C_{bo} and C_{bi}, for the buildings of this volume are chosen as the following:

$$C_{fo} = 2/3$$
$$C_{fi} = -1/3.$$

Hence, $$C_{df} = C_{fo} - C_{fi} = 1.$$

$$C_{bi} = 2/3$$
$$C_{bo} = -1/3.$$

Hence, $$C_{db} = C_{bo} - C_{bi} = -1.$$

The drag coefficients and therefore the drag pressures are the same on the upstream sides of both walls; similarly for the downstream sides.

These coefficients had to be selected somewhat arbitrarily. In Chapter E.8 of Vol. I a discussion of the difficulties in choosing drag coefficients is given. In particular, the remarks in Section E.8.3, starting with the tenth paragraph are appropriate. Data in references 11 and 13 were used in selecting the over-all drag coefficient of (plus or minus) one and in splitting this between upstream and downstream faces of each wall. Considerable changes in this split-up could occur without seriously changing the predicted loadings on the walls.

E.1.3.2.2 Drag Coefficients for Flat Roofs and Side Walls

When air flows past a solid rectangular obstacle, the air which strikes the front wall flows around the edges of the front wall. However, at these edges the flow tends to "separate", i.e., to spring away from the roof (and sides) for some distance. This separation causes a suction force on the roof and sides. This suction force, acting transverse to the flow direction, will be referred to as a drag force.

If the same obstacle has openings in its walls which allow flow through the interior, less flow will be diverted around the edges onto the roof and sides. Hence less suction drag will be found on the roof and sides.

Unfortunately no useful data could be found in the literature showing this suction drag on flat roofs and sides of buildings with wall openings. Therefore, drag coefficients for these surfaces are chosen from tests of solid obstacles.

Reference 14 gives the pressure profile across the roof of a rectangular block which is twice as long (in the flow direction) as it is high. This data is shown in Fig. 1 of reference 14 in the curve labelled "U ; r = 0". The average suction pressure given by this profile is -0.55 times p_d. This value is applied in this volume to flat roofs and side walls. Hence,

$$C_{ro} = -0.55$$
$$C_{so} = -0.55.$$

E.1.3.2.3 Drag Coefficients for Sloped Roofs

The first two paragraphs ~~part~~ of the preceeding subsection on flat roofs applies to roofs of moderate or low slope.

The effect of wall openings on the roof drag might be investigated by using data obtained on plates supported at an angle to the flow with no other surfaces present. Such data can then be compared with pressures found on sloped roofs of solid blocks. Presumably, if some openings are present, pressures will lie between those obtained from the two types of tests noted above.

This approach was followed in deducing drag coefficients for the two angles of sloped roofs which are encountered

in this volume: $7°$ on the 3.3.3 and 3.3.8h types and $33°$ on the 3.3.5 type. Only outside drag coefficients are useful in this volume. To distinguish between the roof slopes which "face" upstream or downstream, the terms "front C_{ro}" and "back C_{ro}" are used for upstream and downstream facing slopes, respectively. The results, based on Figs. 42-46, and 48 in reference 11, and Fig. 2 of reference 14, are shown below.

For 3.3.3 and 3.3.8h structures,

"front C_{ro}" $= -0.3$

"back C_{ro}" $= -0.3$.

For the 3.3.5 type structures,

"front C_{ro}" $= +1/3$

"back C_{ro}" $= -0.4$.

It will be noted that, as the slope increases less separation occurs and the drag on the front slope becomes positive.

Data in Fig. 48 of reference 11 are based on tests of an "open shed" with roof sloped at $30°$ but with the air flow approaching from a series of different directions. The drag on roof surfaces of different slopes can be approximated by using all this data. For example, when the flow is in one direction, drag on a $30°$ roof is obtained; when the flow is turned through $90°$, drag on a flat roof surface is represented. Drag on intermediate slope angles (between $0°$ and $30°$) are obtained by using data for intermediate flow directions.

E.1.3.3 Extrapolation of Predictions for Buildings 3.3.3, 3.3.8h, and 3.3.4

In Chapter E.6 of Vol. I it was pointed out that shock tube data and loading predictions (as presented in symbolic expressions) may sometimes be applied over a range of conditions: for various peak overpressures, various durations of the positive pressure phase,[6] for a range of absolute sizes of the structures, and for some changes in the shape of the structures studied. A similar discussion is given here for the industrial type buildings (3.3.3, 3.3.8h, and 3.3.4) only.[7]

The predictions of loading in this volume are based on the assumption that the main building frame remains intact; they are applicable only when substantial deflections or velocities of the main frame have not occurred.

Velocities of the frame up to approximately 20 per cent[8]

---

6 For a given peak overpressure, changes in duration imply changes in the explosive charge weight.

7 As noted already, loading computations for the 3.3.5 type buildings in this volume are primarily illustrative; because of this fact and because of the difficulty of predicting loads for these buildings without specific numerical values in mind, it is not recommended that any extrapolation be made with those predictions.

8 The value of 20 per cent can be tolerated only when instantaneous overpressure is about 5 psi or under; the percentage allowable decreases to about 10 per cent for 20 psi overpressure. These values are based on an allowable error in gage pressure of about 20 per cent using reference 16, Sections 72 and 40.

of _instantaneous_ air velocity (Vol. I, Eq. E.4.17) can occur without rendering the predictions seriously in error. As to deflections, rotation of the main columns up to 10° or 15° will probably not cause serious deviations from the predicted loadings except when this results in secondary failures such as wall collapse, roof breakage, etc.

If these limits of applicability are exceeded, new predictions must be developed, taking into account the velocity and changes in geometry of the structure.

However, these limits are broad enough that if such displacements or velocities are reached, full collapse of the building may follow, regardless of conceivable future loads (e.g., sero loads from that time on).

No check was made for buildings 3.3.3 and 3.3.8h (which are predicted in Part II to collapse) to insure that collapse would have occurred even if loads were sero after the velocity or displacement limits are reached; however, it seems probable that such is the case. In Part II it is found that these limits are not exceeded (maximum velocity at the roof line of about 14 feet per second and very small angular deflection) on building 3.3.4.

Hence, no predictions which take into account the velocity and changes in geometry of the main structural frame of these buildings are necessary in this volume.

The effects of breakage of windows, doors, wall panels, and roof sections are, however, considered in Part I for the particular

peak pressure, wave duration, and size and shape of the structure as specified for the Greenhouse Operation. The extent of breakage of these members and the time at which such failures occur has been included in the predictions wherever these factors affected loadings appreciably. Thus the questions of both main frame and component failure are treated in this volume only for the particular Greenhouse test conditions.

Therefore, loading predictions given here cannot be extrapolated to any other conditions without a study of the time and severity of structural failures. If extrapolated predictions from this volume show that the limits of main frame velocity and deflection are exceeded, the predictions are invalid from that time onward. If the time and degree of collapse of components (windows, doors, walls, roofs) differ considerably from what is found in this volume, then the predictions are inapplicable from that time on. Exactly what constitutes "considerable" differences must be a matter of judgement based on a study of the development of predictions as reported in Part I.

E.1.3.3.1   Change in Peak Side-on Pressure (Overpressure)

Within the rather severe limitations outlined in the foregoing paragraphs, predictions for the industrial type buildings (3.3.3, 3.3.8h, and 3.3.4) are believed to be valid for peak overpressures up to about 20 psi. It seems likely that when the overpressure is in the upper part of this range, the limitations noted will not allow use of these predictions for more than a small fraction of the positive pressure phase.

E.1.3.3.2 Changes in Shock Wave Duration

For the industrial type structures, the duration should approximately satisfy the relation, $U t_o \geq 4 \ell$, if the predictions of this volume are to apply.

In Vol. I (Chapter E.6), it was stipulated that for certain simple shapes, $U t_o \geq 30 \ell$ must be satisfied. The less severe restriction can be made for the industrial buildings because, with side walls absent, the shock front is predicted to reform in the interior at practically full strength; hence the front wall does not influence the loadings on the rear wall and the length of the structure does not influence the loading to as large a degree as for the simple shapes.

E.1.3.3.3 Changes in Size of Structures

The conditions on t_o given above can be considered as a limitation on the length, ℓ, of the buildings. Within that limit the absolute sizes may be changed without rendering the predictions invalid. Of course, if the size is so reduced as to be comparable with the size of local variations in the terrain, the predictions could not be used.

E.1.3.3.4 Changes in Shape

The loadings on these buildings are probably quite sensitive to structural details, such as the size and spacing of purlins on buildings 3.3.3 and 3.3.8h and to the monitor sizes on all the industrial buildings. Thus alterations in the form of these buildings

may change loadings substantially and, in case of alterations, predictions
of Part I would not apply. However it is probably safe to apply the pre-
dictions for the industrial buildings if their height to length ratio is
changed by no more than 25 per cent, provided that the entire roof
structure (or the entire front and rear wall structure) is scaled as a
unit. The width to height ratio can also be changed somewhat on condi-
tion that side walls are not erected.

E.1.4 NOTATION AND OTHER CONVENTIONS

E.1.4.1 General

The terminology of this volume follows that adopted for
Vol. I and presented in Section E.3.1, of Volume I. However, it will be attempted to
briefly characterize each term as it first appears in this volume. A
discussion of the term, "pressure", which will be used in a special sense
in this volume is given below. This section also comments on the sche-
matic diagrams which appear in the later chapters of Part I.

Pressure: In Part I of this volume, "pressure" will
imply overpressure (i.e., gage pressure) unless the context clearly
indicates otherwise. Furthermore, when the term is referred to a sur-
face of a structure, it means the average pressure across the surface.
The predictions of this volume give only the average pressures or total
forces on surfaces, never the pressure at a single point. Hence it is
convenient to adopt the above abbreviated terminology.

Schematic diagrams: In Part I predictions are presented first in a symbolic form, i.e., in terms of equations which may be evaluated for various shock strengths and various absolute sizes (see Section E.1.3.3). These symbolic expressions are then applied to the calculation of numerical loadings for the particular shock strength and structural size involved in the Greenhouse test.

These symbolic expressions for loading predictions are presented by means of schematic diagrams, showing pressure versus time for each surface of each wall or roof of a structure. Since the graphs are only symbolic, they do not necessarily show the correct relative magnitudes between pressures on different surfaces nor, in some cases, the correct trends of pressure variation on an individual surface.

E.1.4.2 Computations

As discussed in some detail in Section E.1.3.3, the predictions of Part I (in symbolic form) may be used to compute loadings under somewhat changed conditions, e.g., for some other shock strengths and building sizes. In order that such use can be made of the predictions in Part I, the development ("method of determination") sections (e.g., Section E.2.2) have been separated from sections on numerical calculation (e.g., Section E.2.3). The development sections need not be read if it is desired to apply the same methods under slightly changed conditions; the minimum which must be read for a clear understanding is the following: Vol. I, Sections E.2.3 and E.3.1; Vol. III, Sections E.1.1, E.1.2, E.1.3.3, and E.1.4; and Vol. III, the introductory section and the

numerical sections for the particular building considered (e.g., Sections E.2.1 and E.2.3). It may also be desirable to refer to the figures which show the predictions graphically (e.g., Figs. E.2.6-E.2.16).

In sections on numerical computations some of the tables show an asterik beside some value of time. This signifies that pressure is predicted to vary approximately linearly with time until the value which is so marked; following that entry, computed points are ₍to be₎ connected with a smooth curve. The time so marked is that at which only drag forces act on the member under consideration.

Whenever the pressure or force on a surface jumps suddenly, the value of time at which this occurs is entered twice with the symbols "-" and "+" indicating the loadings which hold before and after this sudden change.

E.1.4.3   Notation

Symbols which reappear throughout the report are listed below; other symbols are defined in the first section of chapters discussing specific buildings.

In the definitions below, the term "pressure" always refers to gage pressure (pressure greater than P_0 which is defined below) if the adjective "absolute" is not used. The convention of representing absolute pressure by P and representing gage pressures by p is adopted throughout.

For symbols which appear in the following list as functions of time, t, the t may be dropped from the notation whenever

ambiguity will not result (see p_σ below).

E.1.4.3.1 Notation Not Associated with Structures

P_0 = absolute pressure in front of the shock. This is atmospheric pressure for blast in air.

$p_\sigma(0)$ = pressure rise across the shock front = initial side-on pressure or overpressure

$p_\sigma(t)$ = side-on pressure, *at the front wall* at time, t, after passage of the shock front

P_σ = $p_\sigma(t)$, used whenever t may be dropped from the longer notation without ambiguity

t = time since the shock front passed the front wall of a structure

t_0 = duration of positive pressure phase of shock

U = velocity of shock front moving in still air; velocity of shock front relative to the air ahead of it

u(t) = velocity of air

ξ = P_1/P_0; shock strength

$\rho(t)$ = density

E.1.4.3.2 Notation Associated with Structures

A_b, A_f, A_r = total area minus the areas of the windows and doors or monitor openings for the back wall, front wall, and roof, respectively

back C_{ro} = drag coefficient for the outside surface of the back slope of a gabled roof

C or C_d = drag coefficient (additional subscripts designate structural surfaces)

C_{df}, C_{db}, C_{dr} = total drag coefficient for the front wall, back wall, and roof, respectively; positive if drag force is directed toward the interior, e.g., $C_{df} = C_{fo} - C_{fi}$

C_{fi}, C_{bi}, C_{ri}	= drag coefficients for the inside surfaces of the front wall, back wall, and roof, respectively
C_{fo}, C_{bo}, C_{ro}	= drag coefficients for the outside surfaces of the front wall, back wall, and roof, respectively
c_{refl}	= speed of sound in regions of reflected pressure for normal reflection
δ	= length of the shock wave reflected from the inside back wall of buildings with open sides
$\Delta(x)$	= lag of the inside wave front behind the outside wave front for buildings with upstream front-wall openings
e	= distance from the edge of the roof to the center of an upper window of the front wall
$f(t), b(t), r(t)$ or f, b, r	= average net pressure differences on the front wall, back wall, and roof respectively[8]; e.g., $f = f_o - f_i$.
F, B, R	= average net forces on the front wall, back wall, and roof respectively; e.g., $F = fA_f$
$f_i(t), b_i(t), r_i(t)$	= average pressures on the <u>inside</u> front wall, back wall, and roof respectively
$f_{is}(t), b_{is}(t), r_{is}(t)$	= pseudo steady state pressures for the <u>inside</u> front wall, back wall, and roof, respectively (see Eqs. E.1.1 to E.1.3)
$f_o(t), b_o(t), r_o(t)$	= average pressures on the <u>outside</u> front wall, back wall, and roof respectively
$f_{os}(t), b_{os}(t), r_{os}(t)$	= pseudo steady state pressures for the <u>outside</u> front wall, back wall, and roof respectively (see Eqs. E.1.1-E.1.3)
front C_{ro}	= drag coefficient for the outside surface of the front slope of a gabled roof

---

8 Occasionally these symbols will be used to refer to <u>portions</u> of the various surfaces; such usages are made clear when used.

h = height of front or back wall of a structure

H = total horizontal force on a structure

$\bar{h}_{ib}, \bar{h}_{ob}, \bar{h}_{if}, \bar{h}_{of}$ = distances needed for computing loadings on front and back walls (see Eq. E.2.7)

$K(\theta)$ = factor used in computing loadings on sloped roofs, (see Eq. E.1.4)

ℓ = length of a structure in the direction of flow

Ω = ratio of area of openings to gross area of wall for structures with equal openings in front and back walls

$p_d(t)$ = "basic" drag pressure = $\dfrac{\rho(t)\, u^2(t)}{2}$

p_{irefl} = pressure behind the shock reflected from the back wall of a hollow structure

$p_{obl\ refl}$ = pressure behind a shock after oblique reflection

p_{refl} = pressure behind a shock after normal reflection

$p_{\sigma i}$ = side-on pressure behind a shock which enters a hollow structure

τ = time measured from a zero other than t = 0 (each usage of this symbol is defined as used)

t = time elapsed since the shock front passed the front of structure

t^* = time required for windows to break after being struck by a shock front (taken constant for a particular structure)

θ = angle with the horizontal of a gabled roof (in degrees)

x = distance of the shock front from the front wall of a building = Ut

ξ_i = strength of the shock which enters a hollow structure = $\dfrac{(p_{\sigma i} + P_0)}{P_0}$

E.1.5 INITIAL LOADING OF FRONT PART OF SLOPED ROOF

In this section
The loading on the front part of a sloped roof (see Fig. E.1.4)
is determined at the time when the shock front has reached the roof peak,
a distance $l/2$ from the upstream edge. The results will be applied to
roofs of various slope angles (θ) in this volume: the 33° slopes on
building types 3.3.5, and the 7° slopes on buildings 3.3.3 and 3.3.8h.
For the latter buildings, the distance $l/2$ must be replaced by $l/6$
throughout in applying results of this section.
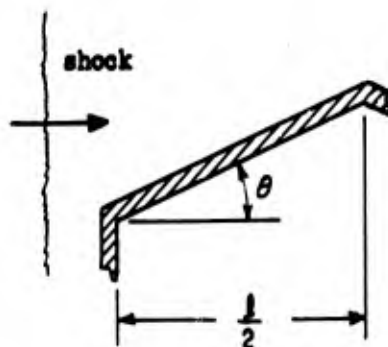
Fig. E.1.4 Front Slope of A Sloped Roof

When the shock front strikes a roof slope oriented as in Fig.
E.1.4, oblique reflection of the shock front occurs. The instantaneous
reflected pressure, $P_{obl \; refl}$, has been studied extensively in the litera-
ture, both theoretically and experimentally, and the value of this pres-
sure is known for various shock strengths and for most slope angles
between zero and 90°.

By the time the shock front reaches $\ell/2$, however, the pressure at most points has dropped considerably below $p_{obl\ refl}$, due primarily to clearing of these higher pressures into the free stream surrounding the building. This section will utilize shock tube data which gives this reduced pressure (less than $p_{obl\ refl}$) for two particular slope angles. A comparison of this data with $p_{obl\ refl}$ will be used to obtain a general relation between $p_{obl\ refl}$ and the average pressure on a roof slope at the time when the shock front has reached the roof peak. These results are obtained for slope angles up to about 45° and for moderate shock strengths.

Reference 18 (Fig. 5.18) gives values of $p_{obl\ refl}$ for a range of shock strengths; for convenience, a series of these curves is reproduced here in Fig. E.1.7 with additional intermediate curves included from the basic references. These original references are computed values from Polachek and Seeger[9] in the domain of regular reflection (angles approaching "normal" or head-on reflection) and experimental results from L. G. Smith[10] for the region of Mach and other types of reflection (for angles approaching glancing incidence at which no reflection occurs). Some of

---

9 H. Polachek and R. J. Seeger, "Regular Reflection of Shocks in Ideal Gases", Explosives Research Report No. 13 Navy Dept, BUORD, 1944. (Confidential).

10 L. G. Smith, "Photographic Investigation of The Reflection of Plane Shocks in Air", NDRC Rept No. A350, 1945.

the difficulties in present studies of oblique reflection are mentioned ~~given~~ in Vol. I at the end of Section E.4.3.2; as noted there, reference 15 presents a summary of recent studies on oblique reflection.

In Fig. E.1.7 a heavy dashed line joins the data for regular reflection and Mach reflection as was done in reference 18; values in this middle zone have not been satisfactorily established.

Curve A in Fig. E.1.5 shows values of $p_{obl\ refl}$ from Fig. E.1.7 for $\xi = 2$. Curve B is based on shock tube data from references 1 and 2 for a 45° and a 10° slope, respectively and on the fact that $p_{obl\ refl} = p_\sigma(0)$ for $\theta = 0°$. The data of curve B give $r_o(\ell/2U)$, the average pressure on the front roof slopes when the shock front has reached the roof peak at $\ell/2$. These two curves are used in deducing predicted loadings for all slope angles up to 45° for a range of shock strengths, ξ .

To obtain the loading predictions the average pressures from curve B and the instantaneous pressures from curve A are used as follows.

It is believed that, for any given angle, θ , the ratio of average pressure to instantaneous pressure is a constant for moderate shock strengths if the pressures are expressed in terms of their deviation from the free stream pressure, $p_\sigma(t)$.

Since the data in Fig. E.1.5 are based on flat-topped shocks, $p_\sigma(t) = p_\sigma(0)$ for that figure. Hence, for peaked shocks, the above assumption is equivalent to stating that the following quantity is a constant; i.e.,

$$K(\theta) = \frac{r_o(\ell/2U) - p_\sigma(\ell/4U)}{P_{obl\ refl} - p_\sigma(\ell/4U)} \qquad (E.1.4)$$

does not vary with shock strength (for moderate strengths up to say, $\xi = 2.5$) but depends only on the slope angle, θ. Here, $r_o(\ell/2U)$ is the average roof pressure when the shock front is at $\ell/2$ and $p_\sigma(\ell/4U)$ is the average side-on pressure in the free stream above the roof at the same time.

The data in Fig. E.1.5 may be used to determine $K(\theta)$ by subtracting one from the values on curve B and A and taking their ratio. The results of such a computation appear in Fig. E.1.6. Clearly $K(\theta)$ responds sensitively to changes in either of these curves; hence, Fig. E.1.6 is to be considered as quite approximate.

Finally, to apply these results to other shock strengths, Eq. E.1.4 is written as

$$r_o(\ell/2U) = p_\sigma(\ell/4U) + K(\theta)\left[P_{obl\ refl} - p_\sigma(\ell/4U)\right] \qquad (E.1.5)$$

To use this expression, $K(\theta)$ and $P_{obl\ refl}$ are found in Figs. E.1.6 and E.1.7, respectively and p_σ is obtained from the side-on pressure curve which is derived for the problem at hand (from Eq. E.4.16 in Vol. I).
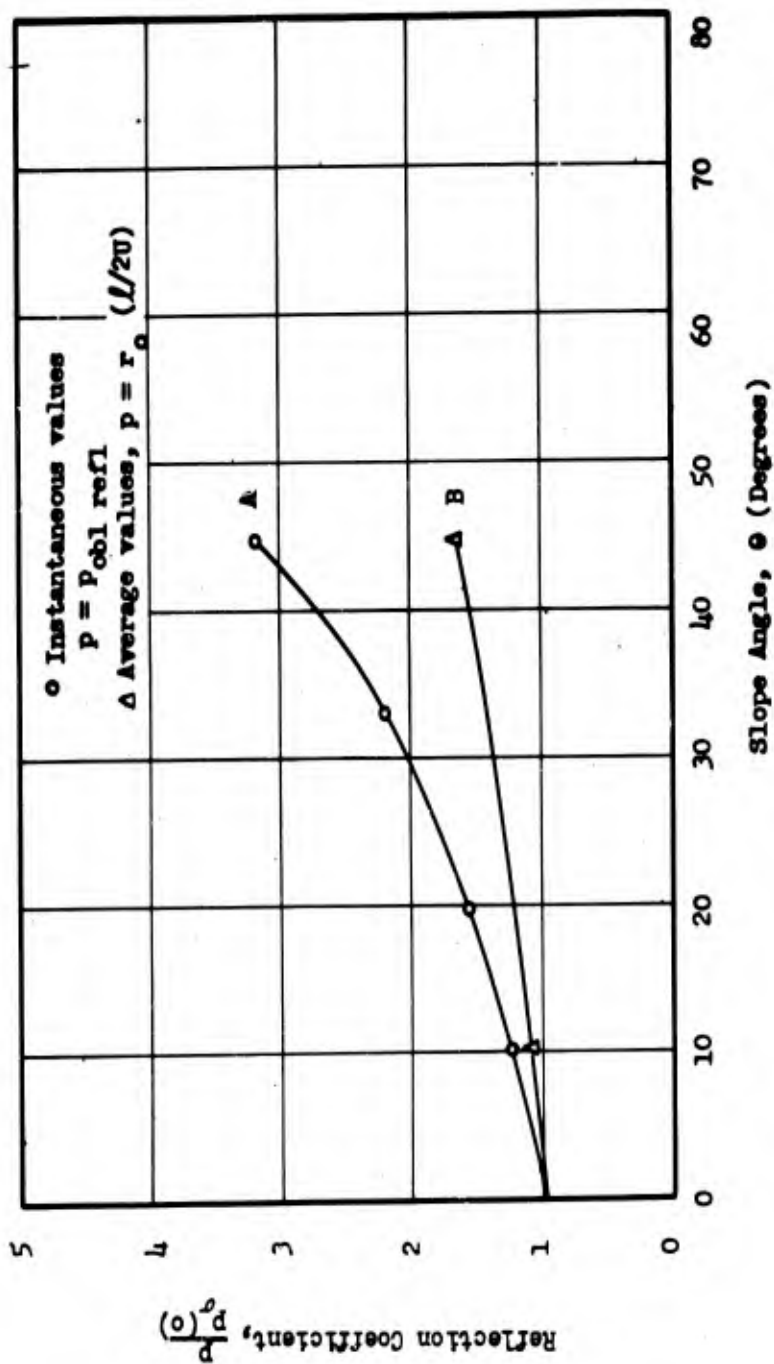
Fig. E.1.5 Instantaneous and Average Reflection Coefficients for Oblique Shock Reflection. Data for Curve A from Fig. E.1.7 for $\xi = 2$; Data for Curve B from references 1 and 2 for $1.92 \leqslant \xi \leqslant 2.06$
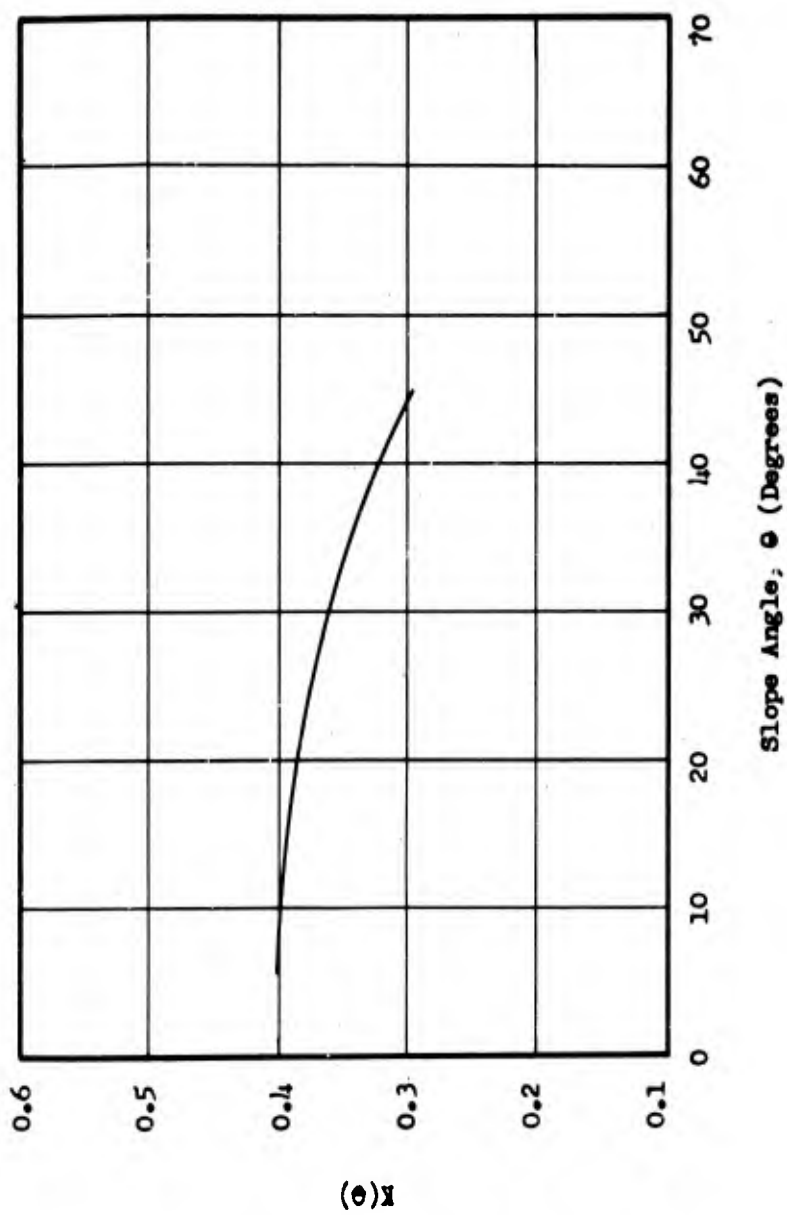
Fig. E.1.6 $K(\Theta)$ as a Function of the Slope Angle, Θ (Not valid for $\xi > 2.5$)
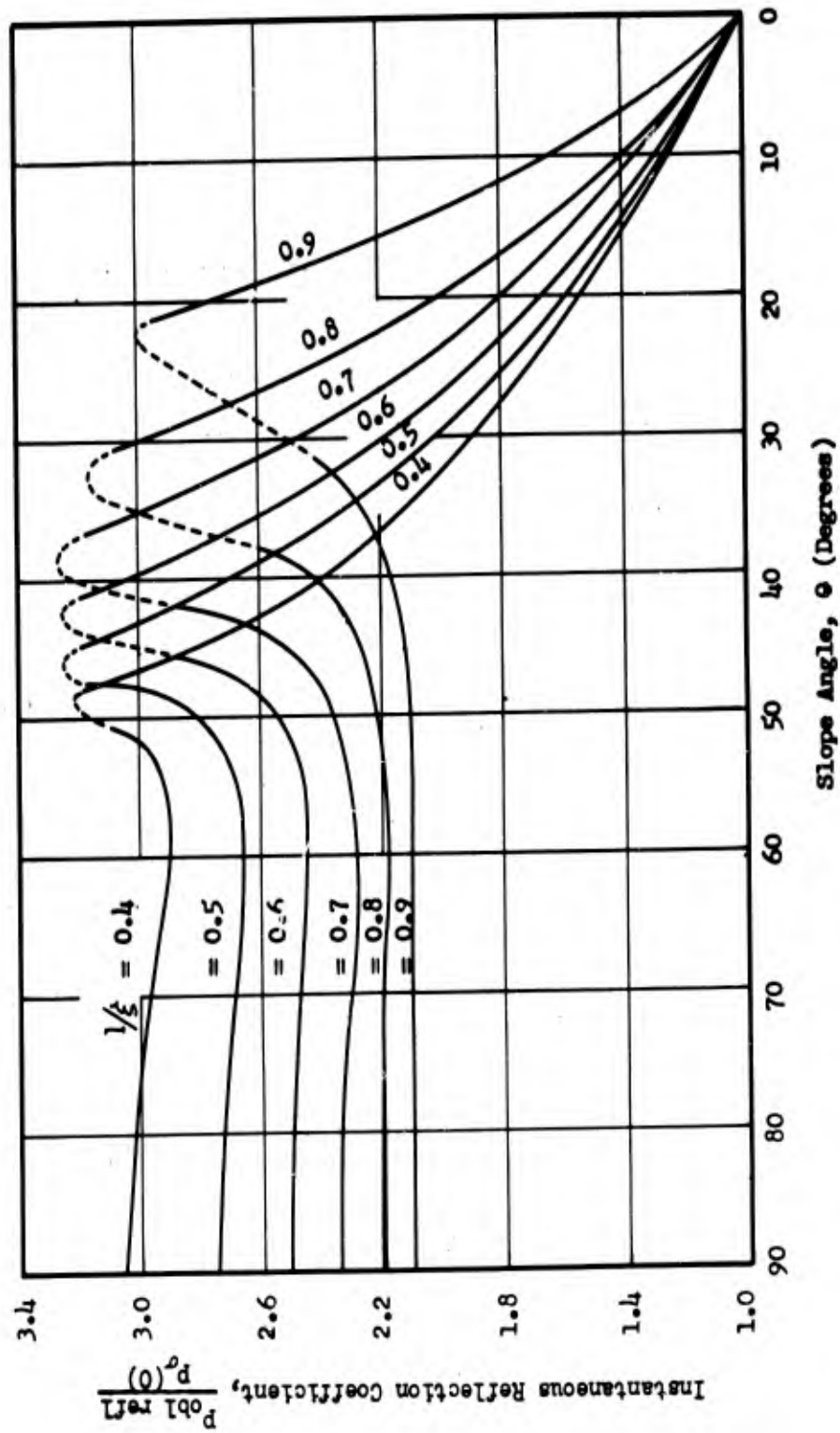
Fig. B.1.7 Instantaneous Reflection Coefficients for Oblique Shock Reflection

CHAPTER E.2

BUILDING 3.3.3

E.2.1 GENERAL

Building 3.3.3 is of the type possessing a sawtooth roof with monitors; it has no side walls. Figure E.1.1 presents a three-dimensional view of the building, with Figs. E.2.1 and E.2.2 showing the front and side details. The back wall, which is similar to the front wall, is not shown.

Also omitted from these drawings is an extensive trusswork, which includes purlins, struts, monitor girts, exposed columns, etc. The projected area of this trusswork, projected into a vertical plane transverse to the flow direction, is roughly 7800 sq ft.[1] For purposes of computation the trusswork is assumed to be linearly distributed along the 240-ft dimension.

The computation of roof loadings utilizes an average slope length, $l = 31.3$ ft, obtained by weighting the two lengths of the roof slopes according to their associated areas. The two lengths arise from the fact that the monitors do not extend across the full width of the building. (See Figs. E.1.1 and E.2.1.)

[1] Computed from Drawing No. 100-252-1, Dept. of Air Force, Hq. AMC, Office of Air Installation, Wright-Patterson Air Force Base, Dayton, Ohio.
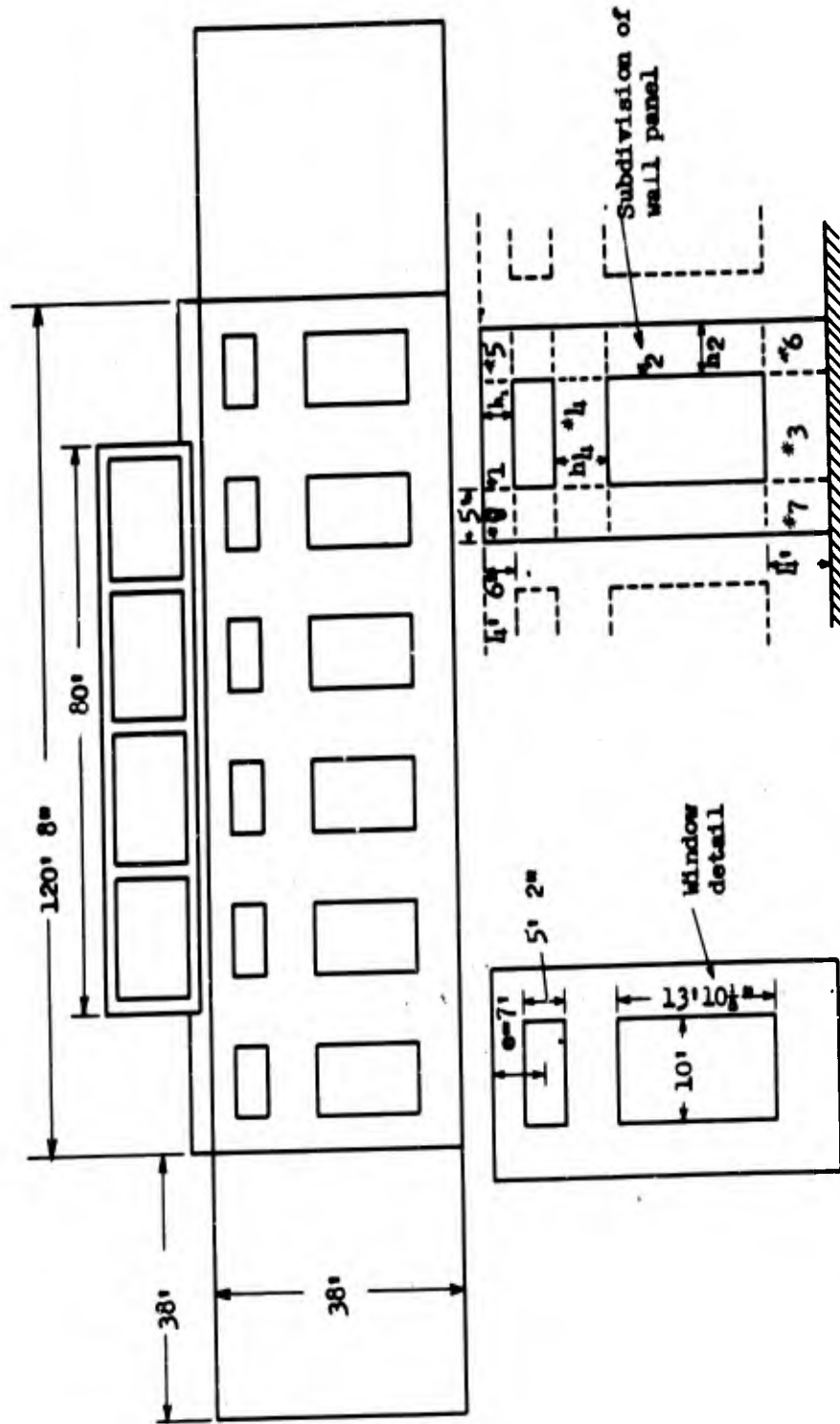
Fig. E.2.1 Front Wall of Building 3.3.3 (Building 3.3.6a is 1/4 of size indicated)

Fig. E.2.2 Side View of Building 3.3.3 (Building 3.3.8a is 1/4 of size indicated)

The structure is subjected to a shock wave of 3.4 psi overpressure (ξ = 1.23).

Notation used in addition to that listed in Section E.1.4.3 is listed below.

a   = length of one bay (see Fig. E.2.2)

α = reduction factor for effect of purlins on inside roof pressure

A_{fn} = area of subdivision of front wall panel (see text associated with Eq. E.2.7)

A_d = projected area of trusswork, projected into a vertical plane transverse to flow direction

C_{dd} = average drag coefficient for trusswork

$d(t)$ = average pressure on trusswork (or average force per unit area in the direction of flow)

D   = force on trusswork = dA_d

δ_n = a quantity which is equal to either 1/2 or 1, depending on a type of subdivision of a wall panel (see Eq. E.2.7)

H_r = horizontal component of the force on the roof

$\bar{L}$ = a weighted average distance on the front or rear wall (Eq. E.2.7)

L = weighted average length used for time computations on the roof slopes (see Section E.2.1)

V_r = vertical component of the force on the roof

E.2.2   METHOD OF DETERMINATION OF LOADING

The development of methods for determining the loadings on building 3.3.3 is based on the qualitative ideas expressed in Section E.1.2. Schematic diagrams are presented in Figs. E.2.6 to E.2.17, showing average

pressures on the front wall, back wall, roof, and trusswork.

E.2.2.1 Some General Topics on Loading

This section treats the pressures anticipated on various subportions of the 3.3.3 structure and on its model, building 3.3.8h. These topics are also applicable to many other building types with similar subportions. In particular, some of the treatments given here will be applied to building 3.3.4 (Chapter E.4).

E.2.2.1.1 Effect of Window Breakage on Clearing of Reflected Pressures

Since glass windows do not break for a certain time after the shock front strikes a building, pressures can be relieved only from the edges of the front wall during this time. The relief time formula of Vol. I (Fig. E.5.25) must therefore be modified to take into account the presence of the glass.

If the glass would never break, the relief time would be based on the height of the building, h, as shown by curve (1) in Fig. E.2.3.

If, however, the building [*windows*] contained no windows [*glass*], the relief time would be based on an average height $\bar{h}$, curve (2), obtained by the method of averaging relief time for subareas outlined in Section E.2.2.1.7.

If the glass panes are subjected to the loading from the lowest of the curves of Fig. E.2.3, curve (2), they will take the longest time to break.
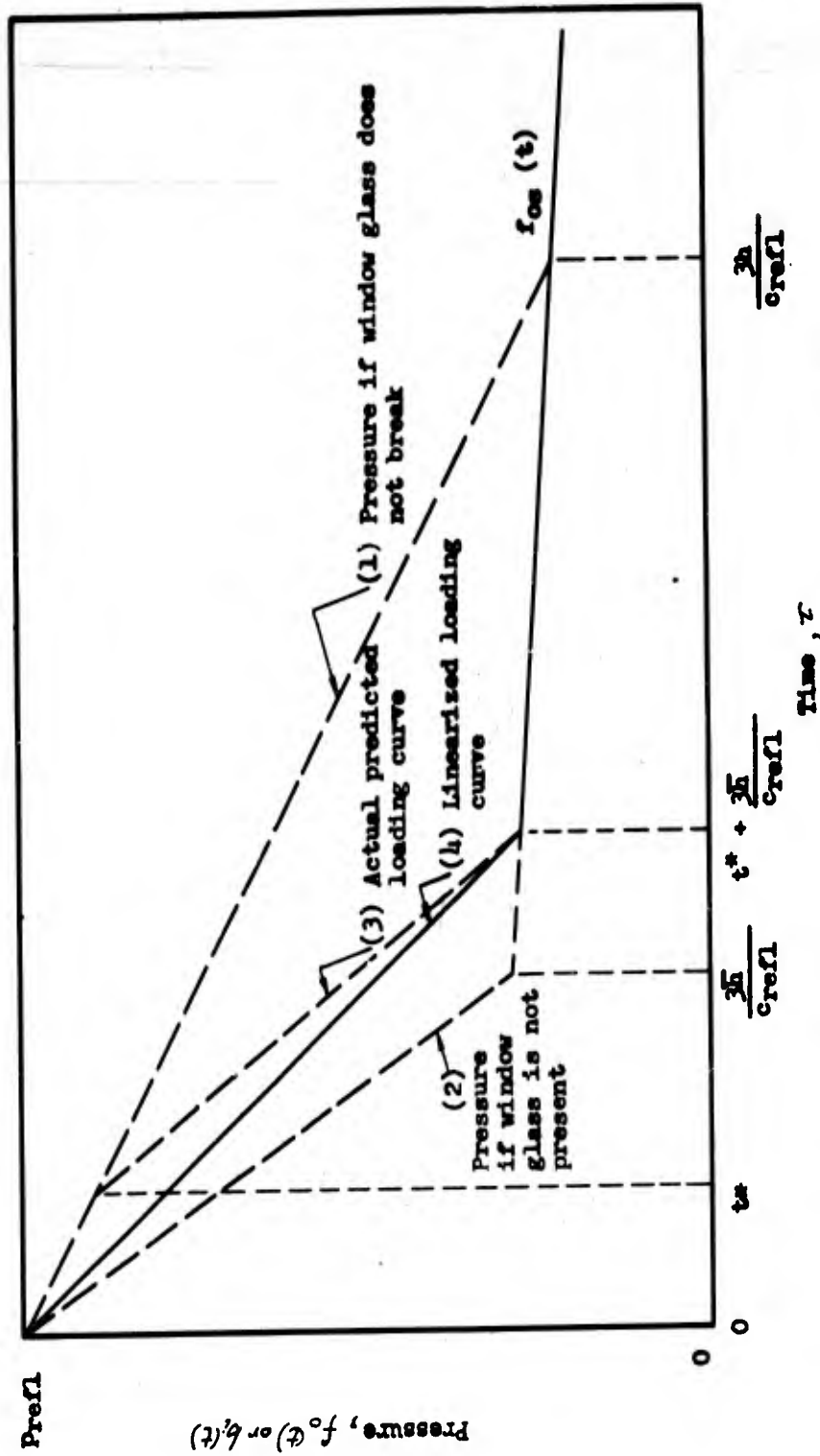
Fig. E.2.3 Relief Time for Walls with Glass Windows of Building 3.3.3

Applying the elementary beam or plate theory to the windows, and using loading curve (2), it can be shown (see Part II, Section E.8.1) that the glass will break in time t^*, where t^* is always less than $3\bar{h}/c_{refl}$ for the Greenhouse Buildings. If the glass pane were subjected to the higher loading given by curve (1) they would break earlier. Hence, t^* is an upper bound for the true breaking time as produced by the actual loading. Assuming that the glass shatters completely at the time of breaking, t^*, the most probable loading would follow curve (1) until t^*. Since the time t^* found in the calculations referred to above was found to be small, it may be assumed that the clearing after the windows break occurs in the usual manner in time $\frac{3\bar{h}}{c_{refl}}$. Thus it will then drop linearly to $f_{os}(t)$ (see Eq. E.1.1) reaching it at approximately $t^* + 3\bar{h}/c_{refl}$. This curve is labeled (3) in Fig. E.2.3. Since the impulse is changed only slightly if the two line segments of curve (3) are replaced by a single straight line, a single straight line between $t = 0$ and $t = t^* + 3\bar{h}/c_{refl}$ shall be used as illustrated by curve (4).

On the basis of the above considerations and for all walls with glass windows, the relief time shall be given by

$$t_c = t^* + \frac{3\bar{h}}{c_{refl}} \tag{E.2.1}$$

where t_c = relief time,

t^* = time when window breaks, shown to be less than 2 msec for the Greenhouse buildings under consideration,

$\bar{h}$ = the average height of sub areas, computed as if no glass
were present as in Section E.2.2.1.7,

c_{refl} = sound velocity in the reflected pressure region.

The front wall pressure is assumed to vary
linearly between p_{refl} at $t = 0$ and $f_{os}(t_e)$ at $t = t_e$.

The value of t_e as derived above is applied
to the computations of average pressure-time relations on the upstream
side of the front and back walls of the 3.3.3, 3.3.8h and 3.3.4 structures
and to an outside section of the 3.3.5b front wall.

E.2.2.1.2   Lag Between Outside and Inside Shock Fronts Along Roofs

Utilizing the Michigan shock tube shadow-
graphs, (reference 8) it is seen that the wave formed inside a hollow model
with an upstream opening initially has nearly a spherical shape. On large
structures this effect can be expected to cause a lag between the inside
shock front and the outside front at the roof, in addition to the lag
induced by the window breaking time. The analysis of the total lag, given
below, shall be used for the roof sections of buildings 3.3.3, 3.3.8h,
and 3.3.4.

Assuming the velocity of the shock front
inside the building to be constant, an elementary analysis shows this
lag, $\Delta(x)$, to be, for the 3.3.4 average roof pressures,

$$\Delta(x) = x - \left[(x - Ut^*)^2 - c^2\right]^{1/2} \tag{E.2.2}$$

where $\Delta(x)$ = lag in ft when shock front is at a point x,

   x = horizontal distance from front wall to shock front, $= Ut$

   U = shock velocity, taken to be the same for inside and
   outside waves,

   t^* = window breaking time,

   e = distance from center of upper windows in the front wall
   to the roof.

For the 3.3.4 structure, $\Delta(x)$ is taken as zero after the shock wave passes the beginning of the third roof section, since the inside shock at this point is equal in strength to and coincides in position with the outside shock. (See also Section E.2.2.1.6.)

In the case of buildings 3.3.3 and 3.3.8h, however, the presence of the sloped roof and purlins make Eq. E.2.2 appear to be too great a refinement to predict the lag between inside and outside waves used in computations of net average pressures. Since inside and outside shock fronts are assumed to coincide at the end of the first bay (see Section E.2.2.1.6), the lag $\Delta(x)$ between inside and outside waves (for the 3.3.3 and 3.3.8h average roof pressures) is taken as

$$\Delta(x) = \Delta(0) \left[1 - \frac{x - \Delta(0)}{a - \Delta(0)} \right] \qquad (E.2.3)$$

where $\Delta(0) = Ut^* + e$. Thus, the lag $\Delta(x)$ decreases linearly from the value $Ut^* + e$ when the inside wave front first reaches the underside of the roof to zero when both inside and outside waves have covered the

first bay length, a.

E.2.2.1.3 Effect on Roof of Reflection of Shock Front From Back Wall

A wave reflecting from the inside back wall of building 3.3.3, 3.3.8h, or 3.3.4 will lead to an upward thrust on the roof near the back wall. This reflected wave is assumed to decay to p_σ (τ) when it has reached the rearmost monitor, a distance $\overline{l}$. This is due to relief through the open sides and through the large window area of the back wall.

As soon as relief is completed on the back wall, a rarefaction wave pursues the above discussed reflected wave at approximately the same velocity. It will lag the shock wave by the distance δ, where

$$\delta = \left[\frac{3\overline{K}_{1b}}{c_{refl}} + t^*\right] U. \qquad (E.2.4)$$

and where $\overline{K}_{1b}$ = average clearing distance for inside back wall,

c_{refl} = velocity of sound behind reflected wave,

t^* = window breaking time,

U = velocity of shock wave.

The pressure between the reflected shock front and the rarefaction wave which follows at a distance, δ, at any time shall be assumed to be constant. After passage of the rarefaction wave the pressure shall be taken to be the same as the pressure on the outside of the roof, r_{os} (see Eq. E.1.3). Thus the net pressure on the roof for any time, as a function of distance, will be, *idealized* in the form of a step-wave of width δ. The magnitude

of the net pressure in the step-wave shall be assumed to decay linearly from the reflected pressure minus side-on pressure when the reflected wave is at the rear wall to a value of zero when the reflected wave has traveled the distance I. Thus the value of the net pressure will be

$$\left[P_{refl} - P_\sigma \ (I/2U) \right] \left[1 - U\tau / I \right] \tag{E.2.5}$$

where the side-on pressure has been taken at its average value during this period, P_σ ($I/2U$) and τ is the time at which the inside wave (of strength P_σ (0))reflects from the back wall. The reflected wave at a certain time is shown schematically in Fig. E.2.4.

The average pressure on the roof, then, will increase linearly until the time δ /U when the rarefaction wave enters the building. The average pressure at this time will have the value

$$r = \frac{1}{I} \left[P_{refl} - P_\sigma \ (I/2U) \right] \left[1 - \delta/I \right] , \tag{E.2.6}$$

since the peak pressure at the time $\tau = I/U$ may be considered to be distributed over all of the roof section instead of over a width of only δ. After this peak pressure is reached the average net pressure will decay linearly to zero when the wave has traveled a distance I, i.e. at a time $\tau = \frac{I}{U}$. This is illustrated in Fig. E.2.5 where the average net pressure on the wall is given as a function of time.

E.2.2.1.4 Drag Coefficient for the Trusswork

The trusswork of building 3.3.3 consists of two types of members, roughly equal in projected area, but subjected to entirely different drag effects. The first type consists of purlins,

which shield each other, supporting the roof planks; the second type consists principally of trusses and cross-bracings whose members are far enough apart on the average so that shielding effects may be neglected.

The ratio of the height of the purlins to the distance between them is approximately 1 to 8 for the 3.3.3 and 3.3.8h structures. Although the literature gives no information regarding the shielding effect of a series of identical flat plates, qualitative knowledge can be gained from Fig. 42 of reference 11, where Irminger and Nøkkentved study the steady state drag pressures on a solid square block shielded by a solid screen of the same height and located at several different distances from the block. Selecting a height to distance ratio corresponding to the purlin geometries of the Greenhouse structures, the drag coefficient for the wind forces acting on these purlins is found to be $C_d \approx 0.2$.

The drag coefficients for the wind forces acting on the isolated truss components of shapes such as occur in Greenhouse structures have been studied by Howe, reference 10. From Fig. 1 of this reference, $C_d \approx 1.9$.

Since the projected areas of members with $C_d \approx 0.2$ and $C_d \approx 1.9$ are roughly equal (see footnote, Section E.2.1), the average drag coefficient of the total trusswork is given by the arithmetic mean as $C_{dd} \approx 1$. The drag coefficient C_{dd} is used in Fig. E.2.17 in conjunction with the pseudo steady state pressures acting on the 3.3.3 and 3.3.8h trusswork.

$$\left[\text{Pres.} - P_0\left(\tfrac{\bar{\ell}}{20}\right)\right]\left(1 - \tfrac{U_c}{\ell}\right)$$

Additional Point Pressure, r_1 reflected shock effect

Distance from Back Wall Measured in Upstream Direction
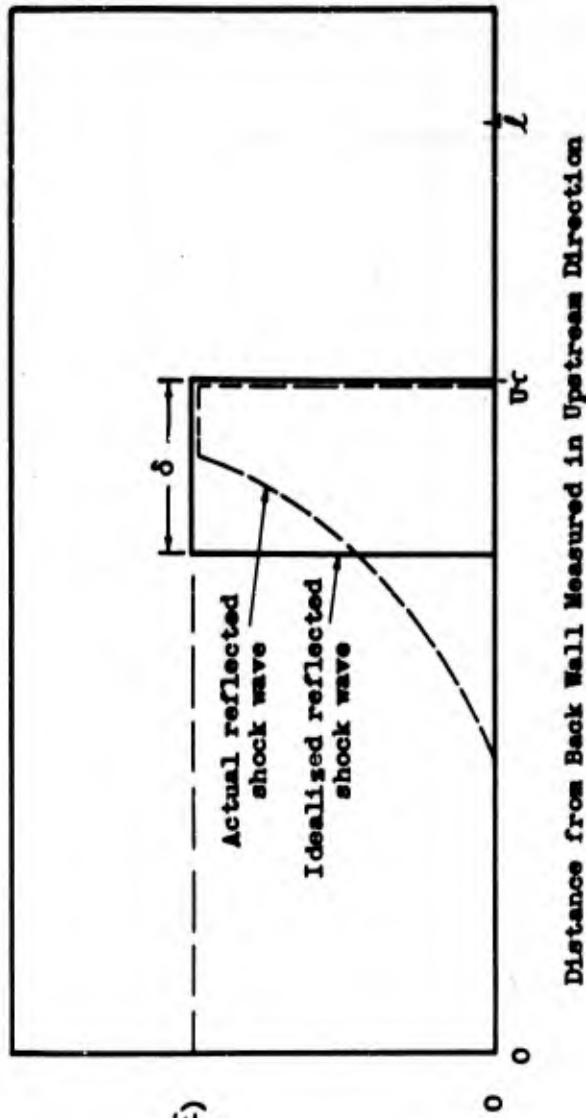
Fig. E.2.4 Additional Pressure at Points on Underside of Third Bay Rear Roof Slope Affected by Reflected Shock for Buildings 3.3.3 and 3.3.8h; $\ell = t - \tfrac{\ell}{U}$

$$r_1^i = \frac{\delta}{L}\left[P_{refl} - P_0\left(\frac{L}{2U}\right)\right] \cdot \left[1 - \frac{\delta}{L}\right]$$
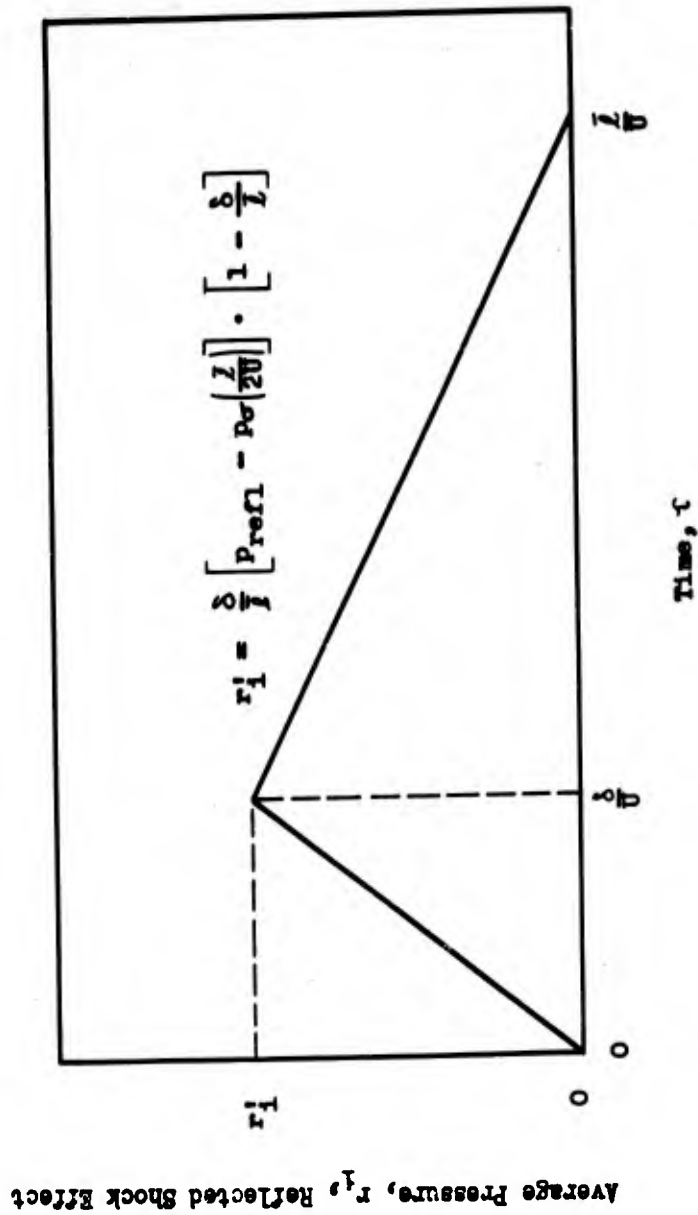
Fig. E.2.5   Additional Average Pressure Due to Reflected Shock on Underside of Third Bay Rear Roof Slope of Buildings 3.3.3 and 3.3.8; $\tau = t - \frac{L}{U}$

E.2.2.1.5   Effect of Purlins on Roof Loadings

The purlins supporting the roof of building 3.3.3 are I-beams, while for building 3.3.8h they are channels made up of two angles. Since the height of the purlins is small compared to the length of the wave (height = 10 in.; Ut_o = 1700 ft for building 3.3.3), it is assumed that steady state flow conditions are applicable for studying the effect of turbulence, due to the purlins, on the roof between two purlins. The presence of turbulence and vortices would lessen the pressure below that which would be felt if there were streamline flow.

The ratio of the height of the purlins to the distance between them is approximately 1 to 8 for both buildings. Figure 42 of reference 11 shows steady state pressures on a block shielded by a solid screen with the same height to distance ratio. Utilizing this figure for qualitative notions and considering the shape of the purlins as affecting the degree of turbulence and vorticity present between them, reduction factors α are chosen, with α being the ratio of the pressures on the roof with and without the purlins. These reduction factors are applied to pressures on the undersides of the roofs computed on the basis that no purlins are present.

The reduction factors were assumed to be α = 0.75 for building 3.3.3, and α = 0.85 for building 3.3.8h.

The factors α are used in Figs. E.2.11, E.2.13, E.2.15 and E.2.16.

E.2.2.1.6 Build-Up of Pressure Behind the Inside Shock Front

As pointed out in Section E.1.2, the shock entering the inside of buildings 3.3.3, 3.3.8h, and 3.3.4 through the front wall openings lags behind the outside shock front because of the delay imposed by the window-breaking time. Furthermore, the inside shock is initially weaker than the outside shock, because the ratio of window and door area to total front wall area, Ω is fairly small, a phenomenon which was studied in considerable detail in Vol I (See Fig. E.5.4 Vol I.)

As both outside and inside waves sweep down the length of the buildings, the inside shock is reinforced by the outside shock which enters from the sides, from the edges of the roof, and through the broken monitors.

It is believed that in the case of the 3.3.3 and 3.3.8h structures, the inside wave has caught up with the outside wave at the end of the first bay (at a distance a from the front wall) and that they are of equal strength there. In the case of 3.3.4, the point at which the shock has reformed to initial strength is taken at the end of the second monitor, a distance ℓ_4 from the front wall.

Summarizing, the inside shock, initially of overpressure $p_{\sigma i}$ (obtained by interpolation from Fig. E.5.4 Vol I) builds up linearly to p_σ (0) in time $t = \frac{a}{U}$ for the 3.3.3 and 3.3.8h structures or in time $t = \frac{\ell_4}{U}$ for the 3.3.4 structure.

E.2.2.1.7   Mean Clearing and Build-Up Distances for Walls with Openings

The time required for reflected pressure on the front of a solid wall struck by a shock wave to clear to pseudo steady state pressure (see Fig. E.5.25, Vol I) is based on multiples of the time h/c_{refl} (the time necessary for a rarefaction wave to sweep the wall once). The time required for the pressure on the back of a wall to build up to pseudo steady state pressure (see Fig. E.5.33, Vol I) is based on multiples of the time h/U (the time required for a shock wave to sweep the wall once). In the above times h is either one-half the width or the height of the wall, whichever is smaller, c_{refl} is the speed of sound in the reflected pressure region, and U is the velocity of the shock front.

When walls with numerous openings are considered, however, clearing from reflected pressure can take place through the openings, and pressure on the back of a wall can build up from flow through the openings. These considerations necessitate a modification of the method of determining clearing and build-up times because the rarefaction wave on the front or the shock fronts on the back of the wall travels a much shorter distance to cover the wall once than was mentioned above.

The distance $\bar{h}$ is introduced as the "weighted average" distance rarefaction waves or shock fronts must travel to cover the wall once. With $\bar{h}$ determined by the method explained in the following discussion, the basic time intervals are chosen as $\bar{h}/c_{refl}$

for clearing time (by rarefactions) on the front of the wall and $\bar{h}/U$ for build-up time (by shocks) on the back of the wall. The method of determining $\bar{h}$ is shown for the front face of a wall, but is equally applicable for the back face.

As shown in Fig. E.2.1, the wall is subdivided into rectangular areas of three types: (a) areas with opposite edges exposed to the free stream, e.g., areas 1 and 4; (b) areas with one edge touching the ground and the opposite edge exposed to the free stream, e.g., area 3; (c) all remaining portions of the wall, e.g., areas 5 to 8. Area 2 acts as a type b area.

Each of the above sub-areas has a width h_n chosen as shown in Fig. E.2.1. Type c areas (areas 5 to 8) are treated as if they were of Type a or b; for each Type c area a fictitious width h_n is chosen which is the same as that for a neighboring Type a or Type b area, whichever has the smallest h_n. This treatment is necessary because the manner in which a shock or rarefaction wave covers Type c areas is relatively unknown; however, by assuming that pressure on such areas builds up or clears in the same time as the fastest neighboring area, a fairly valid approximation should be obtained.

For the front side of a wall the "average" distance which rarefaction waves must travel to cover the wall is now defined as

$$\bar{h} = \sum_n \delta_n h_n A_{fn}/A_f \tag{E.2.7}$$

where $\delta_n = 1/2$ for Type a areas

$\delta_n = 1$ for Type b areas

$\delta_n = 1/2$ or 1 for Type c areas, depending upon whether treated as Type a or b areas.

The distance rarefaction waves must travel from some edge to cover sub-area n is $\delta_n h_n$; thus $\bar{h}$ is the average of such distances weighted according to the relative sizes of the sub-areas.

For the back side of a wall the formula may be interpreted as giving the average distance which shock fronts must travel to cover the wall.

This method is used to determine clearing and build-up times for the front and back walls of buildings 3.3.3, 3.3.4, and 3.3.8h, and a section of the front wall of building 3.3.5b.

Although there is a slight difference in geometry between the front and back walls, due to the presence of wing walls on the front wall (and the door in the back walls in the case of buildings 3.3.3 and 3.3.8h) these differences do not affect the numerical values for the $\bar{h}$'s computed in Sections E.2.2, E.3.2 and E.4.2.

E.2.2.2 Development of Computational Methods

The development of methods for computing pressures on building 3.3.3 is divided into four parts, based on computations for the front wall, the back wall, the roof, and the trusswork. Section E.1.2, which contains the detailed qualitative discussion underlying the average pressure predictions for these surfaces, forms the basis for a

clear understanding of the development of these predictions.

The concept of pseudo steady state pressures as used in this section is discussed in detail in Section E.1.3.2. These pseudo steady state pressures are: f_{os} and f_{is} for the front wall; b_{is} and b_{os} for the back wall; and "front r_{os}" and "back r_{os}" for the roof slopes.

The results of this section are summarized in Figs. E.2.6 through E.2.17 in the form of symbolic expressions for predicted loadings.

E.2.2.2.1 Pressures on Front Wall

The average pressure on the **outside** of the front wall, shown in Fig. E.2.6, follows the predictions developed in Vol I (Fig. E.5.25) for a wall without openings. However, the relief time is replaced by $t^* + \dfrac{3\bar{h}_{of}}{c_{refl}}$ as discussed in Section E.2.2.1.1 (see Eq. E.2.1). The calculation of $\bar{h}_{of}$ is to be made from Eq. E.2.7; its use is justified in that section (E.2.2.1.7).

The average pressure on the **inside** front wall, shown in Fig. E.2.7, is based partly on data in Vol I for the rear of a thin wall and partly on data in Vol II for the inside front wall of a hollow block. The data in Vol I (Fig. E.5.12) show that the average pressure on the back of the thin wall builds up to roughly one-half the side-on pressure in time 6 h/U, where h is the height of the (two-dimensional) wall. The data in Vol II (Fig. E.3.4), show that the average pressure on the inside upper lip of the hollow block reaches ~~one-half-the~~ **inside** side-on pressure in a time which would correspond to

something between approximately 6 h/U and 15 h/U for the thin wall.

Thus, build-up time will be about 6 h/U. The pressure is expected to depend primarily on <u>inside</u> side-on pressure, and not on outside side-on pressure; hence, the data from the hollow block must be used - i.e., full inside side-on pressure, p_{σ_1}, is reached.

Changing h to $\bar{h}_{1f}$ to allow for openings in the wall, the pressure on the inside front wall is predicted to build up to p_{σ_1} in time 6 $\bar{h}_{1f}/U$; $\bar{h}_{1f}$ is computed by Eq. E.2.7 and p_{σ_1} is obtained by interpolation from Fig. E.5.4, Vol I. The time t^* required for the windows to break delays the beginning of pressure build-up on this surface; hence a time shift of t^* is added to the build-up time.

From Section E.2.2.1.6 the inside pressure builds up to outside side-on pressure at t = a/U. Therefore, at this time the pressure on the inside front wall should reach $f_{1s}(t)$, as given in Eq. E.1.1.

These predictions are summarized in Fig. E.2.7.

E.2.2.2.2   Pressure on Back Wall

The prediction of the average pressure on the <u>front</u> of the back wall, shown in Fig. E.2.8, show exactly the same sequence of events as those predicted for the front of the front wall. This is so because the back wall probably is not shielded at all by the front wall (as implied by the reinforcement of the inside shock to full outside shock strength discussed in Section E.1.2). Therefore,

Fig. E.2.8 shows the same loadings as Fig. E.2.6, except for changes to back wall "parameters" $\left[E_{1b} \text{ and } b_{1s}(t)\right]$ and except for the time shift, l/U, which is the time the shock front takes to reach the back wall.

Similarly, predictions for the <u>rear</u> of the back wall, shown in Fig. E.2.9, correspond to the sequence on the rear of the front wall (Fig. E.2.7). However, here $p_{\sigma 1}$ is not applicable; hence, the average pressure builds up directly to $b_{os}(t)$.

E.2.2.2.3 <u>Pressures</u> <u>on</u> <u>Roof</u>

<u>First bay front slope</u>: The <u>outside</u> pressure on this surface (shown in Fig. E.2.10) from time $t = 0$ to $t = l/U$ is computed by the methods of Section E.1.5 as given in Eq. E.1.5. It builds up linearly from zero overpressure at $t = 0$ to a modified reflected value at $t = l/U$. After time l/U, continued clearing effects cause the pressure on the front slope to decrease to pseudo steady state pressure. From data of reference 2 for a 10° gabled roof block, it is deduced that the pseudo-steady state is reached at about 2 l/U. After that time, the pressure follows the pseudo steady state curve for this surface, $r_{os}(t + \frac{l - l}{2U})$. (Note the appropriate time shift in the argument of r_{os}.) No alternative predictions for "maximum" and "minimum turbulence" effects are given because it is believed that vortex and turbulence effects are roughly the same on the outside and inside surface of the roof and would, to a large extent, cancel.
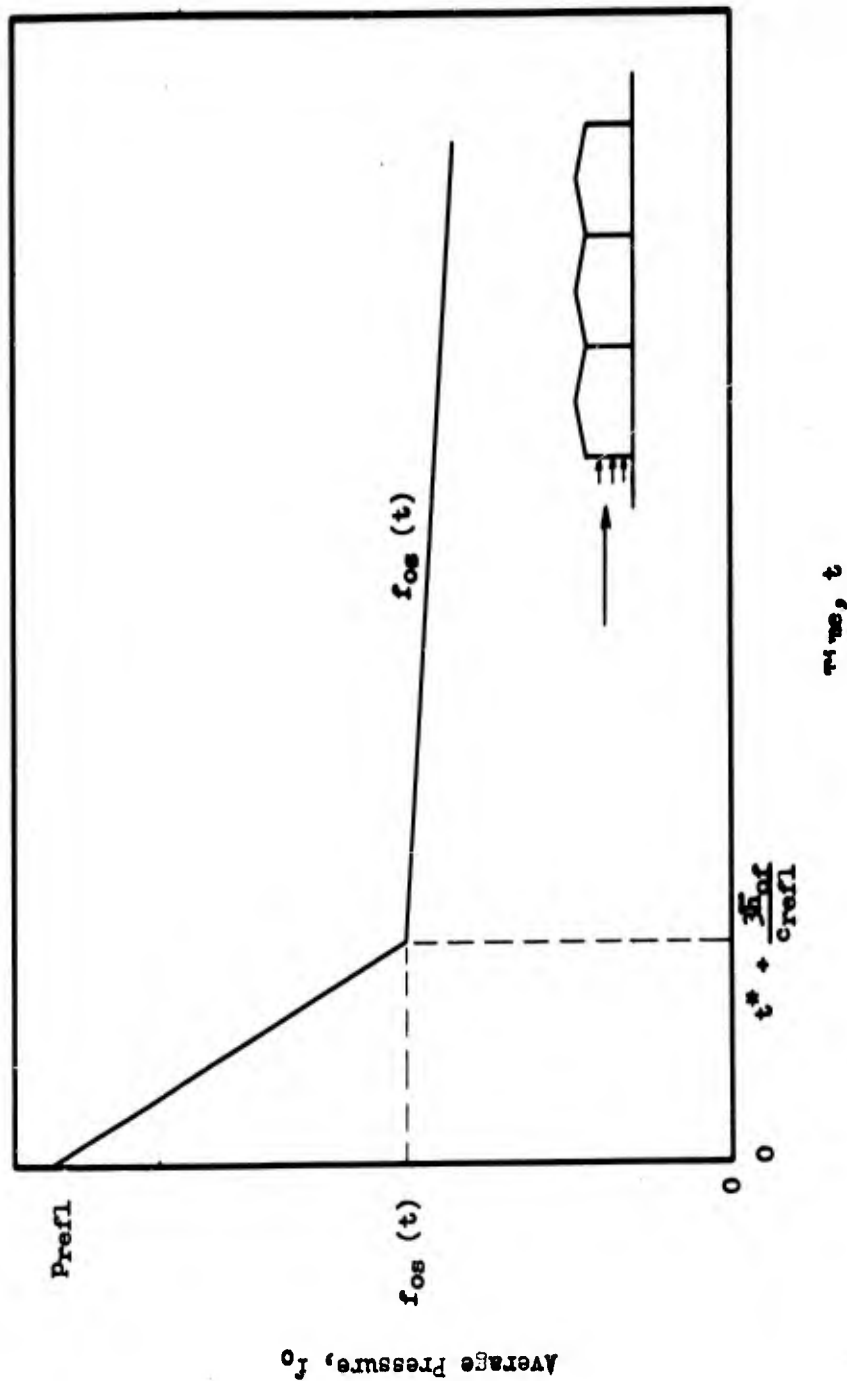
Fig. E.2.6   Predicted Average Pressure on Outside of Front Wall of
Buildings 3.3.3 and 3.3.8h
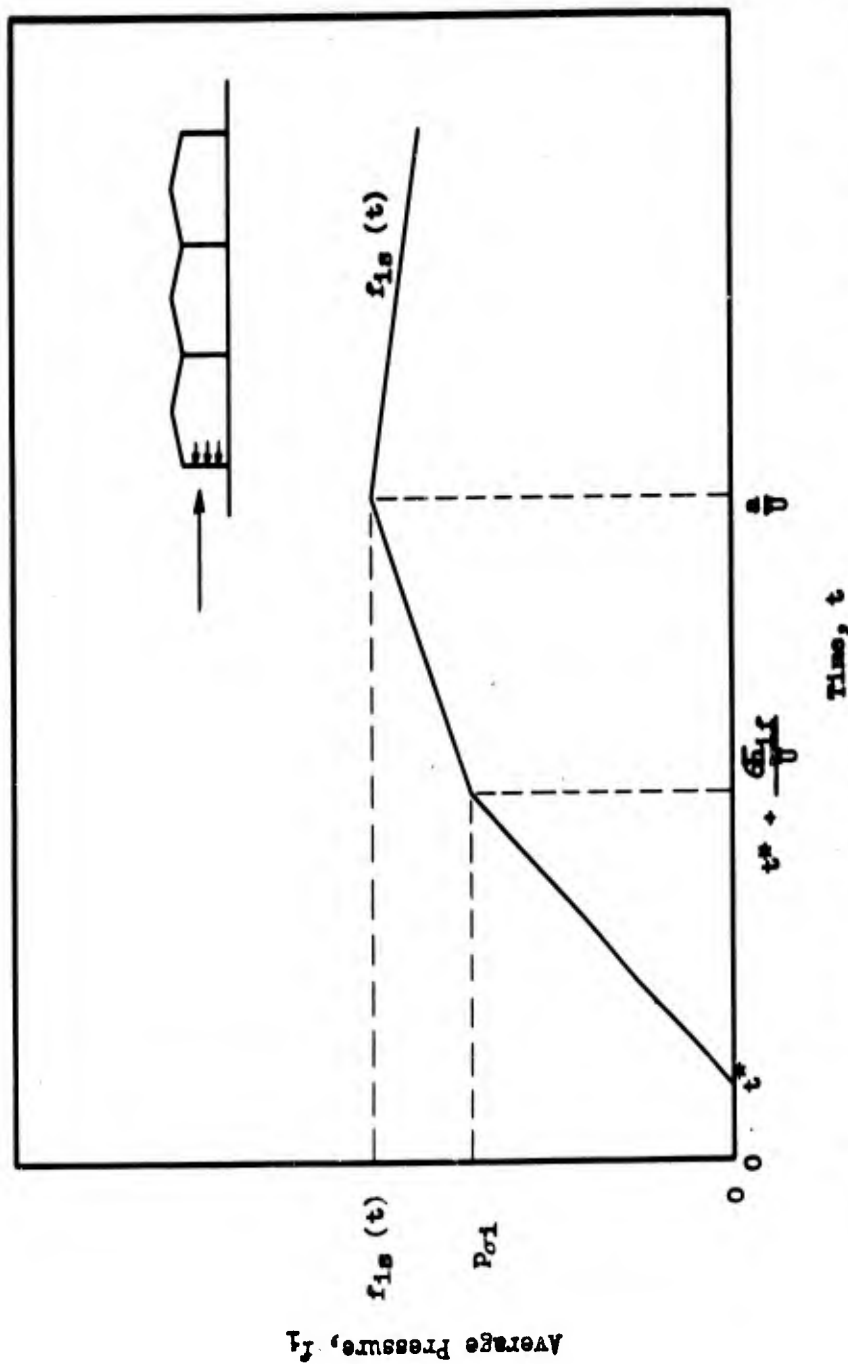
Fig. E.2.7 Predicted *Average* Pressure on Inside Front Wall of Building 3.3.3 and Building 3.3.6h
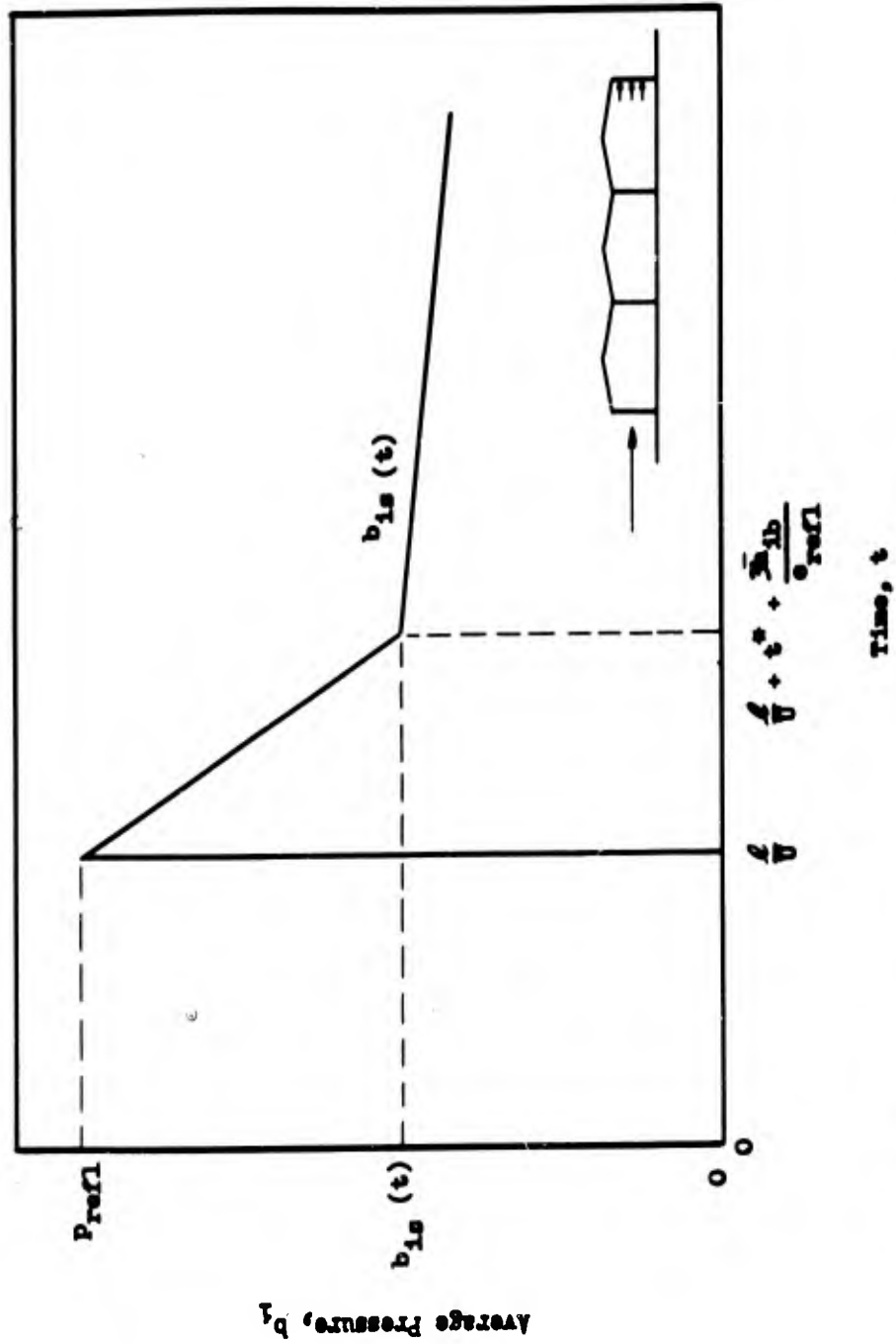
Fig. E.2.8   Predicted Average Pressures on Inside of Back Wall of
Buildings 3.3.3 and 3.3.8h
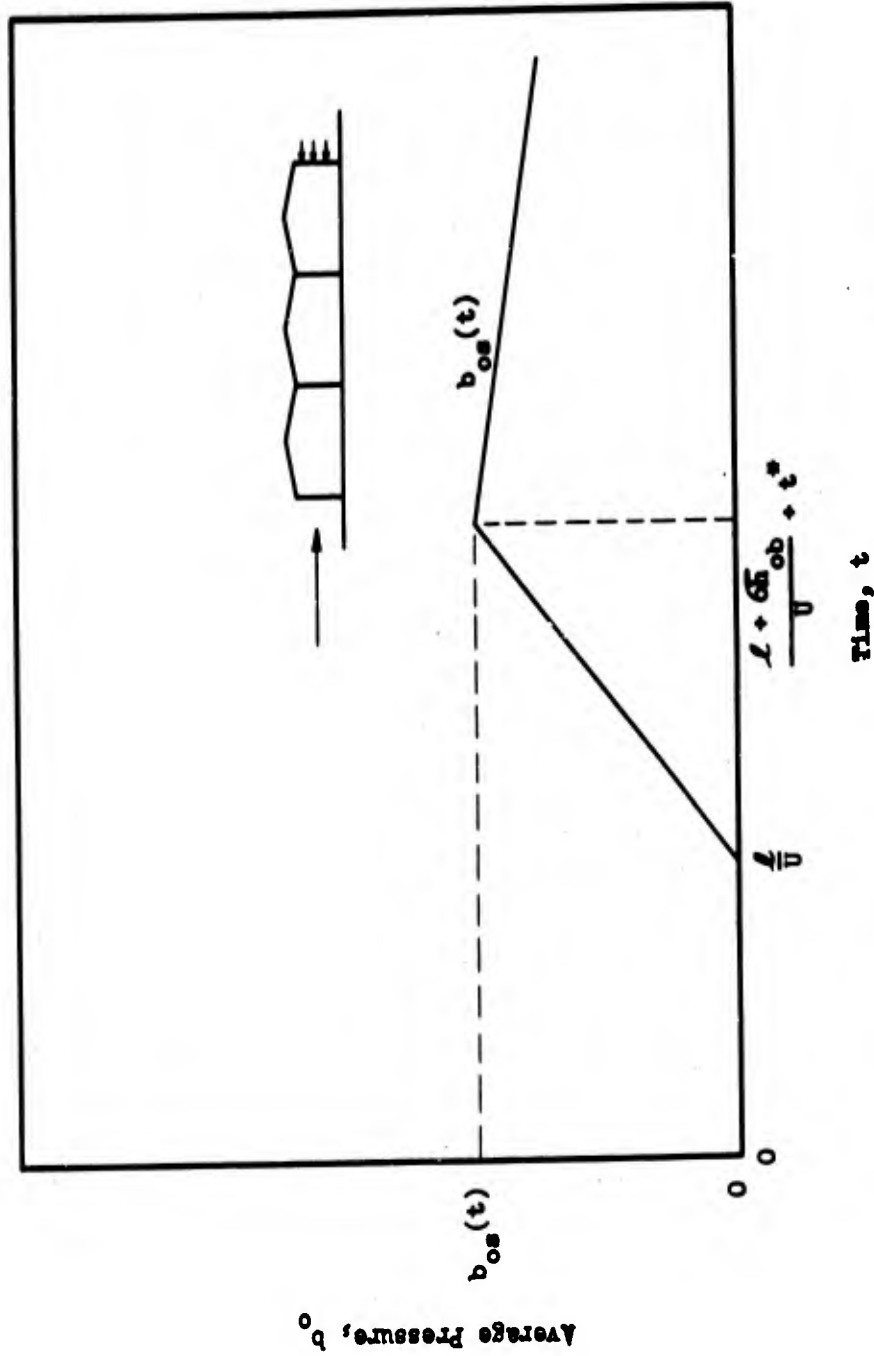
Fig. E.2.9   Predicted Average Pressure on Outside of Back Wall of
Buildings 3.3.3 and 3.3.8h

The _inside_ pressure on the first bay front slope is shown in Fig. E.2.11. The pressure build-up on the underside of the roof is delayed until $t = e/U + t^*$ to allow for the window-breaking time and the lag of the inside wave behind the outside wave at the roof due to the curved shape of the inside wave (see Eq. E.2.2, Section E.2.2.1). It builds up to ϵ times the pressure behind the inside shock in time $\frac{e + \bar{l}}{U} + t^*$ (i.e., when the inside wave covers the average length of the roof slope, $\bar{l}$). The factor ϵ allows for the reduction of inside roof pressure due to the purlin interference. The pressure behind the inside shock wave builds up linearly from $p_{\sigma\,i}$ at $t = t^*$ to $p_\sigma (0)$ at $t = a/U$ (i.e. when the shock front has swept across the first bay). The computation of α is discussed in Section E.2.2.1.5. Pressure behind the inside shock is discussed in Section E.2.2.1.6 and its value at $t = (e + \bar{l})/U + t^*$ is approximately equal to $0.7\, p_\sigma \left(t - \bar{l}/2U\right)$. ~~(t = $\bar{l}/2U$)~~. At $t^* + (e + 2\,\bar{l})/U$ the inside wave is full strength and full pseudo steady state pressure[2] is imposed, $r_{os}\left(t + \frac{\ell - \bar{l}}{2U}\right)$.

First bay rear roof slope: The pressure on the _outside_ of this slope (see Fig. E.2.12) builds up in a manner similar to the outside pressure on the front roof slope. No oblique reflection phenomena take place, however, as was the case on the front roof slope. The pressure builds up

---

[2] The quantity, $r_{os}(t)$, defined in Eq. E.1.3, is based on a time shift referred to the mid-length of the structure, $\ell/2$ from the front wall. The middle of the first bay front roof slope is $(\ell - \bar{\ell})/2$ forward of that line; hence, the time shift $(\ell - \bar{l})/2U$ is introduced in r_{os} to apply it to this slope.

linearly from zero at $t = (a - \mathcal{I})/U$ to pseudo steady state pressure for this surface, $r_{os} \left[t + (a + \mathcal{I})/2U \right]$, at $t = a/U$. The time shift,[3] $a - \mathcal{I}/U$, is imposed on all times pertaining to this surface to allow for the outside wave to reach the upstream edge of the surface.

The pressure variation on the <u>inside</u> of the first bay rear roof slope (see Fig. E.2.13) is similar to that on the inside of the front roof slope illustrated in Fig. E.2.11. In this case, however, the time lag of the inside shock front is $(t^{*} + e/U)$ *times* $(\mathcal{I}/a)$, computed from Eq. E.2.3, instead of $(t^{*} + e/U)$; further, the time shift $(a - \mathcal{I})/U$ is added to all times in obtaining the data for Fig. E.2.13, and the inside pressure has risen to $0.9\, p_{\sigma} \left[t - (2a - \mathcal{I})/2U \right]$ instead of the lower value used on the front roof slope.

<u>Second bay front roof slope:</u>
<u>The outside pressures on the</u> front roof slope of the second bay are shown in Fig. E.2.14. The wave striking this slope is assumed to be so weakened by the monitor of the first bay that reflection merely raises the pressure to pseudo steady state. Under this assumption the pressure on the outside of the front roof slope of the second bay is identical to that on the outside of the rear roof slope of the first bay shown in Fig. E.2.12. The pressure builds up linearly from zero at $t = a/U$ to pseudo steady state pressure for this surface $r_{os} \left[t + (a - \mathcal{I})/2U \right]$ at $t = (a + \mathcal{I})/U$ and follows the pseudo steady state curve from that time on. The time shift in this case equals a/U.

---

[3] The time shift, in effect, shifts zero time from the time that the outside wave strikes the front wall to the time that it reaches the leading edge of the structural member being studied.

The pressure build-up on the __inside__ of the second bay front roof slope is illustrated in Fig. E.2.15. The build-up is identical to that on the inside of the front and back roof slopes of the first bay, except that by the time the shock reaches this point, pressure behind the inside shock has become full outside side-on pressure, p_σ $(t - (2a + T)/2U)$, according to Section E.2.2.1.6. Again, the initial pressures are reduced by the factor α to allow for the purlin effect. There is no longer a lag between the inside and the outside waves, since the inside and outside wave fronts are assumed to coincide at the end of the first bay.

Second bay rear roof slope and third bay front roof slope: The pressures on these surfaces are not illustrated since they are assumed to be identical with those on the front roof slope of the second bay, except for a time shift. For the rear roof slope of the second bay the predictions of Figs. E.2.14 and E.2.15 are shifted by adding $(a - T)/U$ to all times; for the front roof slope of the third bay, a/U is added. There is one exception, however, the shifts must be subtracted from t in the expressions for r_{os}.

Third bay rear roof slope: The average pressures on the third bay rear roof slope are illustrated in Fig. E.2.16. The upper curve includes the purlin effect, but not the effect of the shock reflected from the rear wall.

The latter effect imposes an upward thrust on the roof and has been described in detail in Section E.2.2.1.3, Fig. E.2.5. The lower curve in Fig. E.2.16 shows these loads caused by the
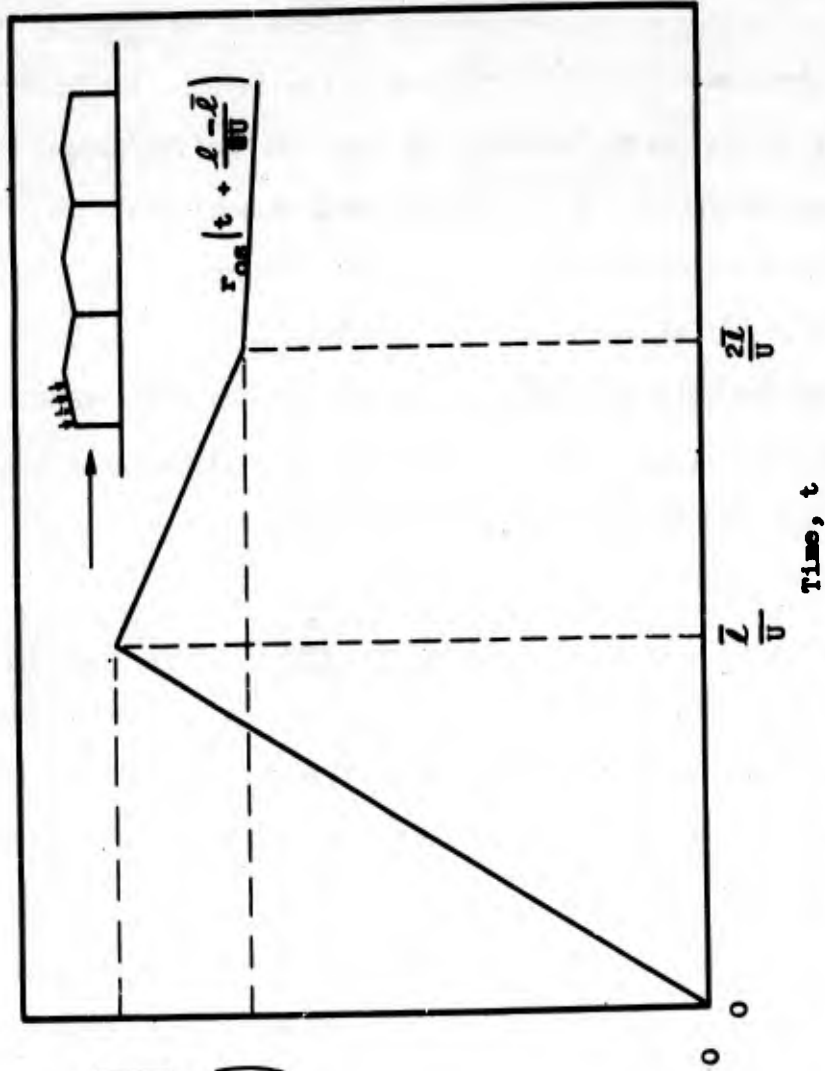
Fig. E.2.10   Predicted Average Pressures on Outside of First Bay Front Roof
Slope of Buildings 3.3.3 and 3.3.8h
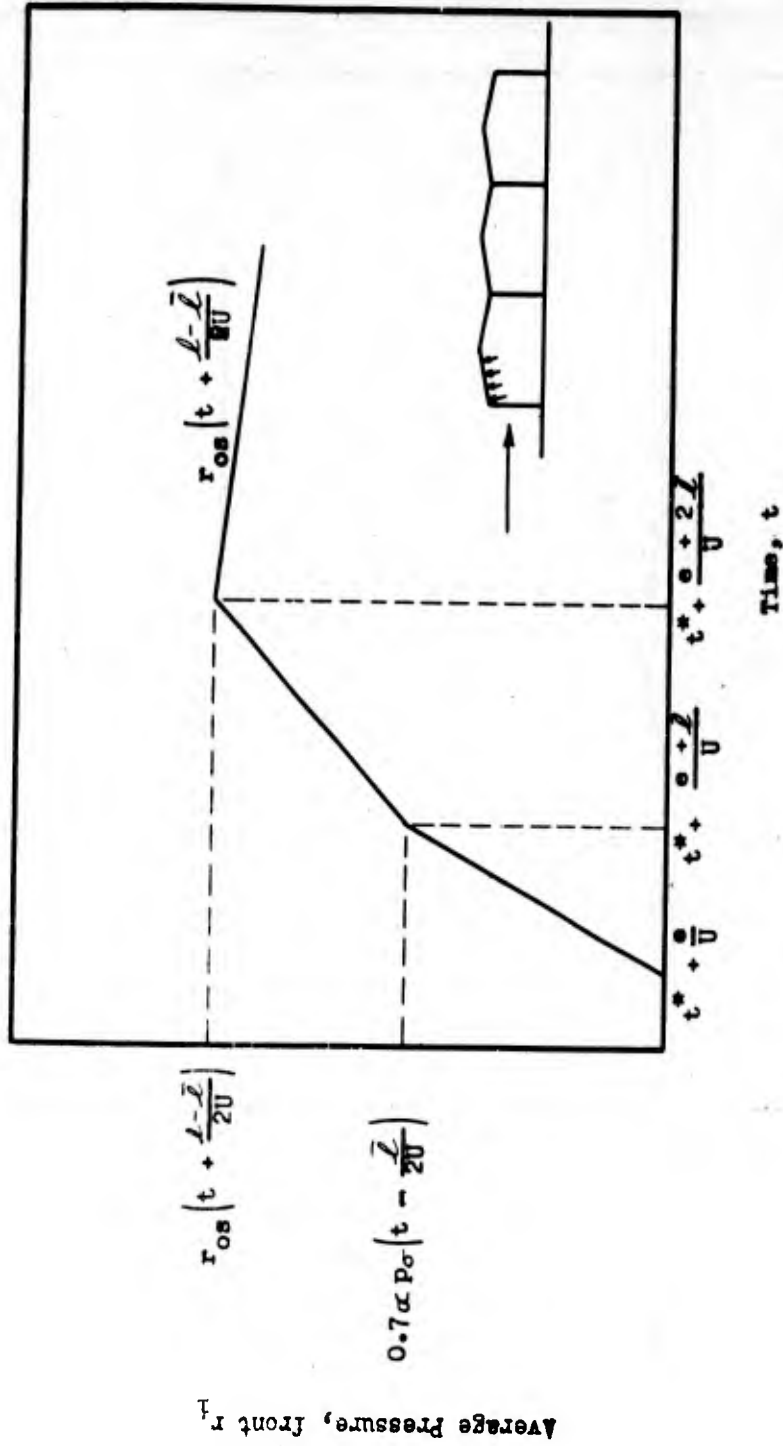
Fig. E.2.11   Predicted Average Pressure on Inside of First Bay Front
Roof Slope of Buildings 3.3.3 and 3.3.8h
(Note: $\alpha = 0.75$ for Building 3.3.3 and 0.85 for 3.3.8h)
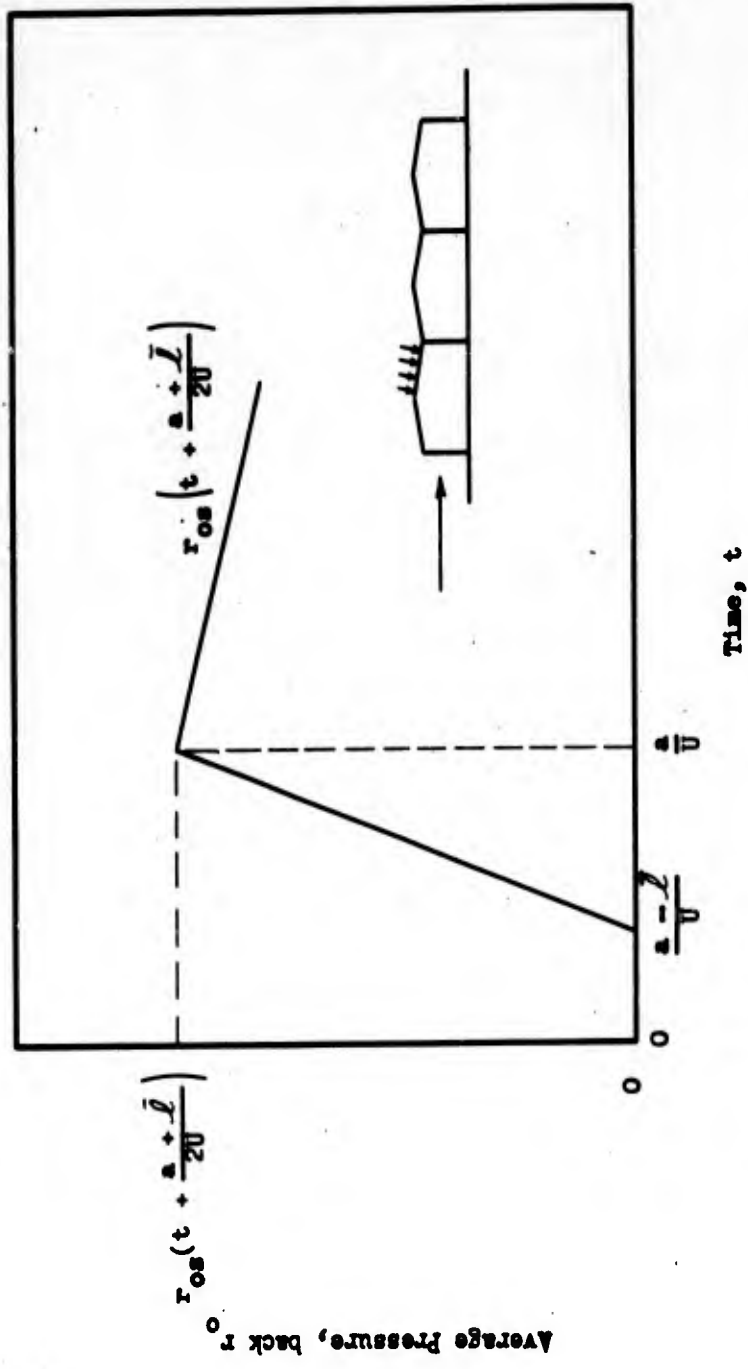
Fig. E.2.12   Predicted Average Pressure on Outside of First Bay Rear Roof Slope of Buildings 3.3.3 and 3.3.8h
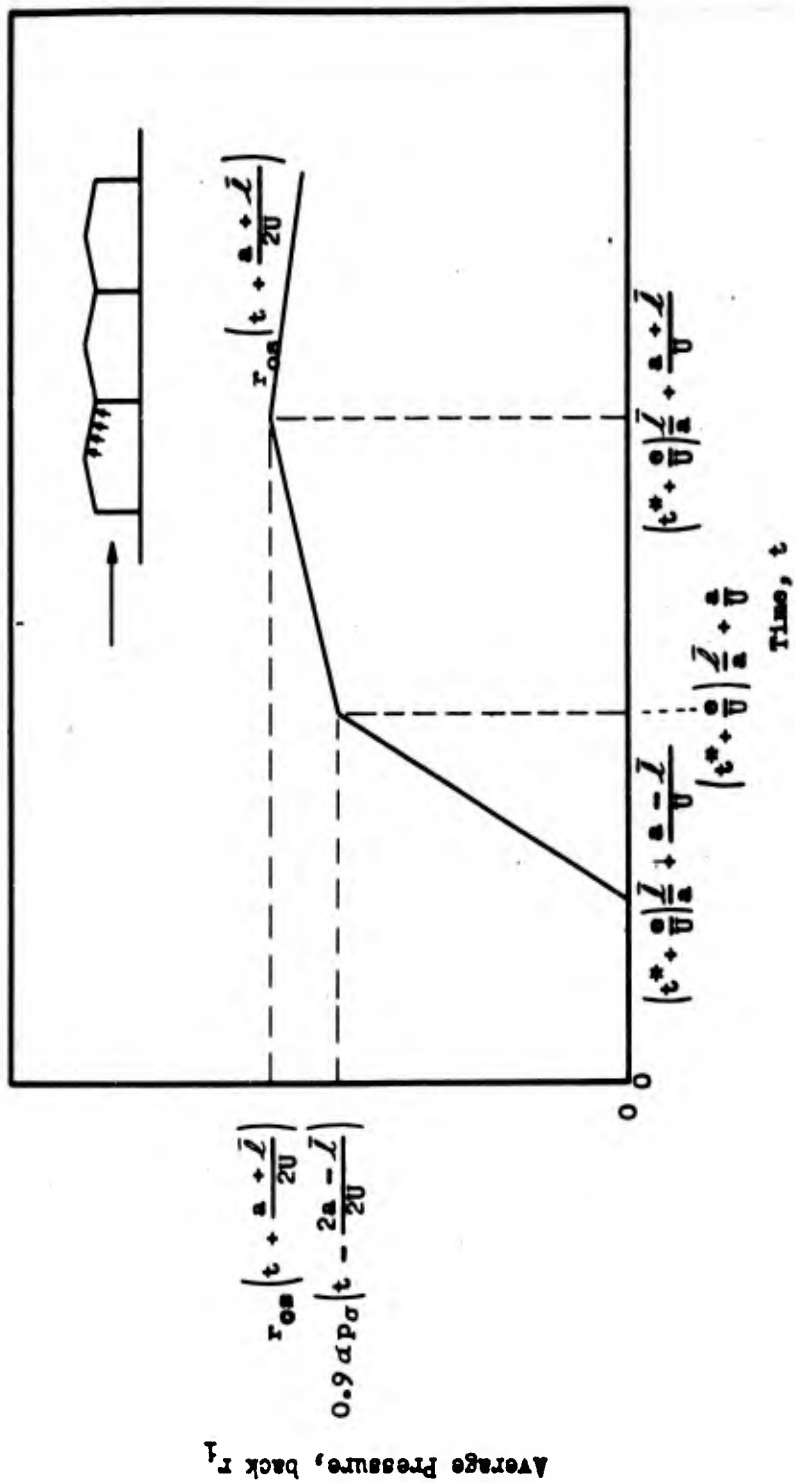
Fig. E.2.13   Predicted Average Pressure on Inside of First Bay Rear Roof
Slope of Buildings 3.3.3 and 3.3.8h
(Note: α = 0.75 for Building 3.3.3 and 0.85 for 3.3.8h)
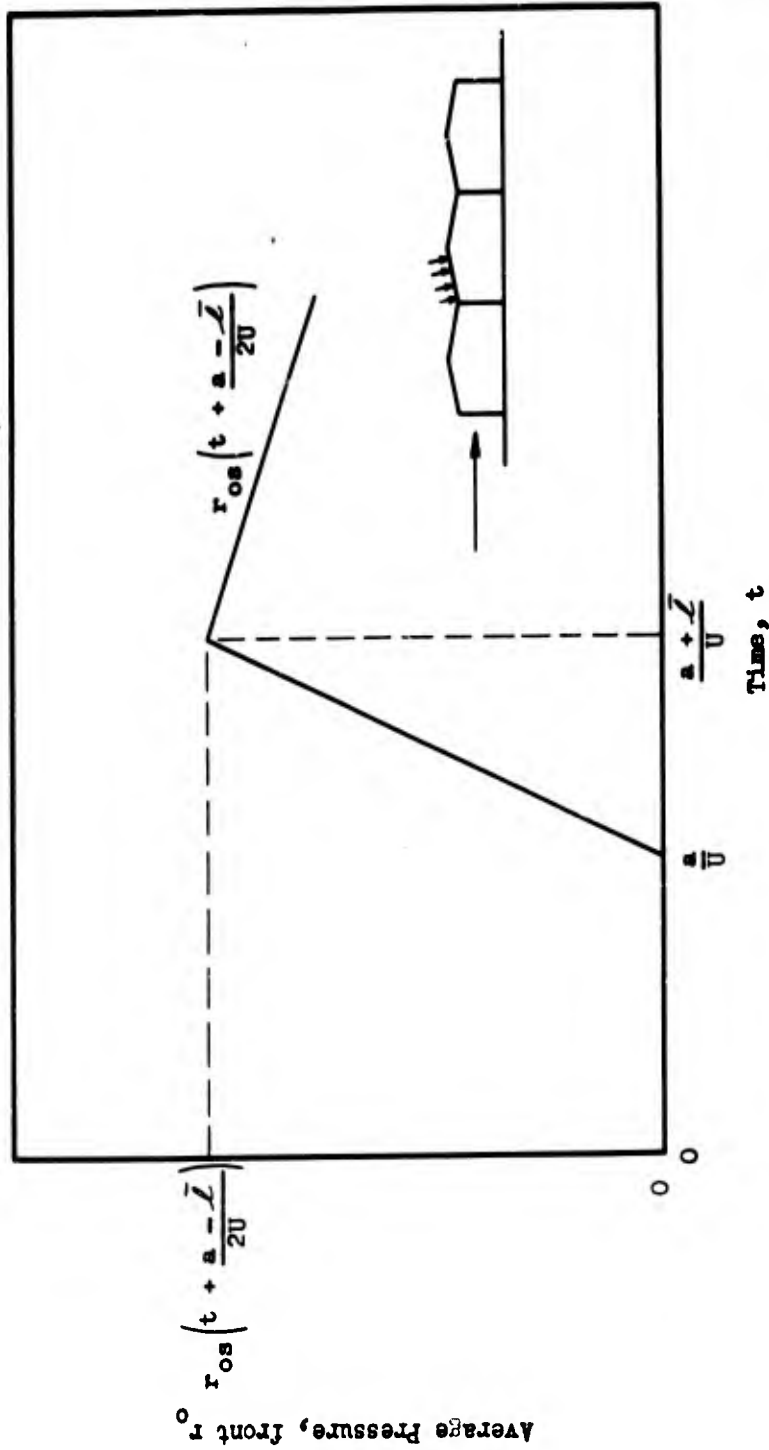
Fig. E.2.14   Predicted Average Pressure on Outside of Second Bay Front Roof
Slope of Buildings 3.3.3 and 3.3.8h
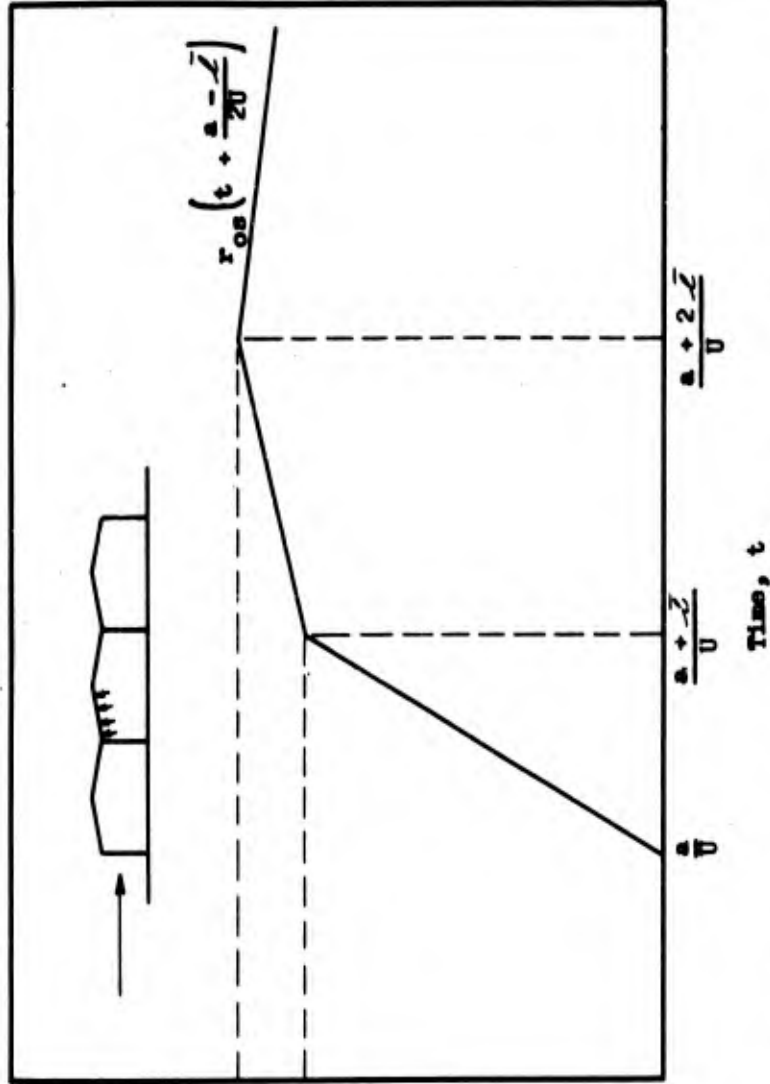
Fig. E.2.15   Predicted Average Pressures on Inside of Second Front Roof Bay
Slope of Buildings 3.3.3 and 3.3.8h
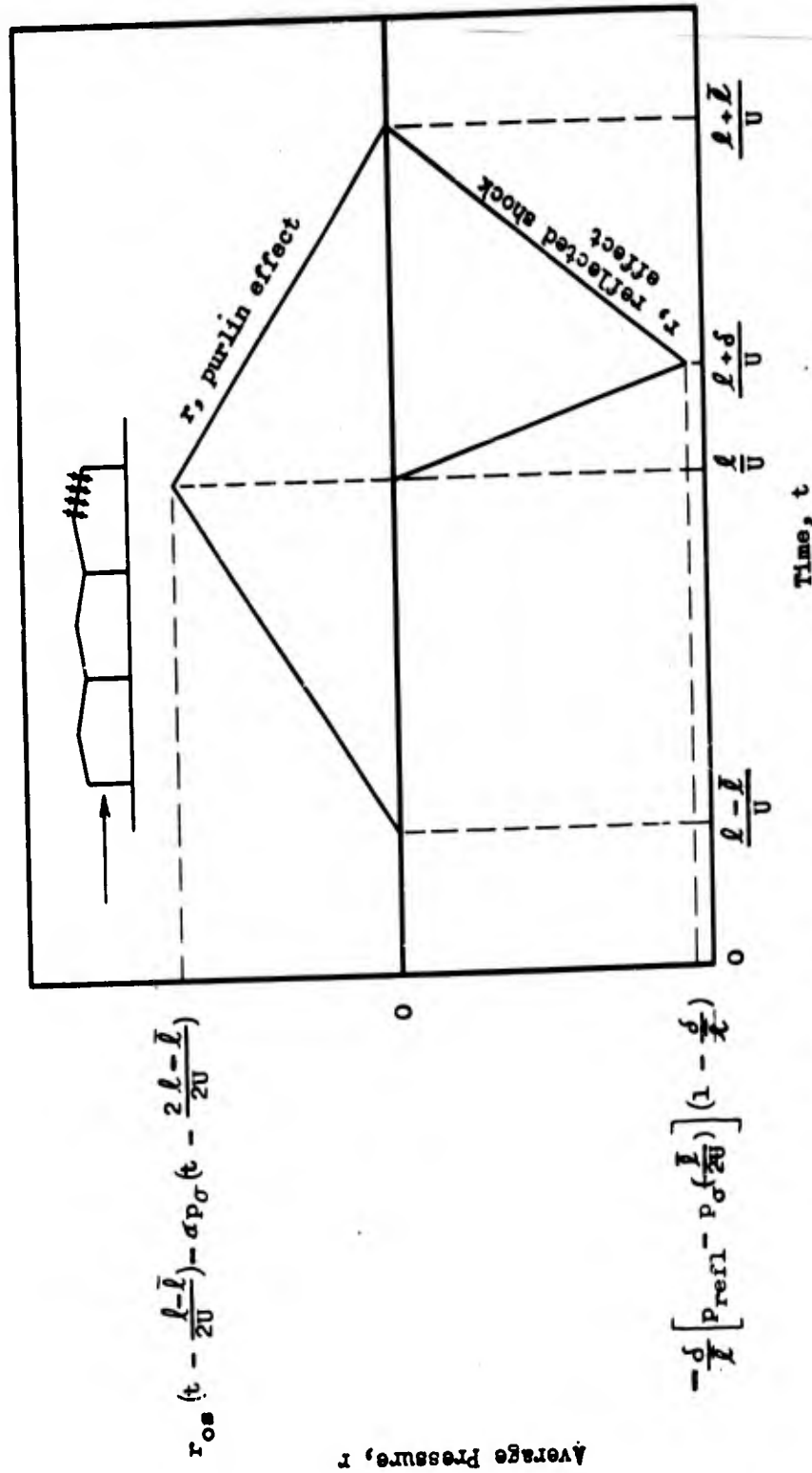
Fig. E.2.16 Predicted Average Pressures on Third Bay Rear Roof Section of Buildings 3.3.3 and 3.3.8h
(Note: $\alpha = 0.75$ for Building 3.3.3 and 0.85 for 3.3.8h)
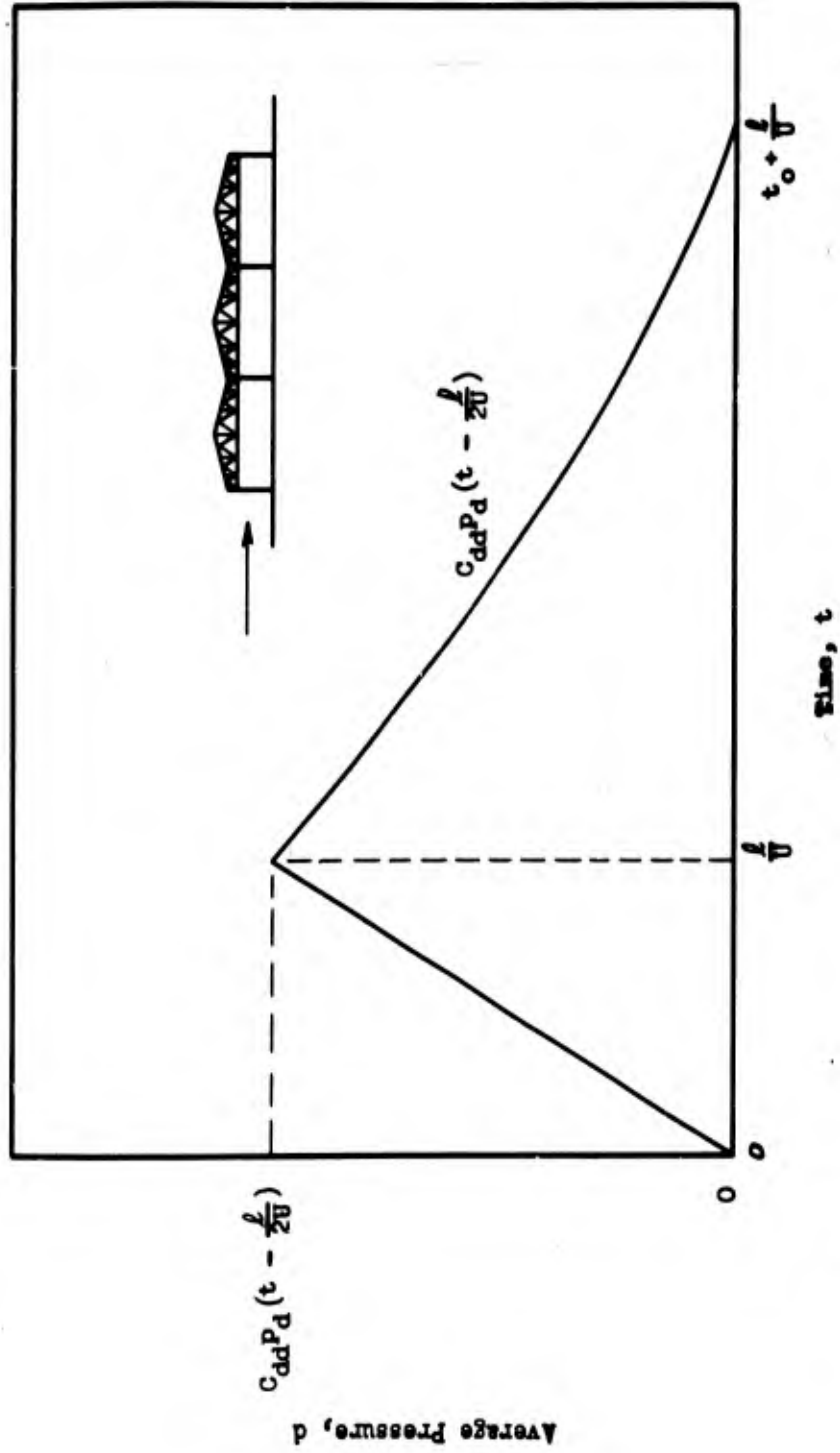
Fig. E.2.17 Predicted Average Pressure on Trusswork of Buildings 3.3.3 and 3.3.8h

reflected shock; the two curves must be added to give the net pressure on the roof slope.

The upper curve is the net pressure which would be felt by this surface if there were no back wall. It is equal to the net pressure on second bay front roof slope and is obtained by subtracting the pressures exhibited in Fig. E.2.15 from those on Fig. E.2.14 and adding the time shift, $\frac{2a - l}{U}$, to all times.

E.2.2.2.4 Pressures on Trusswork

The loading on the trusswork is shown in Fig. E.2.17. As pointed out in Section E.1.2, the pseudo steady state forces on the trusswork are mainly drag forces, since the small width and depth of the individual truss components lead to relatively small forces before drag is established on each member.

The projected area (see Section E.2.1) of the trusswork may be assumed to be linearly distributed along the length of the building with little risk of error and with considerable simplification in calculation.

The average pressure on the trusswork, $d(t)$, builds up linearly from zero at $t = 0$ to the steady state drag pressure $C_{dd}P_d(t - l/2U)$ at the time $t = l/U$ when the wave reaches the back wall. The pressure follows the steady state drag pressure curve from that time on until the tail of the wave has passed the entire trusswork at $t = t_o + l/U$, when it becomes zero.

E.2.3 NUMERICAL COMPUTATION OF LOADING

E.2.3.1 Loadings on Total Structure

The calculation of forces and average pressures on building 3.3.3 is based on the computational methods developed in Section E.2.2. The results from that section which are needed in the numerical computation of loading are repeated in Tables E.2.2, E.2.4, E.2.6, E.2.8, E.2.10, and E.2.16 in the columns labeled "Symbolic". These data are also presented schematically in Figs. E.2.6 through E.2.17.

The side-on pressure and drag pressure throughout the 3.4-psi shock wave which strikes the structure are plotted in Fig. E.2.18. These were computed from Vol I, Eq. E.4.16, and Fig. E.4.3, respectively.

The numerical values of all other quantities necessary for computation of loadings on individual components and on the total structure are given in Table E.2.1 and are grouped into three sections: shock constants, geometric constants, and combined geometric and shock constants.

The shock constants are various numerical values which are independent of the geometry of the building. Among these are the following specified numbers: shock strength, ξ ; duration of the wave, t_o; and atmospheric pressure, P_o. Under the same heading certain important derived quantities are listed, including the velocity of the shock front, U; the reflected pressure, p_{refl}; and the velocity of sound in the reflected region, c_{refl}. (See Fig. E.4.2, Vol I.)

The geometric constants necessary for the computation of loadings on the structure include the following: the total length of the structure, l ; the bay length, a ; the "equivalent length" of a front or back slope, $\bar{l}$; the distance from the center of an upper window in the front wall to the roof, e ; the mean relief distances, $\bar{h}_{of}$, on the outside of the front wall and $\bar{h}_{ib}$ on the inside of the back wall; the mean build-up distances, $\bar{h}_{if}$ on the inside of the front wall and $\bar{h}_{ob}$ on the outside of the back wall; the areas A_f, A_b, A_r of the front wall, back wall and roof, respectively; the total projected area of the trusswork, A_d, including purlins, struts, monitor members, exposed columns, etc.; the ratio of window and door area to the gross area of the front or back wall, Ω; and the roof slope angle, θ. The quantities $\bar{h}_{of}$, $\bar{h}_{ib}$, $\bar{h}_{if}$ and $\bar{h}_{ob}$ are computed as described in Section E.2.2.1.7; $\bar{l}$ and A_d are computed as described in Section E.2.1.

The combined geometric and shock constants are certain characteristic time units which underlie the calculations, such as $\bar{l}/U$, a/U, $(\bar{h}_{if})/U$, etc.; the inside shock overpressure, $p_{\sigma 1}$, computed from the equation $p_{\sigma 1} = P_0(\xi_1 - 1)$ where ξ_1 is read by interpolation from Fig. E.5.4 Vol I; the drag coefficients on the outside and inside of the front wall, C_{fo} and C_{fi}, and on the outside and inside of the back wall, C_{bo} and C_{bi}; the drag coefficients on the front and back slopes of the roof, "front C_{ro}", and "back C_{ro}", all obtained from Section E.1.3.2; and an average drag coefficient on the trusswork, C_{dd} from Section E.2.2.1.4. These drag coefficients are used to compute the

pseudo steady state pressures f_{os}, f_{is}, etc. and the series of quantities "front r_{os}" and "back r_{os}" from Eqs. E.1.1-E.1.3. From Section E.1.5 the instantaneous reflected pressure on the oblique roof, $p_{obl\ refl}$ (Fig. E.1.7), and the factor, $K(\theta)$, needed for loading computations on the sloped roofs (Fig. E.1.6), are listed. In addition there is given the constant α obtained from Section E.2.2.1.5, the "length" of the wave reflected from the back wall, δ, obtained from Eq. E.2.9, and t^*, the window-breaking time, obtained from Part II, Section E.8.1.

Tables E.2.2-E.2.16 give the average pressures and forces on the 3.3.3 structure for the front wall, back wall, roof and trusswork, computed on the basis of the geometric constants and shock quantities listed in Table E.2.1.

In the left-hand columns of Tables E.2.2, E.2.4, E.2.6, E.2.8, E.2.10 and E.2.16, under the heading "Symbolic", are listed the discrete values of time at which pressures are computed. These symbolic values were deduced in Section E.2.2.2 (See Figs. E.2.6-E.2.17) and are listed up to such times when wind forces alone constitute the net force on a particular component. In some instances these wind forces are predicted to be equal to zero. In the right-hand columns of this group of tables, the numerical values of the average pressures on the front wall, back wall, roof and trusswork are shown.

The remaining tables give the numerical values of the net pressure differences and forces until the end of the positive phase. Where intermediate points between those shown on the first group of tables are needed, linear interpolation has been used. Once the forces acting on
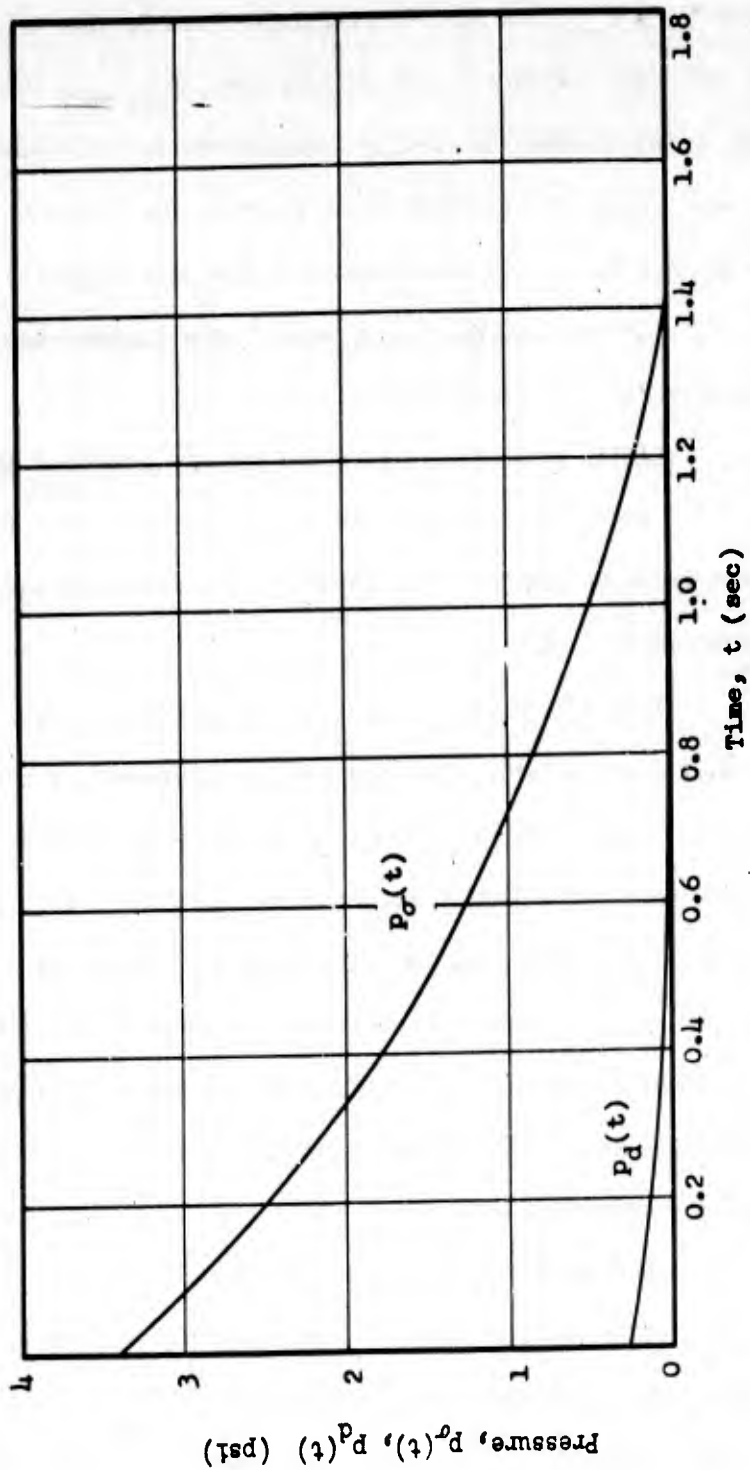
Fig. E.2.18 Side-on Pressure and Drag Pressure for Building 3.3.3 for $p_\sigma(0) = 3.4$ psi

each member become purely wind forces, only the net average pressure differences (total drag coefficient times p_d) are computed. For the front wall the total drag coefficient, C_{df}, $= C_{fo} - C_{fi} = 1$, whereas for the back wall $C_{db} = C_{bo} - C_{bi} = -1$.

The superscripts "-" and "+", shown on certain values of time, indicate that at that time the pressure (and force) undergoes a sudden change. An asterisk at a certain value of time in some tables indicates that until that time force-time relations are considered to be linear, after which they follow a smooth curve through the given points.

Tables E.2.2 to E.2.5 give the average pressures on both sides of front and back wall, as well as the net average pressures and forces on these walls. Their symbolic columns were deduced from Figs. E.2.6 to E.2.9.

Tables E.2.6 to E.2.14 give the pressures and forces on each slope of all three bays of the saw-tooth roof. The fourth and fifth roof sections have the same loading as the third, except for appropriate time displacements, and only the net pressures are listed. Until the wave reflects from the rear wall, the loading on the sixth section (next to the rear wall) will also be the same, but the reflected wave causes an upward thrust on this roof section, which is given in terms of net pressures. The symbolic notations for these tables come from Fig. E.2.5, and Figs. E.2.10 to E.2.16.

Table E.2.15 lists the total force on the roof, together with the horizontal and vertical roof forces, obtained from the total force by proper superposition (i.e. with due regard for the upstream or downstream

direction of the force components given in Tables E.2.6 to E.2.14).

Table E.2.16 shows the pressures and forces on the entire trusswork deduced from Fig. E.2.17. These are exclusively drag forces, since the diffraction forces were shown to be negligible.

The results computed in Tables E.2.2 to E.2.16 during the early periods are shown in Figs. E.2.19 to E.2.25. Figures E.2.19 and E.2.20, depicting loading on the front wall, are based upon data from Tables E.2.2 and E.2.3, while Figs. E.2.21 and E.2.22, illustrating the back wall loading, are associated with Tables E.2.4 and E.2.5.

Figure E.2.23 summarizes the roof loadings from Tables E.2.6 to E.2.14, and Fig. E.2.24, showing horizontal and vertical roof forces, illustrates Table E.2.15.

Figure E.2.25 is based upon Tables E.2.15 and E.2.16. It illustrates the force on the trusswork and the combined force obtained by superposing this trusswork force on the horizontal component of the roof force of Fig. E.2.24.

As discussed more fully in Section E.1.1, the calculated forces are only approximate. Slide rule calculations were used throughout these computations and in each result listed, the third figure has no significance.

E.2.3.2   Component Computations

Monitor windows: The loading on a windowpane (20 1/2 in. by 14 1/2 in.) located at the top outside edge of the monitor is computed in this section. An outside upper pane is chosen since an upper bound on the breaking of all monitor glass is desired. The panes at the
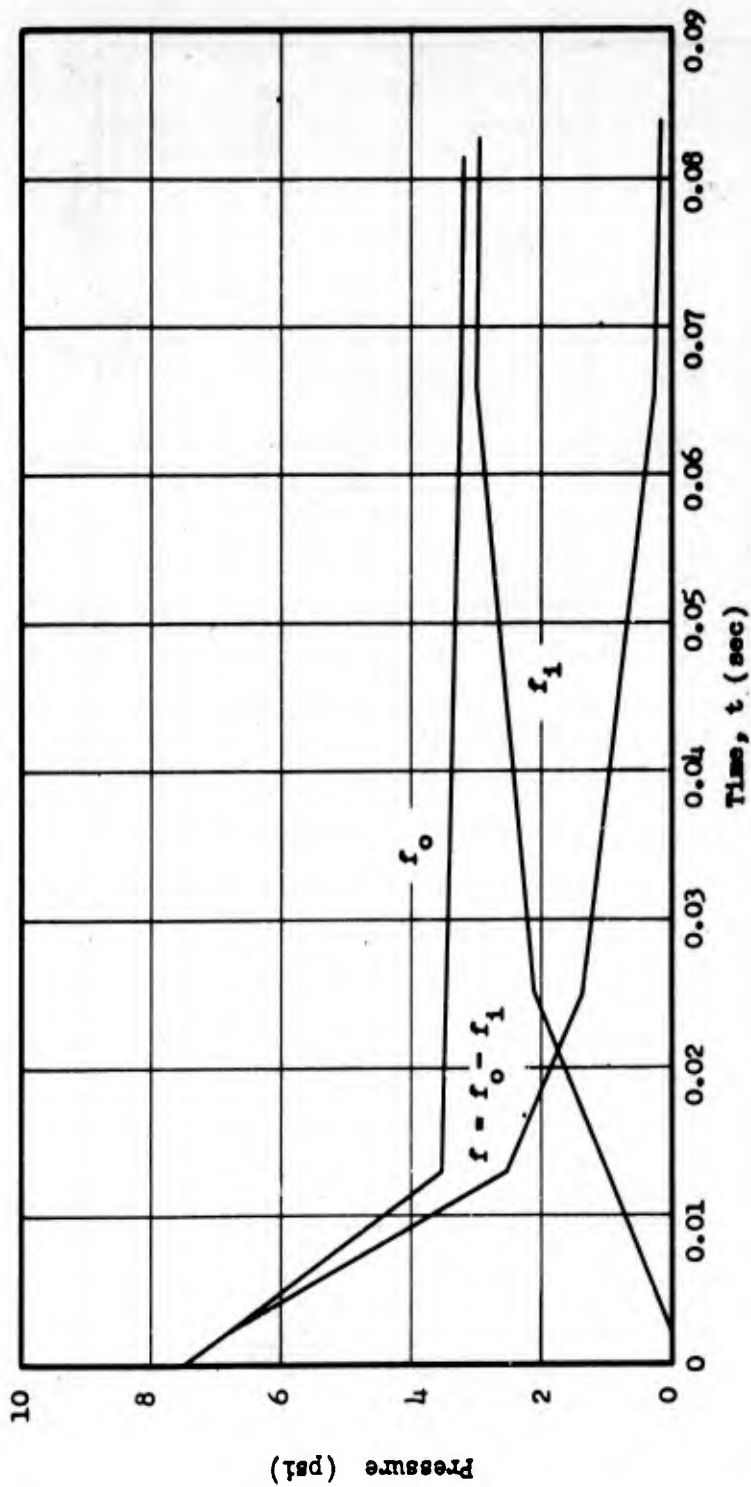
Fig. E.2.19   Pressures on Front Wall of Building 3.3.3
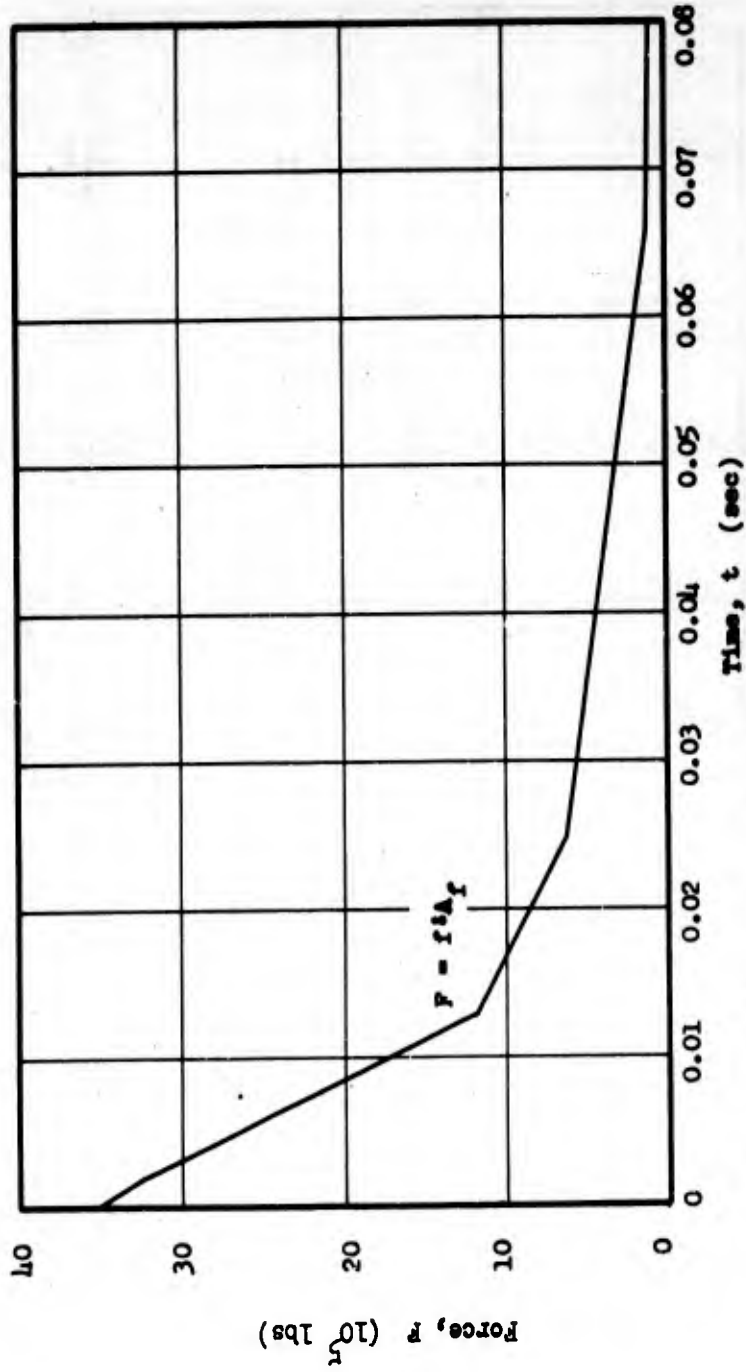
Fig. E.2.20 Force on Front Wall of Building 3.3.3
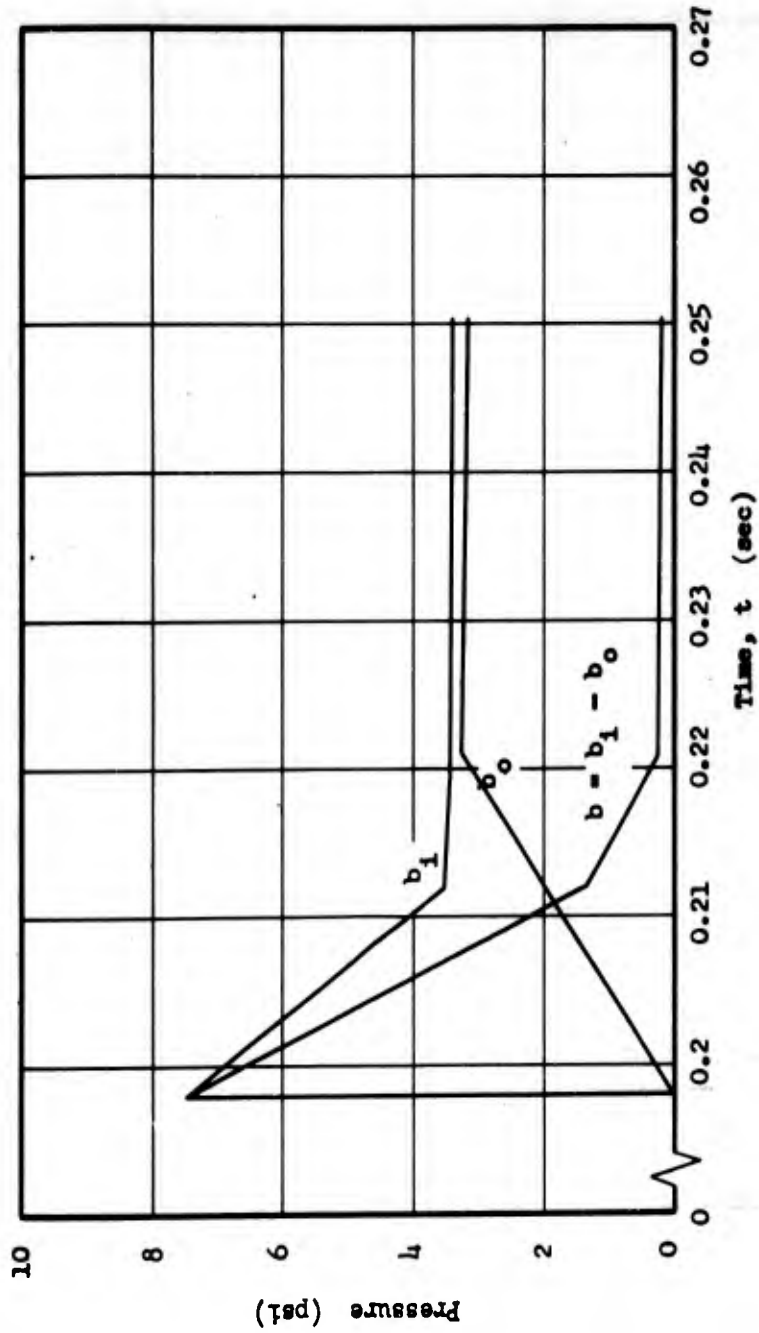
Fig. E.2.21 Pressures on Back Wall of Building 3.3.3
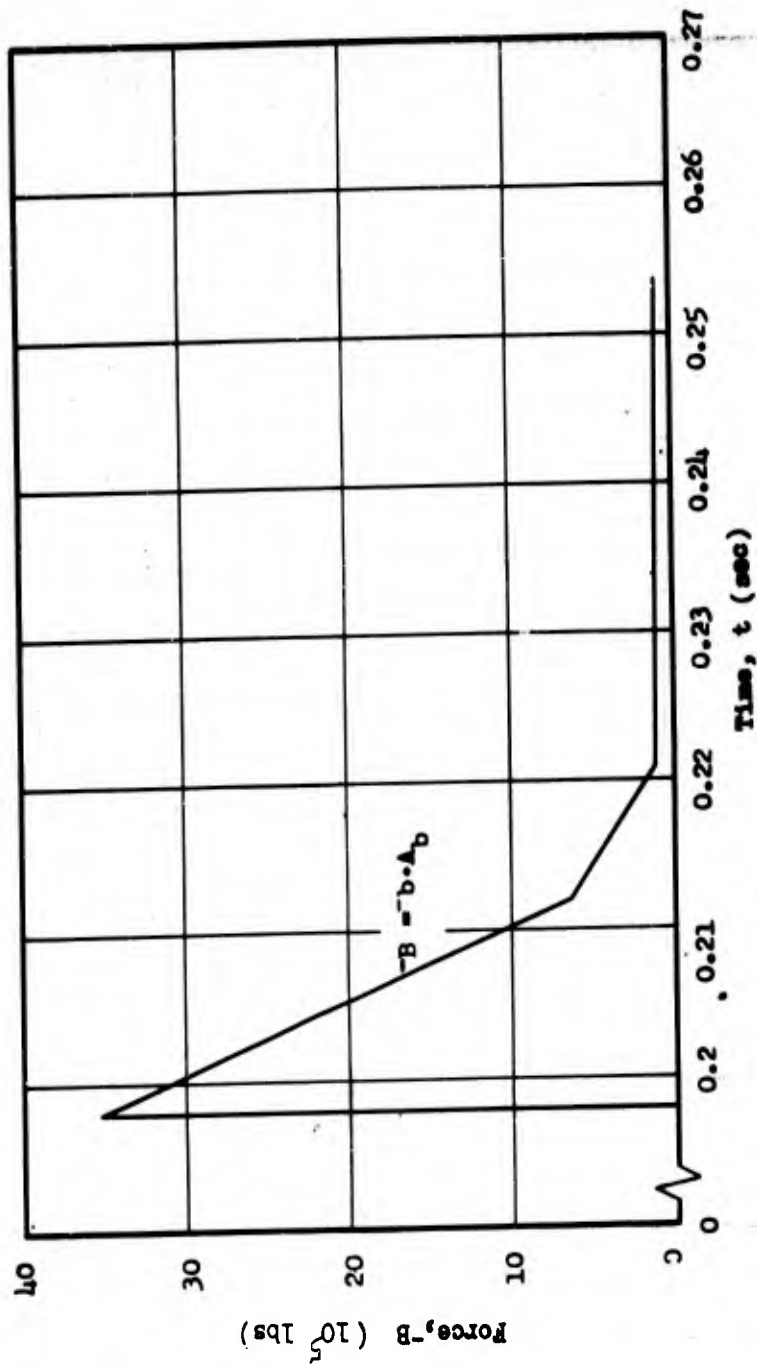
Fig. E.2.22 — Forces on Back Wall of Building 3.3.3
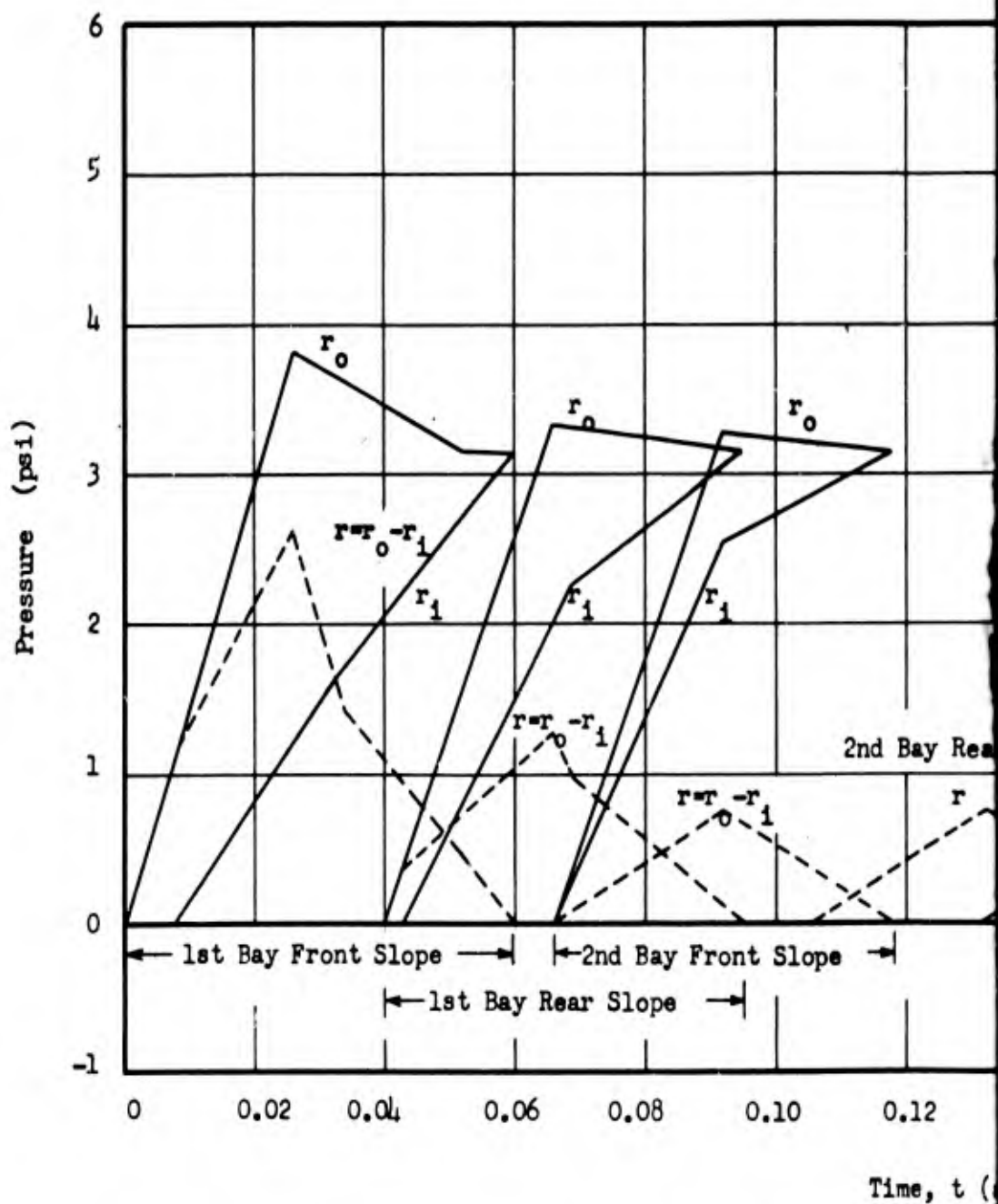
Fig. E.2.23   Pressures on Roo

r_o

2nd Bay Rear Slope   3rd Bay Front Slope

$-r_1$ r r r 3rd Bay Rear Slope

nt Slope

0.10   0.12   0.14   0.16   0.18   0.20   0.22   0.24   0.26

Time, t (sec)
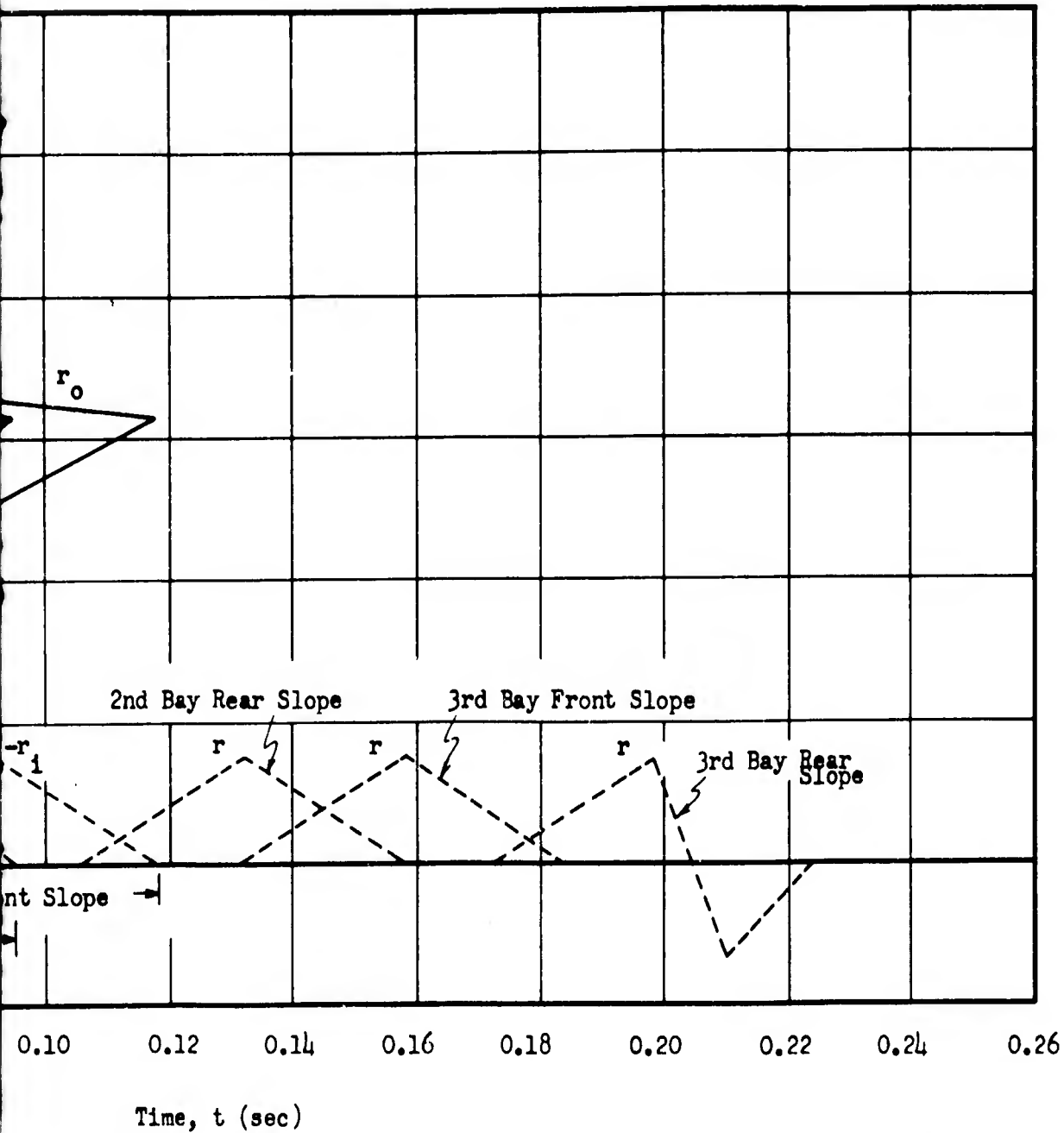
Pressures on Roof Slopes of Building 3.3.3

−114−

2
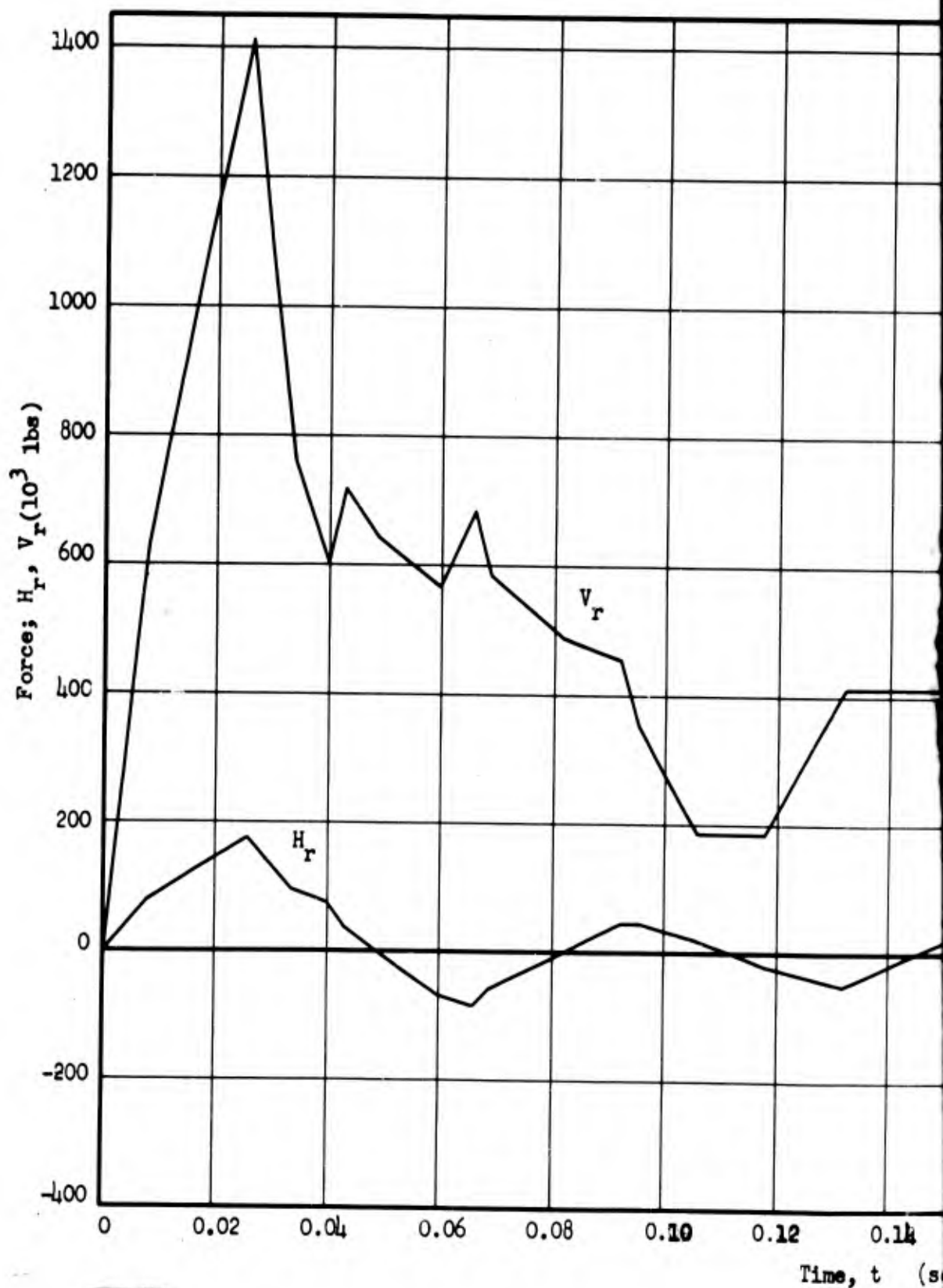
Fig. E.2.24   Horizontal and Vertical F
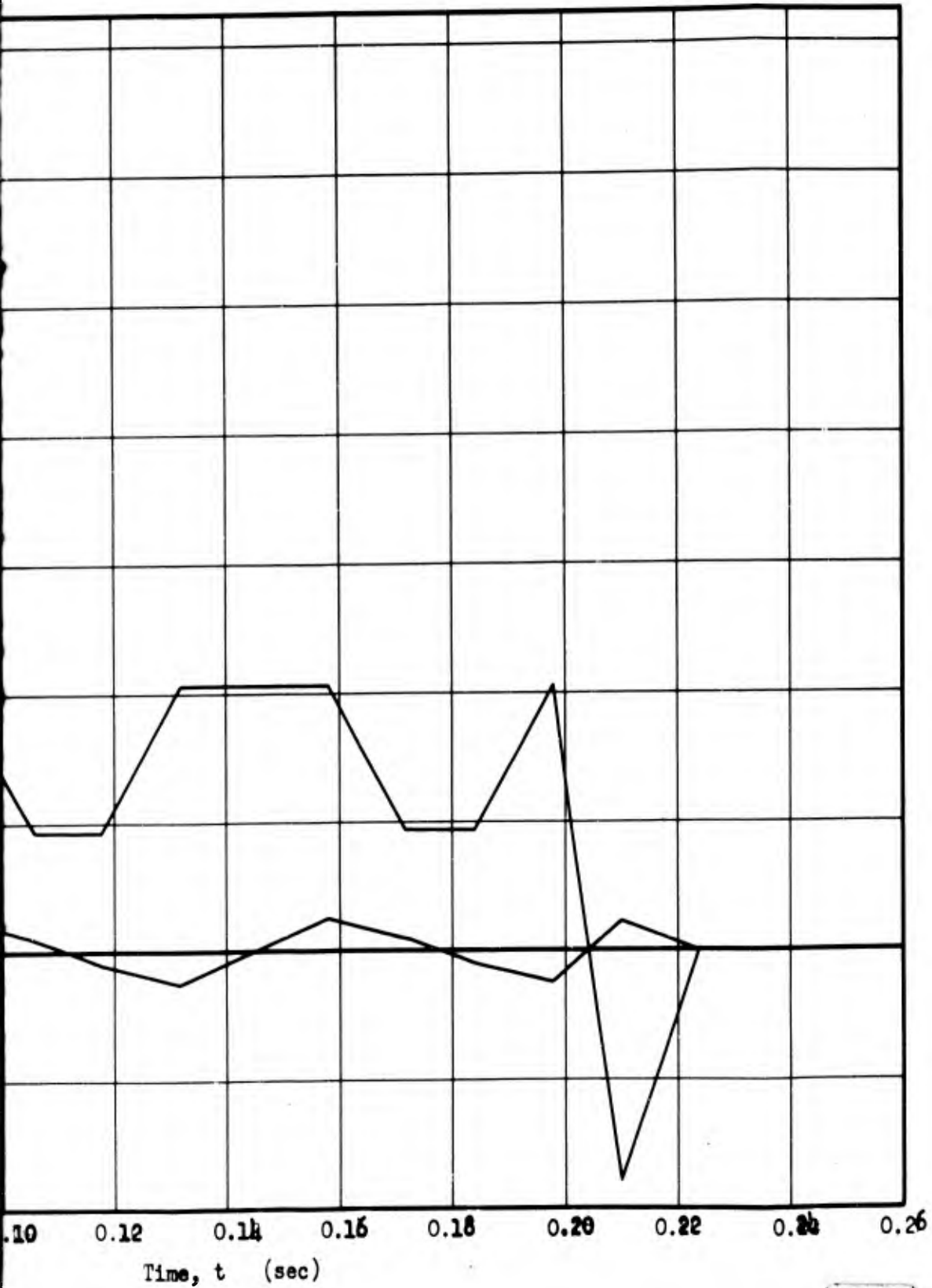
Time, t (sec)

orizontal and Vertical Forces on Roof of Building 3.3.3

-115-

2
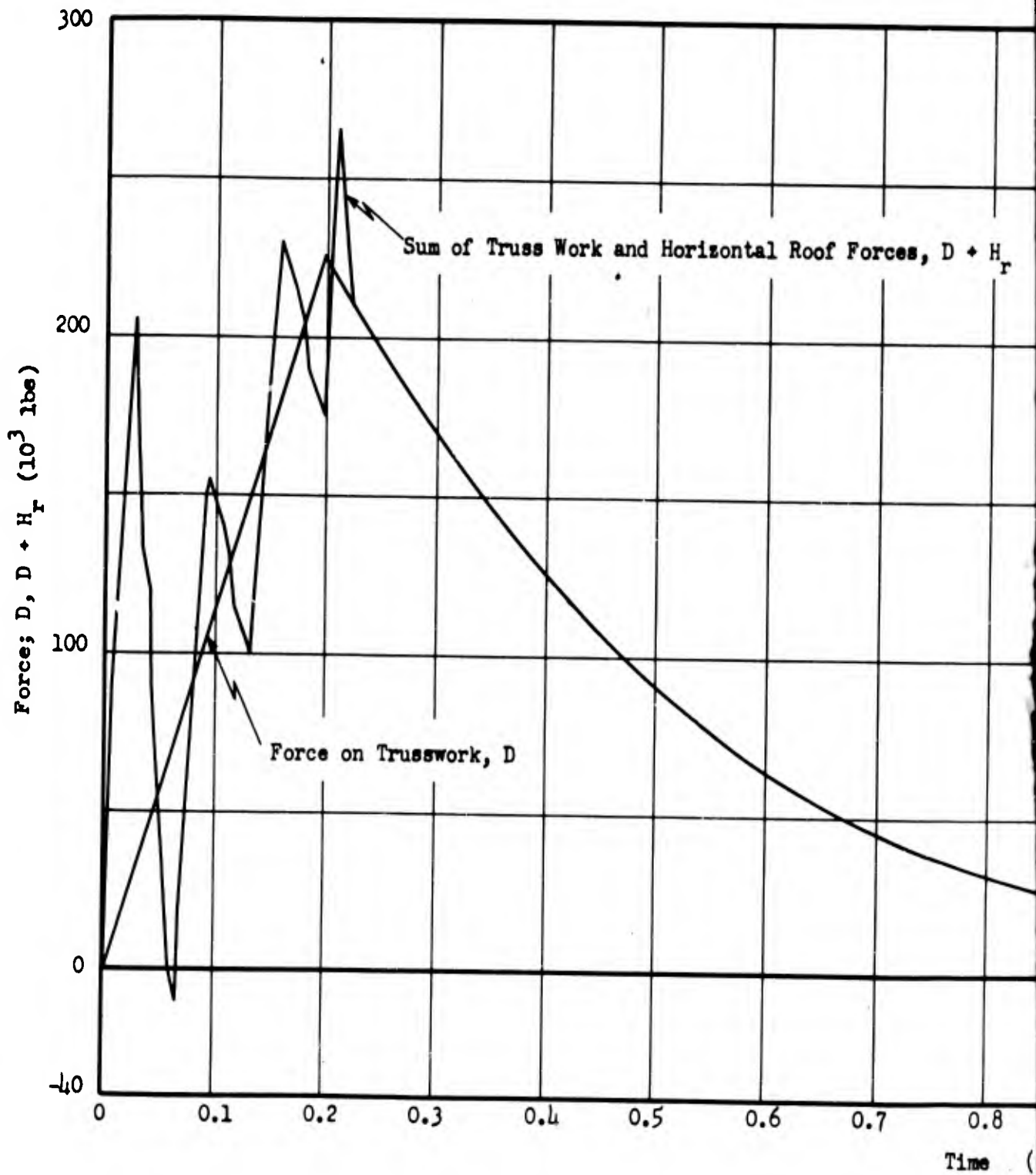
Fig. E.2.25   Force on Trusswork and Sum of Trusswork
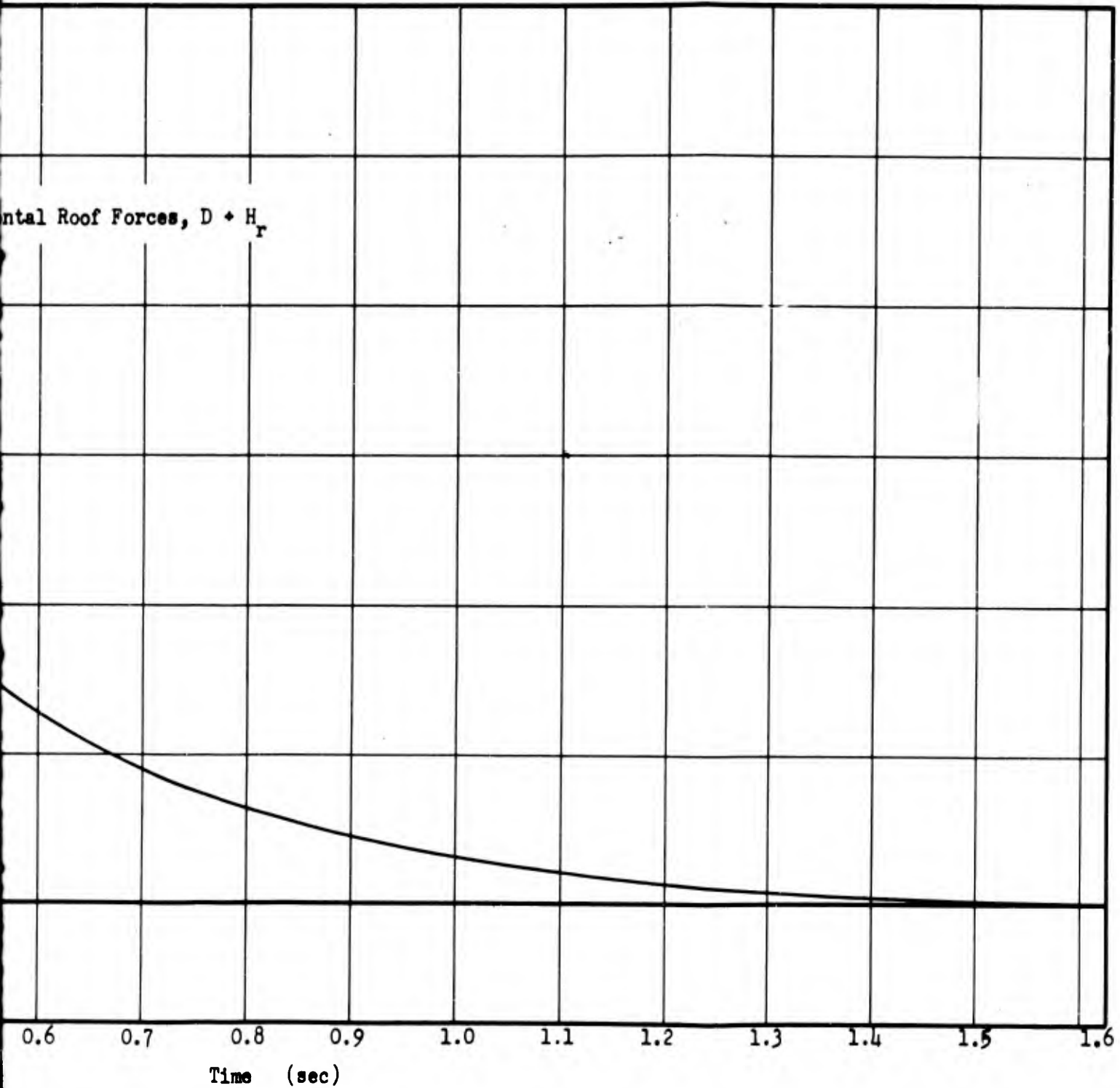
ntal Roof Forces, D + H$_r$

Time   (sec)

sswork and Sum of Trusswork and Horizontal Roof Forces on Building 3.3.3

chosen position will be cleared from reflected pressure faster than any other window panes and hence should be the slowest to break.

The computational method essentially follows the outline in Fig. E.5.25 of Vol I. At time, $\tau = 0$, the shock front ($p_o = 3.4$ psi) strikes the pane, raising the pressure instantaneously from atmospheric pressure ($f_o = 0$) to reflected pressure ($f_o = p_{refl} = 7.45$ psi from Table E.2.1).

As a lower bound for the clearing time, $\frac{20 \text{ in.}}{c_{refl}} = \frac{20}{(12)(1185)} = 0.00146$ sec is chosen. This is believed shorter than the shortest time in which the pressure could drop to pseudo steady state pressure, $f_o = f_{os} = 3.56$ psi.

After this time the pressure follows the pseudo steady state curve until the end of the positive phase ($\tau = t_o = 1.42$ sec), at which time it reaches zero.

Table E.2.17 gives the loading-time relation in terms of average pressures and forces until the window breaks, unless inside pressures reach the back of the pane before this time.[4]

A plank of the first bay front roof slope: The roofing of building 3.3.3 consists of 2-in. roofing planks parallel to the direction of flow (perpendicular to the front wall). The planks are supported by

---

[4] Results of Part II, Section E.8.1 indicate that the window breaking time, $t^* \approx 0.002$ sec, and hence the loadings of Table E.2.17 are permissible for this pane. This derived window breaking time applied to the other monitors is also of the correct magnitude for the majority of the panes.

purlins spaced approximately 6 1/2 ft apart. The loading on one plank of the roof located 20 ft from the front wall and at the center of the roof will be determined here and will be used in Part II to analyze the roof for failure. If this board does not fail, then the entire front slope of the roof is assumed to stand, since the loading on this plank is expected to be (on the average) more severe than on the rest of the front slope.

From Section E.2.2.1, Eq. E.2.2, the lag between the inside and outside waves at the chosen roof plank is Δ (20) = 6.5 ft, and the associated lag time is Δ (20)/U = 0.0053 sec.

The pressure on the outside of the plank is assumed to build up linearly from zero at τ = 0 to oblique reflected pressure minus drag pressure, 4.61 psi - 0.30 psi = 4.31 psi (obtained from Table E.2.1 and Fig. E.2.18) at $\tau = l_{plank}/U$ = 0.0053 sec. The location of the plank in the center of the roof permits this plank to be treated almost as a two-dimensional problem (i.e. relief from reflected pressure takes place relatively slowly since the plank is located quite far from either edge of the building); therefore high pressures would exist for a considerable period on the outside of this plank. Only the variation of net pressure is considered from time $\tau = l_{plank}/U$ on.

The inside pressure, computed as outlined in Section E.2.2.1.6, builds up linearly from $p_{\sigma i}$ = 2.13 psi at x = 0 to p_{σ} = 3.55 psi at x = 40 ft; hence at x = 20 ft the inside pressure is 2.84 psi. The inside pressure acting on the roof is this pressure minus "front C_{ro}" times the drag pressure, or 2.84 psi - 0.19 psi = 2.65 psi.

The net pressure on the roof is therefore taken to build up from zero at τ = 0 to 4.31 psi at τ = 0.0053 sec, and then to de-

ARMOUR RESEARCH FOUNDATION OF ILLINOIS INSTITUTE OF TECHNOLOGY

crease linearly to 4.31 psi - 2.65 psi = 1.66 psi at $\tau = \left[\ell_{plank} + \Delta(20)\right]/U =$
0.0106 sec. At the time both inside and outside waves have reached the
end of the first bay, 0.060 sec, the pressure has dropped linearly to zero.

The following, Table E.2.18, summarizes the net average
pressures on the roof plank.

Table E.2.18

Net Average Pressures on Roof Plank Twenty Feet from Front Wall of
Building 3.3.3

Time, t (sec)	Pressure, (psi)
0	0
0.0053	4.31
0.0106	1.66
0.06	0

Planking in third bay rear roof slope: The wave re-
flected from the inside back wall of building 3.3.3 creates a relatively
high pressure on the inside of the third rear roof slope (see Section
E.1.2). Two planks parallel to the flow in this section of the roof
(each 6.5 ft long with the downstream ends 1 ft and 13 ft from the back
wall, respectively) are analyzed.

The reflection of the inside shock wave from the back
wall and the resultant net pressures on the roof near the back wall have
been discussed in Section E.2.2.1.3 (Eq. E.2.6) and a symbolic method has

been developed.

Substituting the values of the required constants for building 3.3.4 conditions (i.e., $p_{refl} = 7.45$ psi, $p_o(\frac{l}{20}) = 3.18$ psi, $\delta = 14.5$ ft) into Eq. E.2.6, the net pressures listed in Tables E.2.19 and E.2.20 are obtained using the symbolic expressions of Fig. E.2.6. In addition to this pressure, there is a net pressure on each plank before it is completely engulfed by the reflected wave; this effect is due to the difference in pressure between the inside and outside waves. This pressure difference is of the order of 0.75 psi and opposes the net pressure difference due to the reflected wave. However, because of the uncertainty of this effect, only the more severe loading[5] is considered, i.e. that due to the difference in pressure between the outside wave and the reflected wave.

---

[5] Response computations of Section E.8.5.1, Part II show that the planks do not break under the more severe loading.

TABLE E.2.1

Constants for Building 3.3.3

Shock Constants	
$p_o(o)$ = 3.4 psi	c_{refl} = 1185 fps
U = 1220 fps	P_o = 14.7 psi
ξ = 1.23	t_o = 1.42 sec
P_{refl} = 7.45 psi	

Geometric Constants	
l = 240 ft	A_f = 0.473 x 10^6 sq in
a = 80 ft	A_b = A_f
$\mathcal{I}$ = 31.3 ft	A_r = 3.25 x 10^6 sq in
ℓ = 7 ft	A_d = 1.123 x 10^6 sq in
$\bar{h}_{of}$ = 4.3 ft	Ω = 0.28
$\bar{h}_{1f}$ = 4.7 ft	θ = 7°
$\bar{h}_{1b}$ = 4.7 ft	
$\bar{h}_{ob}$ = 4.3 ft	

TABLE E.2.1 (CONTD)

Constants for Building 3.3.3

Combined Geometric and Shock Constants	
$\dfrac{l}{U} = 0.198$ sec	$P_{o1} = 2.1$ psi
$\dfrac{a}{U} = 0.066$ sec	$\xi_1 = 1.14$
$\dfrac{\bar{l}}{U} = 0.026$ sec	$c_{fo} = c_{bi} = \dfrac{2}{3}$
$\dfrac{e}{U} = 0.006$ sec	$c_{fi} = c_{bo} = -\dfrac{1}{3}$
$\dfrac{\bar{h}_{of}}{l_{refl}} = 0.0038$ sec	$c_{df} = 1$
	$c_{db} = -1$
$\dfrac{\bar{h}_{1f}}{U} = 0.0038$ sec	front $c_{ro} = -0.30$
$\dfrac{\bar{h}_{1b}}{l_{refl}} = 0.004$ sec	back $c_{ro} = -0.30$
	$P_{obl\ refl} = 4.28$ psi
	$K(\theta) = 0.4$
$\dfrac{\bar{h}_{ob}}{U} = 0.0035$ sec	$t^* = 0.002$ sec
$\delta = 14.5$ ft	

TABLE E.2.2.

Average Pressures on Front Wall of Building 3.3.3

Outside			
Symbolic		Numerical	
Time, t	Pressure, f_o	Time, t (sec)	Pressure, f_o (psi)
0	P_{refl}	0	7.45
$\frac{3H_{of}}{c_{refl}} + t*$	$f_{os}(t)$	0.013	3.5
a/U	$f_{os}(t)$	0.066	3.22

Inside			
Symbolic		Numerical	
Time, t	Pressure, f_1	Time, t (sec)	Pressure, f_1 (psi)
0	0	0	0
$t*$	0	0.002	0
$\frac{6H_{1r}}{U} + t*$	P_{s1}	0.025	2.1
$\frac{a}{U}$	$f_{1s}(t)$	0.066	2.97

TABLE E.2.3

Net Average Pressures and Forces on Front Wall
of Building 3.3.3

Time, t (sec)	Pressure			Force
	f_o (psi)	f_1 (psi)	$f = f_o - f_1$ (psi)	$F = f A_f$ (lb×10³)
0	7.45	0	7.45	3520
0.002	6.80	0	6.80	3220
0.013	3.5	1.00	2.50	1180
0.025	3.45	2.10	1.35	638
* 0.066	3.22	2.97	0.25	118
0.1			0.20	95
0.2			0.15	71
0.4			0.08	38
0.6			0.04	19
0.8			0.02	9.5
1.0			0.01	4.7
1.2			~	~
1.42			0	0

TABLE E.2.4

Average Pressures on Back Wall of Building 3.3.3

Inside

Symbolic		Numerical	
Time, t	Pressure, b_i	Time, t (sec)	Pressure, b_i (psi)
0	0	0	0
$\left(\frac{t}{U}\right)^-$	0	$0.198-$	0
$\left(\frac{t}{U}\right)^+$	P_{refl}	$0.198+$	7.45
$\frac{t}{U} + \frac{3\sqrt{L_{lb}}}{z_{refl}} + t*$	$b_{1s}(t)$	0.212	3.50
$\frac{L}{U} + \frac{6L_{ob}}{U} + t*$	$b_{1s}(t)$	0.221	3.46

Outside

Symbolic		Numerical	
Time, t	Pressure, b_o	Time, t (sec)	Pressure, b_o (psi)
0	0	0	0
$\frac{t}{U}$	0	0.198	0
$\frac{L}{U} + \frac{6L_{ob}}{U} + t*$	$b_{os}(t)$	0.221	3.23

TABLE E.2.5

Net Average Pressures and Forces on Back Wall
of Building 3.3.3

Time, t (sec)	Pressure			Force
	b_1 (psi)	b_0 (psi)	$-b = b_1 - b_0$ (psi)	$-B = -bA_b$ (lbx10)
0	0	0	0	0
0.198-	0	0	0	0
0.198+	7.45	0	7.45	3520
0.212	3.50	2.15	1.35	638
* 0.221	3.46	3.23	0.23	109
0.4			0.15	71
0.6			0.08	38
0.8			0.04	19
1.0			0.02	9.5
1.2			0.01	4.7
1.4			~	~
1.62			0	0

TABLE E.2.6

Average Pressures on First Bay Front Roof Slope of Building 3.3.3

Outside

Symbolic		Numerical	
Time, t	Pressure, r_o	Time, t (sec)	Pressure, r_o (psi)
0	0	0	0
$\dfrac{Z}{U}$	$p_\sigma\left(\dfrac{Z}{20}\right)+K(\theta)\left[P_{obl\ refl}-p_\sigma\left(\dfrac{Z}{20}\right)\right]$	0.026	3.81
$\dfrac{2Z}{U}$	$r_{os}\left(t+\dfrac{\ell-\frac{Z}{20}}{}\right)$	0.052	3.15
$\dfrac{e+2Z}{U}+ts$	$r_{os}\left(t+\dfrac{\ell-Z}{20}\right)$	0.060	3.13

Inside

Symbolic		Numerical	
Time, t	Pressure, r_1	Time, t (sec)	Pressure, r_1 (psi)
0	0	0	0
$\dfrac{e}{U}+ts$	0	0.008	0
$\dfrac{e+Z}{U}+ts$	$0.7(0.75)p_o\left(t-\dfrac{Z}{20}\right)$	0.034	1.70
$\dfrac{e+2Z}{U}+ts$	$r_{os}\left(t+\dfrac{Z}{20}\right)$	0.060	3.13

TABLE E.2.7.

Net Average Pressures on First Bay Front Roof Slope of Building 3.3.3

Time, t (sec)	r_o (psi)	r_1 (psi)	$r = r_o - r_1$ (psi)
0	0	0	0
0.008	1.18	0	1.18
0.026	3.81	1.18	2.63
0.034	3.12	1.70	1.42
0.052	3.15	2.67	0.48
0.060	3.13	3.13	0

TABLE E.2.8

Average Pressures on First Bay Rear Roof Slope of Building 3.3.3

Outside

	Symbolic		Numerical	
Time, t	Pressure, r_o		Time, t (sec)	Pressure, r_o (psi)
0	0		0	0
$\dfrac{a-Z}{U}$	0		0.040	0
$\dfrac{a}{U} + \dfrac{a}{U}$	$r_{os}(t + \dfrac{a+Z}{20})$		0.066	3.28
$(t^* + \dfrac{a}{U}) \dfrac{Z}{a} + \dfrac{a-Z}{U}$	$r_{os}(t + \dfrac{a+Z}{20})$		0.095	3.15

Inside

	Symbolic		Numerical	
Time, t	Pressure, r_1		Time, t (sec)	Pressure, r_1 (psi)
0	0		0	0
$(t^* + \dfrac{a}{U}) \dfrac{Z}{a} + \dfrac{a-Z}{U}$	0		0.043	0
$(t^* + \dfrac{a}{U}) \dfrac{Z}{a} + \dfrac{a}{U}$	$0.9[0.75)p_o(t - \dfrac{2a-Z}{20})$		0.069	2.26
$(t^* + \dfrac{a}{U}) \dfrac{Z}{a} + \dfrac{a+Z}{U}$	$r_{os}(t + \dfrac{a+Z}{20})$		0.095	3.15

TABLE E.2.9

Net Average Pressures on First Bay Rear Roof Slope of Building 3.3.3

Time, t (sec)	r_o (psi)	r_i (psi)	$r = r_o - r_i$ (psi)
0	0	0	0
0.040	0	0	0
0.043	0.38	0	0.38
0.066	3.28	2.00	1.28
0.069	3.25	2.26	0.99
0.095	3.15	3.15	0

TABLE E.2.10

Average Pressures on Second Bay Front Roof Slope of Building 3.3.3

Outside

Symbolic		Numerical	
Time, t	Pressure, r_o	Time, t (sec)	Pressure, r_o (psi)
0	0	0	0
$\frac{a}{U}$	0	0.066	0
$\frac{a+Z}{U}$	$r_{os}(t + \frac{a-Z}{2U})$	0.092	3.28
$\frac{a+2Z}{U}$	$r_{os}(t + \frac{a-Z}{2U})$	0.118	3.15

Inside

Symbolic		Numerical	
Time, t	Pressure, r_1	Time, t (sec)	Pressure, r_1 (psi)
0	0	0	0
$\frac{a}{U}$		0.066	0
$\frac{a+Z}{U}$	$0.75\, p_o(t - \frac{2a+Z}{2U})$	0.092	2.53
$\frac{a+2Z}{U}$	$r_{os}(t + \frac{a-Z}{2U})$	0.118	3.15

TABLE E.2.11

Net Average Pressure on Second Bay Front Roof Slope of Building 3.3.3

Time, t (sec)	r_0 (psi)	r_1 (psi)	$r = r_0 - r_1$ (psi)
0	0	0	0
0.66	0	0	0
0.92	3.28	2.53	0.75
0.118	3.15	3.15	0

TABLE E.2.12

Net Average Pressure on Second Bay Rear Roof Slope of Building 3.3.3

Time, t (sec	r_0 (psi)	r_1 (psi)	$r = r_0 - r_1$ (psi)
0	0	0	0
0.106	0	0	0
0.132	3.28	2.53	0.75
0.158	3.15	3.15	0

TABLE E.2.13

Net Average Pressure on Third Bay Front Slope of Building 3.3.3

Time, t (sec)	r_0 (psi)	r_1 (psi)	$r = r_0 - r_1$ (psi)
0	0	0	0
0.132	0	0	0
0.158	3.28	2.53	0.75
0.184	3.15	3.15	0

TABLE E.2.14

Net Average Pressure on Third Bay Rear Roof Slope of Building 3.3.3

	Symbolic			Numerical			
		r				r, psi	
Time, t	Purlin Effect	Refl Shock Effect		Time, t (sec)	Purlin	Refl Shock	Total Pressure
0	0	0		0	0	0	0
$\frac{l-\bar{l}}{U}$	0	0		0.172	0	0	0
$\frac{l}{U}$	$r_{os}(t-\frac{l-Z}{20})-0.75p_o(t-\frac{2l-Z}{20})$	0		0.198	0.75	0	0.75
$\frac{l+\delta}{U}$		$-\frac{\delta}{l}\left[p_{refl}-p_o(\frac{Z}{20})\right](1-\frac{\delta}{l})$		0.210	0.40	-1.03	-0.63
$\frac{l+Z}{U}$	0	0		0.224	0	0	0

TABLE E.2.15

Vertical and Horizontal Roof Forces on Building 3.3.3.

Time, t (sec)	psi	Vertical Force, ($lb \times 10^3$)V_r	psi	Horizontal Force, ($lb \times 10^3$)H_r
0	0	0	0	0
0.008	1.18	635	0.144	80
0.026	2.63	1410	0.32	175
0.034	1.42	765	0.173	95
0.040	1.12	600	0.137	75
0.043	1.33	715	0.069	40
0.049	1.20	645	0	0
0.060	1.05	565	-0.128	-70
0.066	1.28	685	-0.156	-85
0.069	1.09	585	-0.109	-60
0.082	0.90	485	0	0
0.092	0.85	455	0.079	45
0.095	0.66	355	0.081	45

TABLE E.2.15 (CONTD)

Vertical and Horizontal Roof Forces of Building 3.3.3.

Time, t (sec)	psi	Vertical Force, $(lb \times 10^3) V_r$	psi	Horizontal Force, $(lb \times 10^3) H_r$
0.106	0.34	185	0.041	20
0.112	0.34	185	0	0
0.118	0.34	185	-0.041	-20
0.132	0.75	410	-0.091	-50
0.145	0.75	410	0	0
0.158	0.75	410	0.091	50
0.172	0.34	185	0.041	20
0.178	0.34	185	0	0
0.184	0.34	185	-0.041	-20
0.198	0.75	410	-0.091	-50
0.210	-0.66	-360	0.081	45
0.224	0	0	0	0

Table E.2.16

Average Pressures and Forces on Trusswork of Building 3.3.3

Symbolic		Numerical		
Time, t	Pressure, d $(C_d = 1)$	Time, t (sec)	Pressure, d (psi)	Force, $D = d \cdot A_d$ (10^3 lb)
0	0	0	0	0
* $\frac{l}{U}$	$p_d\left(t - \frac{l}{2U}\right)$	* 0.198	0.2	225
	$p_d\left(t - \frac{l}{2U}\right)$	0.3	0.15	170
	$p_d\left(t - \frac{l}{2U}\right)$	0.5	0.08	90
	$p_d\left(t - \frac{l}{2U}\right)$	0.7	0.04	45
	$p_d\left(t - \frac{l}{2U}\right)$	0.9	0.02	25
	$p_d\left(t - \frac{l}{2U}\right)$	1.1	0.01	10
	$p_d\left(t - \frac{l}{2U}\right)$	1.3	~	~
	$p_d\left(t - \frac{l}{2U}\right)$	1.5	~	~
$t_o + \frac{l}{U}$	0	1.618	0	0

Table E.2.17

Average Pressures on an Upper Corner First Monitor Windowpane

of Building 3.3.3

Time, t (sec)	Pressure, f_o (psi)	Force, $F = A \cdot f_o$ (10^3 lb)
0	7.45	2.25
0.00146	3.56	1.08
0.1	3.06	0.93
0.2	2.61	0.79
0.4	1.85	0.56
0.6	1.28	0.39
1.0	0.51	0.16
1.42	0	0

Table E.2.19

Net Pressures on Plank in Third Bay Rear Roof Slope of Building 3.3.3

Located with Downstream End One Foot from Back Wall

Time, τ (sec)	Pressure, r (psi)
0	0
0.0049	3.45
0.012	2.25
0.017	0

Table E.2.20

Net Pressures on Plank in Third Bay Rear Roof Slope of Building 3.3.3

Located with Downstream End Seventeen Feet from Back Wall

Time, τ (sec)	Pressure, r (psi)
0	0
0.0049	1.65
0.012	0.50
0.015	0

ARMOUR RESEARCH FOUNDATION OF ILLINOIS INSTITUTE OF TECHNOLOGY

CHAPTER E.3

BUILDING 3.3.8h

E.3.1 GENERAL

Building 3.8.8h has a saw-tooth roof with monitors and no side walls. Figures E.2.1 and E.2.2 give detailed views of the front wall (nearly identical with the back wall) and a side view of the structure. The trusswork of the structure is omitted in these figures. The area of this trusswork, projected into a vertical plane transverse to the flow direction, is roughly 486 sq. ft.[1] The trusswork includes purlins, struts, monitor girts, exposed columns, etc., and for purposes of computation is assumed to be uniformly distributed along the 60-ft length of the structure. The structure is struck by a shock wave of 3.68-psi overpressure ($\xi = 1.25$). The notation is the same as was used in Section E.2.1.

E.3.2 METHOD OF DETERMINATION OF LOADING

The 3.3.8h structure is a quarter-scale model of building 3.3.3. The method of predicting loading is identical to that for building 3.3.3. Sections E.2.1 and E.2.2, including all symbolic graphs, are applicable to the building 3.3.8h.

---

[1] The area of the trusswork can be computed from Drawing No. 100-259-1 Dept. of Air Force Hd. AMC, Office of Installation, Wright-Patterson Air Force Base, Dayton, Ohio.

E.3.3 NUMERICAL COMPUTATION OF LOADING

Since the numerical calculations for the 3.3.8h structure follow exactly the same pattern as for the 3.3.3 structure, no extensive discussion of the procedure is necessary. The discussion in Section E.2.3 of loading on building applies here except for obvious changes in numbering of tables and figures and a slight change in the given shock strength (3.7 psi for building 3.3.8h, 3.4 psi for building 3.3.3).

Figures E.3.2-E.3.8 illustrate the results computed in Tables E.3.2-E.3.16 for the early period.

The following comments summarize the qualitative changes between the loadings on the 3.3.8h and 3.3.3 structures. Since the 3.3.8h structure is a quarter model of the 3.3.3 structure, linear building dimensions, including those time units based upon these dimensions, are reduced by one-quarter; areas and forces acting on these areas are reduced by one-sixteenth. Furthermore, building 3.3.8h is struck by a shock wave of 3.7 psi overpressure instead of the 3.4-psi shock of building 3.3.3. This change, though minor, causes a change in all numerical values depending upon shock strength, such as shock velocity, reflected pressure, etc. In addition, deviation from the purlin shape changes the constant α (obtained from Section E.2.2.1.5) from 0.75 for building 3.3.3 to 0.85 for building 3.3.8h. Glass breaking time, t^*, was arbitrarily taken as one half of the value found for building 3.3.3 since no information was available on the glass thickness used.

TABLE E.3.1

Constants for Building 3.3.8h

Shock Constants	
$p_\sigma(0)$ = 3.7 psi	c_{refl} = 1190 fps
U = 1230 fps	P_o = 14.7 psi
ξ = 1.25	t_o = 1.39 sec
P_{refl} = 8.13 psi	

Geometric Constants	
a = 20 ft	$A_f \approx$ 30,000 sq in.
$\bar{l}$ = 7.84 ft	$A_b \approx$ 30,000 sq in.
e = 1.75 ft	$A_r \approx$ 203,000 sq in.
$\bar{h}_{of}$ = 1.1 ft	$A_d \approx$ 70,000 sq in.
$\bar{h}_{if}$ = 1.2 ft	$\Omega \approx$ 0.22
$\bar{h}_{ib}$ = 1.2 ft	θ = 7°
$\bar{h}_{ob}$ = 1.1 ft	

TABLE E.3.1 (CONTD)

Constants for Building 3.3.8h

Combined Geometric And Shock Constants			
$\frac{\ell}{U} = 0.048$		$P_{\sigma i}$	= 2.2 psi
$\frac{s}{U} = 0.016$ sec		ξ_i	= 1.15
$\frac{I}{U} = 0.0064$ sec		$c_{fo} = c_{bi}$	= $\frac{2}{3}$
$\frac{a}{U} = 0.001$ sec		$c_{fi} = c_{bo}$	= $\frac{-1}{3}$
$\frac{\bar{h}_{of}}{c_{refl}} = 0.0009$ sec		c_{df}	= 1
		c_{db}	= -1
$\frac{\bar{h}_{if}}{U} = 0.001$ sec		front c_{ro}	= -0.30
		back c_{ro}	= -0.30
$\frac{\bar{h}_{ib}}{c_{refl}} = 0.001$ sec		$P_{obl\ refl}$	= 4.64 psi
$\frac{\bar{h}_{ob}}{U} = 0.0009$ sec		$K(\theta)$	= 0.4
		t^*	= 0.004 sec
$\delta = 3.72$ ft			

TABLE E.3.2

Average Pressures on Front Wall of Building 3.3.6h

Outside

Symbolic		Numerical	
Time, t	Pressure, f_o	Time, t (sec)	Pressure, f_o (psi)
0	P_{refl}	0	8.13
$\dfrac{35_{af}}{c_{refl}}+t^*$	$f_{os}(t)$	0.004	3.86
a/U	$(f_{os})t$	0.0163	3.84

Inside

Symbolic		Numerical	
Time, t	Pressure, f_1	Time, t (sec)	Pressure, f_1 (psi)
0	0	0	0
t^*	0	0.001	0
$\dfrac{35_{1r}}{U}+t^*$	$P_{\sigma 1}$	0.007	2.2
a/U	$f_{1s}(t)$	0.0163	3.54

TABLE E.3.3

Net Average Pressures and Forces on Front Wall

of Building 3.3.8h

Time, t (sec)	Pressure			Force
	f_0 (psi)	f_1 (psi)	$f = f_0 - f_1$ (psi)	$F = fA_f$ (lb $\times$ 10^3)
0	8.13	0	8.13	258
0.001	7.06	0	7.06	225
0.004	3.86	1.10	2.76	87.8
0.007	3.85	2.2	1.65	52.1
* 0.0163	3.84	3.54	0.30	9.5
0.1			0.25	8.0
0.2			0.20	6.3
0.4			0.15	4.8
0.6			0.12	3.8
0.8			0.10	3.2
1.0			~	~
1.2			~	~
1.39			0	0

TABLE E.3.4

Average Pressures on Back Wall of Building 3.3.8a

Inside

Symbolic		Numerical	
Time, t	Pressure, b_1	Time, t (sec)	Pressure, b_1 (psi)
0	0	0	0
$\left(\dfrac{l}{U}\right)^-$	0	0.049^-	0
$\left(\dfrac{l}{U}\right)^+$	P_{refl}	0.049^+	8.13
$\dfrac{l}{U} + \dfrac{3\bar{h}_{1b}}{c_{refl}} + t*$	$b_{1s}(t)$	0.053	3.86
$\dfrac{l + 6\bar{h}_{ob}}{U} + t*$	$b_{1s}(t)$	0.055	3.86

Outside

Symbolic		Numerical	
Time, t	Pressure, b_o	Time, t (sec)	Pressure, b_o (psi)
0	0	0	0
$\dfrac{l}{U}$	0	0.049	0
$\dfrac{l + 6\bar{h}_{ob}}{U} + t*$	$b_{os}(t)$	0.055	3.54

TABLE E.3.5

Net Average Pressures and Forces on Back Wall

of Building 3.3.8h

| Time, t (sec) | Pressure | | | Force |
	b_1 (psi)	b_0 (psi)	$-b = b_1 - b_0$ (psi)	$-B = -bA_0$ (lb $\times 10^3$)
0	0	0	0	0
0.049⁻	0	0	0	0
0.049⁺	8.13	0	8.13	258
0.053	3.86	2.83	1.03	32.8
* 0.055	3.86	3.54	0.32	10.2
0.1			0.25	8.0
0.2			0.20	6.3
0.4			0.15	4.8
0.6			0.12	3.8
0.8			0.10	3.2
1.0			$\sim$	$\sim$
1.2			$\sim$	$\sim$
1.44			0	0

TABLE E.3.6

Average Pressures on First Bay Front Roof Slope of Building 3.3.8h

Outside

Symbolic		Numerical	
Time, t	Pressure, r_o	Time, t (sec)	Pressure, r_o (psi)
0	0	0	0
$\dfrac{\bar{\ell}}{U}$	$p_\sigma\left(\dfrac{\bar{\ell}}{2U}\right) + K(\theta)\left[P_{obl\ refl} - p_\sigma\left(\dfrac{\bar{\ell}}{2U}\right)\right]$	0.0064	4.1
$\dfrac{2\bar{\ell}}{U}$	$r_{os}\left(t + \dfrac{\ell - \bar{\ell}}{2U}\right)$	0.0128	3.57
$\dfrac{e+2\bar{\ell}}{U} + t*$	$r_{os}\left(t + \dfrac{\ell - \bar{\ell}}{2U}\right)$	0.0151	3.55

Inside

Symbolic		Numerical	
Time, t	Pressure, r_i	Time, t (sec)	Pressure, r_i (psi)
0	0	0	0
$\dfrac{e}{U} + t*$	0	0.0024	0
$\dfrac{e+\bar{\ell}}{U} + t*$	$0.7\,(0.85)\,p_\sigma\left(t - \dfrac{\bar{\ell}}{2U}\right)$	0.0088	2.17
$\dfrac{e+2\bar{\ell}}{U} + t*$	$r_{os}\left(t + \dfrac{\ell - \bar{\ell}}{2U}\right)$	0.0151	3.55

TABLE E.3.7

Net Average Pressures on First Bay Front Roof Slope of

Building 3.3.8h

Time, t (sec)	r_o (psi)	r_1 (psi)	$r \approx r_o - r_1$ (psi)
0	0	0	0
0.0024	1.52	0	1.52
0.0064	4.10	1.40	2.70
0.0088	3.91	2.17	1.74
0.0128	3.57	3.03	0.54
0.0151	3.55	3.55	0

TABLE E.3.7

Net Average Pressures on First Bay Front Roof Slope of

Building 3.3.8h

Time, t (sec)	r_0 (psi)	r_1 (psi)	$r \approx r_0 - r_1$ (psi)
0	0	0	0
0.0024	1.52	0	1.52
0.0064	4.10	1.40	2.70
0.0088	3.91	2.17	1.74
0.0128	3.57	3.03	0.54
0.0151	3.55	3.55	0

TABLE E.3.8

Average Pressures on First Bay Rear Slope of Building 3.3.8h

Outside

Symbolic		Numerical	
Time, t	Pressure, r_o	Time, t(sec)	Pressure, r_o (psi)
0	0	0	0
$\dfrac{a-\bar{l}}{U}$	0	0.0099	0
$\dfrac{a}{U}$	$r_{os}(t+\dfrac{a+\bar{l}}{2U})$	0.0162	3.57
$(t*+\dfrac{e}{U})\dfrac{\bar{l}}{a}+\dfrac{a+\bar{l}}{U}$	$r_{os}(t+\dfrac{a+\bar{l}}{2U})$	0.0235	3.54

Inside

Symbolic		Numerical	
Time, t	Pressure, r_1	Time, t(sec)	Pressure, r_1 (psi)
0	0	0	0
$(t*+\dfrac{e}{U})\dfrac{\bar{l}}{a}+\dfrac{a-\bar{l}}{U}$	0	0.0108	0
$(t*+\dfrac{e}{U})\dfrac{\bar{l}}{a}+\dfrac{a}{U}$	$0.9(0.85)P_o(t-\dfrac{2a-\bar{l}}{2U})$	0.0172	2.80
$(t*+\dfrac{e}{U})\dfrac{\bar{l}}{a}+\dfrac{a+\bar{l}}{U}$	$r_{os}(t+\dfrac{a+\bar{l}}{2U})$	0.0235	3.54

TABLE E.3.9

Net Average Pressures on First Bay Rear Roof Slope of

Building 3.3.8h

Time, t (sec)	r_o (psi)	r_1 (psi)	$r = r_o - r_1$ (psi)
0	0	0	0
0.0099	0	0	0
0.0108	0.50	0	0.50
0.0162	3.57	2.38	1.19
0.0172	3.56	2.80	0.76
0.0235	3.54	3.54	0

TABLE E.3.10

Average Pressures on Second Bay Front Roof Slope of Building 3.3.8h

Outside

| | Symbolic | | Numerical |
Time, t	Pressure, r_o	Time, t (sec)	Pressure, r_o (psi)
0	0	0	0
$\dfrac{a}{U}$	0	0.0162	0
$\dfrac{a + \bar{\ell}}{U}$	$r_{os}(t + \dfrac{a - \bar{\ell}}{2U})$	0.0226	3.57
$\dfrac{a + 2\bar{\ell}}{U}$	$r_{os}(t + \dfrac{a - \bar{\ell}}{2U})$	0.030	3.55

Inside

| | Symbolic | | Numerical |
Time, t	Pressure, r_i	Time, t (sec)	Pressure, r_i (sec)
0	0	0	0
$\dfrac{a}{U}$	0	0.0162	0
$\dfrac{a + \bar{\ell}}{U}$	$0.85 p_\sigma(t - \dfrac{2a + \bar{\ell}}{2U})$	0.0226	3.12
$\dfrac{a + 2\bar{\ell}}{U}$	$r_{os}(t + \dfrac{a - \bar{\ell}}{2U})$	0.030	3.55

TABLE E.3.11

Net Average Pressures on Second Bay Front Roof Slope of

Building 3.3.8h

Time, t (sec)	r_0 (psi)	r_1 (psi)	$r = r_0 - r_1$ (psi)
0	0	0	0
0.0162	0	0	0
0.0226	3.57	3.12	0.45
0.030	3.55	3.55	0

TABLE E.3.12

Net Average Pressures on Second Bay Rear Roof Slope of

Building 3.3.8h

Time, t (sec)	r_0 (psi)	r_1 (psi)	$r = r_0 - r_1$ (psi)
0	0	0	0
0.0261	0	0	0
0.0325	3.57	3.12	0.45
0.0389	3.55	3.55	0

TABLE E.3.13

Net Average Pressures on Third Bay Front Roof Slope of

Building 3.3.8h

Time, t (sec)	r_0 (psi)	r_1 (psi)	$r = r_0 - r_1$ (psi)
0	0	0	0
0.0325	0	0	0
0.0389	3.57	3.12	0.45
0.0452	3.55	3.55	0

TABLE E.3.14

Net Average Pressures on Third Bay Rear Roof Slope of Building 3.3.8h

| Time, t | Symbolic, r | | Numerical | | | |
	Purlin Effect	Refl Shock Effect	Time, t (sec)	r, psi Purlin	r, psi Refl Shock	Total Pressure
0	0	0	0	0	0	0
$\frac{l-\bar{l}}{U}$	0	0	0.0425	0	0	0
$\frac{l}{U}$	$r_{os}(t-\frac{l-\bar{l}}{20}) - 0.85 p_\sigma(t-\frac{2l-\bar{l}}{20})$	0	0.0488	0.45	0	0.45
$\frac{l+\delta}{U}$	$-\frac{\delta}{\bar{l}}\left[p_{refl}-p_\sigma(\frac{\bar{l}}{20})\right](1-\frac{\delta}{\bar{l}})$	0	0.0513	0.27	-1.14	-0.87
$\frac{l+\bar{l}}{U}$	0	0	0.0552	0	0	0

TABLE E.3.15

Vertical and Horisontal Roof Forces on Building 3.3.8h

Time, t (sec)	Pressure psi	Vertical Force, V_r (lb x 10^3)	Pressure psi	Horisontal Force, H_r (lb x 10^3)
0	0	0	0	0
0.0023	1.55	52.3	0.17	5.7
0.0063	2.71	91.5	0.33	11.3
0.010	1.35	45.5	0.16	5.4
0.011	1.55	52.3	0.07	2.4
0.0122	1.35	45.5	0	0
0.0151	1.05	35.5	-0.12	-4.1
0.0161	1.20	40.6	-0.14	-4.7
0.0171	0.85	28.7	-0.08	-2.8
0.0225	0.58	19.6	0.04	1.4
0.0238	0.39	13.2	0.04	1.4
0.026	0.20	6.7	0.02	0.7
0.029	0.20	6.7	-0.02	-0.7
0.0325	0.45	15.2	-0.05	-1.7
0.039	0.45	15.2	0.05	1.7
0.0425	0.20	6.7	0	0
0.0455	0.20	6.7	-0.02	-0.7
0.049	0.45	15.2	-0.05	-1.7
0.051	-0.88	-29.8	0.11	3.7
0.0555	0	0	0	0

TABLE E.3.16

Average Pressures and Forces on Trusswork of Building 3.3.8h

Symbolic		Numerical		
Time, t	Pressure, d $(C_{d} = 1)$	Time, t (sec)	Pressure, d (psi)	Force, $D = dA_d$ (lb x 10^3)
0	0	0	0	0
* $\frac{l}{U}$	$P_d(t - \frac{l}{2U})$	* 0.0488	0.29	20.3
	$P_d(t - \frac{l}{2U})$	0.2	0.20	14.0
	$P_d(t - \frac{l}{2U})$	0.4	0.10	7.0
	$P_d(t - \frac{l}{2U})$	0.6	0.04	2.8
	$P_d(t - \frac{l}{2U})$	0.8	0.03	2.1
	$P_d(t - \frac{l}{2U})$	1.0	$\sim$	$\sim$
	$P_d(t - \frac{l}{2U})$	1.2	$\sim$	$\sim$
$t_o + \frac{l}{U}$	0	1.44	0	0
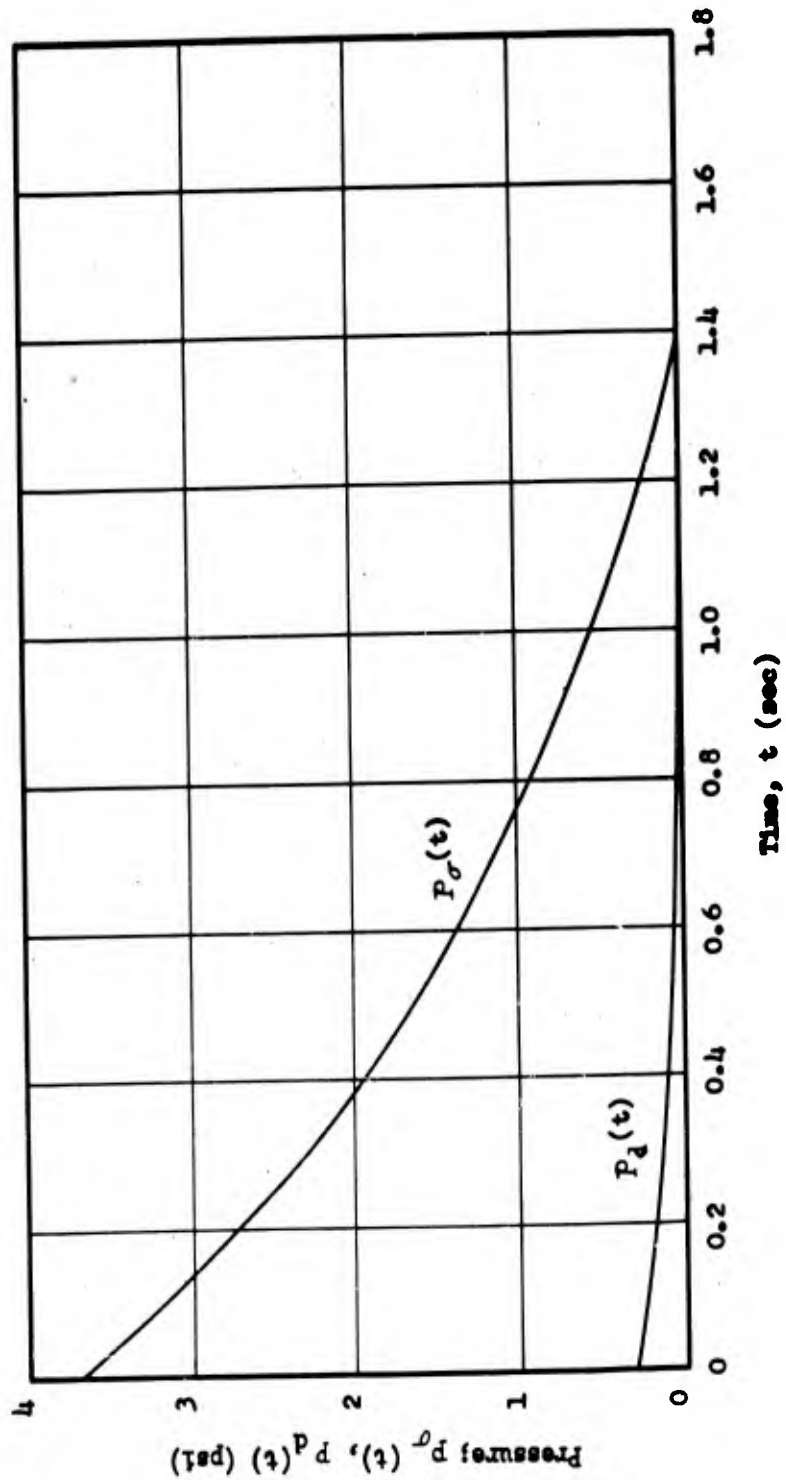
Fig. E.3.1 Side-On Pressure and Drag Pressure on Building 3.3.8h for $P_\sigma(0) = 3.7$ psi
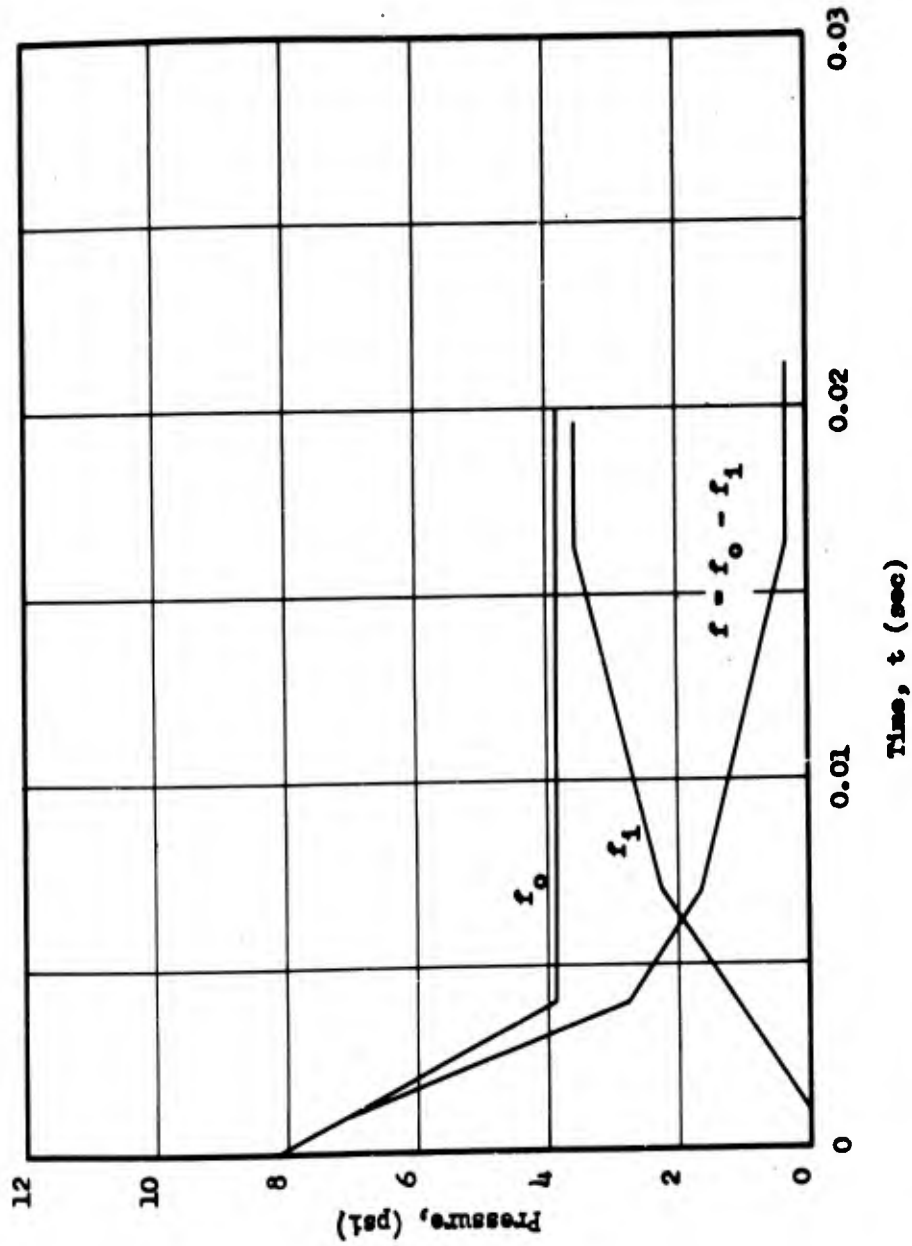
Fig. E.3.2 Average Pressures on Front Wall of Building 3.3.8a
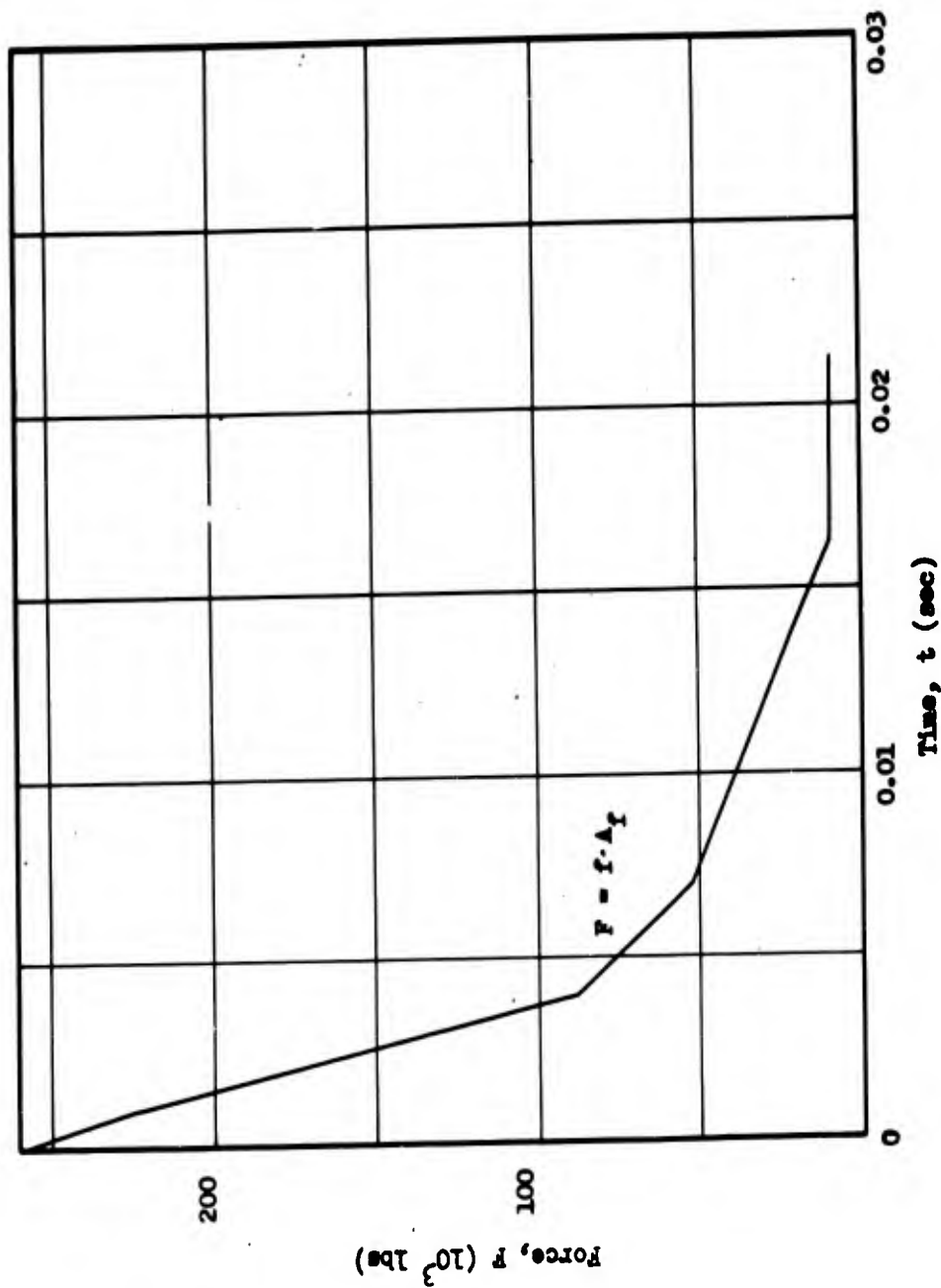
Fig. E.3.3. Force on Front Wall of Building 3.3.8h
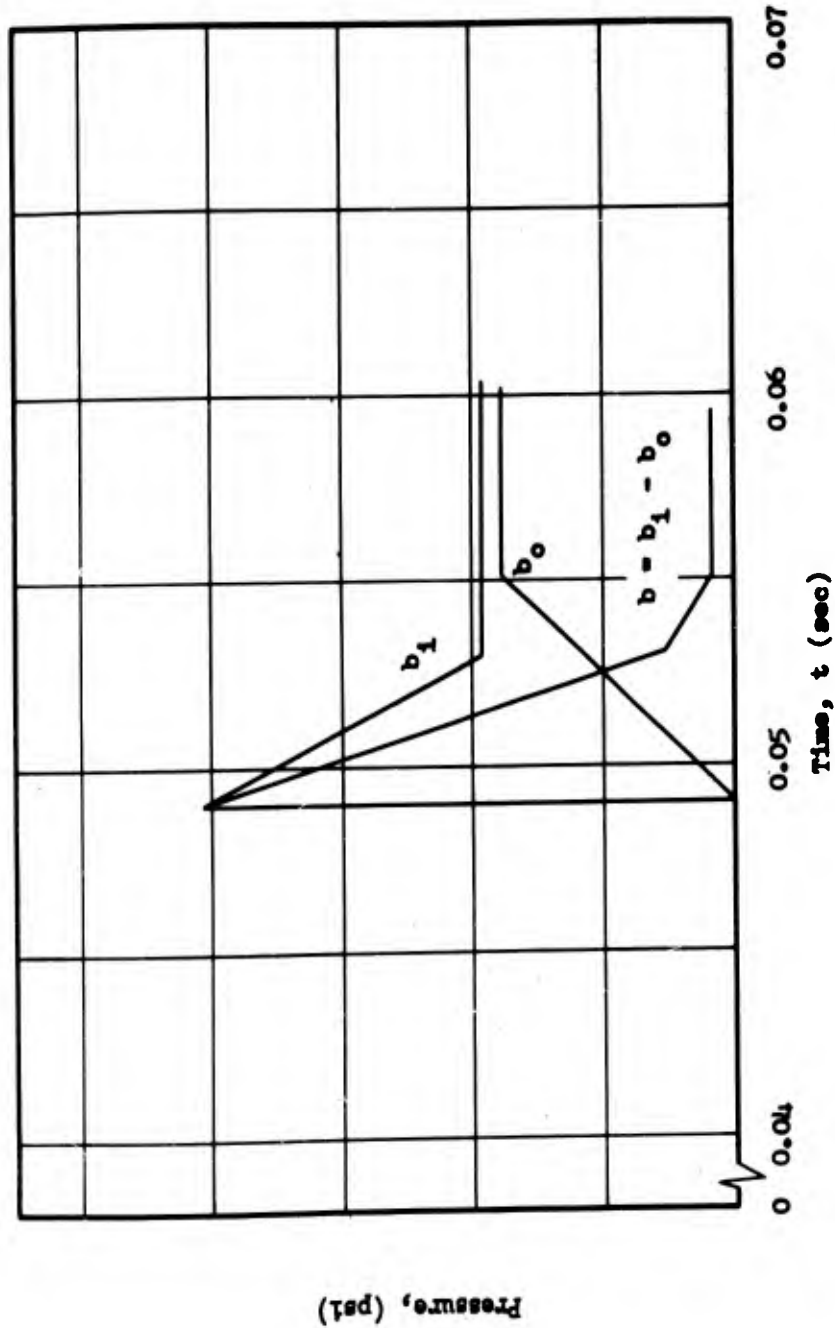
Fig. B.3.4 Average Pressures on Back Wall of Building 3.3.8h
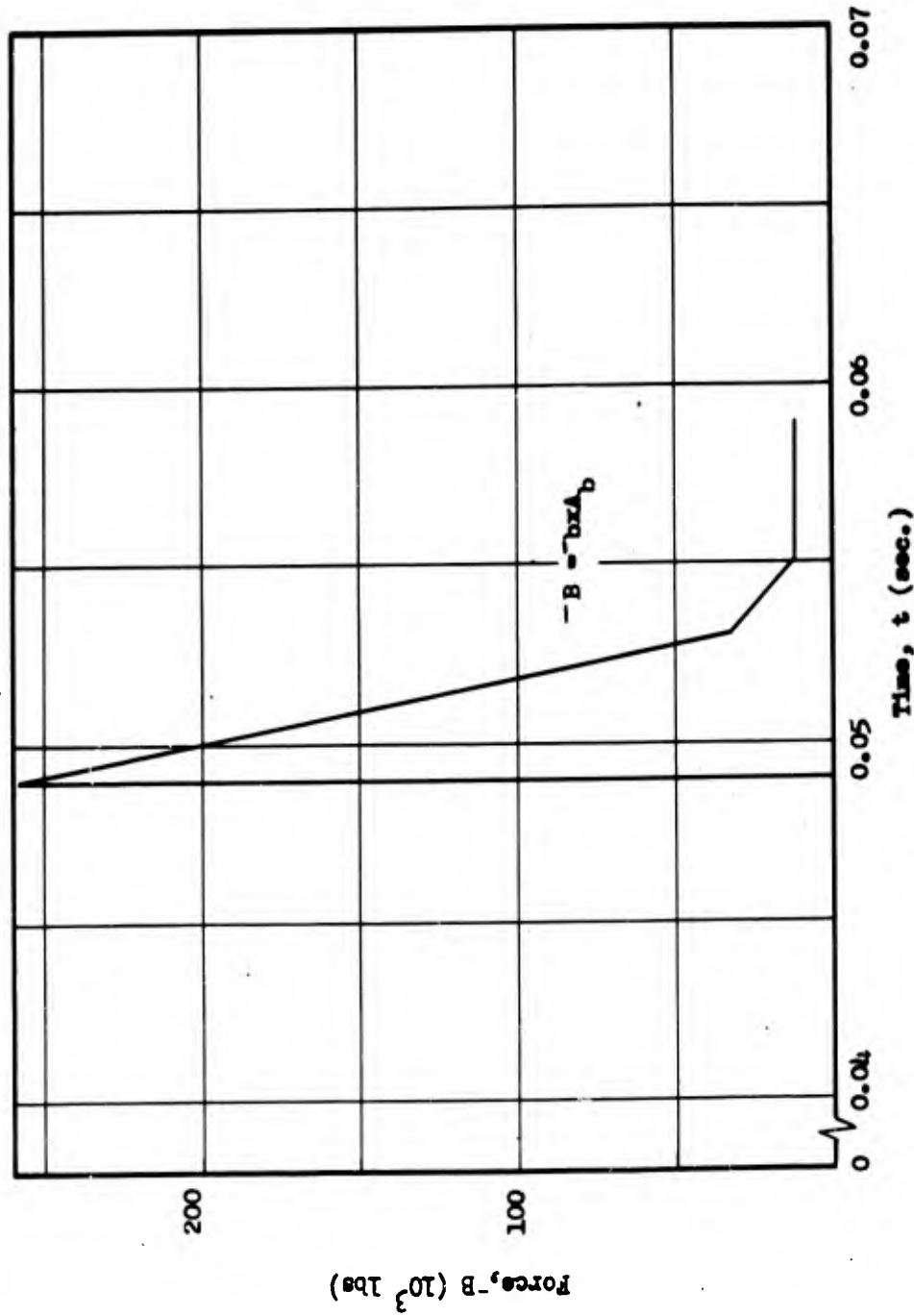
Fig. E.3.5 Force on Back Wall of Building 3.3.8h
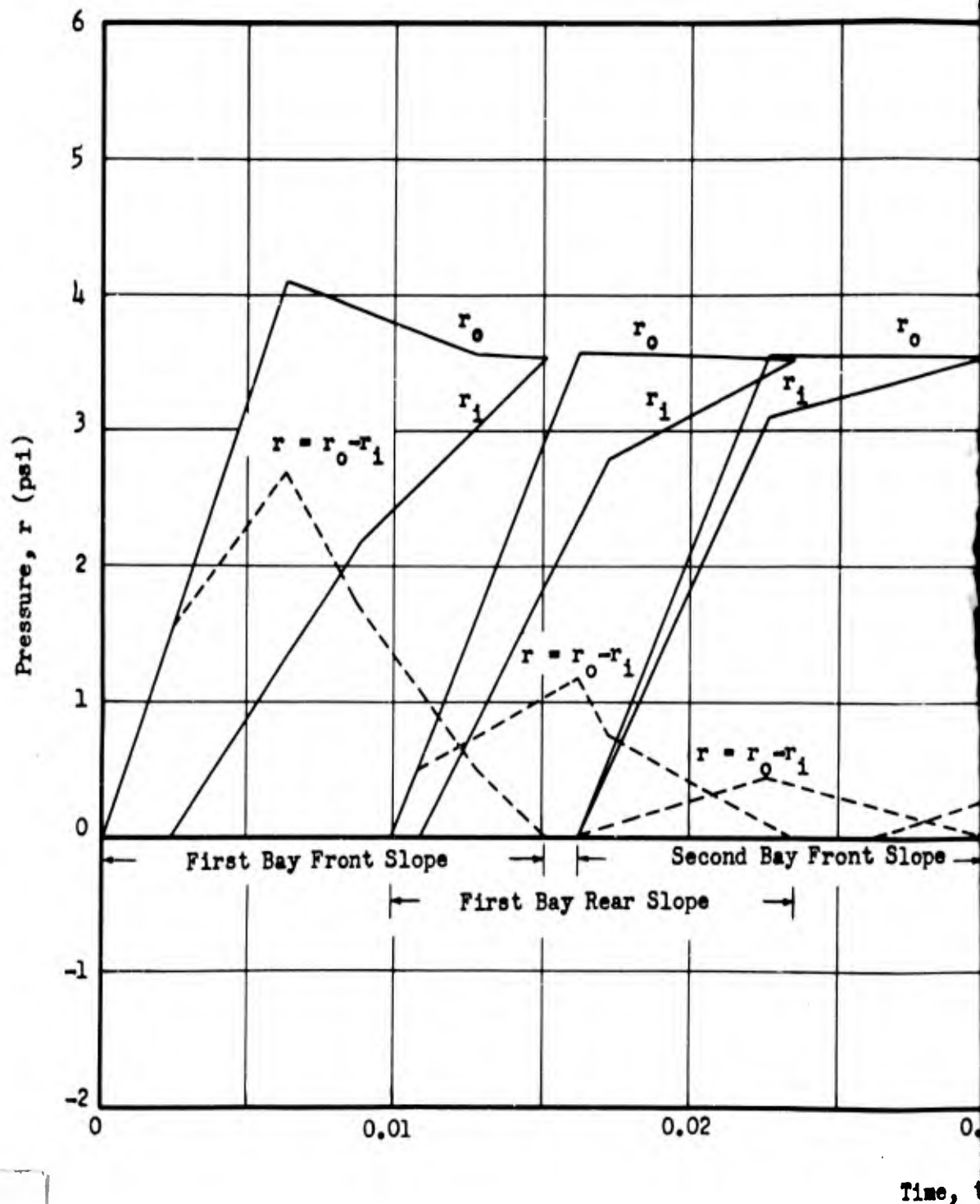
Fig. E.3.6   Pressures on Roof Slopes of Building 3.3.8h

Time, t (sec)

3.3.8h

2
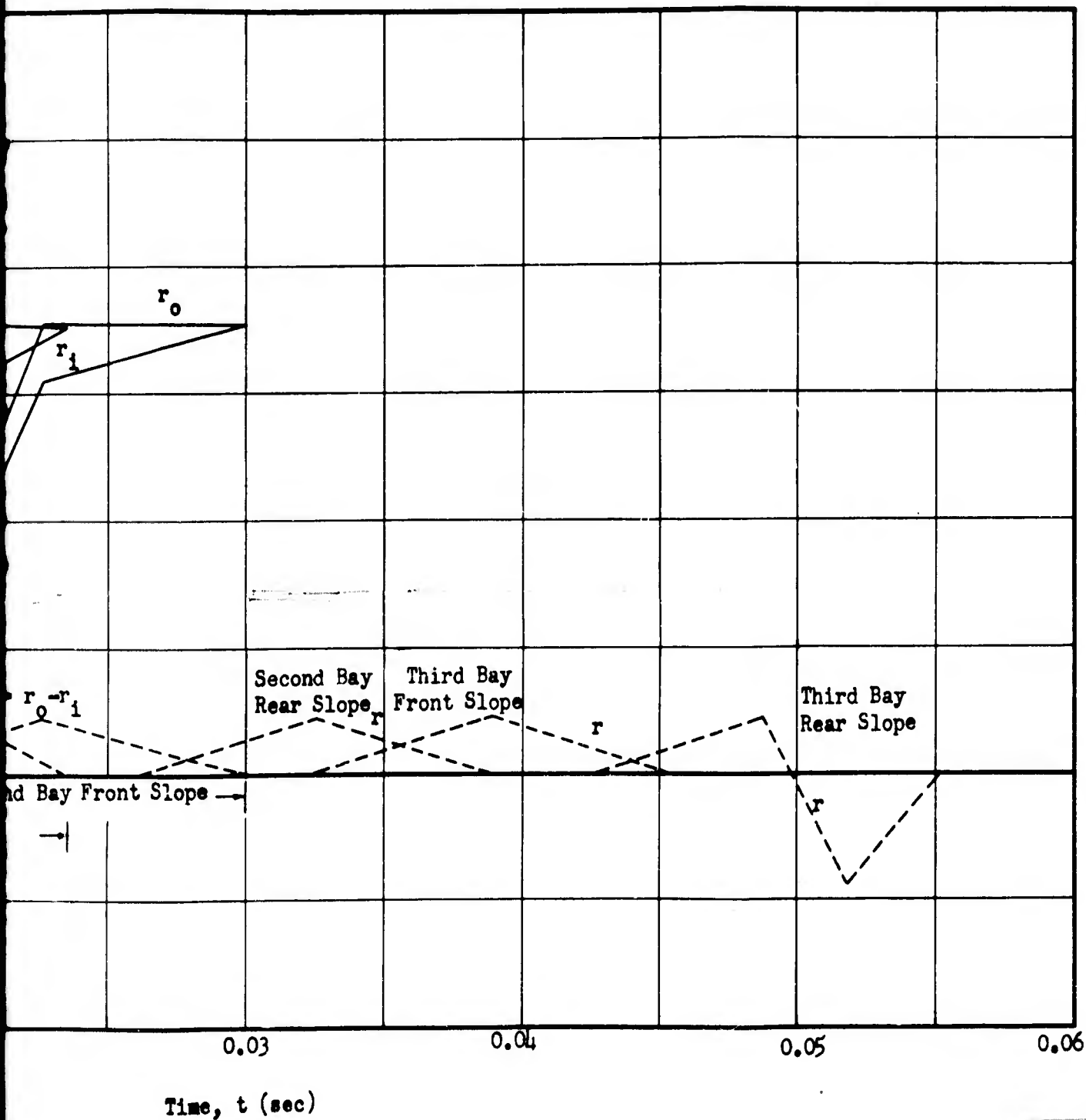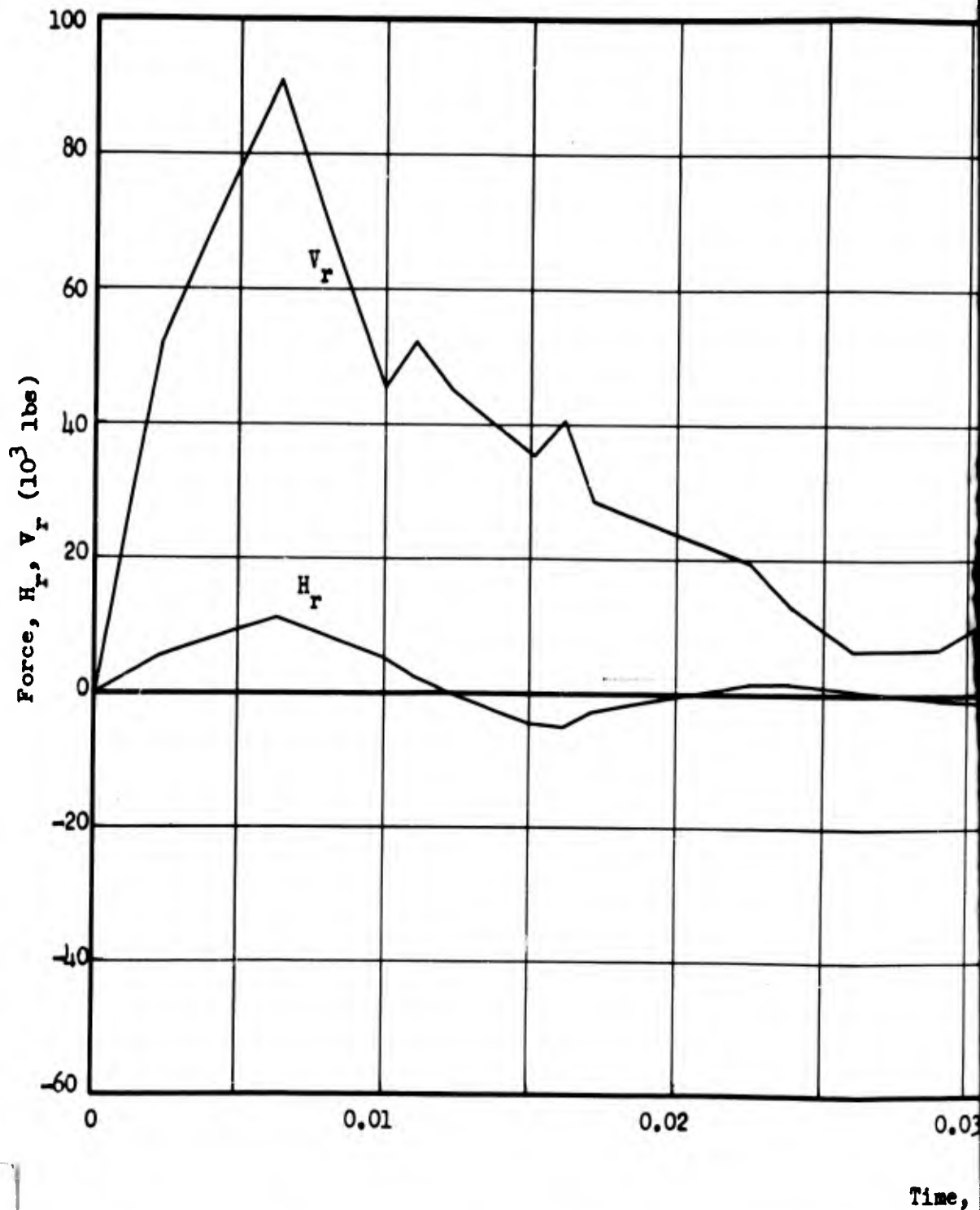
Fig. E.3.7   Horizontal and Vertical Forces on Roof of Building 3.3.8h
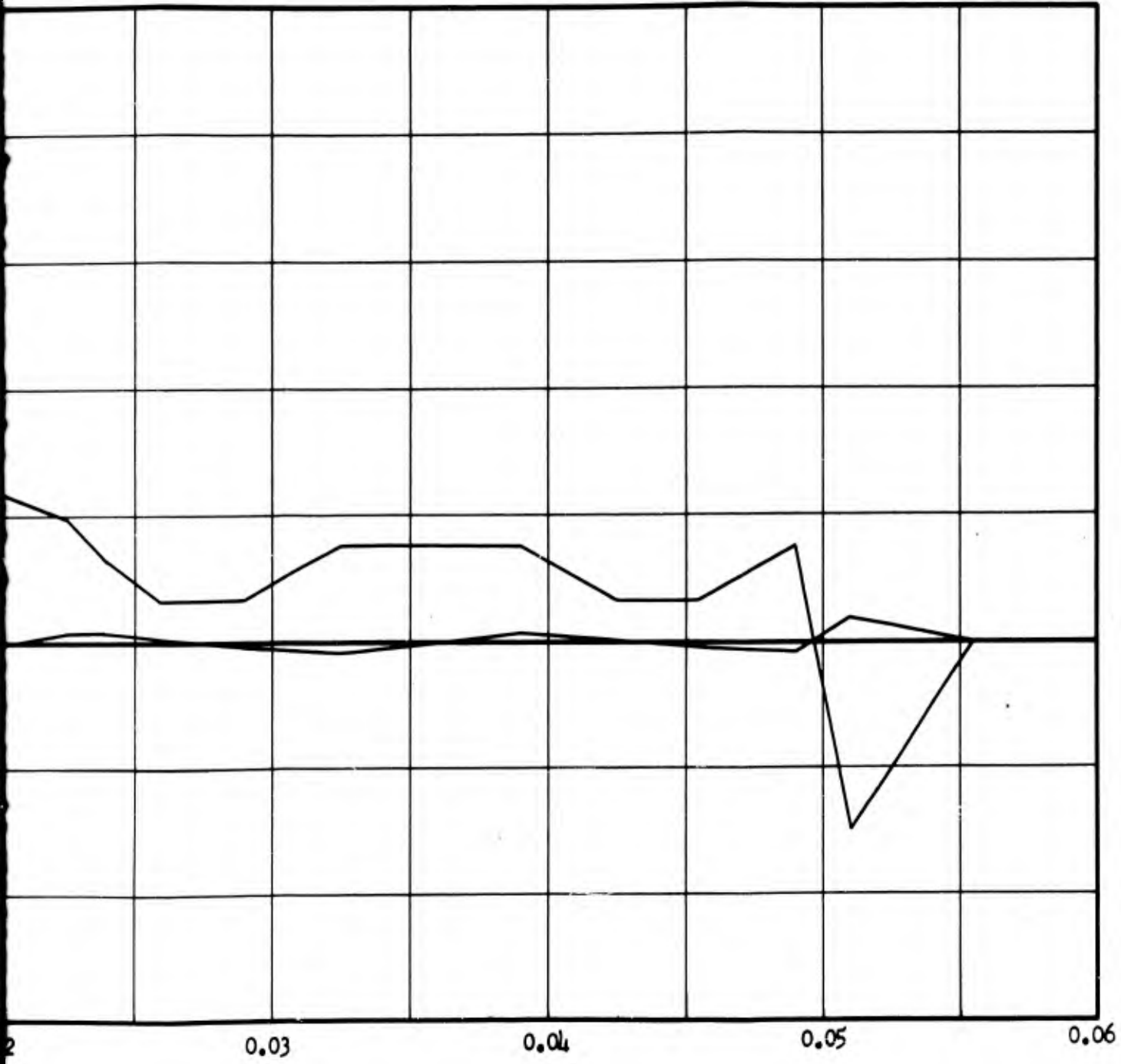
-162-

Time, t (sec)

of of Building 3.3.8h

2
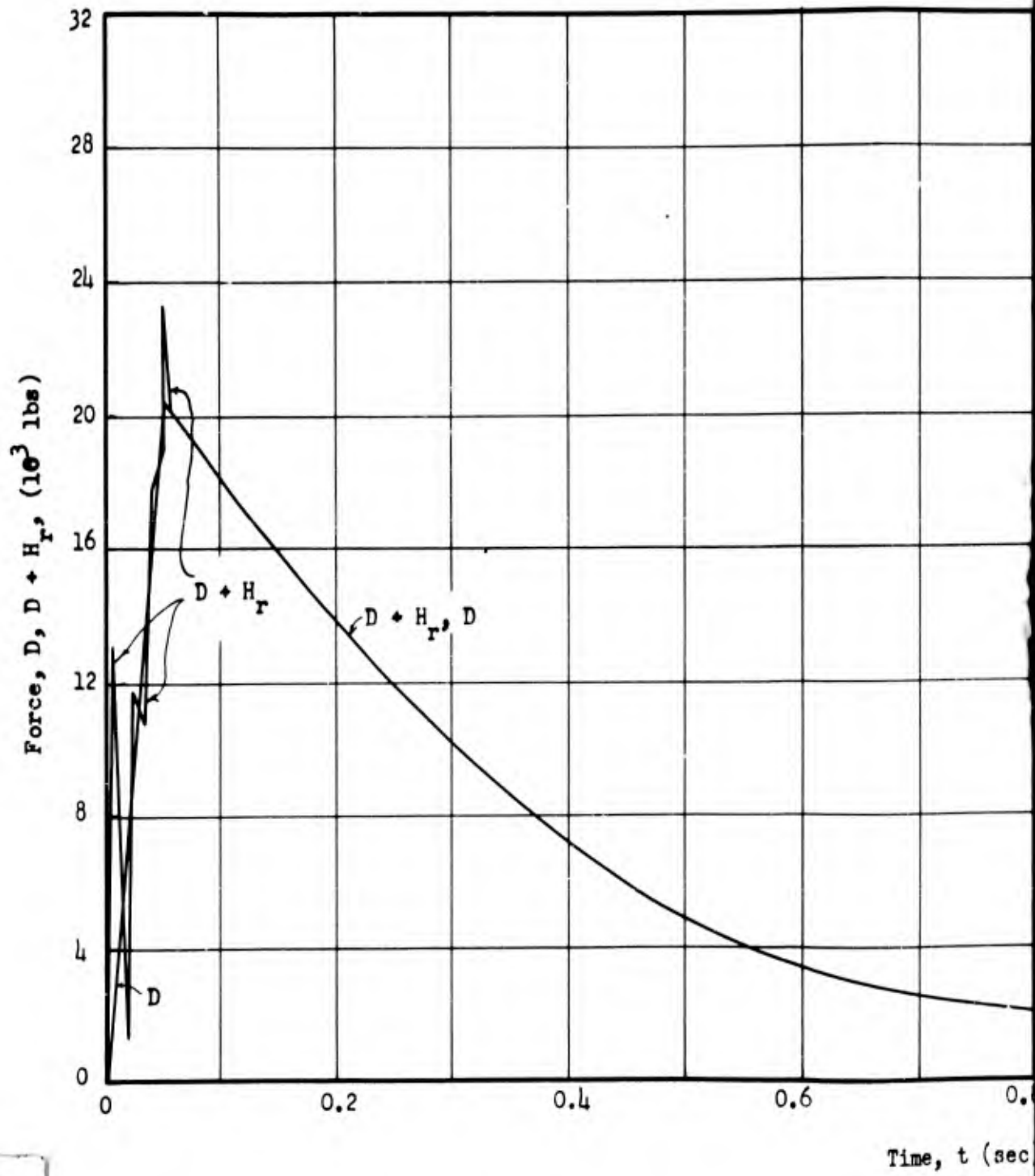
Fig. E.3.8   Force on Trusswork and Sum of Trusswork and Horizontal Roof For
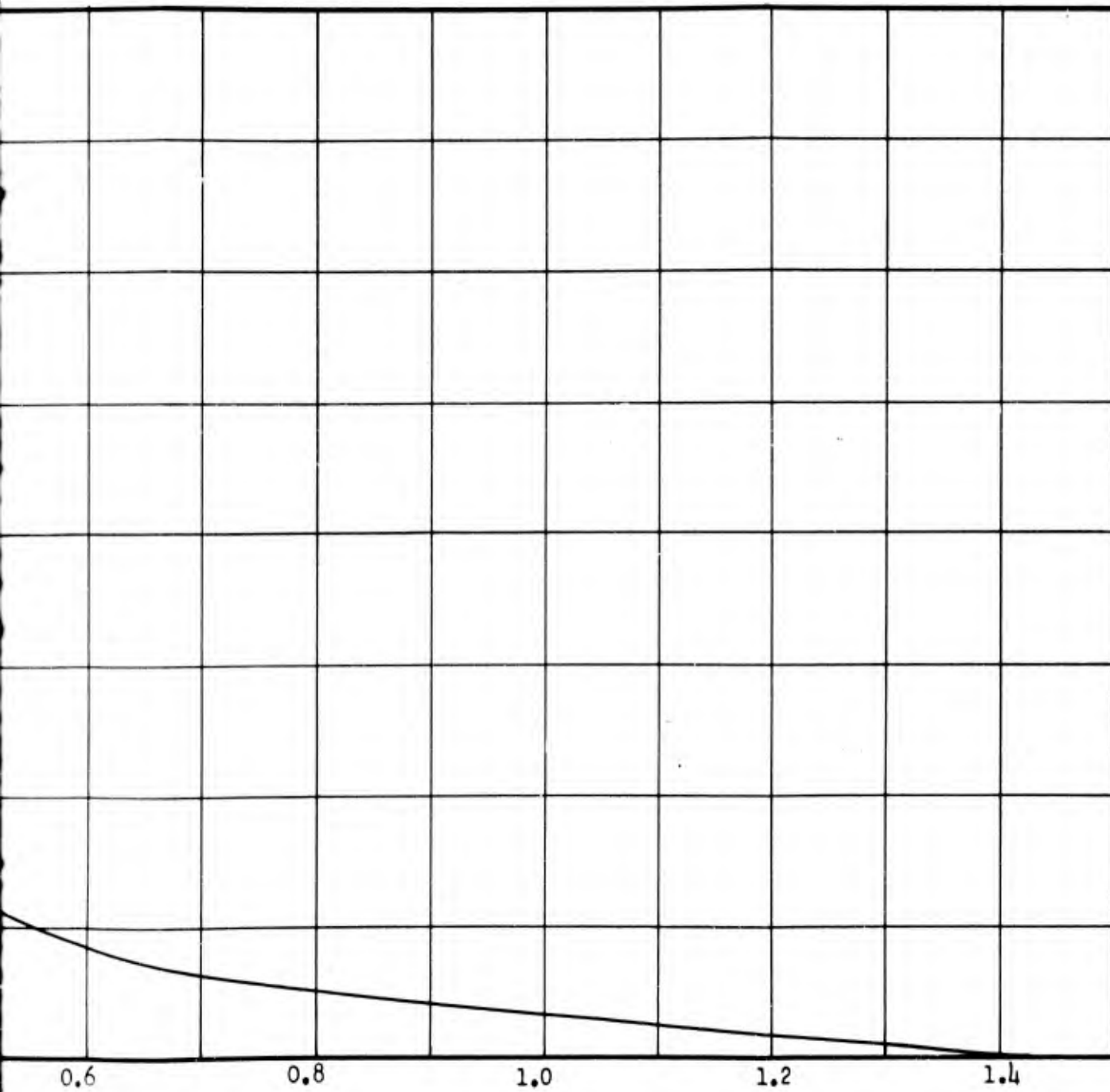
Time, t (sec)

ork and Horizontal Roof Forces on Building 3.3.8h

2

CHAPTER E.4

BUILDING 3.3.4

E.4.1 GENERAL

Building 3.3.4 is an industrial type structure of reinforced-concrete construction, and has a flat roof, two monitors, and no side walls. Figures E.4.1 and E.4.2 give a detailed view of the front wall (nearly identical with the back wall) and a side view. The structure is exposed to a shock wave of 3.55 psi overpressure (ξ = 1.25).

Symbols used in addition to those listed in Section E.1.4.3 are listed as follows:

A_{r1}	= area of the first roof section (from the front wall to the first monitor),
A_{r2}	= area of the second roof section (between the monitors),
A_{r3}	= area of the third roof section (from the second monitor to the rear wall),
l_1, l_2, l_3, l_4	= lengths (see Fig. E.4.2),
$P_i(t)$	= reference pressure inside of structure, i. e., pressure behind inside shock wave.

E.4.2 METHOD OF DETERMINATION OF LOADING

Methods for the determination of loadings on building 3.3.4 are based on the qualitative ideas expressed in Section E.1.2. The predictions are presented in the form of schematic diagrams in Figs. E.4.3 to E.4.11, and include the average pressures on the front wall, back wall,
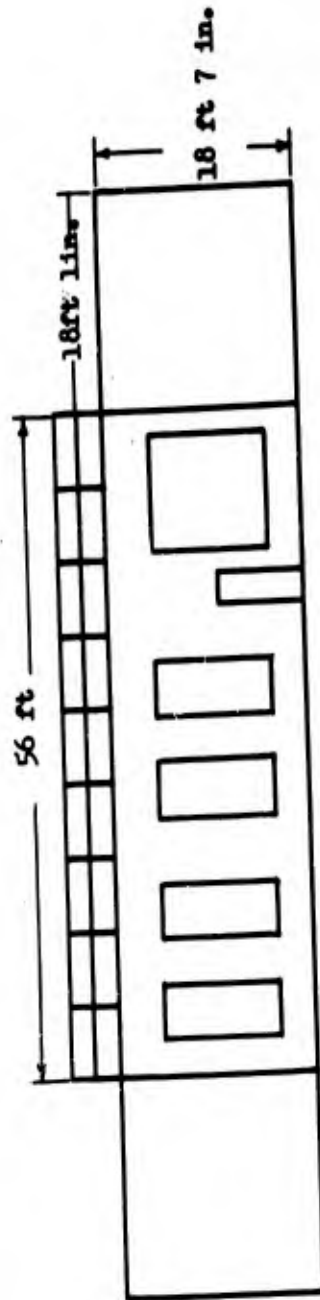
Fig. E.4.1 Front Wall of Building 3.3.4
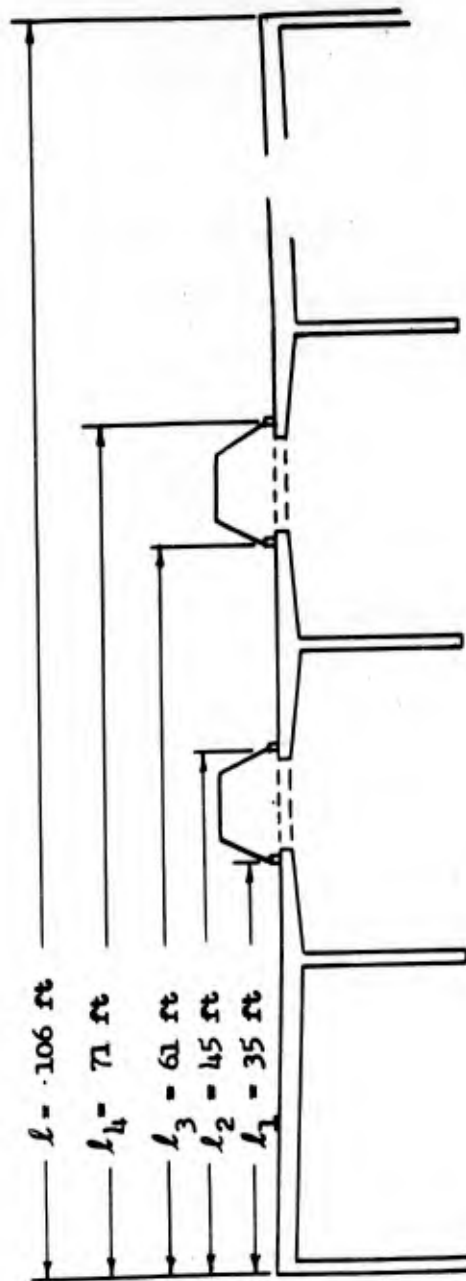
ℓ - 106 ft
ℓ_4 - 72 ft
ℓ_3 - 61 ft
ℓ_2 - 45 ft
ℓ_1 - 35 ft

Fig. B.4.2   Side View of Building 3.3.4

and roof.

To insure a more continuous discussion of the development of the methods, a few topics of general applicability to other structures were presented in Section E.2.2.1. These topics will be used in the following development.

E.4.2.1 Pressures on Front and Back Walls

The average pressures on the outside and inside of the front and back walls of building 3.3.4 are shown in Figs. E.4.3 to Fig. E.4.6.

The method of computing loadings on these surfaces is identical with that on buildings 3.3.3 and 3.3.8h (Figs. E.4.3 to E.4.6 correspond to Figures E.2.6 to E.2.9), and hence the discussion in Section E.2.2 applies for these walls. For building 3.3.4, however, the front wall opening ratio is larger than that of buildings 3.3.3 and 3.3.8h. Therefore, the pressure on the inside front wall builds up to $p_i(t)$ (Fig. E.4.4) rather than to $p_i(0) = p_{\sigma i}$ (Fig. E.2.7) as was the case with the previous buildings. The equation for $p_i(t)$ (see Fig. E.4.4) is based on Section E.2.2.1.6. It is the pressure at all points behind the inside shock wave; and builds up linearly from $p_{\sigma i}$ at $t = 0$ to $p_\sigma(0)$ at $t = \dfrac{\ell_4}{U}$, i.e. when the wave front has reached the third roof section.

E.4.2.2 Pressures on Flat Roof

First roof section: The outside pressure on this surface is shown in Fig. E.4.7. Essentially, the computational scheme follows the outline of Fig. E.5.29 Vol I ("minimum turbulence" pressure
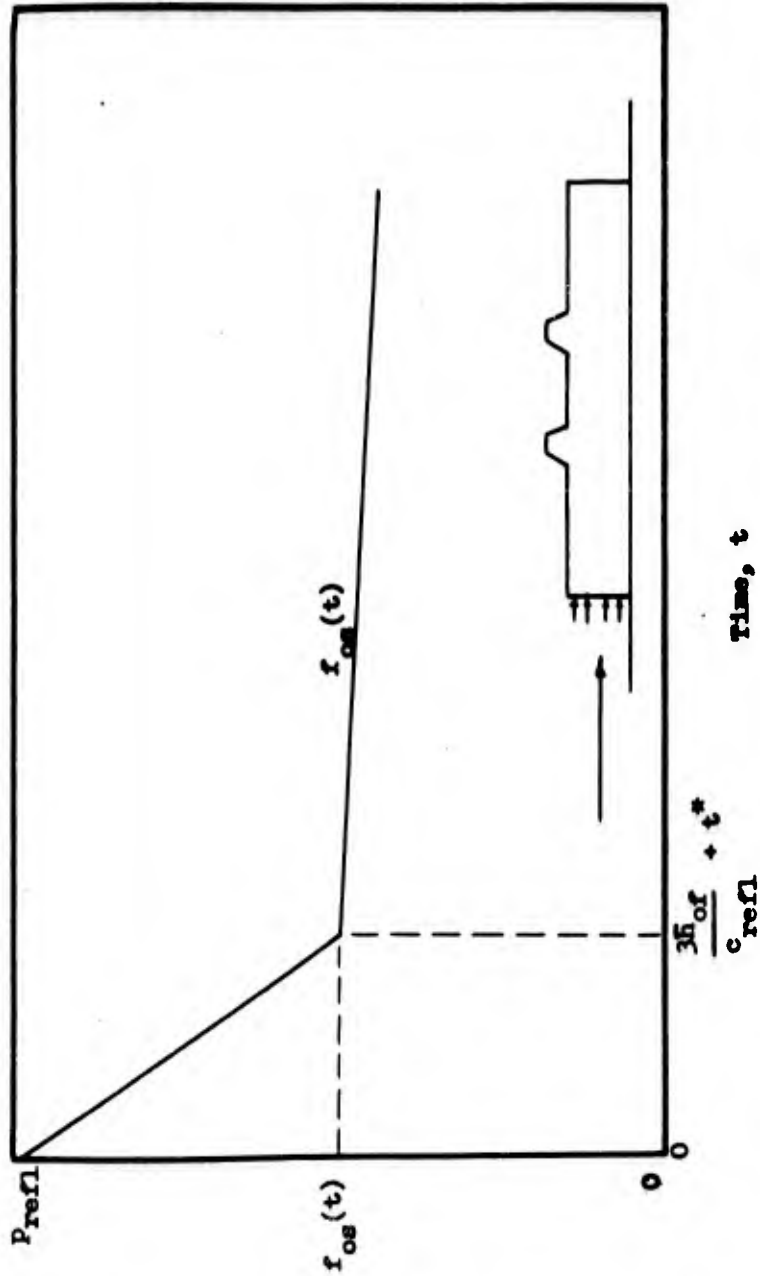
Fig. B.4.3   Predicted Average Pressures on Outside Front Wall of Building 3.3.4
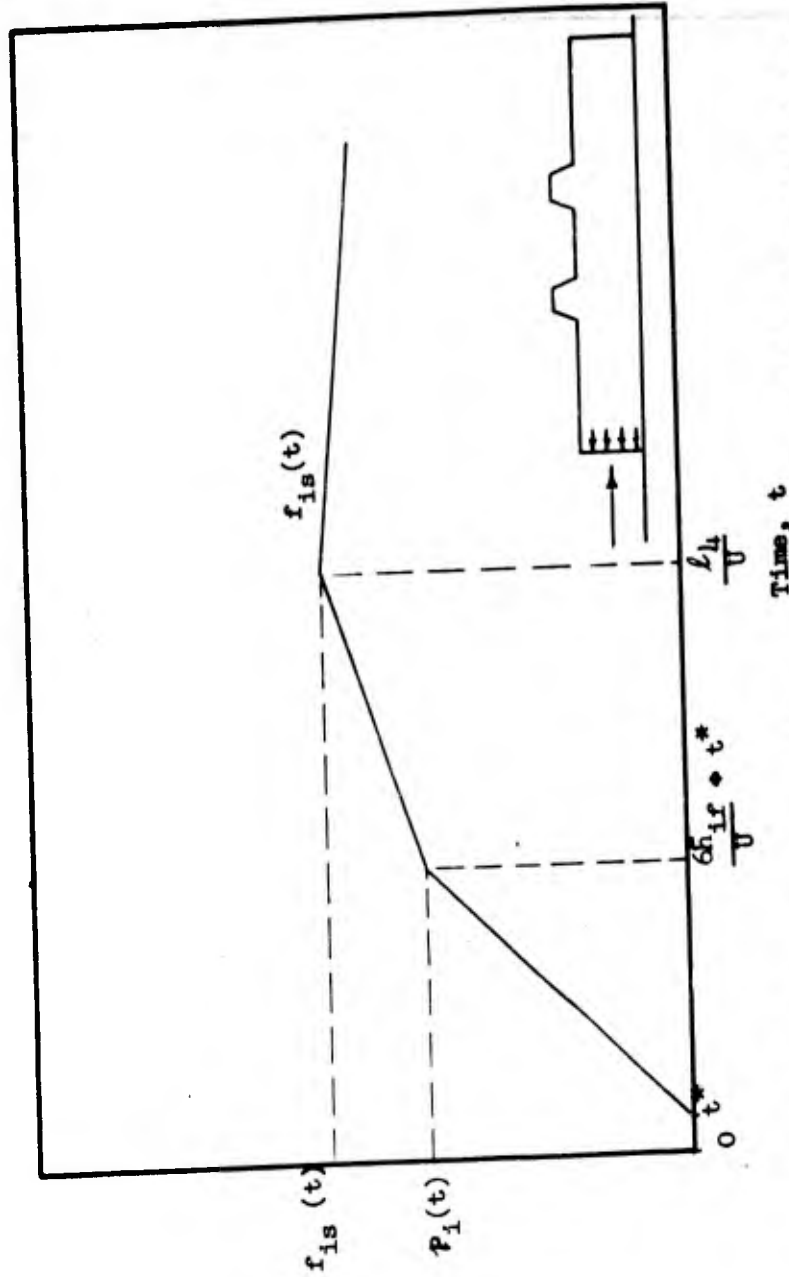
Fig. E.4.4 Predicted Average Pressures on Inside Front Wall of Building 3.3.4

(Note: $P_i(t) = P_{\sigma i} + \left[P_\sigma(0) - P_{\sigma i} \right] \frac{Ut}{\ell_4}$)

- 169 -
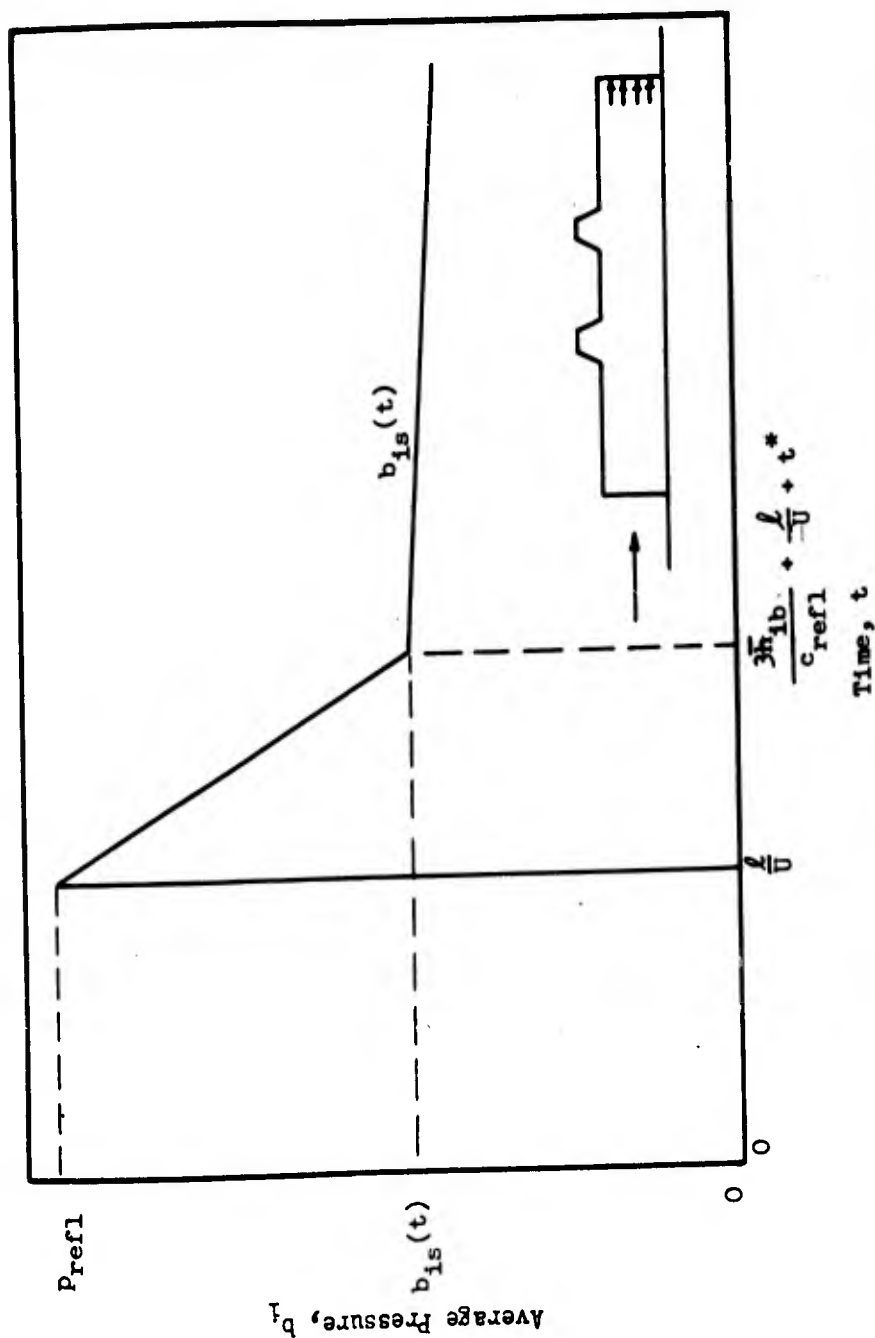
Fig. E.4.5   Predicted Average Pressures on Inside of Back Wall of Building 3.3.4
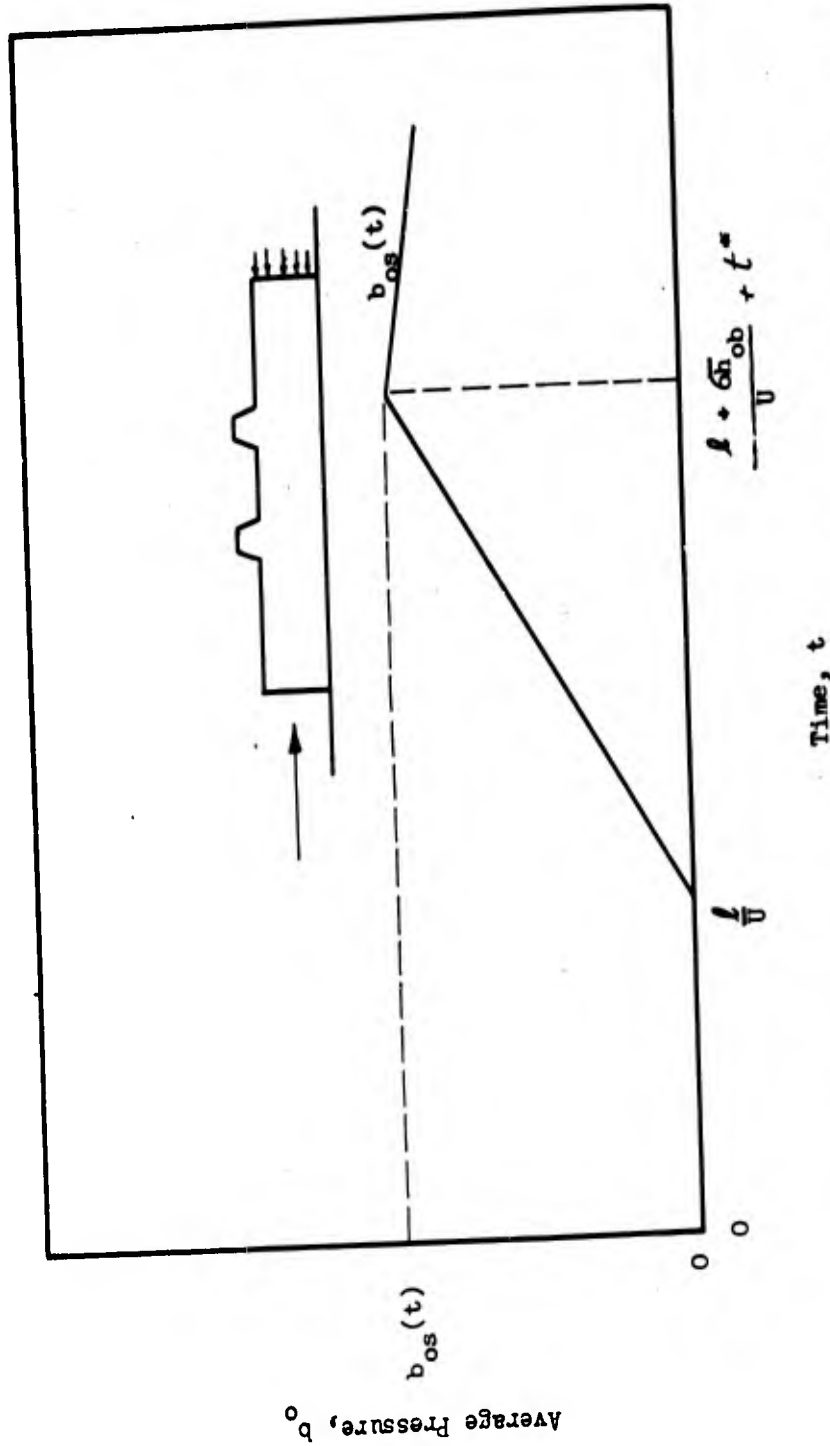
Fig. 3.4.6   Predicted Average Pressures on Outside Back Wall of Building 3.3.4

on the top of a solid rectangular block). The pressure is assumed to
build up linearly from zero at t = 0 to pseudo steady state for this sur-
face at t = l_1/U, at which time the wave front has covered the first
roof section (note the appropriate time shift indicated in Fig. E.4.7).
No alternative predictions for "maximum" and "minimum turbulence" are
given because it is believed that vortex and turbulence effects are
approximately the same on the outside and inside surface of the roof and
will to a large extent, cancel.

The inside pressure on the first roof section is shown
in Fig. E.4.8. The pressure build-up is based on the methods developed
in Sections E.2.2.1.2 and E.2.2.1.6. The various lags, $\Delta(x)$, shown in
Fig. E.4.8 are computed from Equation E.2.2 (Section E.2.2.1.2), and the
value of $p_i(t)$ is obtained from the equation in Fig. E.4.4. The pressure
is zero until the curved inside wave has reached the roof; then it rises
linearly to $p_i(t)$ by the time the inside wave front has reached the end
of the first roof section. Pseudo steady state pressure for that surface
(note the appropriate time shift) is reached when both inside and out-
side wave fronts have reached the beginning of the third roof section.

Second roof section: The outside pressure on the
second roof section is shown in Fig. E.4.9. Except for appropriate
time shifts, the method is identical with that used for computing pressures
on the outside of the first roof section (see Fig. E.4.7). In the time
the outside wave front covers the second roof section the pressure builds
up linearly from zero to pseudo steady state pressure for that surface
and follows the pseudo steady state pressure from that time on.

The inside pressures on the second roof section are shown in Fig. E.4.10. Except for appropriate time shifts the method corresponds exactly to that developed for the underside of the first roof (see Fig. E.4.8). The pressure is zero until the inside wave has reached the second roof section; then it rises linearly to inside pressure $p_i(t)$ by the time the inside wave has reached the end of the second roof section. Pseudo steady state pressure for this surface is established when both inside and outside wave fronts have reached the beginning of the third roof section.

Third roof section: The average pressures on the third roof section are illustrated in Fig. E.4.11. Since the inside and outside waves are taken to be equal in pressure and to coincide when they reach the beginning of the third roof section there is no net pressure on this section of the roof until reflection of the inside wave from the back wall takes place. This reflection imposes an upward thrust on the roof which has been described in detail in Section E.2.2.1.3. The computational scheme follows the outline of Fig. E.2.5. Again the time shift l/U is included to allow for the shock front reaching the back wall.

E.4.3 NUMERICAL COMPUTATION OF LOADING

E.4.3.1 Loadings on Total Building

The calculation of forces and average pressures on building 3.3.4 is based on the computational methods developed in Section E.4.2. The results from that section which are needed here are
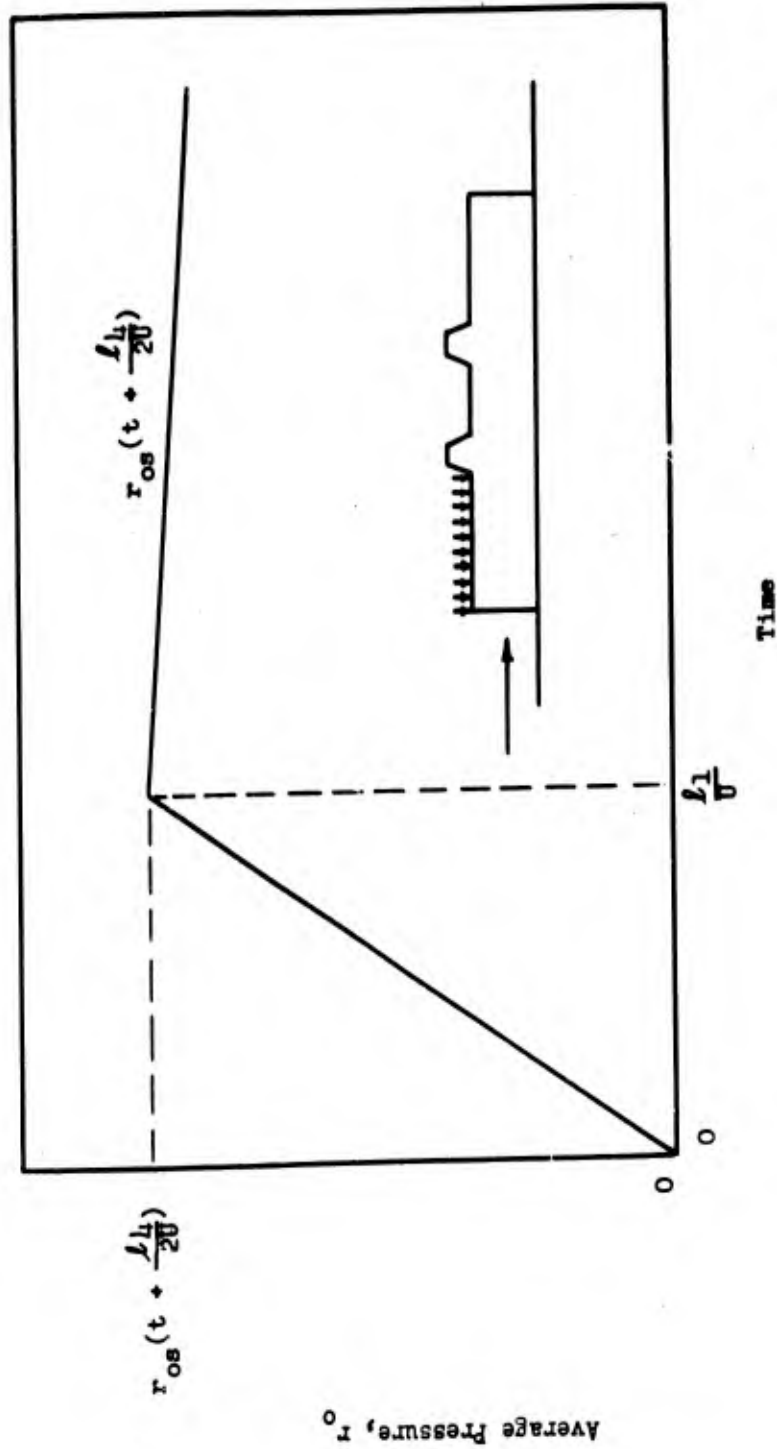
Fig. E.4.7 Predicted Average Pressure on Outside of First Roof Section of Building 3.3.4
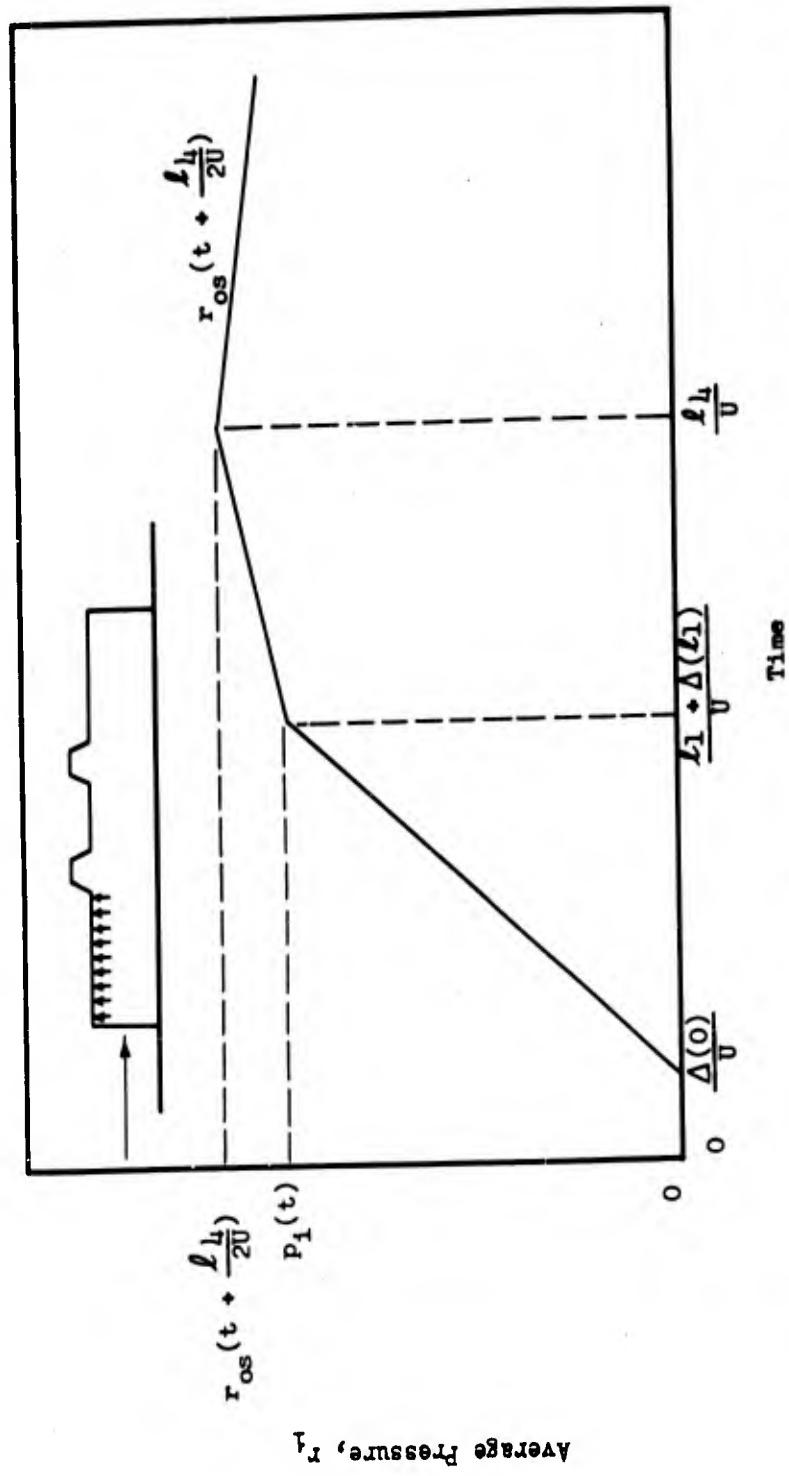
Fig. E.4.8   Predicted Average Pressure on Inside of First Roof Section of Building 3.3.4

repeated in Tables E.4.2, E.4.4, E.4.6, E.4.8, and E.4.10 in the columns
labeled "Symbolic". These data are also given in Figs. E.4.3-E.4.11.
The side-on pressure and drag pressure throughout the 3.55-psi shock
wave which strikes the structure are plotted in Fig. E.4.12. These
were computed from Vol I, Eq. E.4.16 and Fig. E.4.3, respectively.

Table E.4.1 lists the numerical values of all other
quantities necessary for computation of loadings on individual components
and on the total structure according to shock constants, geometric
constants, and geometric and shock constants.

The shock quantities are various numerical values which
are independent of the geometry of the building. Among these are the
following specified numbers: shock strength, ξ ; the duration of the
wave, t_o, and atmospheric pressure, P_o. Under the same heading certain
important derived quantities are listed. These are: the velocity of
the shock front, U; the reflected pressure, p_{refl}; and the velocity of
sound in the reflected region, c_{refl}; (see Fig. E.4.2, Vol I).

The geometric constants necessary for the computation
of loadings on the structure include the following: the structural dimen-
sions, ℓ, ℓ_1, ℓ_2, ℓ_3, ℓ_4, as shown in Fig. E.4.2; the distance, e, from
the center of a window in the front wall to the roof; the mean relief
distances, $\bar{h}_{of}$, on the outside of the front wall and $\bar{h}_{ib}$ on the inside
of the back wall; the mean build-up distances: $\bar{h}_{if}$, on the inside of
the front wall and $\bar{h}_{ob}$ on the outside of the back wall; the net areas A_f,
A_b, A_{r_1}, A_{r_2}, and A_{r_3} of the front wall, back wall and the three
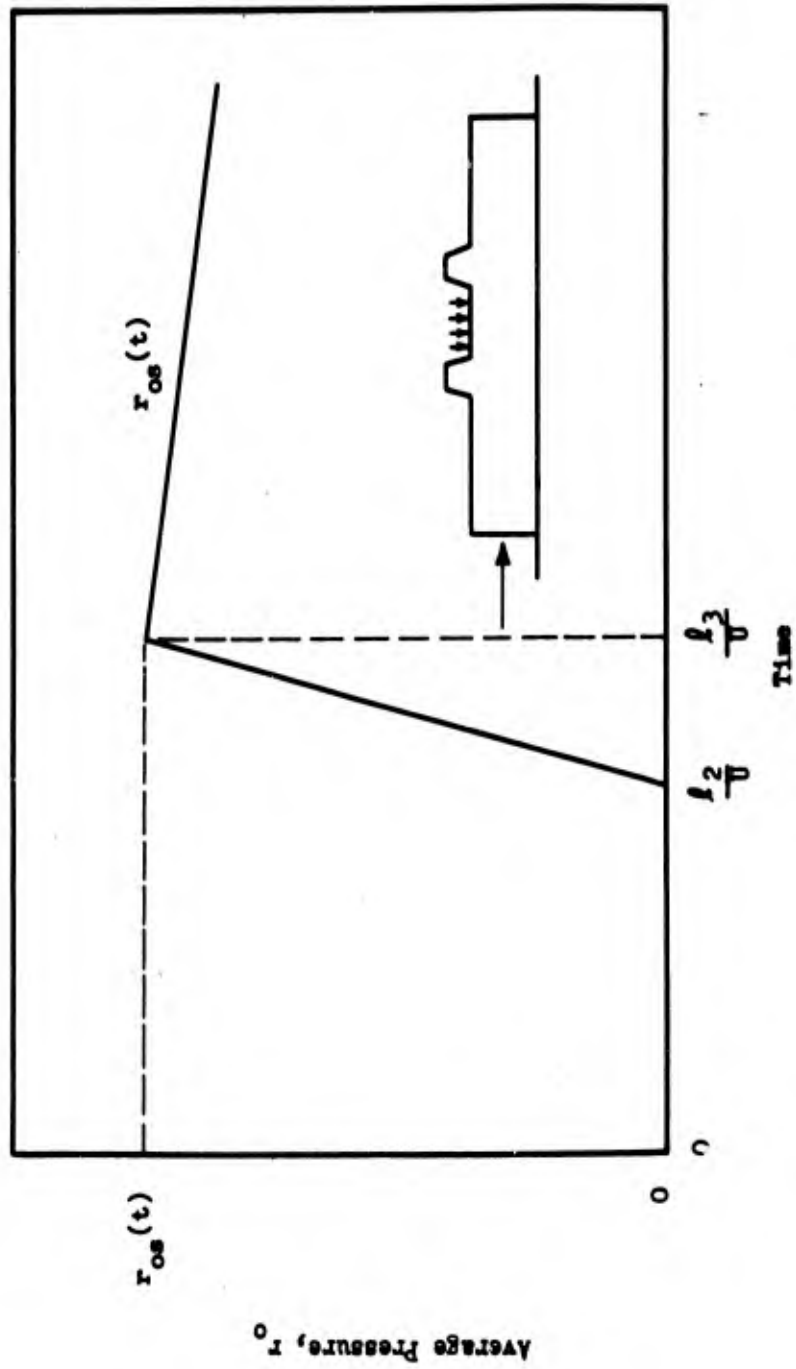
Fig. E.4.9   Predicted Average Pressure on Outside of Second Roof Section of Building 3.3.4
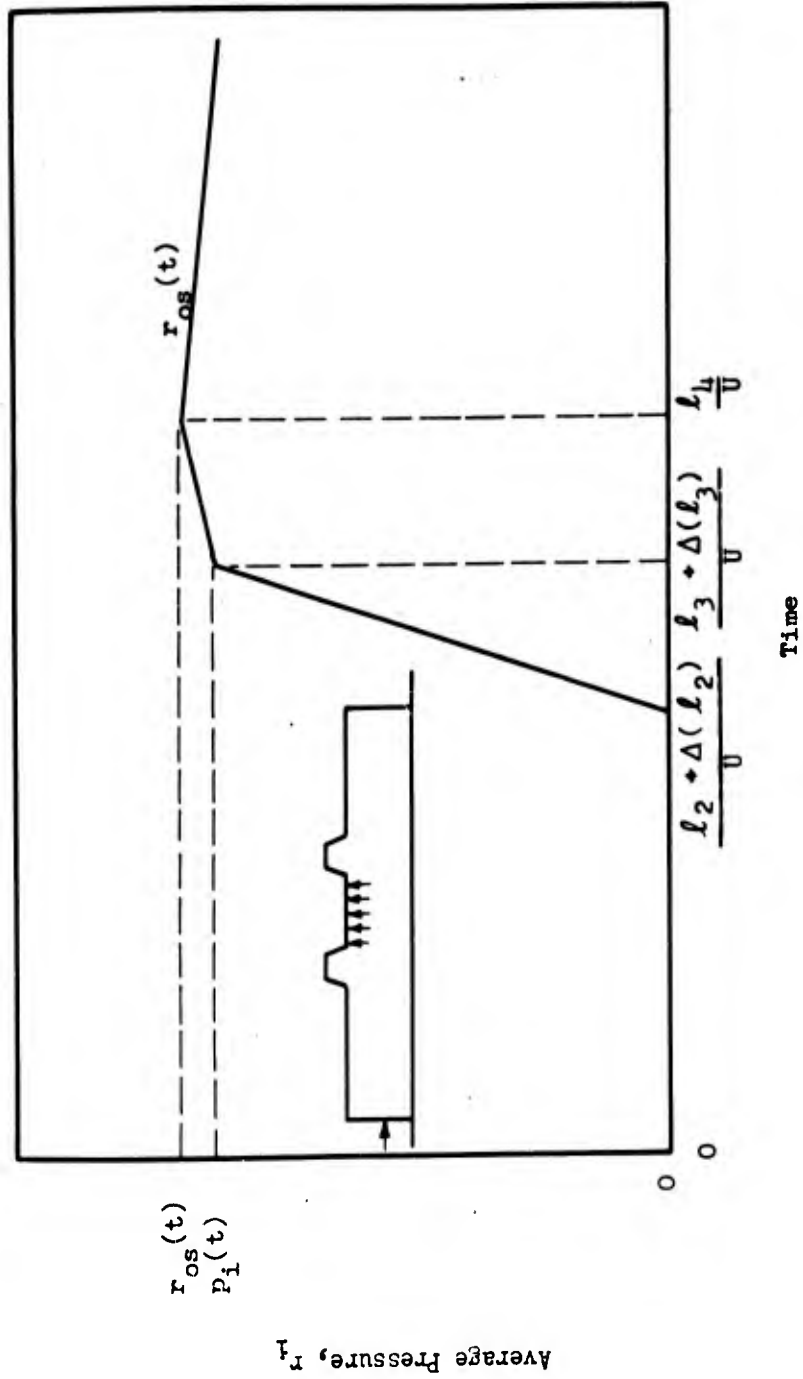
Fig. E.4.10 Predicted Average Pressure on Inside of Second Roof Section of Building 3.3.4
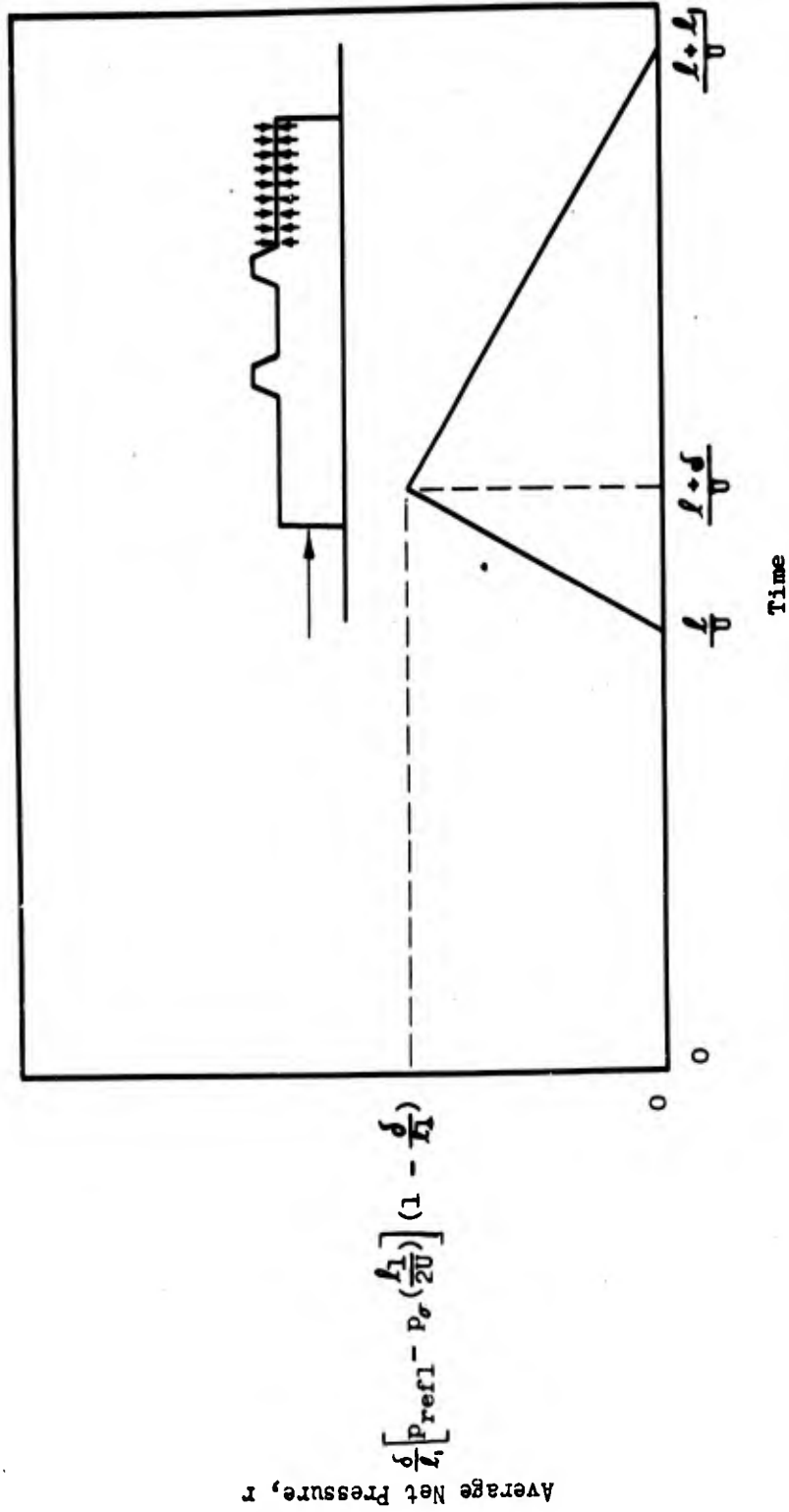
Fig. E.4.11 Predicted Average Net Pressure on Third Roof Section of Building 3.3.4

sections of roof, respectively; and the ratio of wall, window, and door area to the gross wall area of front and back walls, Ω. The quantities $\bar{h}_{of}$, $\bar{h}_{ib}$, $\bar{h}_{if}$, and $\bar{h}_{ob}$ are computed as described in Section E.2.2.1.7.

The combined geometric and shock constants are certain characteristic time units which underlie the calculations, such as ℓ_1/U, ℓ/U, etc.; the inside shock overpressure, $p_{\sigma i}$, computed from the equation $p_{\sigma i} = p_o (\xi_i - 1)$ where ξ_i is read by interpolation from Fig. E.5.4 Vol I; and the drag coefficients on the outside and inside of the front wall, C_{fo} and C_{fi}, on the outside and inside of the back wall, C_{bo} and C_{bi}, and on the roof, C_{ro}, all obtained from Section E.1.3.2. These drag coefficients are used to compute the pseudo steady state pressures f_{os}, f_{is}, etc., from Eqs. E.1.1-E.1.3. Also given are the lag between the outside and inside shock fronts at a distance x from the front wall, $\Delta (x)$, obtained from Eq. E.2.2, the length of the shock wave reflected from the back wall, δ, from Eq. E.2.4, Section E.2.2.1.3 and t^*, the window-breaking time, obtained from Section E.8.1.2.

The expression

$$p_i(t) = p_{\sigma i} + \left[p_\sigma(0) - p_{\sigma i}\right] \frac{Ut}{\ell_4}$$

from Fig. E.4.4 is needed for certain of the tables.

The constants of Table E.4.1 are used to compute the average pressures and forces on the 3.3.4 structure as shown in Tables E.4.2-E.4.10. In the left-hand columns of these tables under the heading "Symbolic" are listed the discrete values of time at which pressures are

computed. These symbolic values are deduced in Section E.4.2 (see Figs. E.4.3-E.4.11) and are listed until such times when wind forces alone constitute the net force on a particular component. These wind forces are predicted to be equal to zero in some instances. In the right-hand columns of this group of tables, the numerical values of the average pressures on each side of the front wall, back wall, and roof are shown.

The remaining tables give the numerical values of the net pressure differences and forces until the end of the positive phase. Where intermediate points between those shown in the first group of tables are needed, linear interpolation has been used. Once the force acting on each member becomes purely wind force, only the net average pressure (total drag coefficient times p_d) is computed. For the front wall the total drag coefficient, C_{df}, $= C_{fo} - C_{fi} = 1$, whereas for the back wall $C_{db} = C_{bo} - C_{bi} = -1$.

The superscripts "-" and "+" shown on certain values of time in the tables indicate that the pressure or force undergoes a sudden change. The symbol "*" at a certain value of time in tables showing the final results indicates that until that time, the force-time relation is considered to be linear between given points, and after that time it follows a smooth curve through the given points.

Tables E.4.2-E.4.5 give the average pressures on both sides of front and back wall, as well as the net average pressures and forces on these walls. Their symbolic columns were deduced from Figs. E.4.3-E.4.6.

Tables E.4.6-11 give the pressures and forces on all three sections of the flat roof. Outside, inside, and net pressures are given on the first and second sections of the roof. The wave reflected from the back wall causes an upward thrust on the third roof section and only net pressures are given. The symbolic notations for these tables were deduced from Figs. E.4.7-E.4.11.

Figures E.4.13-E.4.20 give the loadings computed in Tables E.4.2-E.4.11 for the early period of the blast wave.

As discussed more fully in Section E.1.4-2, the calculated forces are only approximate.

Slide rule calculations were used throughout these computations and in each result listed, the third figure has no significance.

E.4.3.2   Component Computation

Section of front wall: A section unsupported by columns and located between two windows of the front wall of building 3.3.4 is chosen for analysis of failure. Since this panel is probably the weakest portion of the wall, the rest of the wall can be expected to stand if this panel stands.

The loading on this panel is about the same as that on the entire front wall, since the relief time is roughly the same as the average relief time on the total front wall. Hence, the net average pressures on the front wall of building 3.3.4, listed in Table E.4.3 and Fig. E.4.13, are chosen as forcing functions for the response calculations carried out in Part II for this section of the front wall.

TABLE E.4.1

Constants for Building 3.3.4

Shock Constants	
$p_\alpha(0)$ = 3.55 psi	c_{refl} = 1185 fps
U = 1228 fps	P_o = 14.7 psi
ζ = 1.25	t_o = 1.41 sec
P_{refl} = 7.82 psi	

Geometric Constants	
ℓ = 106 ft	Ω = 0.40
ℓ_1 = 35 ft	$A_f = A_b$ = 96,900 sq in.
ℓ_2 = 45 ft	$A_{r_1} = A_{r_2}$ = 282,240 sq. in.
ℓ_3 = 61 ft	A_{r_3} = 124,900 sq in.
ℓ_4 = 71 ft	
$\bar{h}_{of}$ = 2.4 ft	$\bullet$ = 9 ft
$\bar{h}_{1f}$ = 2.92 ft	
$\bar{h}_{1b}$ = 2.92 ft	
$\bar{h}_{ob}$ = 2.4 ft	

TABLE E.4.1 (CONTD)

Constants for Building 3.3.4

Combined Shock and Geometric Constants	
$\dfrac{\ell_0}{U}$ = 0.0865 sec	$\Delta(0)$ = 11 ft
	$\Delta(\ell_1)$ = 5.6 ft
$\dfrac{\ell_1}{U}$ = 0.029 sec	$\Delta(\ell_2)$ = 4.03 ft
$\dfrac{\ell_2}{U}$ = 0.037 sec	$\Delta(\ell_3)$ = 1.55 ft
$\dfrac{\ell_3}{U}$ = 0.05 sec	δ = 9.05 ft
	t^* = 0.002 sec
$\dfrac{\ell_4}{U}$ = 0.058 sec	
	ξ_1 = 1.22
$\dfrac{h_{of}}{c_{refl}}$ = 0.002 sec	p_{σ_1} = 2.31 psi
$\dfrac{h_{1f}}{U}$ = 0.0025 sec	$c_{fo} = c_{bi}$ = 0.66
	$c_{fi} = c_{bo}$ = -0.33
$\dfrac{h_{1b}}{c_{refl}}$ = 0.0025 sec	c_{df} = 1
	c_{db} = -1
$\dfrac{h_{ob}}{U}$ = 0.002 sec	c_{ro} = -0.55

TABLE E.4.2

Average Pressures on Front Wall of Building 3.3.4

Outside

Symbolic		Numerical	
Time, t	Pressure, f_o	Time, t (sec)	Pressure, f_o (psi)
0	P_{refl}	0	7.82
$\dfrac{3t_{of}}{c_{refl}} + t^*$	$f_{os}(t)$	0.008	3.70
$\dfrac{l_4}{U}$	$f_{os}(t)$	0.058	3.45

Inside

Symbolic		Numerical	
Time, t	Pressure, f_1	Time, t (sec)	Pressure, f_1 (psi)
0	0	0	0
t^*	0	0.002	0
$\dfrac{3t_{1f}}{U} + t^*$	$p_1(t)$	0.016	2.57
$\dfrac{l_4}{U}$	$f_{1s}(t)$	0.058	3.20

TABLE E.4.3

Net Average Pressures and Forces on Front Wall

of Building 3.3.4

Time, t (sec)	Pressure			Force
	f_0 (psi)	f_1 (psi)	$f = f_0 - f_1$ (psi)	$F = f \times A_c$ (lb $\times 10^3$)
0	7.82	0	7.82	758
0.002	6.75	0	6.75	655
0.008	3.70	1.25	2.45	238
0.016	3.65	2.57	1.08	105
* 0.058	3.45	3.20	0.25	24.2
0.10			0.22	21.3
0.20			0.16	15.5
0.40			0.08	7.7
0.60			0.04	3.9
0.80			0.02	1.9
1.00			0.01	1.0
1.20				
1.41			0	0

TABLE E.4.4

Average Pressures on Back Wall of Building 3.3.4

Inside

Symbolic		Numerical	
Time, t	Pressure, b_1	Time, t (sec)	Pressure, b_1 (psi)
0	0	0	0
$\dfrac{\ell}{U}^-$	0	0.087^-	0
$\dfrac{\ell}{U}^+ + t^* + \dfrac{3F_{1b}}{c_{refl}}$	P_{refl}	0.087^+	7.82
$\dfrac{\ell}{U} + t^* + t^*$	$b_{1s}(t)$	0.096	3.70
$\dfrac{\ell}{U} + \dfrac{6h_{ob}}{U} + t^*$	$b_{1s}(t)$	0.100	3.67

Outside

Symbolic		Numerical	
Time, t	Pressure, b_0	Time, t (sec)	Pressure, b_0 (psi)
0	0	0	0
$\dfrac{\ell}{U}$	$b_{os}(t)$	0.089 / 0.100	0 / 3.38
$\dfrac{\ell}{U} + \dfrac{6h_{ob}}{U} + t^*$			

TABLE E.4.5

Net Average Pressures and Forces on Back Wall of Building 3.3.4

| Time, t (sec) | Pressure | | | Force |
	b_1 (psi)	b_o (psi)	$-b = b_1 - b_o$ (psi)	$-B = -b \, A_b$ (lb $\times 10^3$)
0	0	0	0	0
0.087^-	0	0	0	0
0.087^+	7.82	0	7.82	758
0.089	7.00	0	7.00	680
0.096	3.70	2.10	1.60	155
*0.1	3.67	3.38	0.22	28.
0.2			0.20	19.5
0.4			0.10	9.7
0.6			0.06	5.8
0.8			0.03	2.9
1.0			0.01	1.0
1.2			~	~
1.5			0	0

TABLE B.4.6

Average Pressures on First Roof Section of Building 3.3.4

Outside

Symbolic		Numerical	
Time, t	Pressure, r_o	Time, t (sec)	Pressure, r_o (psi)
0	0	0	0
$\dfrac{l_1}{u}$	$r_{os}\left(t + \dfrac{l_4}{2u}\right)$	0.029	3.28
$\dfrac{l_4}{u}$	$r_{os}\left(t + \dfrac{l_4}{2u}\right)$	0.058	3.15

Inside

Symbolic		Numerical	
Time, t	Pressure, r_1	Time, t (sec)	Pressure, r_1 (psi)
0	0	0	0
$\dfrac{\Delta(0)}{u}$	0	0.009	0
$\dfrac{l_1 + \Delta(l_1)}{u}$	$p_1(t)$	0.033	2.80
$\dfrac{l_4}{u}$	$r_{ns}\left(t + \dfrac{l_4}{2u}\right)$	0.058	3.15

TABLE E.4.7

Net Average Pressures on First Roof Section of Building 3.3.4

Time, t (sec)	r_0(psi)	r_1(psi)	$r = r_0 - r_1$ (psi)
0	0	0	0
0.009	1.03	0	1.03
0.029	3.28	2.32	0.96
0.033	3.23	2.80	0.43
0.058	3.15	3.15	0

TABLE E.4.8

Average Pressures on Second Roof Section of Building 3.3.4

Outside

Symbolic		Numerical	
Time, t	Pressure, r_o	Time, t (sec)	Pressure, r_o (psi)
0	0	0	0
$\dfrac{l_2}{U}$	0	0.037	0
$\dfrac{l_3}{U}$	$r_{os}(t)$	0.050	3.30
$\dfrac{l_4}{U}$	$r_{os}(t)$	0.058	3.26

Inside

Symbolic		Numerical	
Time, t	Pressure, r_1	Time, t (sec)	Pressure, r_1 (psi)
0	0	0	0
$\dfrac{l_2 + \Delta(l_2)}{U}$	0	0.040	0
$\dfrac{l_3 + \Delta(l_3)}{U}$	$p_1(t)$	0.051	3.10
$\dfrac{l_4}{U}$	$r_{os}(t)$	0.058	3.26

TABLE E.4.9

Net Average Pressures on Second Roof Section of Building 3.3.4

Time, t (sec)	r_o (psi)	r_1 (psi)	$r = r_o - r_1$ (psi)
0	0	0	0
0.037	0	0	0
0.040	0.75	0	0.75
0.050	3.30	3.10	0.20
0.058	3.26	3.26	0

TABLE E.4.10

Net Average Pressures on Third Roof Section of Building 3.3.4

Symbolic		Numerical	
Time, t	Pressure, r	Time, t (sec)	Pressure, r (psi)
0	0	0	0
$\dfrac{l}{U}$	0	0.087	0
$\dfrac{l + \delta}{U}$	$\dfrac{\delta}{l_1}\left[P_{refl} - P_{\!\!\!/}\left(\dfrac{l_1}{2U}\right)\right]$ $times\left[1 - \dfrac{\delta}{l_1}\right]$	0.094	-0.88
$\dfrac{l + l_1}{U}$	0	0.115	0

Plank in frontmost section of roof: The roofing of
building 3.3.4 is built up of two-by-sixes running crosswise (parallel
to the front wall). The loading on a timber 1-1/2 in. in width and
located halfway between the front wall and the front monitor will be
determined here and used in Part II to analyse for roof failure. If
a single timber with no support from adjacent timbers would not fail,
then the timbers as actually placed in this building (with toenailing to
adjacent timbers) will not be expected to fail.

From Section E.2.2.1.2, Eq. E.2.2 the lag between the
inside and outside waves at a roof plank located 17.5 ft from the front
wall is $\Delta(17.5) = 5.6$ ft and the associated lag time is $\frac{\Delta(17.5)}{U} = 0.0045$ sec.

The outside pressure is assumed to build up linearly
from zero at $\gamma = 0$ to $r_{os}(\tau - \frac{\ell}{U})$ at $\tau = \frac{1.5 \text{ in.}}{U}$ and to follow the
r_{os} curve from that time on.

The inside wave is assumed to build up linearly from
$p_{\sigma i} = 2.4$ psi (see Table E.4.1) when the shock front is at $x = 0$ to
$p_\sigma = 3.55$ psi at $x = 74$ ft; hence when the front is at $x = 17.5$ ft,
the inside pressure is 2.65 psi. The inside pressure acting on the roof
is this value minus C_{ro} times the drag pressure at the time, 17.5 ft/U,
i.e., $2.65 - 0.14 = 2.51$ psi.

The net pressure on the roof timber is taken to build
up linearly from zero at $\tau = 0$ to $r = r_{os} = 3.38$ psi at $\gamma = \frac{1.5 \text{ in.}}{U} = 0.0001$ sec. Here γ is time measured from the moment the outside shock

front reaches this point on the roof.

The pressure remains constant at 3.38 psi until $\gamma =$ $\frac{\Delta(17.5)}{U} = 0.0045$ sec. From that time on it decreases linearly to the difference between outside and inside pressures 3.38 psi - 2.51 psi = 0.87 psi at $0.0045 + 1.5$ in/U = 0.0046 sec. The inside pressure builds up to $r_{os}(t)$ at $\gamma = \frac{74-17.5}{U} = 0.0046$ sec. At this time net pressure on the timber reaches zero.

Table E.4.12 lists the net average pressures on this roof member.

One-foot planking in third roof section of building 3.3.4: The wave reflected from the inside back wall of building 3.3.4 creates a relatively high pressure on the inside of the third roof section (see Section E.1.2). Two transverse strips of the roof located between the inner bents and at different distances (1 ft and 17 ft) from the back wall are chosen to be analyzed. Strips 1 ft in width are considered.

The reflection of the inside shock wave from the back wall and the resultant net pressures on the roof near the back wall have been discussed and a method developed for net pressure computations in Eq. E.2.6.

For the given constants (i.e., $p_{refl} = 7.82$ psi, p_o $(\ell_1/2U) = 3.32$ psi, $\delta = 9.05$ ft). The net pressures listed in Tables E.4.13 and E.4.14 are obtained using the symbolic expressions of Fig. E.2.6.

TABLE E.4.11

Vertical Forces on Roof of Building 3.3.4

Time, t (sec)	1st Roof Section		2nd Roof Section		3rd Roof Section		Total Force, V (lb × 10^3)
	Pressure, r (psi)	Force, $V_1 = rA_1$ (lb × 10^3)	Pressure, r (psi)	Force, $V_2 = rA_2$ (lb × 10^3)	Pressure, r (psi)	Force, $V_3 = rA_3$ (lb × 10^3)	
0	0	0	0	0	0	0	0
0.009	1.03	291	0	0	0	0	291
0.029	0.96	271	0	0	0	0	271
0.033	0.43	121.5	0	0	0	0	121.5
0.037	0.36	102.5	0	0	0	0	102.5
0.040	0.32	90.4	0.75	94	0	0	184.4
0.050	0.15	39.5	0.20	25	0	0	64.5
0.058	0	0	0	0	0	0	0
0.087	0	0	0	0	0	0	0
0.094	0	0	0	0	-0.88	-249	-249
0.115	0	0	0	0	0	0	0

TABLE E.4.12

Net Average Pressures on Roof Timber 17.5 Ft from Front Wall

of Building 3.3.4

Time*, τ (sec)	Pressure, r, (psi)
0	0
0.0001	3.38
0.0045	3.38
0.0046	0.87
0.046	0

*Measured from time shock first reaches this timber.

TABLE E.4.13

Pressures on a Strip of the Roof One Foot Wide Located

One Foot from the Back Wall of Building 3.3.4

Time*, γ (sec)	Pressure, r, (psi)
0	0
0.0008	4.24
0.0077	3.15
0.0084	0

*Measured from the time when the shock first contacts this strip.

TABLE E.4.14

Pressures on a Strip of the Roof One Foot Wide Located

Seventeen Feet from the Back Wall of Building 3.3.4

Time*, γ (sec)	Pressure, r, (psi)
0	0
0.0008	2.16
0.0077	1.04
0.0084	0

*Measured from the time when the shock first contacts this strip.
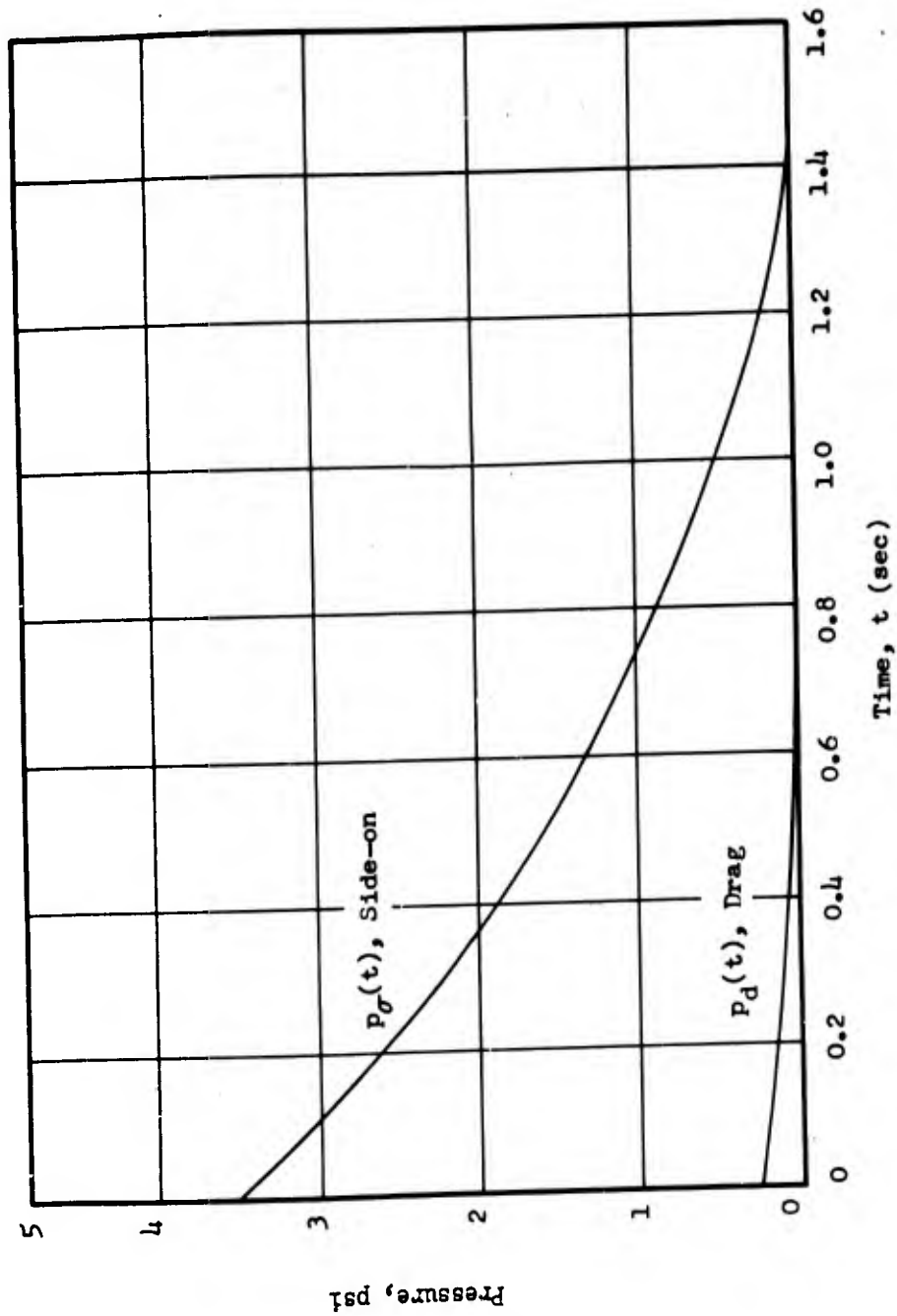
Fig. E.4.12 Side-on Pressure and Drag Pressure for Building 3.3.4 for
$p_\sigma(0) = 3.55$ psi
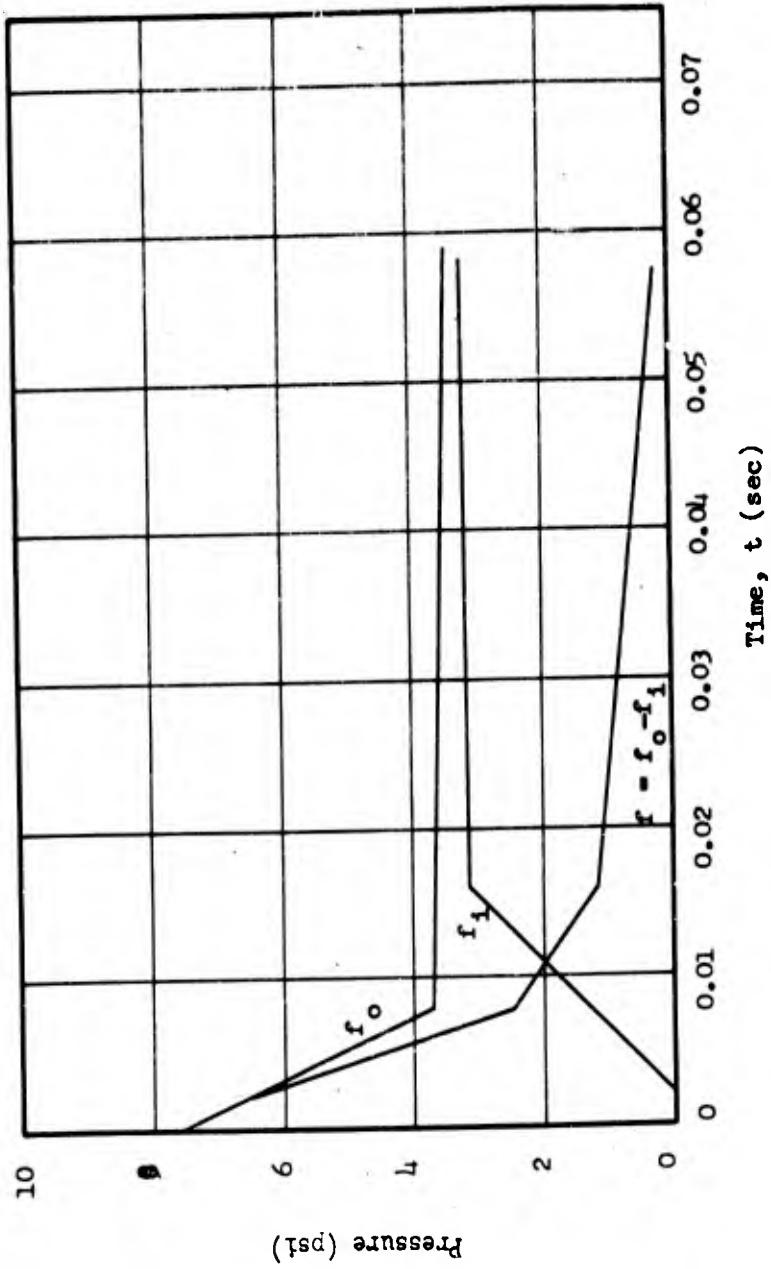
Fig. E.4.13   Pressures on Front Wall of Building 3.3.4
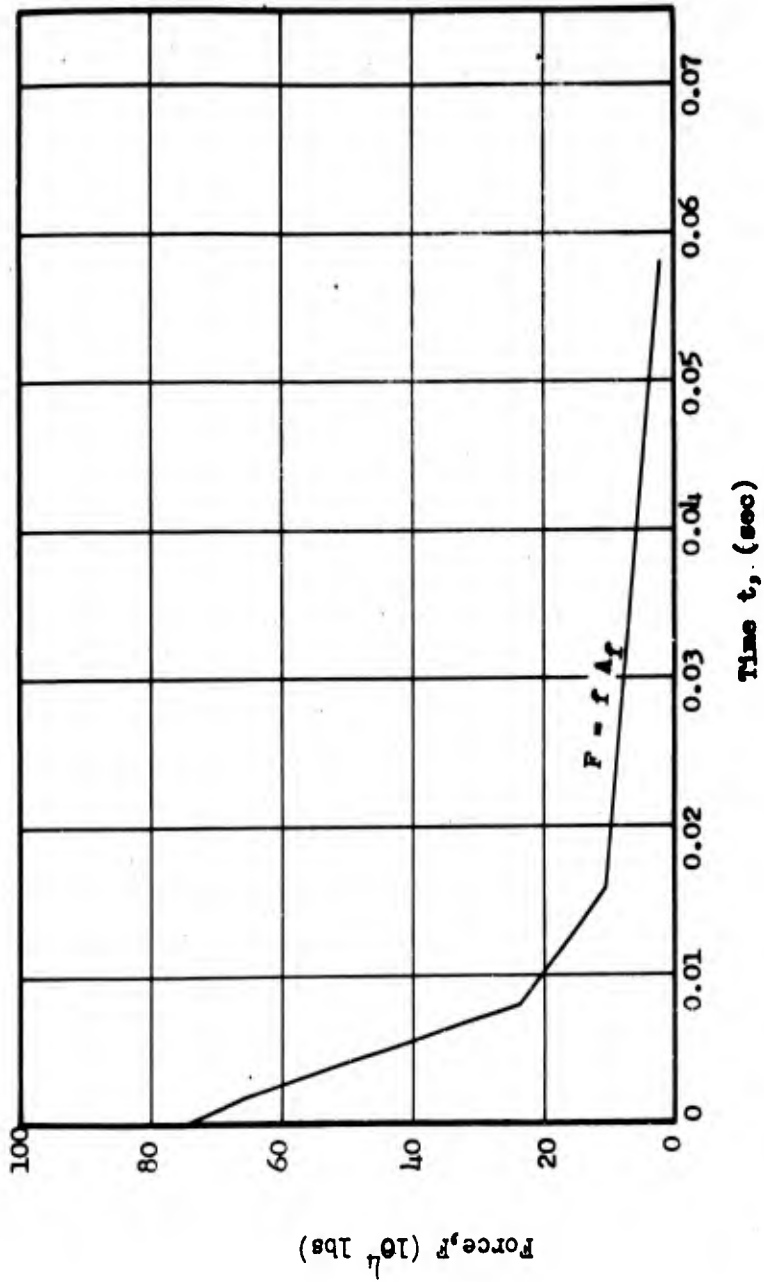
Fig. E.4.14 Force on Front Wall of Building 3.3.4
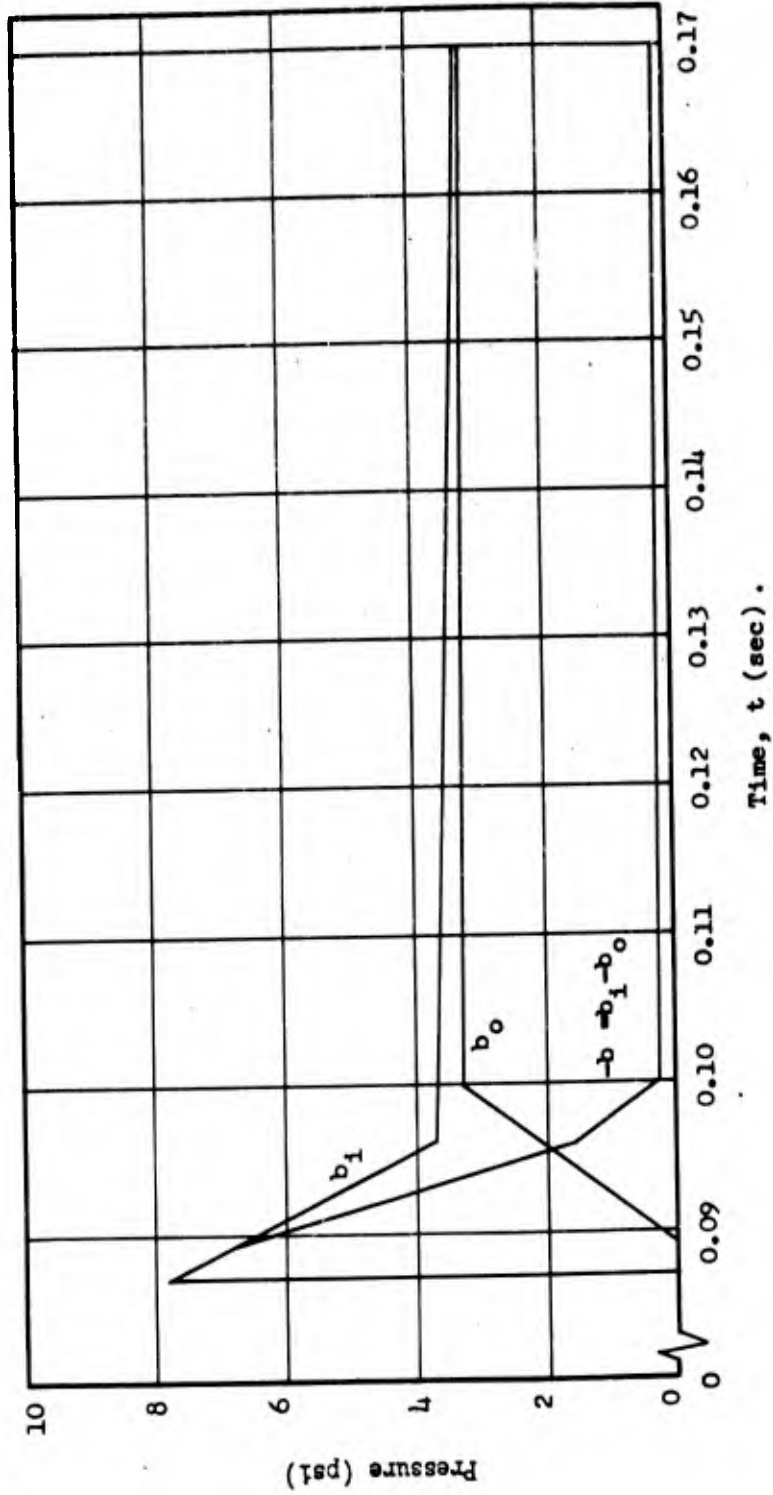
Fig. E.4.15 Pressures on Back Wall of Building 3.3.4
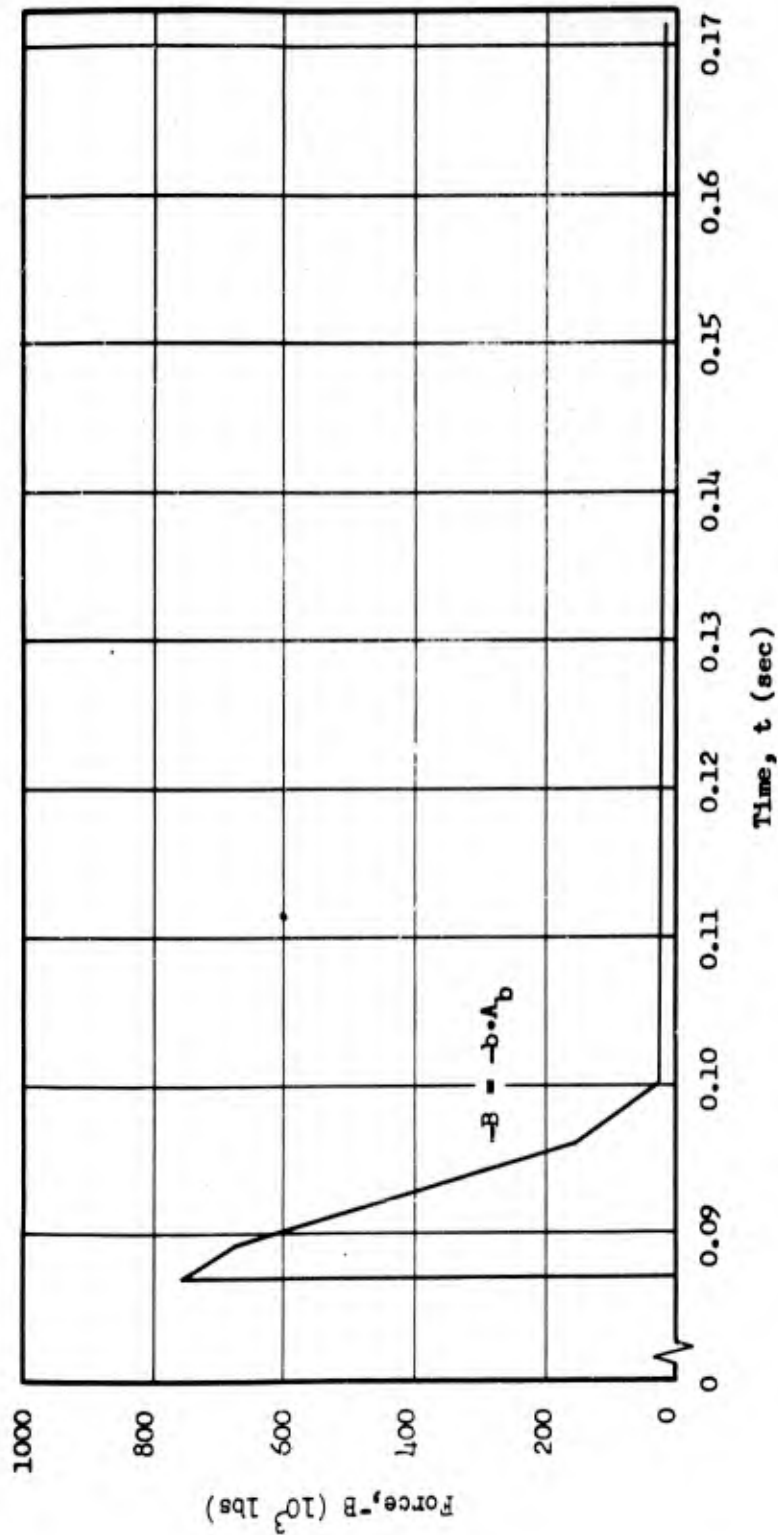
Fig. E.4.16 Force on Back Wall of Building 3.3.4
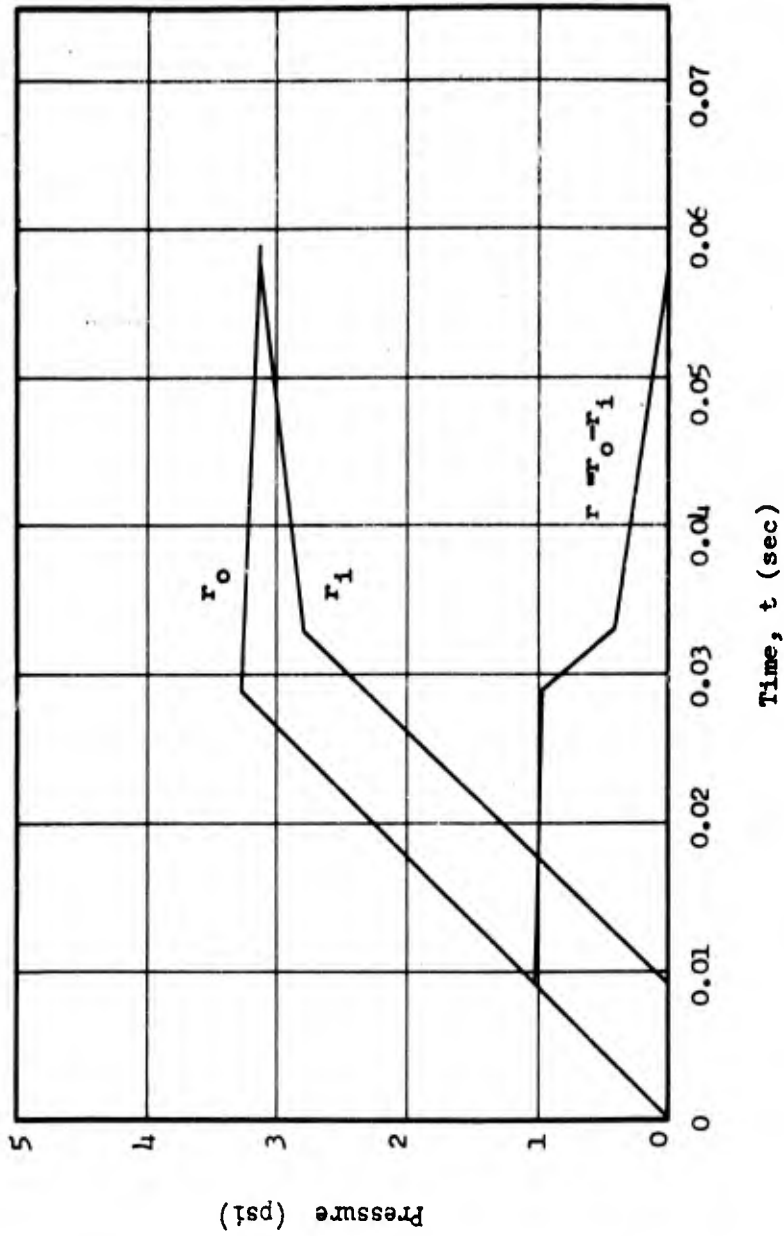
Fig. E.4.17   Pressures on First Roof Section of Building 3.3.4
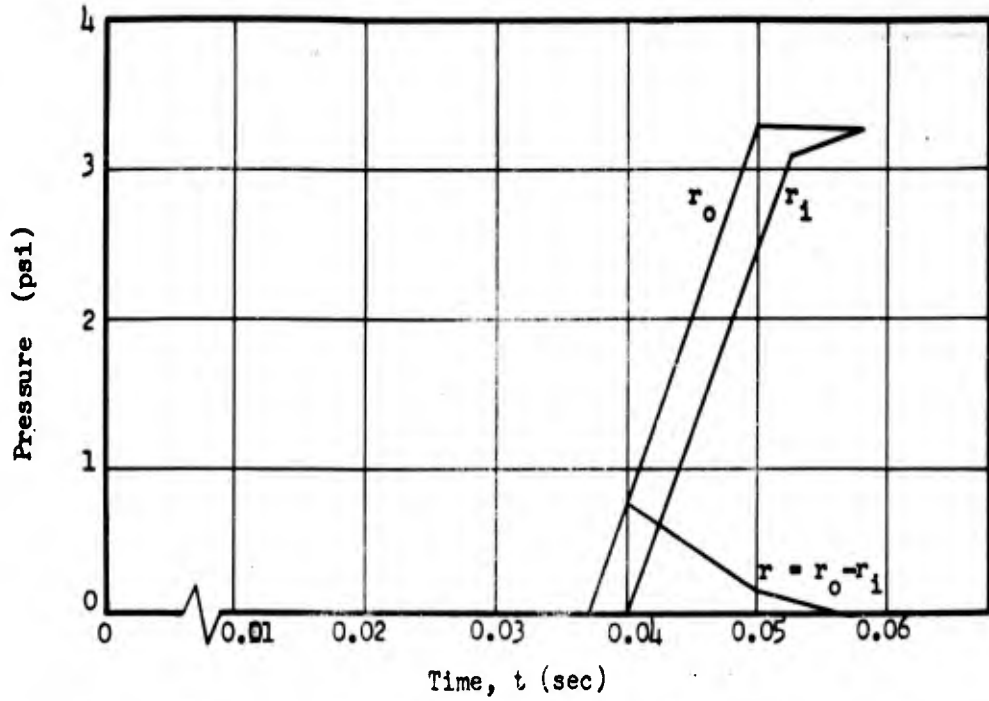
Fig. E.4.18   Pressures on Second Roof Section of Building 3.3.4
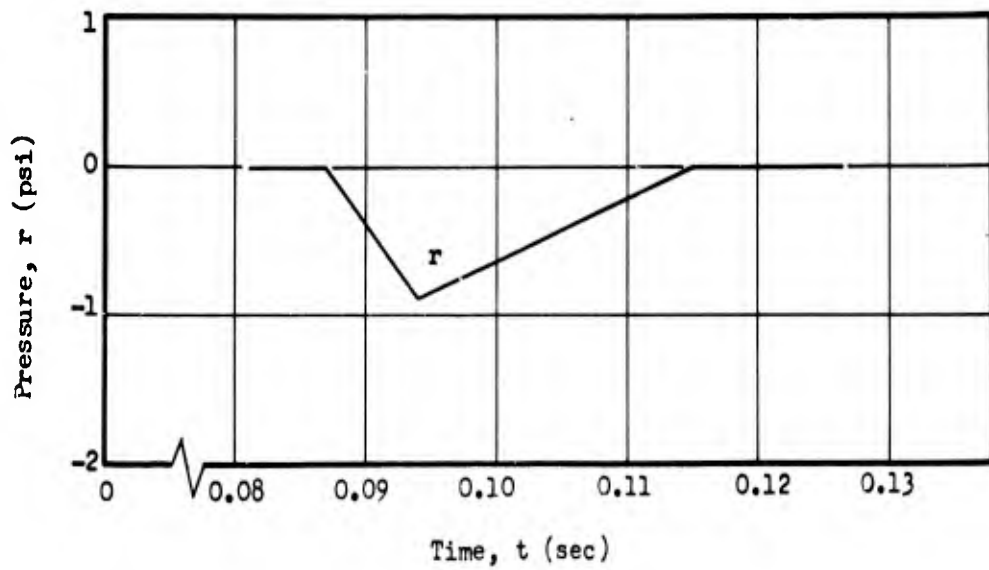
Fig. E.4.19   Pressures on Third Roof Section of Building 3.3.4

204
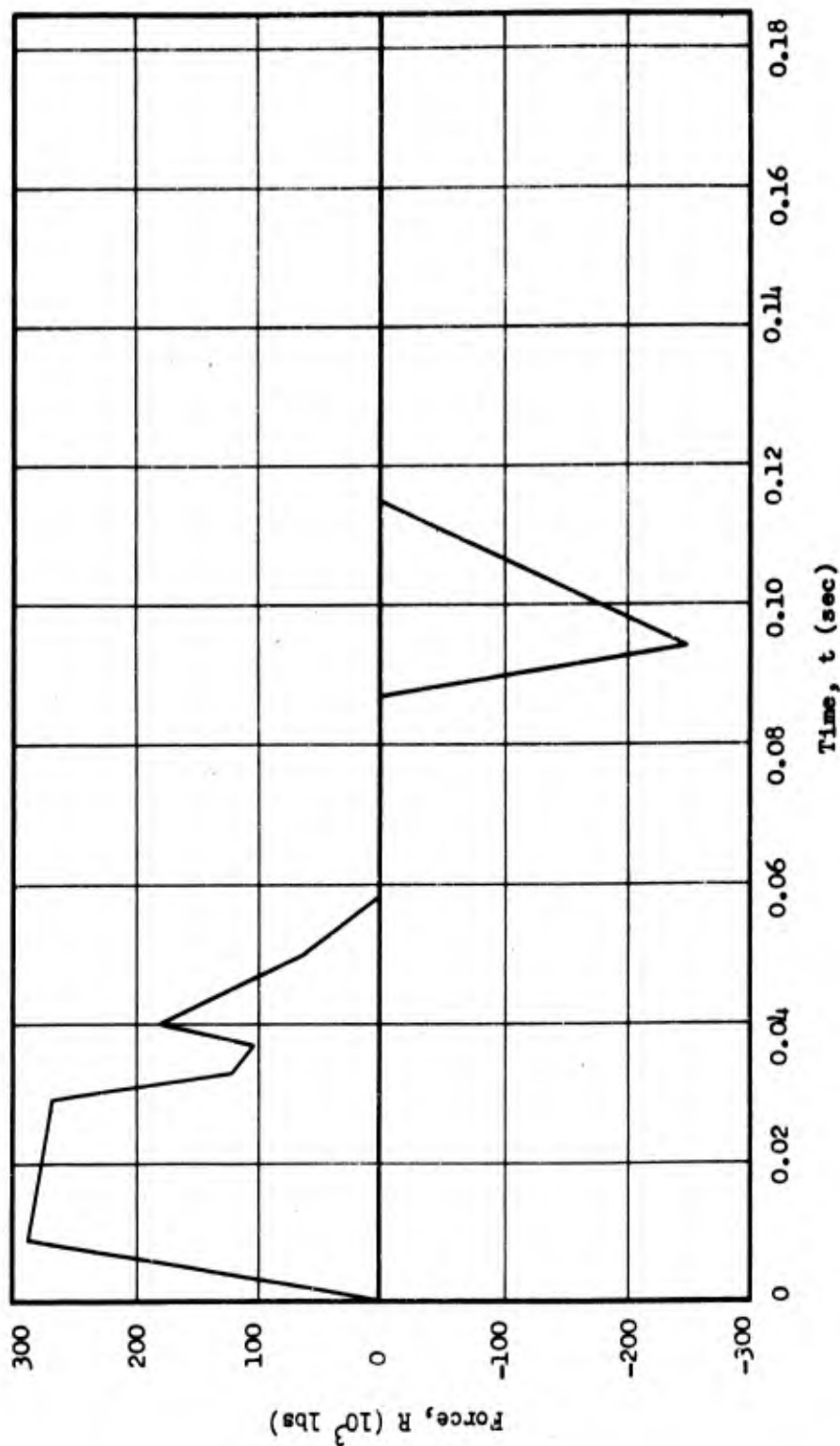
Fig. E.4.20 Force on Roof of Building 3.3.4

CHAPTER E.5

BUILDING 3.3.5b

E.5.1 GENERAL

Building 3.3.5b, as seen in Fig. E.1.3, is a load-bearing brick wall structure somewhat typical of small apartment buildings. It is struck by a shock wave of 3.75 psi peak overpressure and of 1.38 seconds duration.

Structural computations for this building are not made in Part II of this volume, since a meaningful analysis of response for such a structure is practically out of the question. Hence complete estimates of loadings are not made in this chapter; rather, sample predictions are given, mainly for the purpose of illustrating the approach which can be used in determining loadings. The predictions are confined to the determination of forces on the roof and a few typical wall sections.

All walls, roof surfaces, and partitions of the building are assumed to stand. In particular, loadings on the roof and wall surfaces are computed on the basis that these members do not fail. No response calculations are made to check these assumptions.

However, the failure of a few types of members must be recognised if the predictions are to have an illustrative meaning. The windows in the front and rear walls are assumed to break in one millisecond, the same time as for the windows of building 3.3.8h.

Some assumptions must be made about the failure of doors in
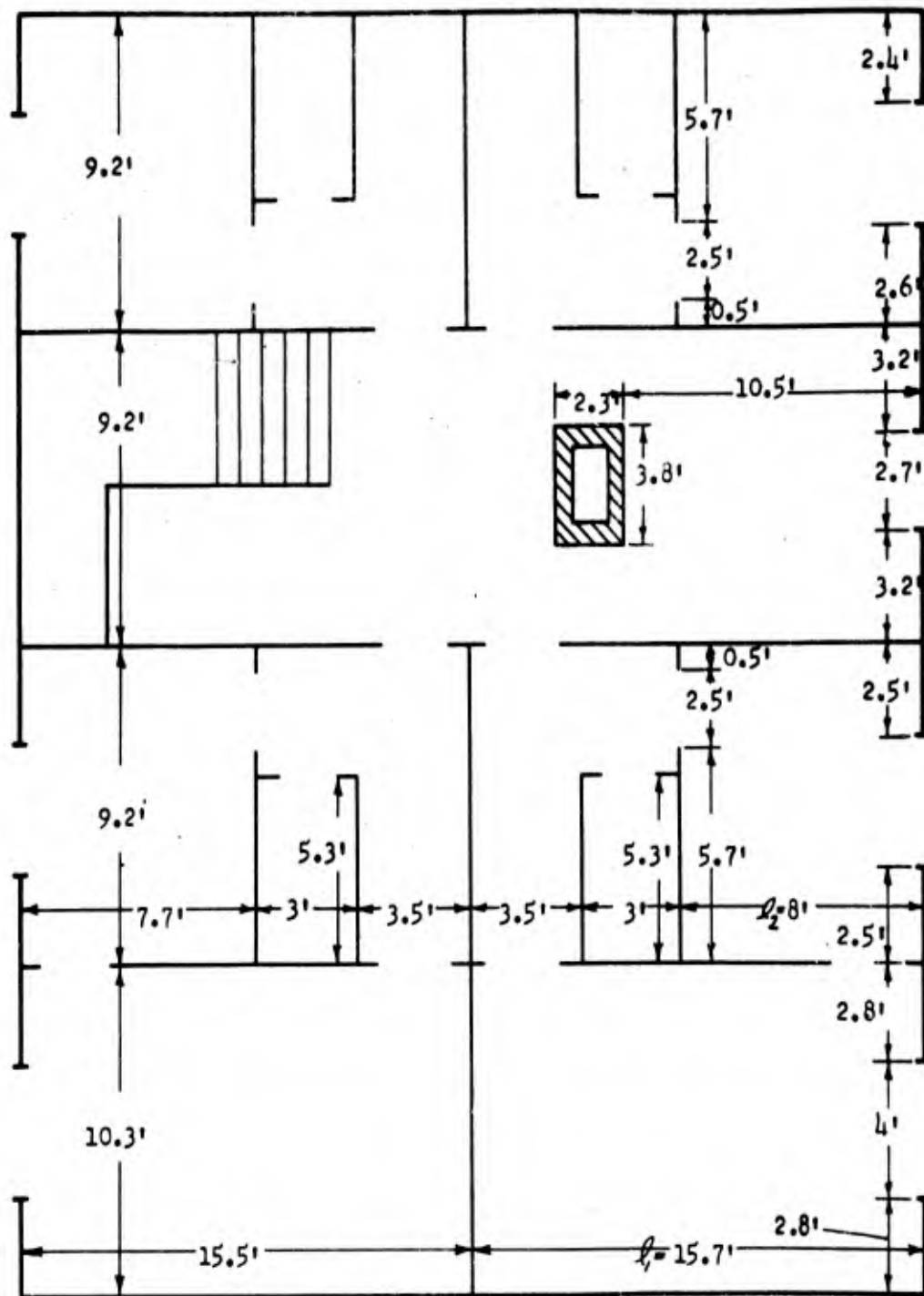
Fig. E.5.1   First Floor Plan Dimensions of 3.3.5 Type Buildings
(Right Hand wall, the front wall, is struck first)
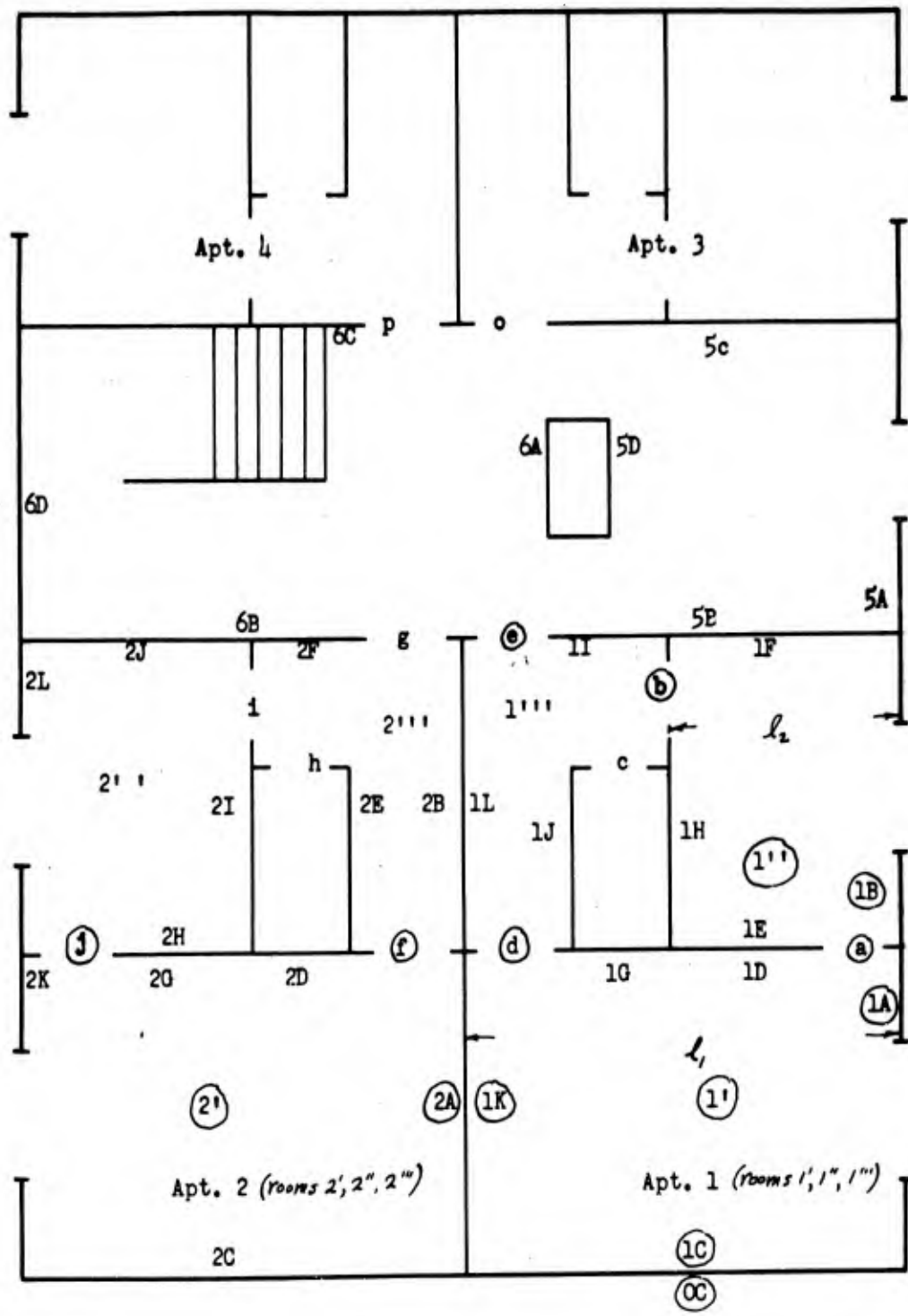
Fig. E.5.2   First Floor Plan Nomenclature of 3.3.5 Type Buildings
(Right hand wall, the front wall, is struck first)

the building. The outside (front wall) door and some of the interior doors (see Section E.5.2.2.1) are assumed to collapse. These assumptions are chosen arbitrarily in order that illustrative predictions can be carried out.

In particular, failure of doors would be quite difficult to analyze if working predictions (rather than the present illustrative ones) were to be made at this time. The possible modes of failure which would have to be treated in any paper analysis seem scarcely ammendable to such analysis. Among such modes are deflection and splitting of panels, tearing out at hinges, splitting of joints between the stiles and rails, failure of latches and failure of the jamb. Empirical data will probably be necessary in developing useful criteria for door collapse.

A qualitative discussion of the loadings on building 3.3.5b is given in Section E.1.2. That section therefore serves as an introduction to this chapter.

Floor plans of building 3.3.5b are shown in Figs. E.5.1 and E.5.2. Additional notation to be used in this chapter (beyond that given in Section E.1.4.3) follows:

b_1, b_2 ■   average pressure on a partition wall, upstream and downstream surfaces, respectively

b_{12} ■   net average pressure difference on a partition wall

back r_{os} ■   pseudo steady state pressure for the rear slope of a gabled roof

C_{so}	-	drag coefficient for the outside surface of a side wall
front r_{os}	-	pseudo steady-state pressure for the front slope of a gabled roof
front $r_0(t)$	-	average pressure on the outside front slope of a gabled roof
h_1	-	distance from the eaves to the ground
h_2	-	distance from the eaves of the roof to the upper edge of first floor windows
$\bar{h}$	-	weighted average distance for determining clearing of the front wall near a first floor window, (see Eq. E.2.7), equals buildup distance; thus $\bar{h} = \bar{h}_{of} = \bar{h}_{if}$
ℓ_1	-	length of Room 1'
ℓ_2	-	length of Room 1' '
1', 1'', 1 '''	-	rooms of building 3.3.5 (see Fig. E.5.2)
1A, 1B, 1C, 0C, 1K, 2A	-	portions of wall surfaces (see Fig. E.5.2)
$p_1(t)$	-	a reference pressure inside the structure (see Section E.5.2.2.2)
s_0, s_1	-	average pressures on the load-bearing side wall of Room 1', outside and inside surfaces, respectively

E.5.2   METHOD OF DETERMINATION OF LOADING

   E.5.2.1   Roof

   The roof of building 3.3.5b has a slope angle, Θ, of

33 degrees. It is struck by a shock wave of 3.75 psi overpressure.

Computations will be based upon the assumption that the roof stands,

as already noted in Section E.5.1. Further, it is assumed that the pressure in the attic remains atmospheric, i.e., the pressure in the lower part of the structure neither breaks the second floor ceiling nor opens the scuttle to the attic. Hence this assumption states that the roof section is closed off from the rest of building 3.3.5b. (See Fig. E.5.3.)

Front slope loadings: Up to the time $t = \ell/2U$ predictions are based on Section E.1.5. From that section, the average pressure on the front slope proceeds linearly with time from zero at $t = 0$ to the following value (from Eq. E.1.5) at $t = \frac{\ell}{2U}$:

$$\text{front } r_0(\frac{\ell}{2U}) = p_\sigma(\frac{\ell}{4U}) + K(\Theta)\left[P_{\text{obl refl}} - p_\sigma(\frac{\ell}{4U})\right] \quad ,$$

$$(E.5.1)$$

where $K(\Theta)$ is found from Fig. E.5.6 and $P_{\text{obl refl}}$ is found from reference 18 (Fig. 5.18, p 123) or Fig. E.1.7 in this volume.

After the time, $\ell/2U$, the pressure on the front slope decreased because of continued clearing effects. Pseudo steady state pressure is assumed at $t = 5\,\ell/2U$. This estimate is based on consideration of shock tube tests in reference 2 (triangular block, slope angle of $45°$) and in reference 1 (peaked top rectangular block, slope angle of $10°$). Therefore,

$$\text{front } r_0(\frac{5\ell}{2U}) = \text{front } r_{os}(\frac{5\ell}{2U}) \quad (E.5.2)$$

From this time on, "front $r_0(t)$" follows the "front $r_{os}(t)$" curve.

The results of the above discussion are shown in
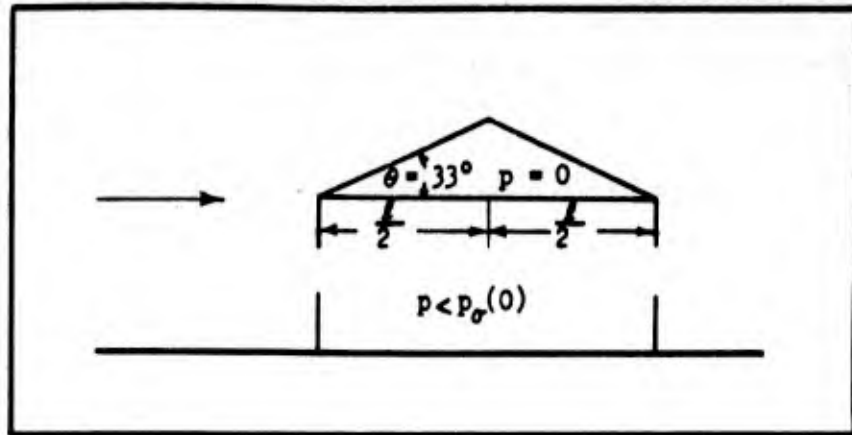
Fig. E.5.3   Roof Section of Building 3.3.5b
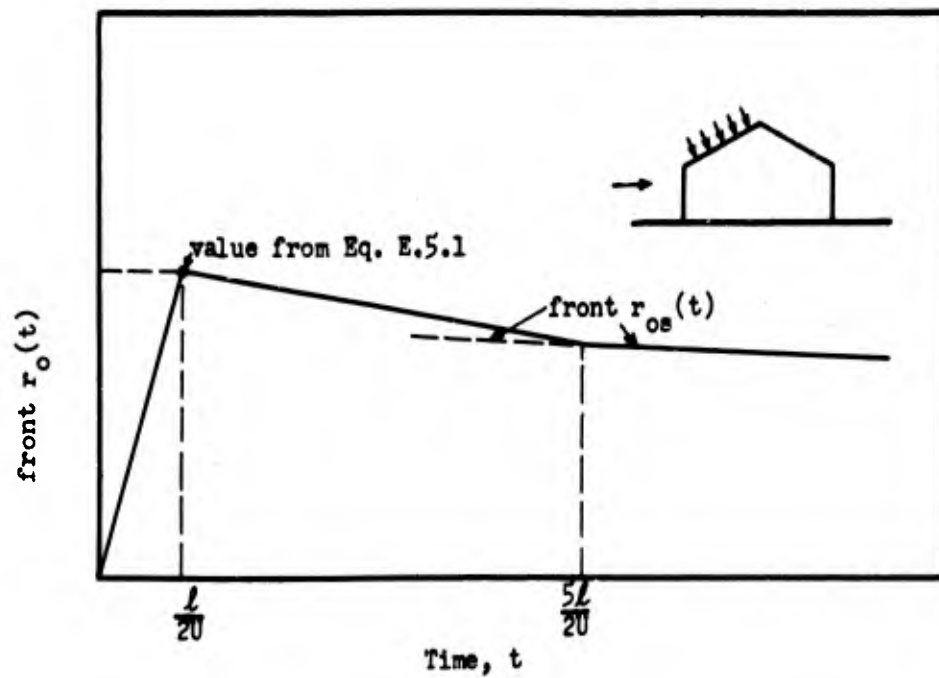
Fig. E.5.4   Predicted Pressures on Front Slope of Building 3.3.5b

Fig. E.5.4 where "front $r_o(t)$" is the total net pressure on the roof slope since atmospheric pressure was assumed on the underside of the roof.

These predictions are for both "maximum" and "minimum turbulence" (See Section E.1.3.1). The water tests of Irminger and Nøkkentved (reference 11, Figs. 1a to 1e and 4a to 4d, and discussion, p 10 to 14) show that any turbulent region, if present at all, is quite limited in extent for roof slopes of 30° to 45°. Since the roof slope of building 3.3.5b, 33°, is within this test range, the above predictions are believed to be valid for cases of both "maximum" and "minimum turbulence" effects.

The drag coefficient, "front Cr_o", for a 33° front sloped roof is given in Sec. E.1.3.2.

Back slope loadings: The average pressures on the back slope of the roof are investigated on the basis that the front slope of the roof suffers no major destruction. The average pressure on the back slope is zero until $t = \mathcal{L}/2U$, since the origin of the time scale is taken when the shock front contacts the front of the building. At this time, the pressure begins to rise to an equilibrium value, "back $r_{os}(t)$".

No shock tube tests are recorded for a 33° sloped roof. The results of shock tube tests conducted for a 10° sloped roof (reference 2) and a 45° triangular block (reference 1) can be used to
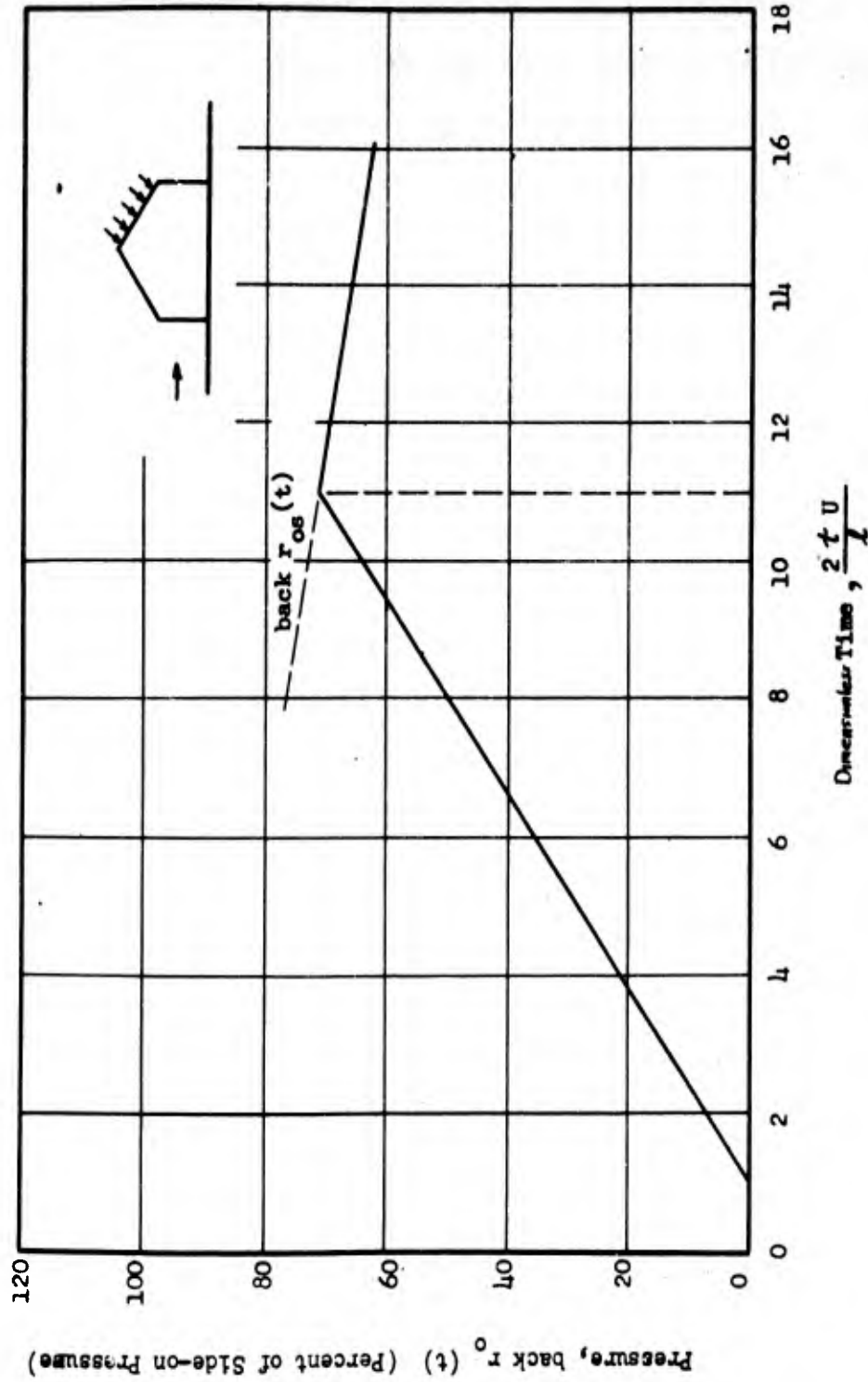
Fig. E.5.5   Predictions for Back Roof Slope of Building 3.3.5b ($\theta = 33°$)

estimate the time at which this equilibrium value is reached. Based on these data it is assumed that at $t = \frac{11\ell}{20}$, pseudo steady state pressure is reached, i.e., back $r_o(\frac{11\ell}{20})$ = back $r_{os}(\frac{11\ell}{20})$, having risen linearly from its earlier value.

The drag coefficient, "back C_{ro}", for a 33° back slope is deduced in Section E.1.3.2.

E.5.2.2.   Analysis of Wall Surfaces

E.5.2.2.1   Introduction and Summary

The wall surfaces of building 3.3.5b to be analyzed are located in Rooms 1', and 1 '', and 2' (see Fig. E.5.2). These surfaces are labeled 1A and 1B (portions of the front wall); 1C and 0C (a portion of the side wall); and 1K and 2A (an interior partition wall).

The equilibrium times and pressures for the three rooms are given in Table E.5.1. The loading predictions on various surfaces are shown in Figs. E.5.7 - E.5.9.

As noted in Section E.5.1, assumptions are made arbitrarily as to the failure of certain interior doors in order that illustrative predictions can be carried out. Doors b, d, and e (see Fig. E.5.2) assumed to collapse; doors a, f, and j are assumed to remain standing in a latched position. It is not necessary to consider other doors in order to carry out the predictions in this chapter.

The flow through the building and the
loadings on the walls are discussed in the remaining subsections. A
summary of the predictions in symbolic form and the numerical compu-
tation of the loadings is given in Section E.5.3.

TABLE E.5.1

Equilibrium Times and Pressures

In Rooms 1', 1' ', and 2' of Building 3.3.5b

Room	Equilibrium Time	Pressure, $P_i(t)$
1'	$8\dfrac{\ell_1}{U} + t*$	$f_{os}(t)$
1' '	$8\dfrac{\ell_2}{U} + t*$	$f_{os}(t)$
2'	$5\dfrac{\ell_3}{U} + \dfrac{8h}{U} + t*$	$b_{os}(t)$

E.5.2.2.2 <u>General</u> <u>Discussion</u> <u>of</u> <u>Pressures</u> <u>in</u> <u>Front</u> <u>Room</u>

Rooms with rear windows only are considered in
Section E.5.2.2.3. The strength of the entering shock wave is de-
termined from Fig. E.5.4 in Vol. I. This wave begins to form after
t* when the windows break.

In treating the pressures on various inside sur-
faces it is convenient to introduce an intermediate step: determination
of an inside "reference pressure". This reference pressure will be
denoted as $p_i(t)$; pressures on some of the inside surfaces will be
shown to be expressible in terms of this pressure. The definition

SECURITY INFORMATION

CONFIDENTIAL

of $p_1(t)$ follows. Until t^*, $p_1 = 0$; it then jumps instantaneously to $p_{\sigma 1}$. Then p_1 rises linearly to become equal to $f_{os}(t)$ at the equilibrium time (see Table E.5.1) and remains equal to $f_{os}(t)$ for the remainder of the positive phase.

The time required (after t^*, when windows break) for $p_1(t)$ to build up to pseudo steady state pressure, $f_{os}(t)$, in Room 1' was taken to be $\frac{8\ell_1}{U}$ where ℓ_1 is the dimension of the room parallel to free stream flow and U is the outside wave velocity. This time (plus t^*) is termed inside "equilibrium" time. The choice, $\frac{8\ell_1}{U}$, was made from the following considerations. The pressure behind the wave reflected from the back wall of the room, p_{1refl}, is nearly equal to initial outside side-on pressure, $p_\sigma(0)$. Hence, if conditions were ideal, the inside pressure would build up to $f_{os}(t)$ at approximately $\frac{2\ell_1}{U}$ (when the inside-reflected shock returns to the front wall). However, the collapse of door, d, will allow considerable flow out of the room so that the time required for reference pressure to reach $f_{os}(t)$ will probably be much longer than $\frac{2\ell_1}{U}$.

Further, examination of shock tube fringe shift diagrams for a hollow rectangular block with an upstream opening (reference 3) reveals that inside equilibrium is reached in about $\frac{6\ell_1}{U}$ for that particular block with $\Omega_f = 0.5$ and no rear opening. It is felt that for 3.3.5b the reference pressure will require longer than $\frac{6\ell_1}{U}$ to reach equilibrium, $f_{os}(t)$. The increase in time over $\frac{6\ell_1}{U}$ was arbitrarily

ARMOUR RESEARCH FOUNDATION OF ILLINOIS INSTITUTE OF TECHNOLOGY

- 217 -

CONFIDENTIAL
Security Information

chosen to be $\frac{2\ell_1}{U}$, thus giving a total equilibrium time of $\frac{8\ell_1}{U}$ for Room 1'.

Correspondingly, $\frac{8\ell_2}{U}$ was chosen to be the equilibrium time for Room 1". Glass breaking time, t^*, is added to each of these to give the values in Table E.5.1. Figure E.5.6 shows the build-up of the reference pressure, $p_1(t)$, in these rooms; it is based on t^*, $f_{os}(t)$, and values of equilibrium times computed in section E.5.3, using the definition of $p_1(t)$ given at the beginning of this section.

E.5.2.2.3 Determination of Average Pressure on a Partition Wall

The partition wall to be analyzed is the back wall of Room 1' (see Fig. E.5.2). Surfaces 1K and 2A are the front and back surfaces of this wall. The pressure on surface 1K is entirely due to the flow through the front window of Room 1', while the pressure on surface 2A is entirely due to flow through the rear window of Room 2' since door f is assumed to stand (section E.5.2.2.1).

1K: The pressure on surface 1K is very similar to that felt by the inside back wall of idealized model 3.3.8b (section E.5.2.3, Vol II). The main difference in the pressures results from the failure of door d. The overpressure on surface 1K is, of course, zero until the surface is struck by the inside shock wave at time $t = \ell_1/U + t^*$; at that time it rises instantaneously to p_{irefl} as determined by Eq. E.4.20, Vol I. Assuming a 3-msec breaking time, door d would fail at about the time it is traversed by the inside-reflected shock wave (which travels against the main inside flow). The collapse of door d would initiate a rarefaction wave spreading across surface 1K relieving inside-

ARMOUR RESEARCH FOUNDATION OF ILLINOIS INSTITUTE OF TECHNOLOGY
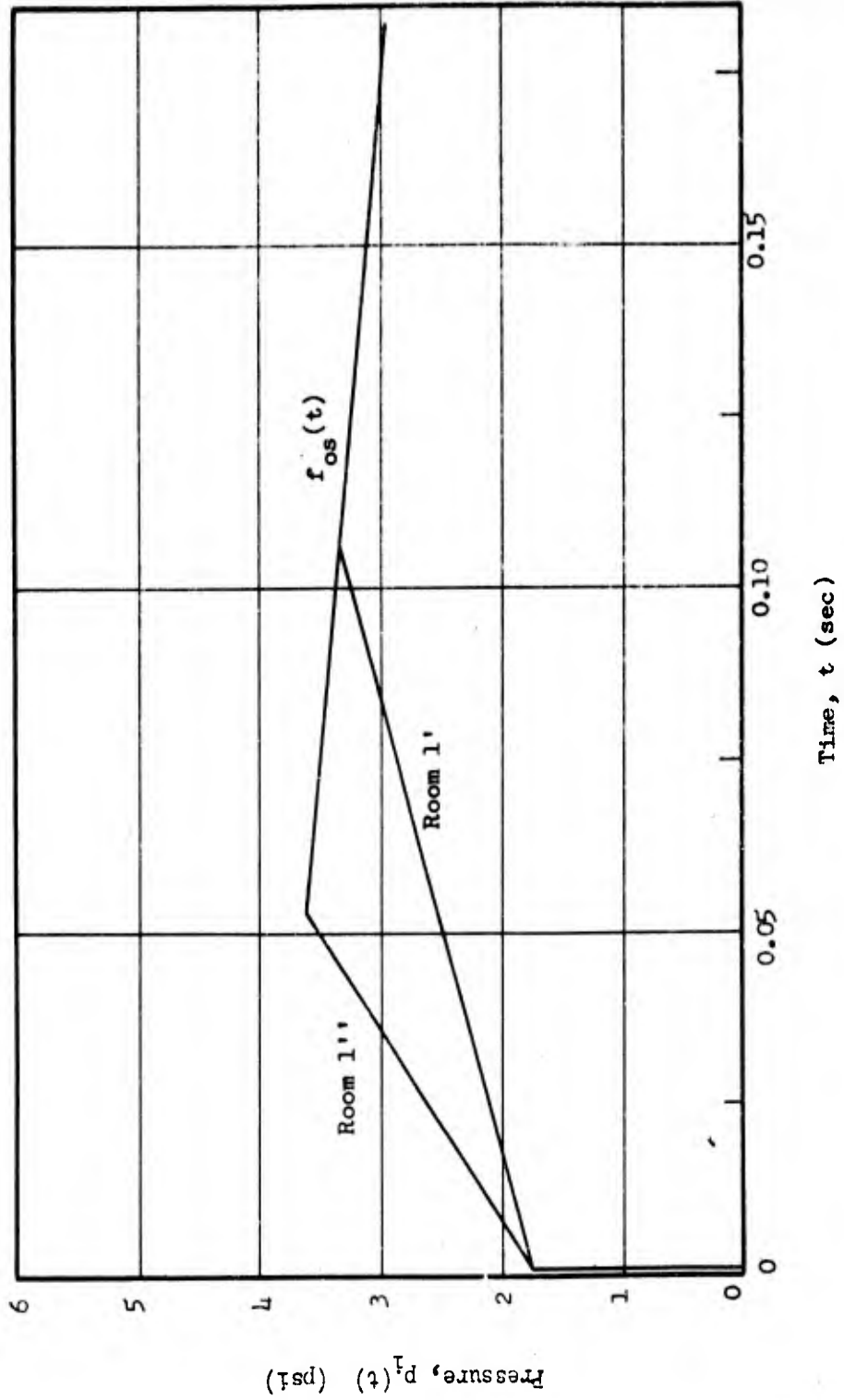
Fig. E.5.6   Build-up of reference pressure, $p_i(t)$, in two Front Rooms of Building 3.3.5b

reflected pressure on that surface. Before complete relief can take place, however, the shock from Room 1" will reflect from surface 1L and door e will break (see Fig. E.5.2). Before the time that the reflected wave (from 1K) reaches the front wall, the pressure on surface 1K will probably be relieved to "reference pressure", $p_i(t)$, shown in Fig. E.5.6. The time $t = \frac{2\ell_1}{U} + t^*$ is chosen for 1K to reach $p_i(t)$. Turbulence effects will not be felt by surface 1K; hence "maximum" and "minimum turbulence" estimates are merged here. The predicted pressures thus derived for surface 1K are illustrated graphically in Fig. E.5.7.

<u>2A</u>: Surface 2A is the rear surface of the back wall of Room 1'. Since doors j and f do not fail (see section E.5.2.2.1), the pressure on 2A must build up through the back window of Room 2'.

The pressure on surface 2A is deduced in part from shock tube experiments, viz., reference 2, Figs. 38-47, which gives fringe shift diagrams for a hollow, rectangular, two-dimensional block with an opening facing downstream. These data (which show some flow from the upstream wall into the interior due to leakage) show a build-up of pressure at approximately the same rate on all inside walls of the block. Unfortunately, the time of observation is not sufficiently long to permit a determination of "equilibrium time" for the inside of the block.

The pressure on all inside surfaces of Room 2' is estimated to build up uniformly, as is indicated by the above experimental data. Thus, pressure on 2A equals $p_i(t)$ for Room 2'. The equilibrium pressure (maximum pressure on the walls) for this room was taken as the pseudo steady state pressure available at the rear windows, namely
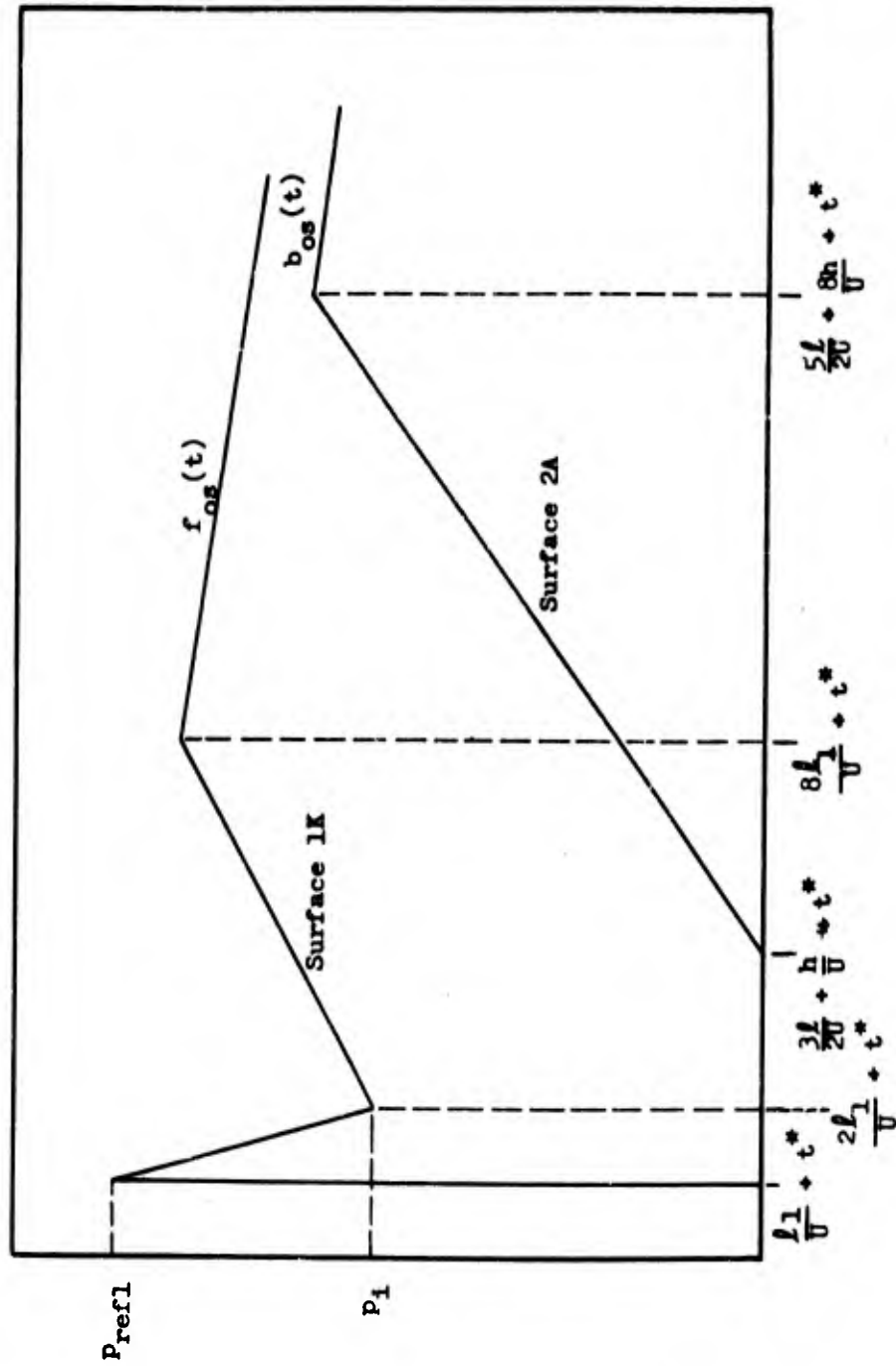
Fig. E.5.7 Predicted Pressure on a Partition Wall of Bldg. 3.3.5b

$b_{os}(t)$, defined in section E.1.3.2. The discussion of the time required for the reference pressure, $p_i(t)$, for Room 2' to build up to equilibrium pressure follows. The pressure inside of Room 2' cannot reach $b_{os}(t)$ until that pressure is established at the back wall. The time required to establish $b_{os}(t)$ on the back wall is approximately $\ell/U + 8h/U$ (section E.3.5.1.3, Vol II) where ℓ is the length of the building and h is the height of the back wall (to the eaves). A somewhat longer period is required to establish this pressure uniformly in Room 2'. This additional increment of time, chosen rather arbitrarily, is $3\ell/2U + t$. Thus, the total time estimated for surface 2A to reach $b_{os}(t)$ is estimated as $5\ell/2U + 8h/U + t$. Turbulence effects will not affect surfaces 2A to any appreciable extent.

The predicted pressure on surface 2A, under the above assumptions is illustrated in Fig. E.5.7.

E.5.2.2.4 Determination of Average Pressures on a Load Bearing Wall

The load bearing wall chosen to be analyzed is the left wall of Room 1' (Fig. E.5.2). Surfaces 1C and OC are the inside and outside surfaces of this wall.

OC: The loading on surface OC is taken directly from the method developed in section E.3.5.1.2, Vol II for the pressures on the outside roof of idealized model 3.3.3b. The method is illustrated graphically in Fig. E.5.8.

1C: Pressures on surface 1C are determined from the method developed in Section E.3.5.2.2, Vol II for the inside roof
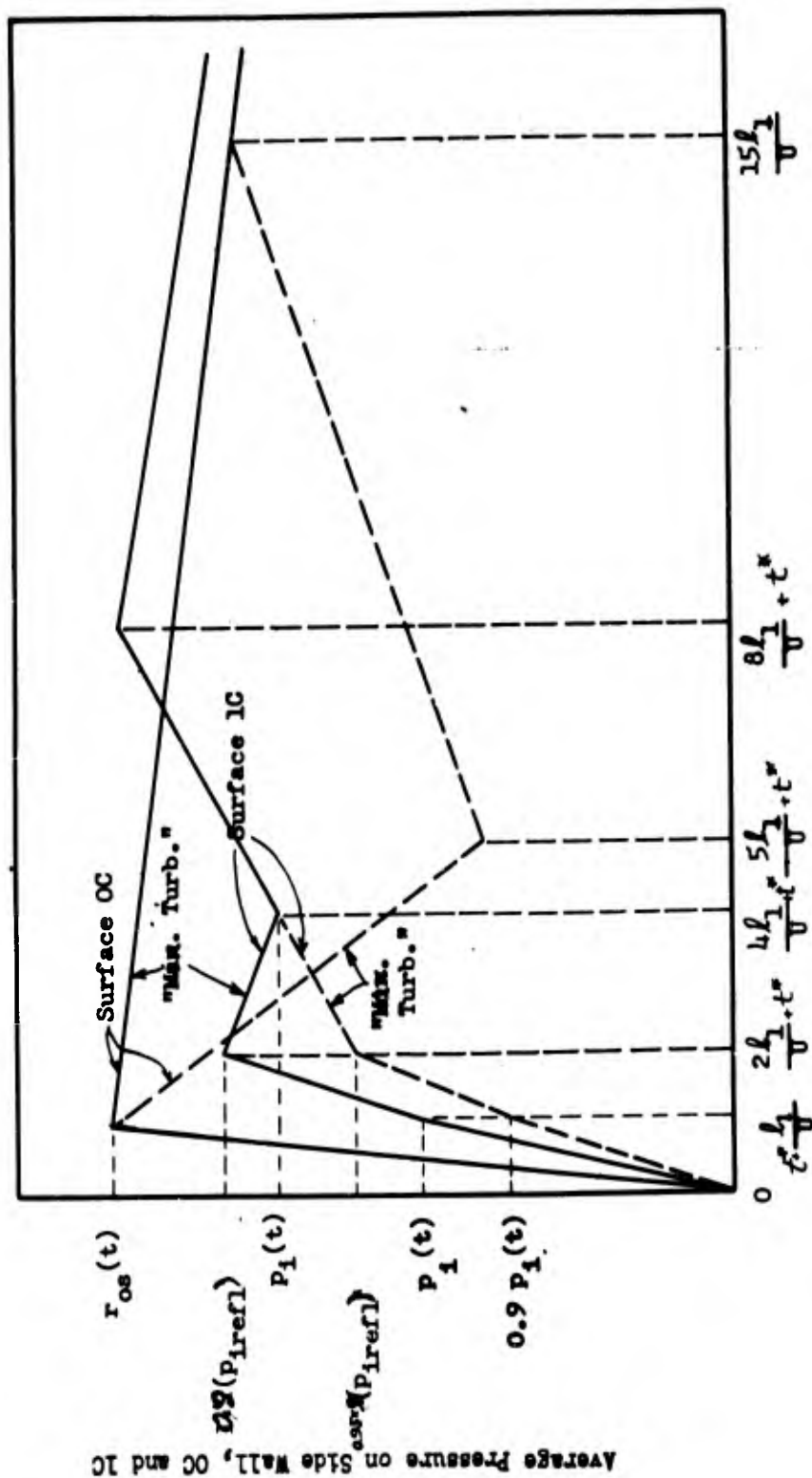
Fig. B.5.8 Predicted Pressure on a Load-Bearning Side Wall of Building 3.3.5b

of idealized model 3.3.8b. The inside of model 3.3.8b and Room 1' of building 3.3.5b are similar; however, modifications must be made in the method for the effect of the destruction of door d of Room 1' by the inside shock wave (noted in Section E.5.2.2.1) and a different time required for inside pressures to reach equilibrium (discussed in Section E.5.2.2.2).

Vortices and turbulence originating at the front windows might influence the front portion of surface 1C. For this reason both "maximum" and "minimum turbulence" predictions are made for the left wall of Room 1'. The "maximum turbulence" prediction from the aforementioned section in Vol II is used.

The pressure on surface 1C is assumed to build up to $p_i(t)$ for Room 1' (Fig. E.5.6) in the "minimum turbulence" case and to 0.9 of this value in the "maximum turbulence" case when the inside shock wave has reached the back wall (i.e. $t = \ell_1/U$). Pressure on the inside wall then rises due to the inside-reflected wave returning to the front wall. The collapse of door d results in a rarefaction wave relieving the pressure behind the inside-reflected shock wave as discussed in Section E.5.2.2.3. The exact pressures distributed by this combination are, however, relatively indeterminate. As a first approximation, the effect of the rarefaction wave is taken to decrease the pressures predicted for the roof of idealized model 3.3.8b by 20 per cent. The result of this adaptation is a pressure on surface 1C of 0.8 P_{1refl} for the "minimum turbulence" case and a pressure of 0.8 (Q95) P_{1refl} for the "maximum turbulence" case at time $t = 2\ell_1/U$ (about the time

when the inside-reflected wave returns to the front wall).

At time $\dfrac{2\ell_1}{U}$, this predicted average pressure on surface 1C is only slightly above the "inside pressure", $p_1(t)$, described in Section E.5.2.2.2, and shown in Fig. E.5.5. Because of this small difference, the pressure on surface 1C will drop to inside pressure in a relatively short time (before equilibrium has been established in Room 1'); $t = \dfrac{4\ell_1}{U}$ was chosen at this time.

The average pressure on surface 1C thus predicted is illustrated in Fig. E.5.8.

E.5.2.2.5 Determination of Average Pressures on a Section of the Front Wall

Part of the front walls of Rooms 1' and 1" is chosen for analysis. The inside surfaces of these portions are indicated as surfaces 1A and 1B in Fig. E.5.2. As before, loadings are computed under the assumption that the wall does not collapse.

Outside surface of the front wall: The pressures on the outside surface of the front wall are determined by the same method as the other buildings of this Vol (see, for instance, Fig. E.2.6). The shock wave strkes the building raising the pressure on the front surface to the reflected pressure given numerically in Fig. E.4.2, Vol I. This pressure is assumed to clear to pseudo steady state pressure, $f_{os}(t)$, at $t_< = 3\bar{h}/c_{refl} + t^*$ and to follow $f_{os}(t)$ from that time on. The definition of $f_{os}(t)$ is given in Section E.1.3.2. The determination of $\bar{h}$, the "mean clearing distance", is carried out by the method given in section
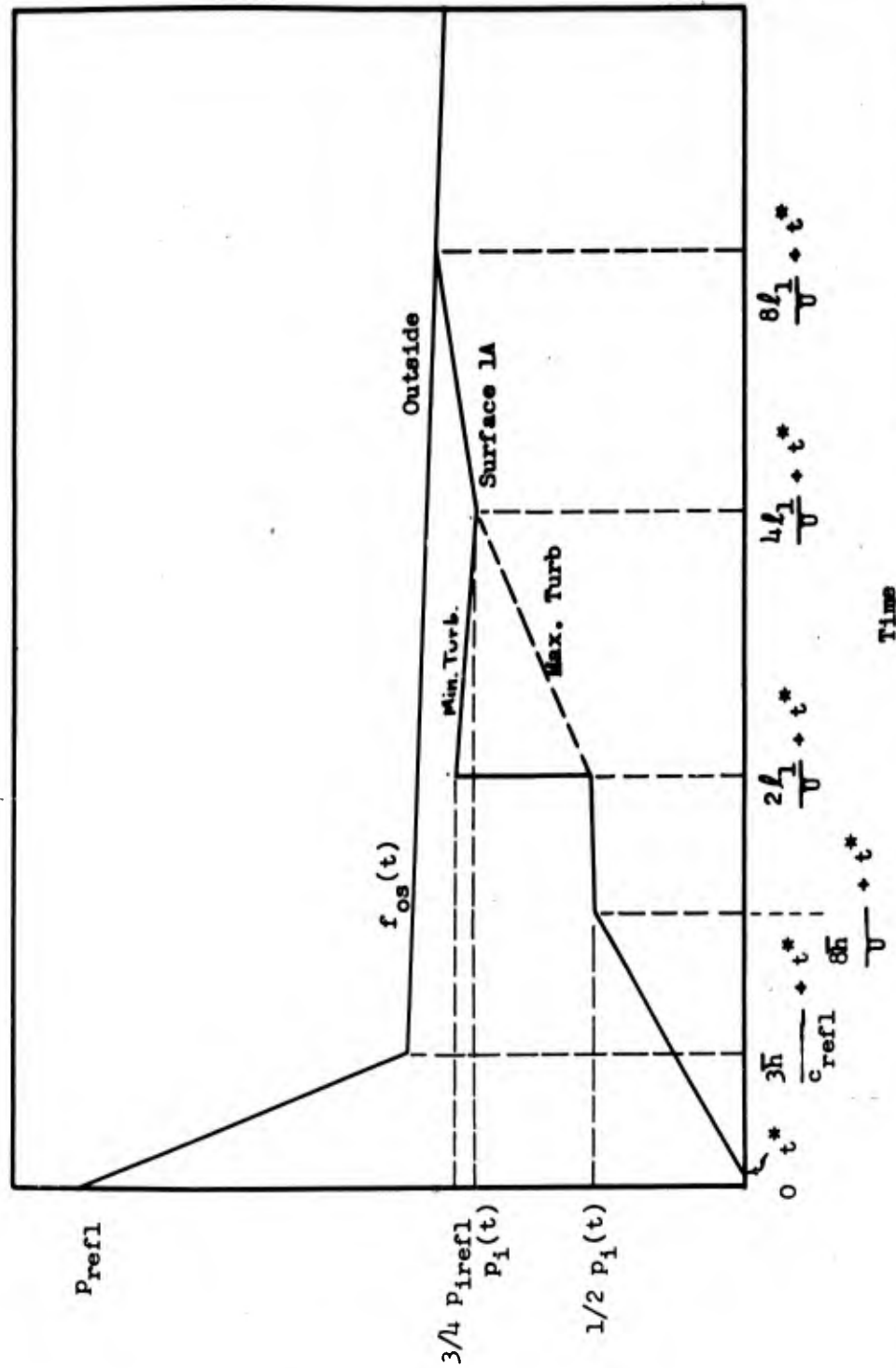
Fig. E.5.9   Predicted Pressures on a Portion of the Front Wall of Building 3.3.5 (For surface 1A, read as shown; for surface 1B, replace ℓ_1 with ℓ_2)

E.2.2.1.7. The value of t_c is obtained from section E.2.2.1 (below Eq. E.2.1).

      1A and 1B: Surfaces 1A and 1B are portions of the inside surfaces of the front wall of Room 1' and 1" respectively. Predictions for surfaces 1A and 1B, shown in Fig. E.5.9, are based on estimates made in Vol II (Fig. E.3.20) for the inside front wall of model building 3.3.8b. In addition to a few minor changes (e.g. t^* added on all times, $\hat{h}$ replaces h_1, U replaces $\bar{U}_{1refl}$, $p_1(t)$ replaces $p_{\sigma 1}$) reductions in pressure were made in applying the material of Vol II to the 3.3.5b structure. The inside-reflected shock wave in building 3.3.5b is weakened by collapse of doors d and b (see Section E.5.2.2.4), hence lower pressures are estimated than in the material of Vol II. Furthermore, equilibrium times, developed independently for building 3.3.5b, are used.

E.5.3 NUMERICAL COMPUTATION OF LOADING

      The calculation of average pressures on building 3.3.5b is based on the predictions developed in Section E.5.2. Only certain surfaces are analyzed rather than the entire structure. The results needed from Section E.5.2 are repeated in Tables E.5.2, 3, 4, 6, and 8 in the columns labeled "Symbolic". These data were given in schematic diagrams in Figs. E.5.4-E.5.9.

      The side-on pressure vs. time, and drag pressure vs. time relations required for the predictions are shown in Fig. E.5.10. These were computed from Eq. E.4.16, Vol I and from Fig. E.4.3, Vol I, respectively.

Table E.5.2 contains the numerical values of other quantities necessary for computation of loadings on the components. It is divided into three sections: shock constants, geometric constants, and combined shock and geometric constants. The shock constants are various numerical values which are independent of the building. Among these are certain specified values: the shock strength, ξ, the duration of the wave, t_0, and atmospheric pressure, P_0. Under the same heading are important derived quantities, viz., the velocity of the shock front, U, the reflected pressure, P_{refl}, and the velocity of sound in the reflected region, c_{refl}. All are obtained from Fig. E.4.2, Vol I.

The geometric constants (see Figs. E.1.3 and E.5.1) are the length of room 1', ℓ_1, the length of room 1", ℓ_2, the length of the building, ℓ, the height of the building from the ground to the eaves, h_1, the distance from the eaves to the top of the first floor window, h_2, the mean clearing distance, $\overline{h}$, and the roof slope angle, Θ.

The combined geometric and shock constants include:

1. certain characteristic time units which underlie the calculations, e.g., $\dfrac{\ell_1}{U}$ and $\dfrac{h_1}{U}$,

2. the inside shock strength, $p_{\sigma 1}$, computed from the equation, $P_{\sigma 1} = P_0(\xi_1 - 1)$, where ξ_1 is obtained by interpolation from Fig. E.5.4, Vol I,

3. inside-reflected pressure, P_{1refl}, obtained by interpolation from Fig. E.5.5, Vol I,

4. the drag coefficient on the front of the front wall, C_{fo}; on the back of the back wall, C_{bo}; the side wall, C_{so};

and the front and back slopes of the roof, "front C_{ro}"

and "back C_{ro}".

These drag coefficients, obtained from Section E.1.3.2, are used
to compute the pseudo steady state pressures, f_{os}, b_{os}, r_{os}, and the
series of quantities, "front r_{os}", and "back r_{os}", from Eqs. E.1.1-
E.1.3. Also listed are:

1. the instantaneous reflected pressure on the sloped roof,
   $P_{obl refl}$, obtained from Fig. E.5.7,

2. the factor, $X(\theta)$, needed for loading computations on the
   oblique roof and obtained from Fig. E.5.6, and

3. the window-breaking time, t^*, obtained from Section E.5.1.

The pressure, $p_1(t)$, for Rooms 1' and 1'' appears in Fig. E.5.6.
The superscripts " - " and " + " shown in certain values of time indicate
that the pressure and force undergo a sudden change. In the tables, the
symbol "*" at a certain value of time (showing the final forces or pres-
sures) indicates that until that time, average pressure-time relations
are considered linear, and after that time follow a smooth curve through
the given points.

Tables E.5.3 and E.5.4 contain the average pressures on the front
and back slopes of the roof. The symbolic values were obtained from
Fig. E.5.4. Tables E.5.5 and E.5.6 give the average pressure and net
average pressure on a portion of the front wall. The symbolic values
are obtained from Fig. E.5.9.

The average and net average pressure on a portion of the side wall
were deduced from Fig. E.5.8 and are given in Tables E.5.7 and E.5.8.

The average pressures deduced in Fig. E.5.7 for a partition wall are listed numerically in Table E.5.9, with Table E.5.10 containing the net average pressure for the partition wall.

Figures E.5.11-E.5.20 give the results computed in Tables E.5.3-E.5.10 during the early periods.

As discussed in Section E.1.1 the computed pressures are quite approximate.

Slide rule calculations were used throughout, and the third figure in each case has no significance.
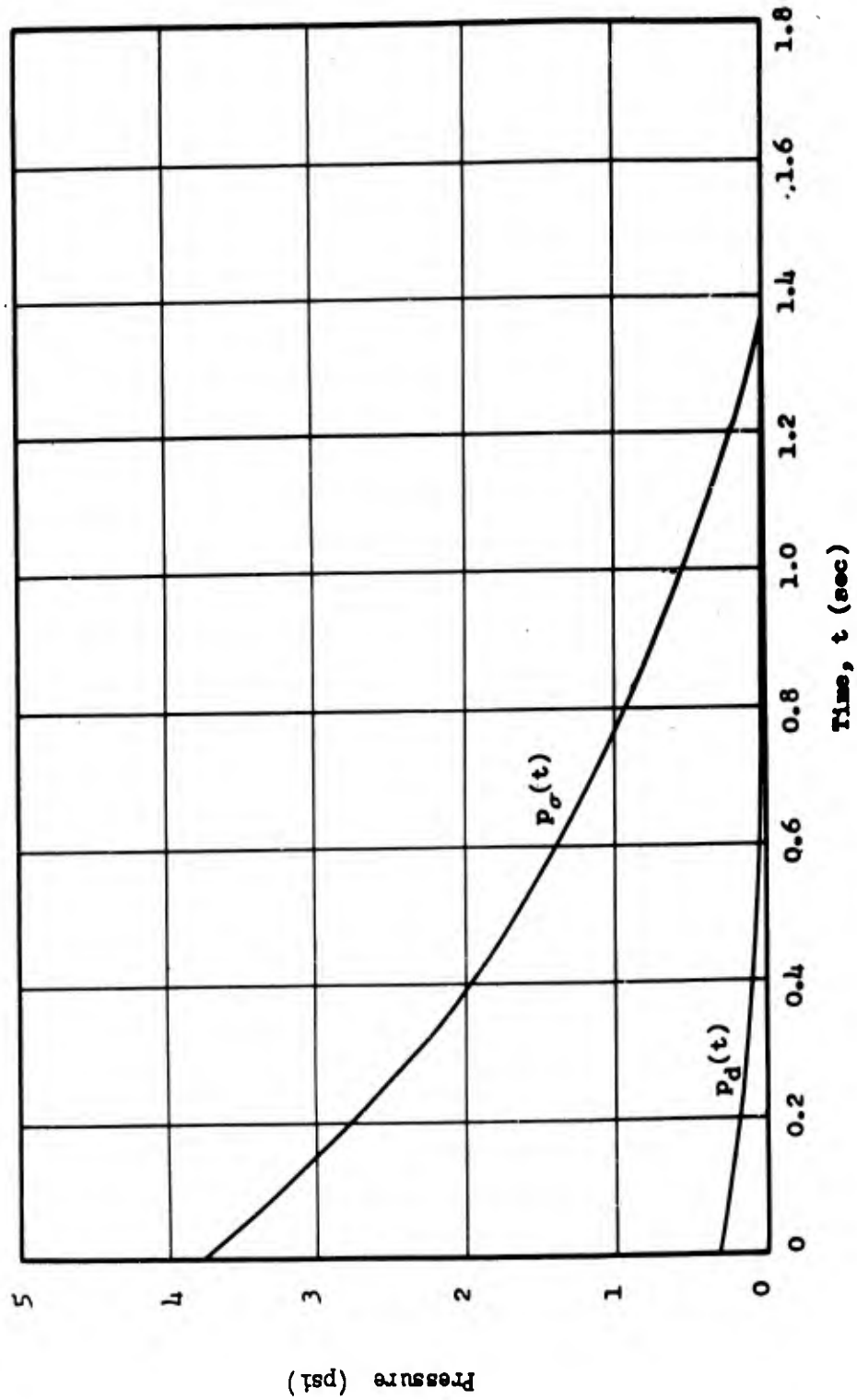
Fig. E.5.10 Side-on Pressure and Drag Pressure on Building 3.3.5 for $p_\sigma(0) = 3.75$ psi

231

TABLE E.5.2

Constants for Building 3.3.5b

Shock Constants	
$p_\sigma = 3.75$ psi	$c_{refl} = 1185$ fps
$U = 1230$ fps	$p_o = 14.7$ psi
$\xi = 1.255$	$t_o = 1.38$ sec
$P_{refl} = 8.4$ psi	

Geometric Constants	
$l_1 = 15.7$ ft	$h_2 = 16$ ft
$l_2 = 8$ ft	$\bar{h} = 2.33$ ft
$l = 33.4$ ft	$\Omega = 0.20$
$h_1 = 23.5$ ft	$\theta = 33°$

Combined Geometric and Shock Constants	
$\dfrac{l_1}{U} = 0.013$ sec	$p_{\sigma 1} = 1.75$ psi
$\dfrac{l_2}{U} = 0.007$ sec	$\xi_1 = 1.12$
$\dfrac{l}{U} = 0.028$ sec	$p_{1refl} = 3.7$ psi
	$C_{fo} = 0.66$
$\dfrac{h_1}{U} = 0.019$ sec	$C_{bo} = -0.33$
$\dfrac{h_2}{U} = 0.013$ sec	$C_{so} = -0.55$
	front $C_{ro} = 0.33$
$\dfrac{\bar{h}}{c_{refl}} = 0.002$ sec.	back $C_{ro} = -0.40$

ARMOUR RESEARCH FOUNDATION OF ILLINOIS INSTITUTE OF TECHNOLOGY

TABLE E.5.2 (CONTD)

Constants for Building 3.3.5b

Combined Geometric and Shock Constants
$t^* = 0.001$ sec $\qquad P_{obl\ refl} = 11.8$ psi $K(0) = 0.35$

TABLE E.5.3

Average Pressures on Front Roof Slope of Building 3.3.5b

Symbolic		Numerical	
Time, t	Pressure, r_o	Time, t (sec)	Pressure, r_o (psi)
0	0	0	0
$\dfrac{\ell}{2U}$	$P_\sigma\!\left(\dfrac{\ell}{2U}\right)+K(\theta)\left[P_{obl\,refl}-P_\sigma\!\left(\dfrac{\ell}{2U}\right)\right]$	0.0135	6.11
$\dfrac{5\ell}{2U}$	front $r_{os}(t)$	0.0675	3.48
		0.1	3.23
		0.2	2.76
		0.4	1.97
		0.6	1.37
		0.8	0.91
		1.0	0.54
		1.2	0.24
		1.4	~
$t_o+\dfrac{\ell}{2U}$	0	1.48	0

TABLE I.5.4

Average Pressures on Rear Roof Slope of Building 3.3.5b

Symbolic		Numerical	
Time, t	Pressure, r_o	Time, t (sec)	Pressure, r_o (psi)
0	0	0	0
$\frac{l}{2U}$	0	0.0135	0
11 $\frac{l}{2U}$	$r_{os}(t)$	0.148	2.87
	$r_{os}(t)$	0.2	2.66
	$r_{os}(t)$	0.4	1.91
	$r_{os}(t)$	0.6	1.35
	$r_{os}(t)$	0.8	0.91
	$r_{os}(t)$	1.0	0.54
	$r_{os}(t)$	1.2	0.25
		1.4	~
$t_o + \frac{l}{U}$	0	1.48	0

TABLE E.5.5

Average Pressures on a Portion of the Front Wall of Building 3.3.5b

Outside of Surface 1A of Room 1" and 1B of Room 1'

Symbolic		Numerical	
Time, t	Pressure, f_o	Time, t (sec)	Pressure, f_o (psi)
0	P_{refl}	0	8.4
$\dfrac{3h_e}{a_{refl}} + t^*$	$f_{os}(t)$	0.007	3.95
$\dfrac{8\ell_2}{U} + t^*$	$f_{os}(t)$	0.053	3.60
$\dfrac{8\ell_1}{U} + t^*$	$f_{os}(t)$	0.105	3.30

Surface 1A of Room 1" (Inside)

Symbolic		Numerical	
Time, t	Pressure, f_1	Time, t (sec)	Pressure, f_1 (psi)
0	0	0	0
t^*	0	0.001	0
$\dfrac{85w}{U} + t^*$	$\tfrac{1}{2} p_1(t)$	0.017	1.00

TABLE E.5.5 (CONTD)

Average Pressures on a Portion of the Front Wall of Building 3.3.5b

Surface 1A of Room 1'

Symbolic		Numerical	
Time, t	Pressure, f_1	Time, t (sec)	Pressure, f_1 (psi)
$\left[\dfrac{2\ell}{U} + t^*\right]^{-}$	$1/2\ p_1(t)$	0.027^{-}	1.07
$\left[\dfrac{2\ell}{U} + t^*\right]^{+(b)}$	$3/4\ p_{1refl}$ (b)	0.027^{+}(b)	2.76(b)
$\dfrac{4\ell}{U} + t^*$	$p_1(t)$	0.053	2.55
$\dfrac{8\ell}{U} + t^*$	$f_{os}(t)$	0.105	3.30

Surface 1B of Room 1"

Symbolic		Numerical	
Time, t	Pressure, f_1	Time, t (sec)	Pressure, f_1 (psi)
0	0	0	0
t^*	0	0.001	0

(b)Denotes "minimum turbulence" predictions. Undesignated values apply to "maximum" and "minimum turbulence" predictions.

TABLE E.5.5 (CONT'D)

Average Pressures on a Portion of the Front Wall of Building 3.3.5b

Surface 1B of Room 1".

Symbolic		Numerical	
Time, t	Pressure, f_1	Time, t (sec)	Pressure, f_1 (psi)
$\left[\dfrac{2\ell_2}{U} + t^*\right]^-$	$\frac{1}{2}\, p_1(t)$	0.013	1.10
$\left[\dfrac{2\ell_2}{U} + t^*\right]^{+(b)}$	$\frac{3}{4}\, p_{1refl}{}^{(b)}$	$0.013^{(b)}$	$2.76^{(b)}$
$\dfrac{4\ell_2}{U} + t^*$	$p_1(t)$	0.027	2.60
$\dfrac{8\ell_2}{U} + t^*$	$f_{os}(t)$	0.053	3.60

(b) Denotes "minimum turbulence" predictions. Undesignated values apply to "maximum" and "minimum turbulence" predictions.

TABLE E.5.6

Net Average Pressures on a Portion of the Front Wall

of Building 3.3.5b

Net Pressure on Surface 1A			
Time, t (sec)	f_0 (psi)	f_1 (psi)	$f = f_0 - f_1$ (psi)
0	8.4	0	8.40
0.007	3.95	0.40	3.55
0.017	3.85	1.00	2.85
0.027[-]	3.78	1.04	2.74
0.027[+(b)]	3.78	2.76[(b)]	1.12
0.053	3.60	2.55	1.05
0.105	3.30	3.30	0
Net Pressure on Surface 1B			
Time, t (sec)	f_0 (psi)	f_1 (psi)	$f = f_0 - f_1$ (psi)
0	8.4	0	8.40
0.007	3.95	0.30	3.65
0.013[-]	3.90	1.10	2.80
0.013[+(b)]	3.90	2.76[(b)]	1.14[(b)]
0.027	3.80	2.60	1.20
0.053	3.60	3.60	0

[(b)] Denotes "minimum turbulence" predictions. Undesignated values apply to "maximum" and "minimum turbulence" predictions.

TABLE E.5.6

Net Average Pressures on a Portion of the Front Wall

of Building 3.3.5b

Net Pressure on Surface 1A			
Time, t (sec)	f_o (psi)	f_1 (psi)	$f = f_o - f_1$ (psi)
0	8.4	0	8.40
0.007	3.95	0.40	3.55
0.017	3.85	1.00	2.85
0.027[-]	3.78	1.04	2.74
0.027[+(b)]	3.78	2.76[(b)]	1.12
0.053	3.60	2.55	1.05
0.105	3.30	3.30	0
Net Pressure on Surface 1B			
Time, t (sec)	f_o (psi)	f_1 (psi)	$f = f_o - f_1$ (psi)
0	8.4	0	8.40
0.007	3.95	0.30	3.65
0.013[-]	3.90	1.10	2.80
0.013[+(b)]	3.90	2.76[(b)]	1.14[(b)]
0.027	3.80	2.60	1.20
0.053	3.60	3.60	0

[(b)] Denotes "minimum turbulence" predictions. Undesignated values apply to "maximum" and "minimum turbulence" predictions.

TABLE B.5.7

Average Pressures on a Portion of a Side Wall of Building 3.3.5b

Outside

	Symbolic		Numerical	
Time, t	Pressure, s_o		Time, t (sec)	Pressure, s_o (psi)
0	0		0	0
$\frac{l}{5}\frac{1}{U}$	$r_{os}(t)$		0.013	3.52
$\frac{l}{5}\frac{1}{U}$	$\left\{0.35\left[1+\left(\frac{1}{2}\right)\Omega\right]r_{os}(t)\right\}$ (a)		0.065 (a)	1.25
$\frac{15l}{U}$	$r_{os}(t)$		0.195	2.70

Surface 1C

	Symbolic		Numerical	
Time, t	Pressure, s_1		Time, t (sec)	Pressure, s_1 (psi)
0	0		0	0
$\frac{l}{U} + t^*$ (b)	$P_1(t)$		0.014 (b)	1.95 (b)

(a) ... (a)

(b) Denotes "minimum turbulence" predictions. Underdesignated values apply to "maximum" and "minimum turbulence" predictions.

TABLE E.5.7 (CONTD)

Average Pressures on a Portion of a Side Wall of Building 3.3.5b

Surface 1C

Symbolic		Numerical	
Time, t	Pressure, B_1	Time, t (msec)	Pressure, B_1 (psi)
$\int_0^{l} \frac{1}{\rho} + t^*$ (a)	$0.9\, P_1(t)$	0.014 (a)	1.75 (a)
$2\int_0^{l} \frac{1}{\rho} + t^*$ (b)	$0.8\, P_{1refl}$	0.027 (b)	2.92 (b)
$2\int_0^{l} \frac{1}{\rho} + t^*$ (a)	$(0.95)(0.8)P_{1refl}$	0.027 (a)	2.76 (a)
$4\int_0^{l} \frac{1}{\rho} + t^*$	$P_1(t)$	0.053	2.57
$8\int_0^{l} \frac{1}{\rho} + t^*$	$f_{os}(t)$	0.105	3.35

(a) Denotes "maximum turbulence" predictions.
(b) Denotes "minimum turbulence" predictions. Undesignated values apply to both cases.

TABLE B.5.8

Net Average Pressures on a Portion of a Side Wall

of Building 3.3.5b

Time, t (sec)	s_0 (psi)	s_1 (psi)	$s = s_0 - s_1$ (psi)
0	0	0	0
0.014[b]	3.52	1.95	1.57
0.014[a]	3.52	1.75	1.77
0.027[b]	3.45	2.92	0.53
0.027[a]	2.90	2.76	0.14
0.053[b]	3.33	2.57	0.76
0.053[a]	1.77	2.57	-0.80
0.065[a]	1.25	2.73	-1.48
0.105[b]	3.10	3.35	-0.25
0.105[a]	1.68	3.35	-1.67
0.195	2.70	2.92	-0.22
0.2			-0.21
0.4			-0.11
0.6			-0.06
0.8			-0.02
1.0			-0.02
1.2			
1.39			00

[a]Denotes "maximum turbulence" predictions.

[b]Denotes "minimum turbulence" predictions. Undesignated values apply to both cases.

TABLE E.5.9

Average Pressures on a Partition Wall of Building 3.3.5b

Surface 1X

Symbolic		Numerical	
Time, t	Pressure, b_1	Time, t (sec)	Pressure, b_1 (psi)
$\frac{l_1}{D} + t^* - $	0	0	0
$\frac{l_1}{D} + t^* + $	0	0.014^-	0
$\frac{2l_1}{D} + t^*$	P_{1refl}	0.014^+	3.7
$\frac{8l_1}{D} + t^*$	$P_1(t)$	0.027	2.15
$\frac{5l_1}{D} + \frac{8R}{D} + t^*$	$f_{os}(t)$	0.105	3.35
	$f_{es}(t)$	0.223	2.73

ARMOUR RESEARCH FOUNDATION OF ILLINOIS INSTITUTE OF TECHNOLOGY

TABLE E.5.9 (CONT'D)

Average Pressures on a Partition Wall of Building 3.3.5b

Surface 2A			
Symbolic		Numerical	
Time, t	Pressure, b_2	Time, t (sec)	Pressure, b_2 (psi)
0	0	0	0
$3\frac{\ell}{D} + \frac{h}{D} + t^*$	0	0.054	0
$5\frac{\ell}{D} + \frac{8h}{D} + t^*$	$b_{os}(t)$	0.223	2.60

TABLE E.5.10

Net Average Pressures on a Partition Wall of Building 3.3.5b

Time, t (sec)	b_1 (psi)	b_2 (psi)	$b_{12} = b_1 - b_2$ (psi)
0	0	0	0
0.014^-	0	0	0
0.014^+	3.7	0	3.70
0.027	2.15	0	2.15
0.054	2.60	0	2.60
0.105	3.35	0.75	2.60
0.223	2.73	2.60	0.13
0.4			0.09
0.6			0.05
0.8			0.02
1.0			0.01
1.2			
1.39			0
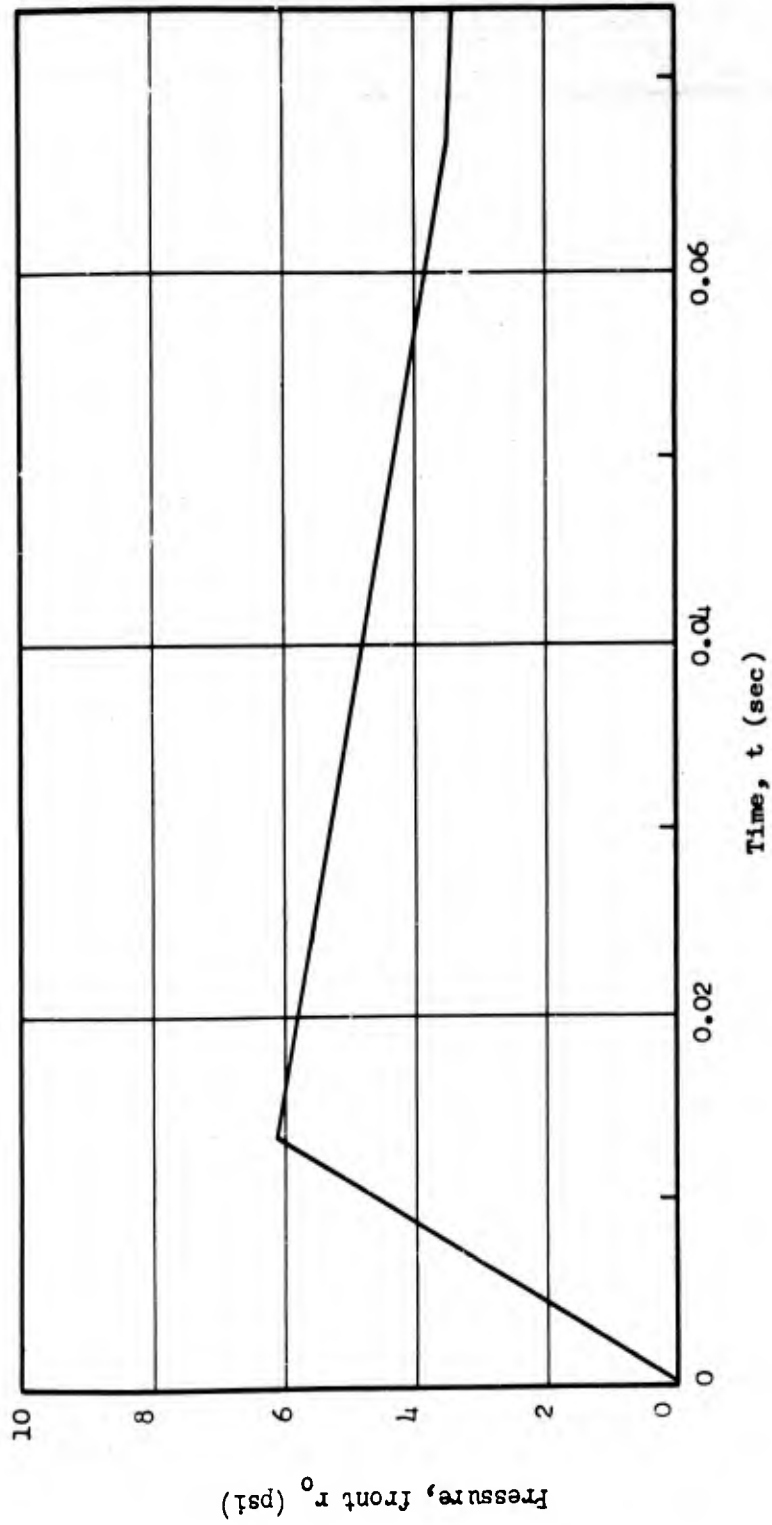
Fig. E.5.11 Average Pressure on Front Roof Slope of Building 3.3.5b
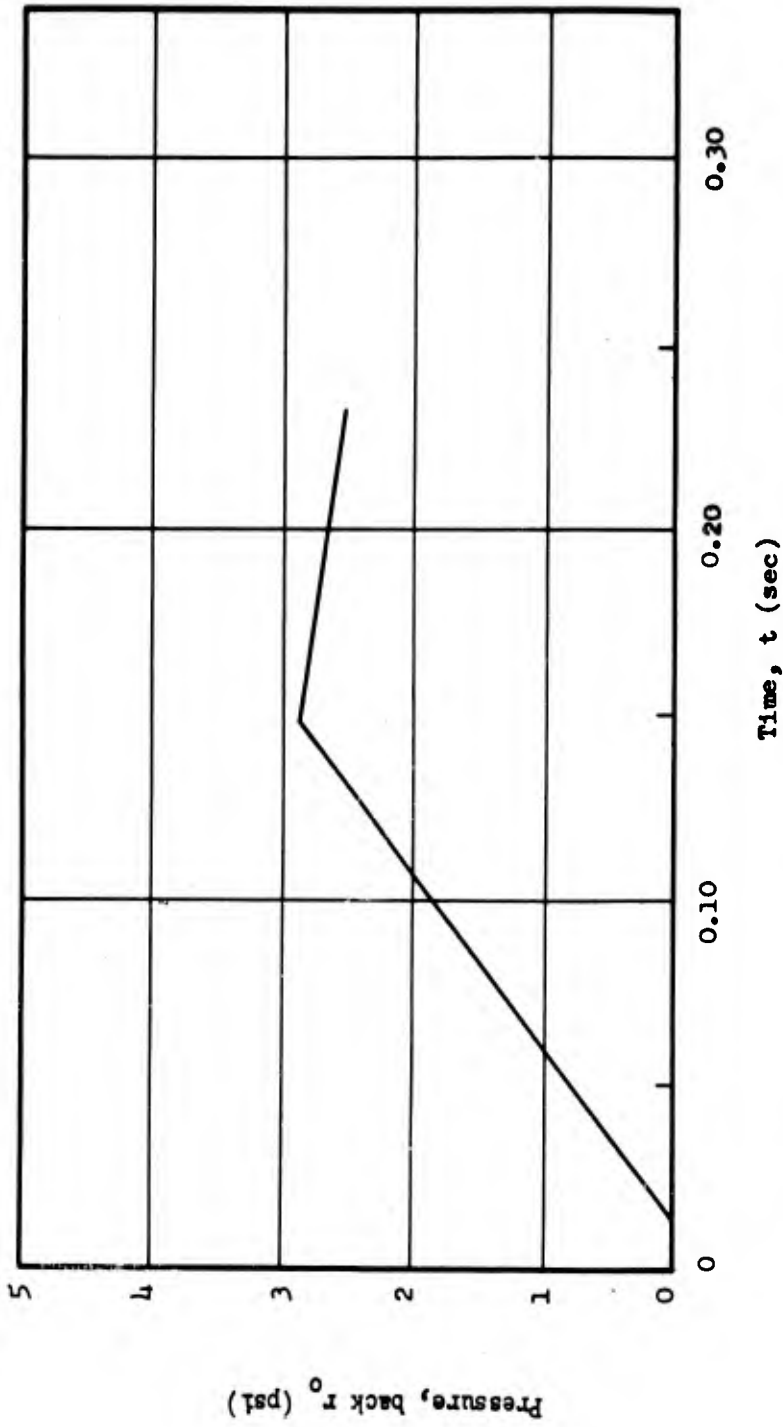
Fig. E.5.12   Average Pressure on Back Roof Slope of Building 3.3.5b
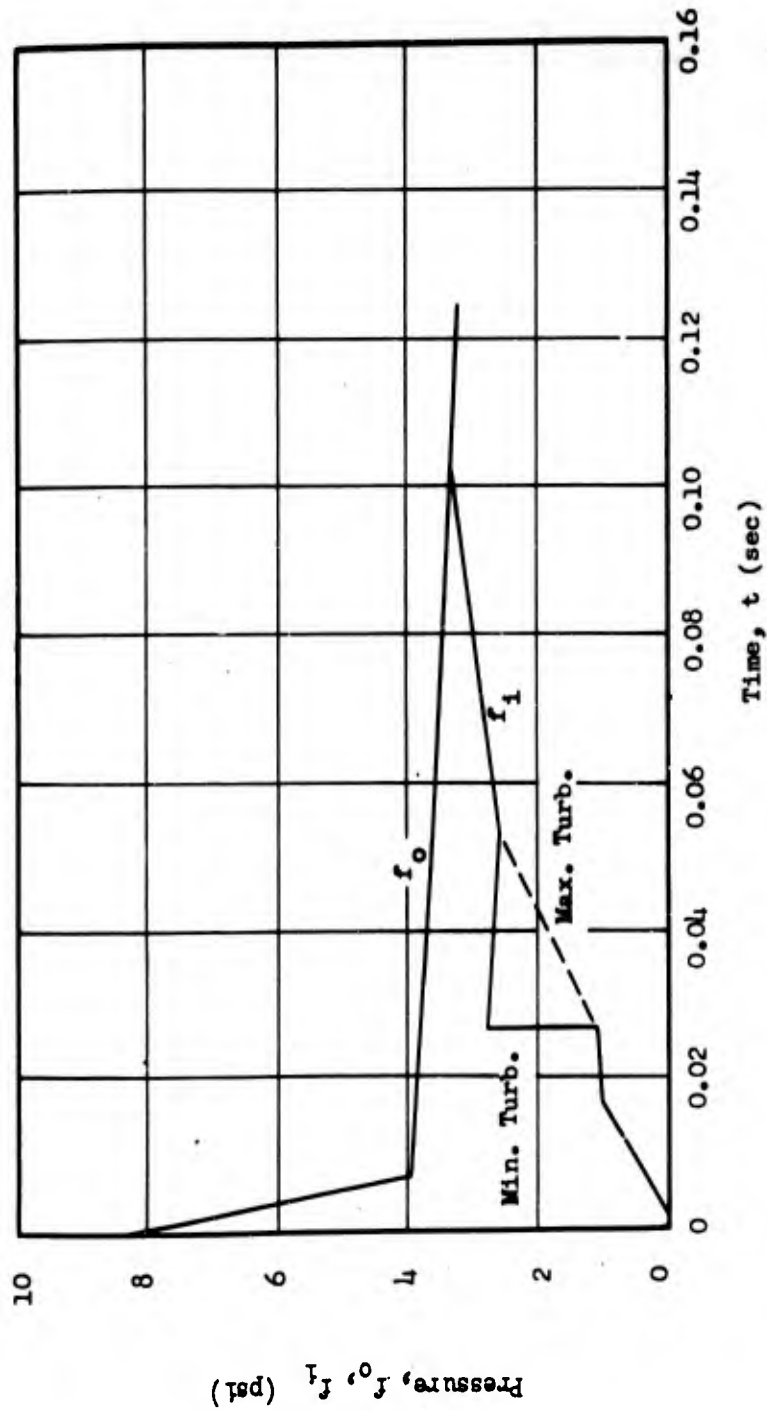
Fig. E.5.13   Average Pressure on a Portion of the Front Wall (Surface 1A) of Bldg. 3.3.5b
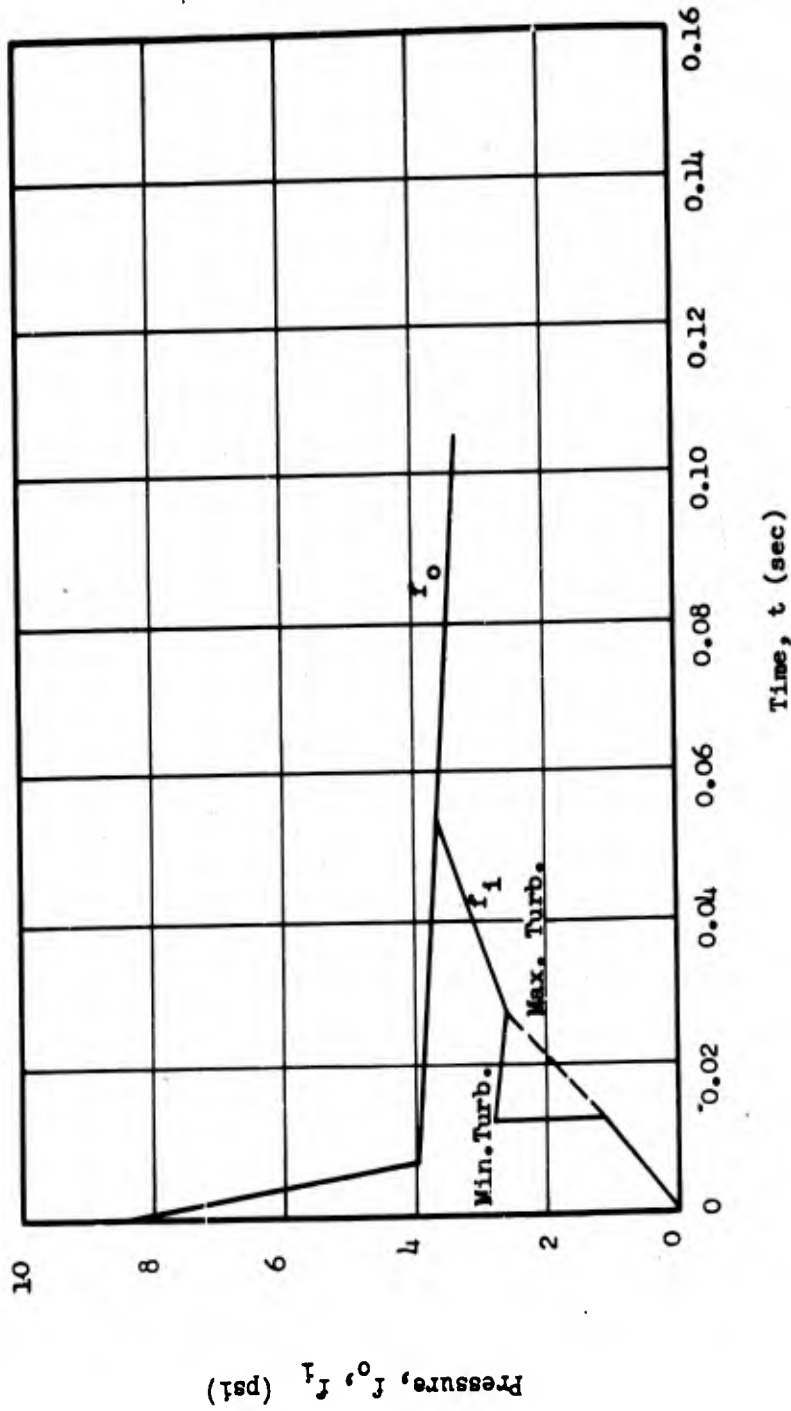
Fig. E.5.14   Average Pressure on a Portion of the Front Wall (Surface(B) of Building 3.3.5b
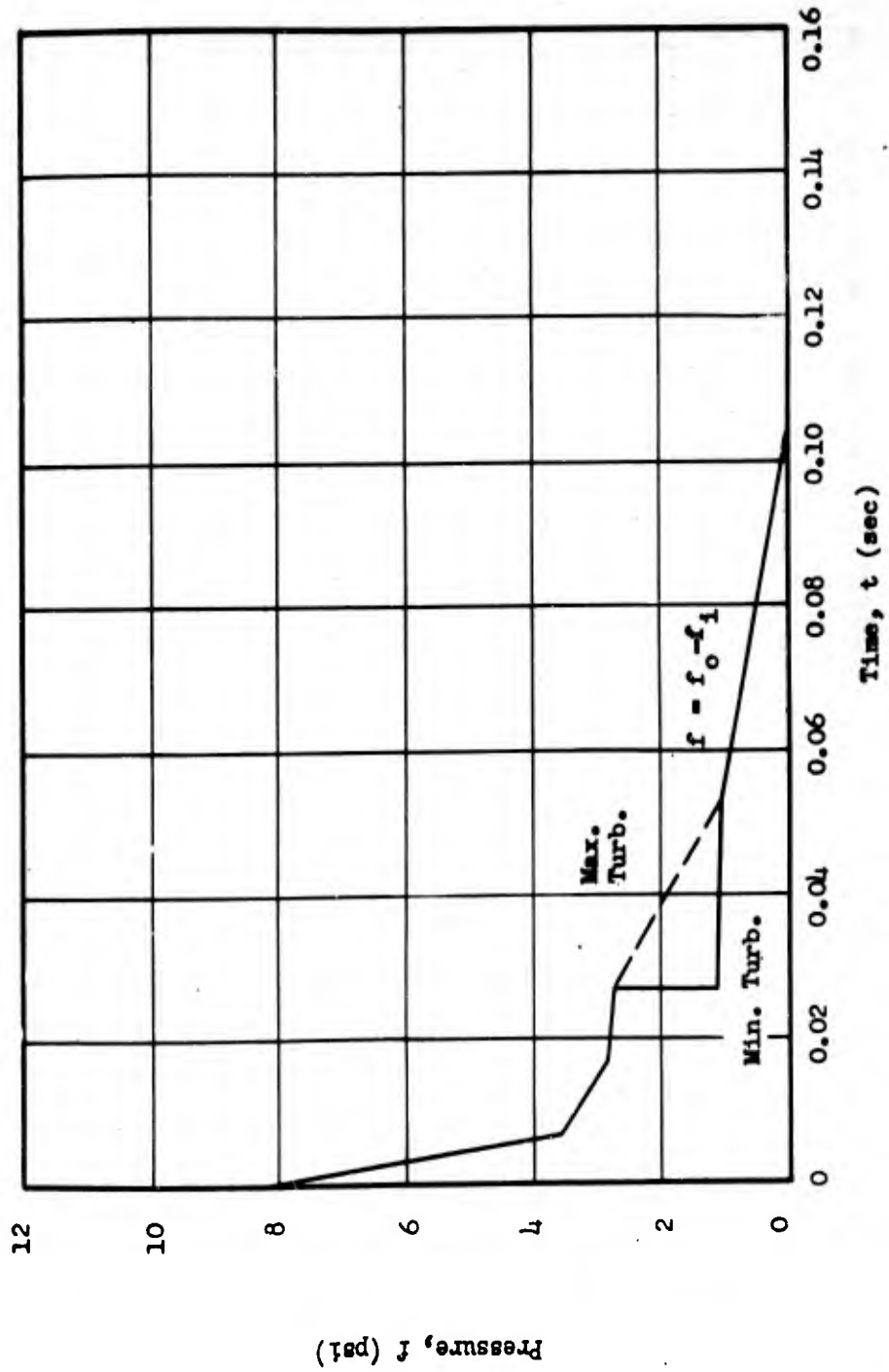
Fig. E.5.15 Net Average Pressure on a Portion of the Front Wall (Surface 1A) of Building 3.3.5b

250
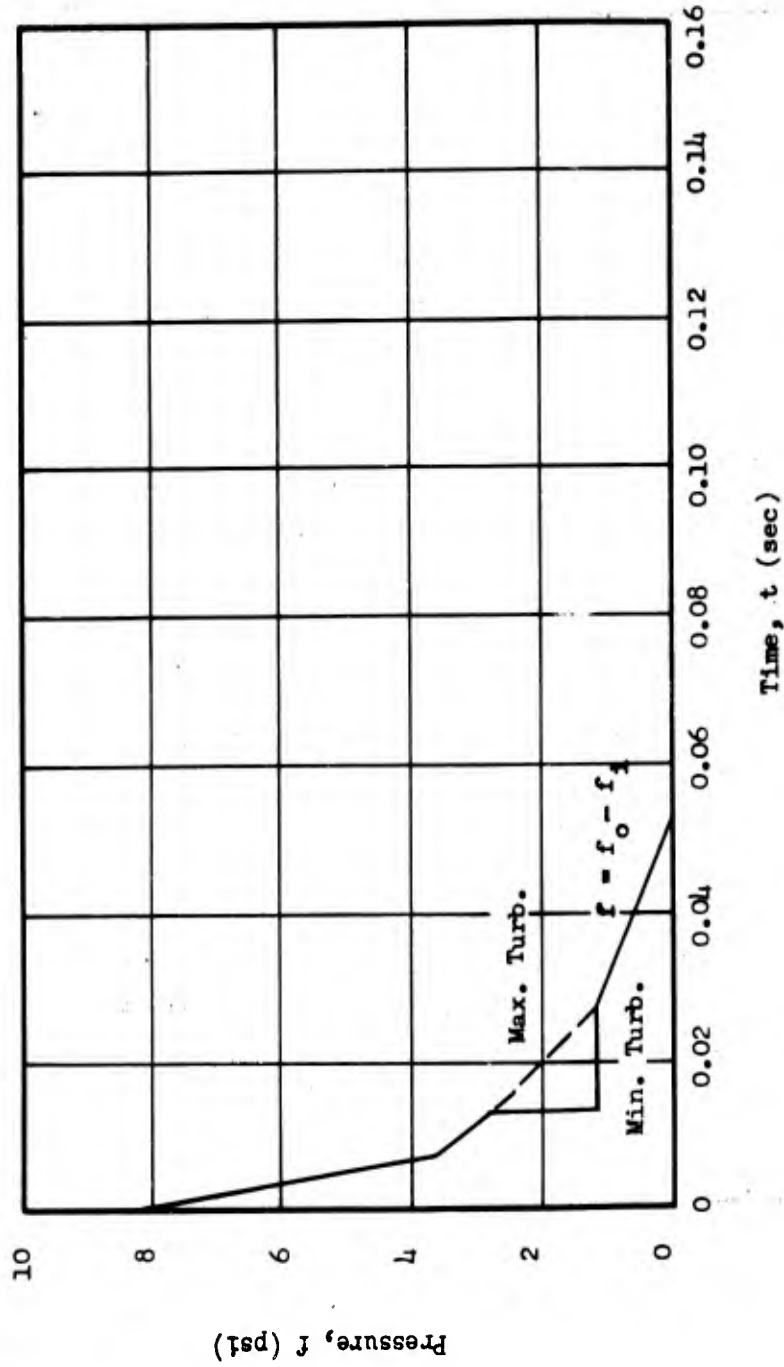
Fig. E.5.16 Net Average Pressure on a Portion of the Front Wall (Surface 1B) of Building 3.3.5b
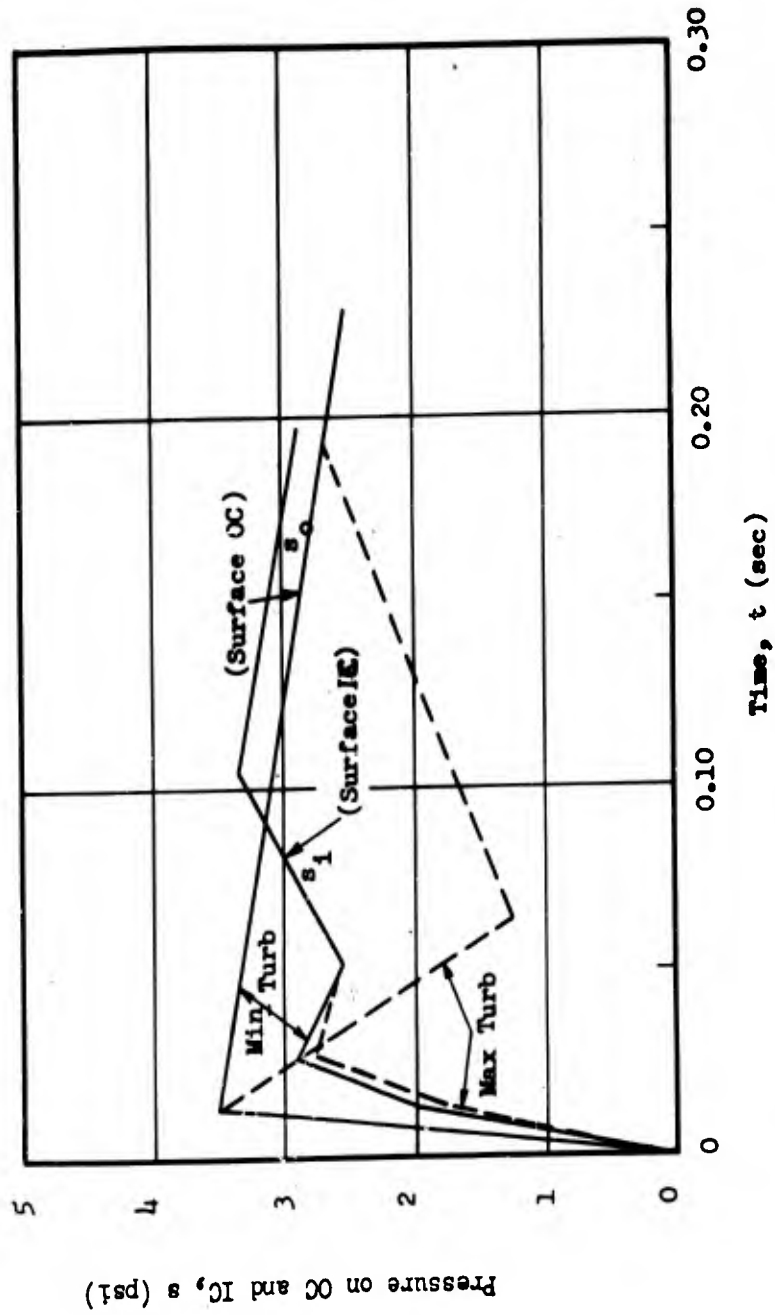
Fig. E.5.17   Average Pressure on a Portion of a Side Wall of Building 3.3.5b
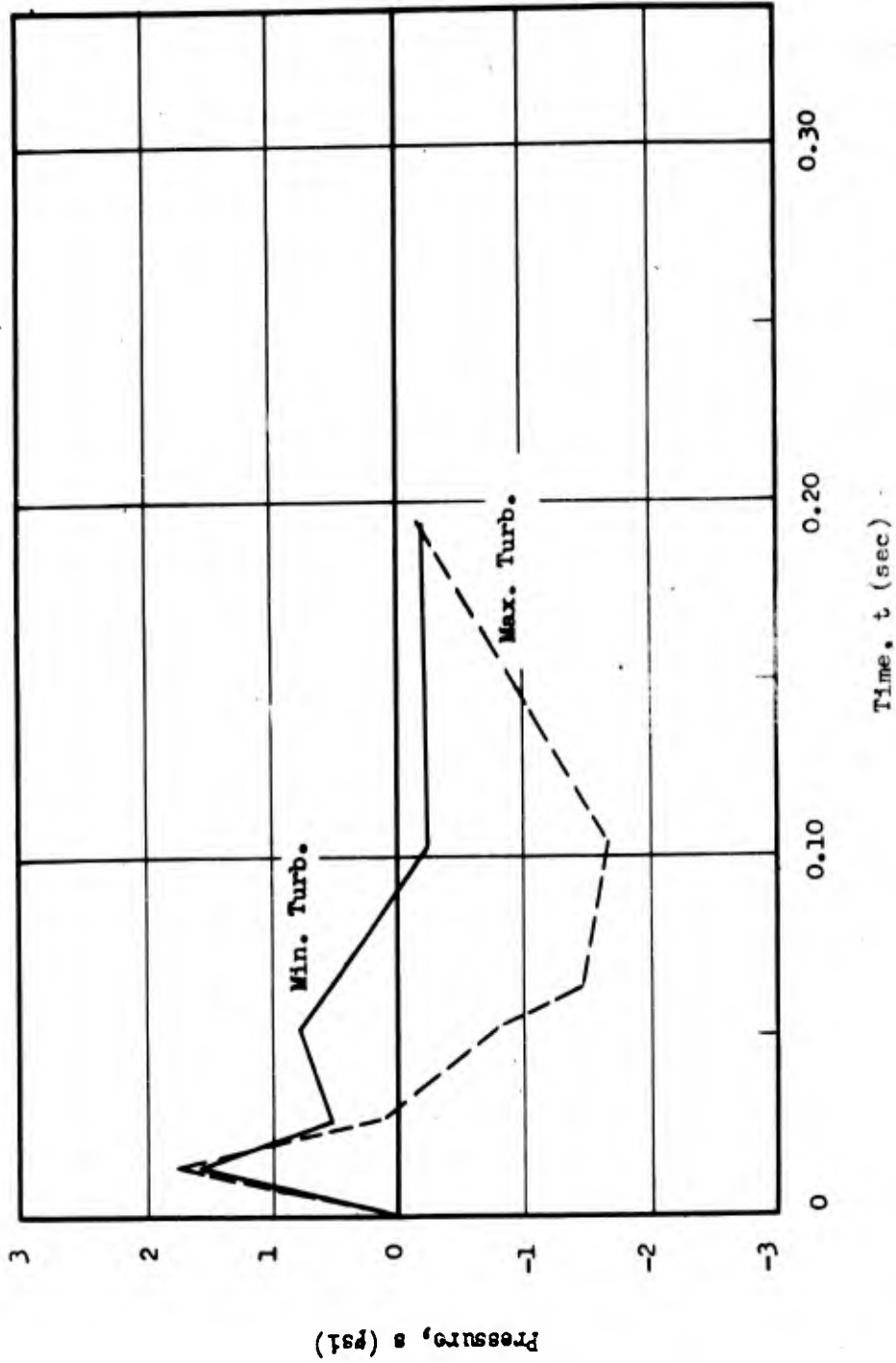
Fig. E.5.18 Net Average Pressure on a Portion of a Side Wall (OG,IC) of Building 3.3.5b
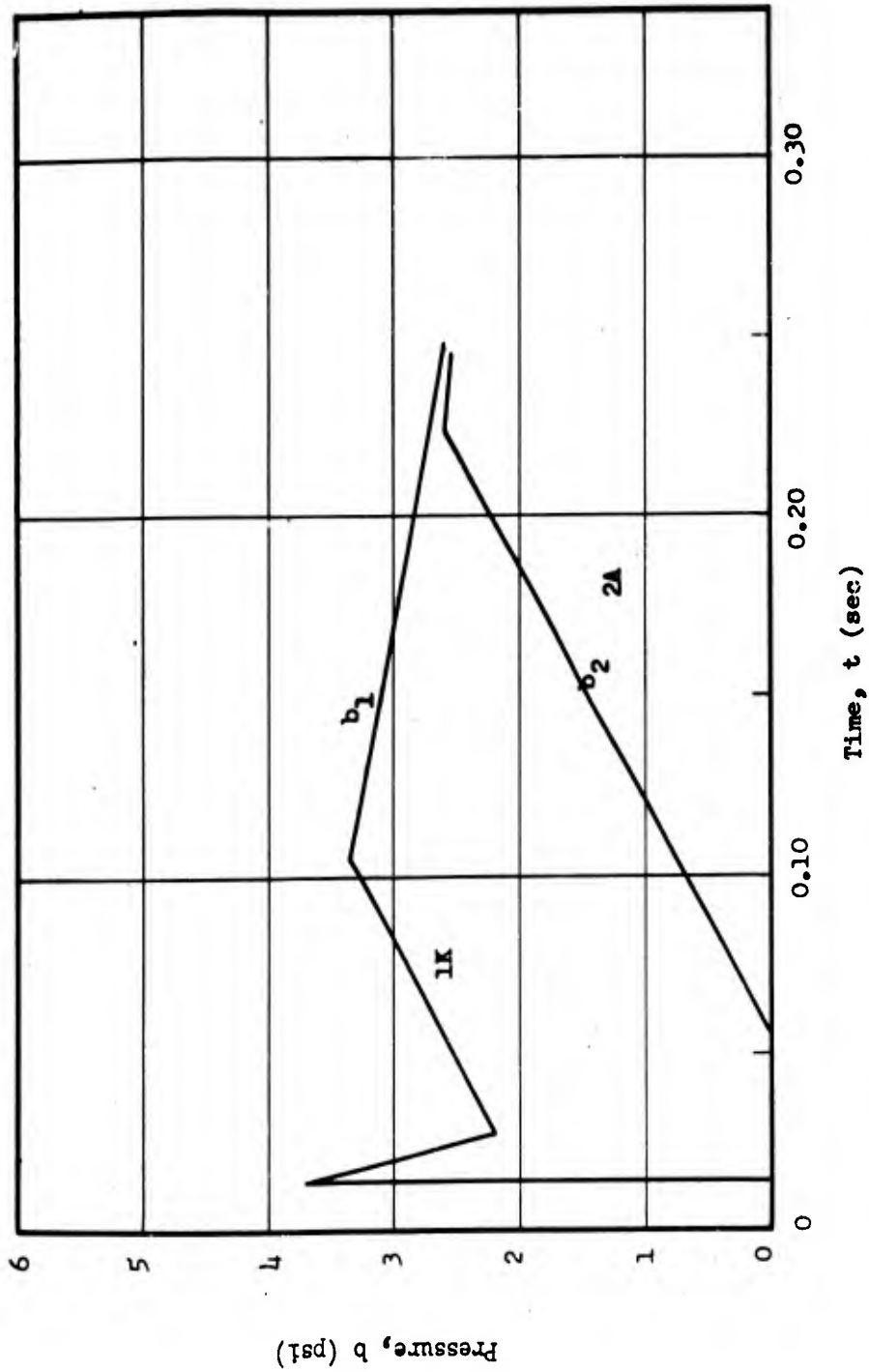
Fig. E.5.19   Average Pressure on a Partition Wall (1K, 2A) of Building 3.3.5b
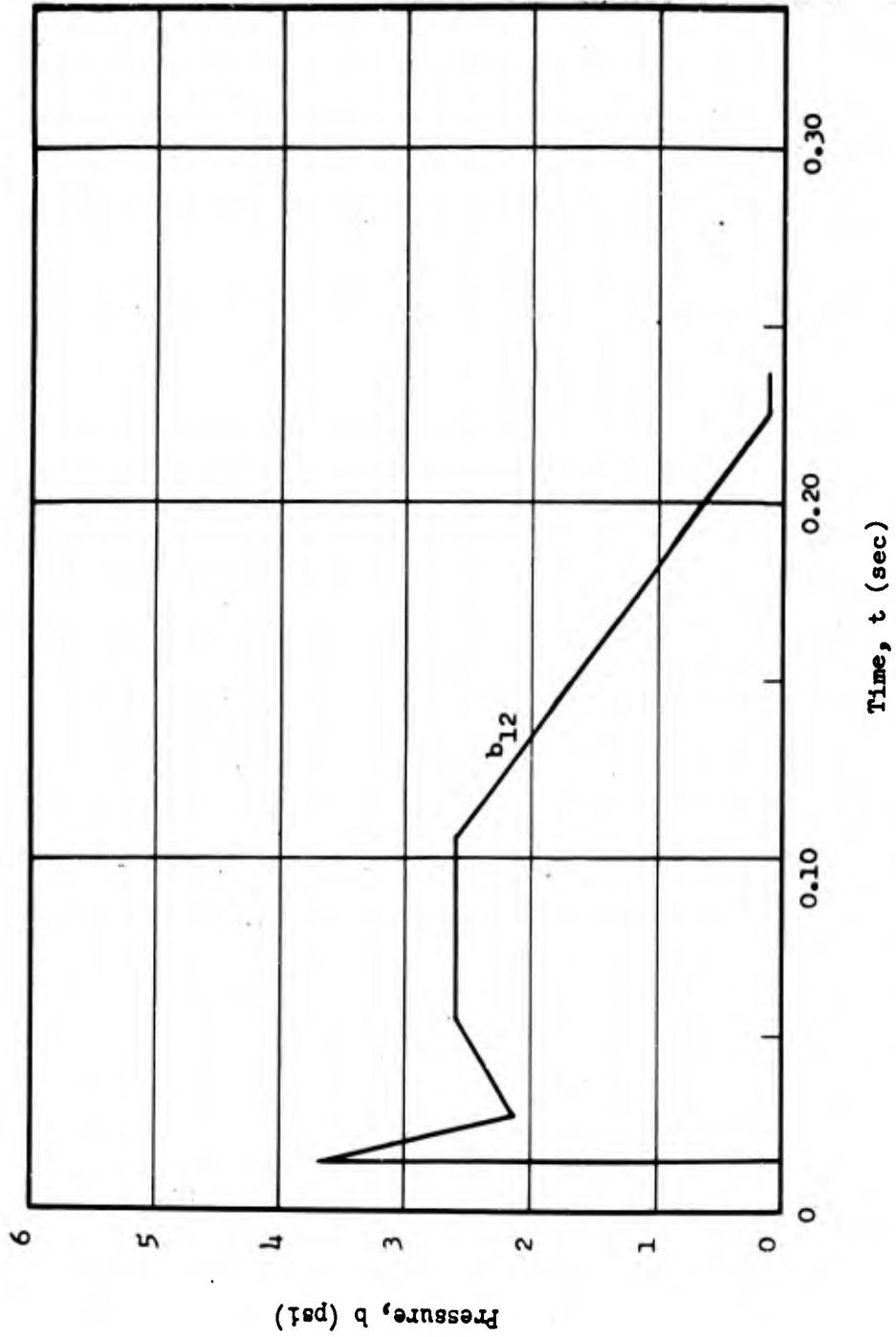
Fig. E.5.20   Net Average Pressure on a Partition Wall (1K, 2A) of Building 3.3.5b

CHAPTER E.6

BUILDING 3.3.5a

E.6.1 GENERAL

Building 3.3.5a is a duplicate of the 3.3.5b structure, but is located considerably closer to ground zero. The local shock has an 8.8 psi overpressure, rather than the 3.75-psi overpressure which struck building 3.3.5b. Figure E.6.1 shows the side-on and drag-pressure variation with time. For building 3.3.5a, as for building 3.3.5b, no response calculations are given in Part II. Since only illustrative loading predictions seem justified in such a case, this chapter presents only a very few results.

E.6.2. METHOD OF DETERMINATION OF LOADING

Applying to building 3.3.5a the methods developed in Chapter E.5.2 for calculating loadings on building 3.3.5b, a few computations of interest were performed. These are the reflected pressure on the outside front wall, given as

$$P_{refl} = 21.7 \text{ psi},$$

the initial inside shock overpressure, given as

$$p_{\sigma 1} = 2.64 \text{ psi},$$

and the pressure-time relation on the front slope of the roof, listed in Table E.6.1 and represented graphically in Fig. E.6.2.
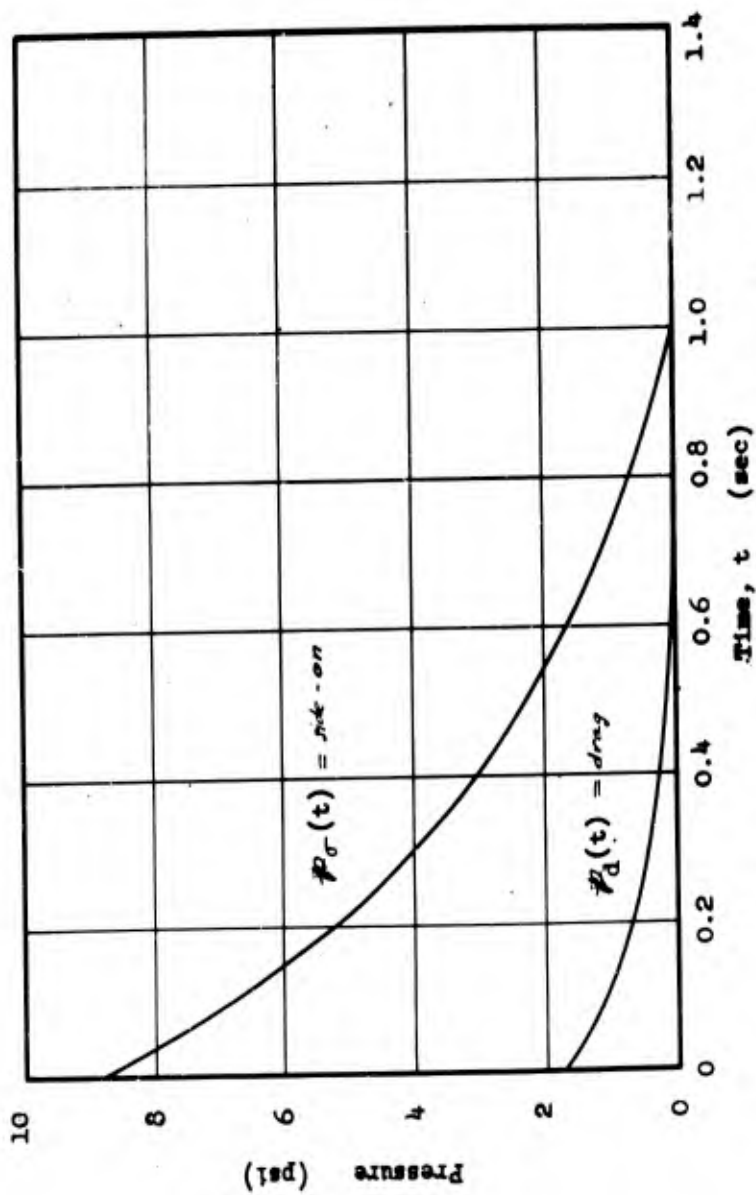
Fig. E.6.1 Side-On Pressure and Drag Pressure for $p_\sigma(0)$ = 8.8 psi
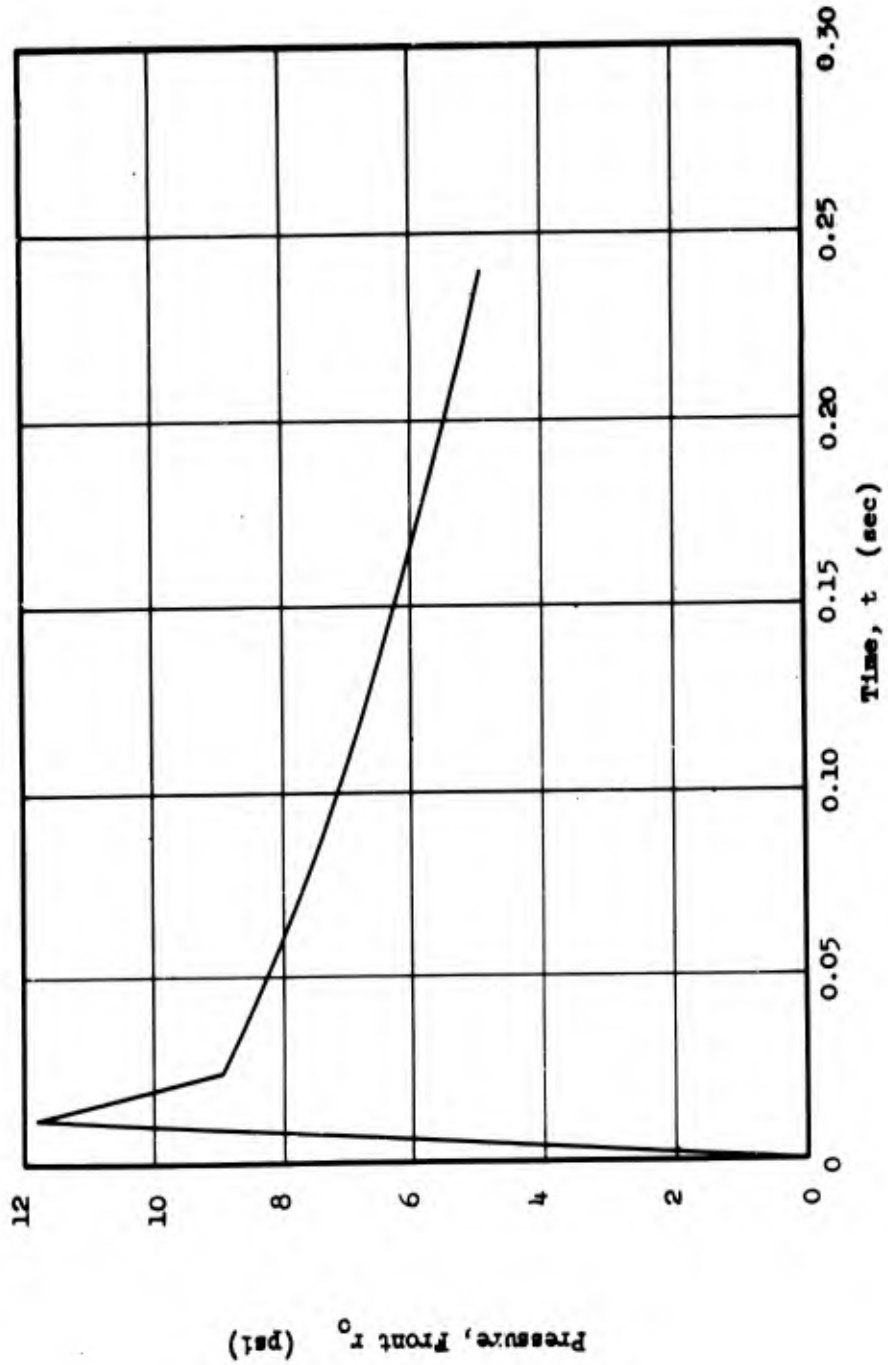
257

Fig. E.6.2 Average Pressure on Front Roof Slope of Building 3.3.5a

258

TABLE E.6.1

Average Pressures on Front Roof Slope of Building 3.3.5a

Symbolic		Numerical	
Time, t	Pressure, r_o	Time, t (sec)	Pressure, r_o (psi)
0	0	0	0
$\dfrac{\ell}{2U}$	$P_o\!\left(\dfrac{\ell}{4U}\right) + K(\theta)\left[P_{obl\ refl} - P_o\!\left(\dfrac{\ell}{4U}\right)\right]$	0.0121	11.8
$\dfrac{\ell}{U}$	$r_{os}(t)$	0.0242	8.91
	$r_{os}(t)$	0.1	7.15
	$r_{os}(t)$	0.2	5.5
	$r_{os}(t)$	0.4	3.14
	$r_{os}(t)$	0.6	1.67
	$r_{os}(t)$	0.8	0.695
$t_o + \dfrac{\ell}{2U}$	0	1.02	0

PART II THE RESPONSE OF STRUCTURES TO BLAST LOADING

CHAPTER E.7

INTRODUCTION

This portion of the test analysis report is intended to predict
the response of the model and prototype building structures to blast
loading. The loadings used herein as forcing functions for the analytical
work are those determined in Part I.

The methods of response analysis applied are fundamentally the
same as those applied in the case of the idealized model buildings as
given in Part II, Vol II. These methods, however, must be somewhat
modified and are certainly less informative here due to the less ideal
character of the structures concerned. This loss of accuracy is due to
the fact that any analytical system is actually a mathematical analogy
to the real situation and that as the buildings become less and less like
the idealized system the analogy is correspondingly more loose. Consequent-
ly, the same accuracy of prediction as was anticipated with the idealized
model structures treated in Vol II cannot reasonably be expected on the
real buildings.

Another complication of the present analyses is the necessity of
treating the components of the over-all structure. The contribution of
the windows and the wall panels during their process of failure to the load
transmitted to the main structural frame must be determined. Because of

the relatively ill-defined nature of these components, it is necessary
to make a number of simplifying assumptions. This is particularly true in
the treatment of brick panels since not only the boundary conditions of
these panels, but their very behavior as engineering materials, are not
well understood.

In this portion of the report, methods are developed for treating
the response of the above-mentioned elements to blast loading, which
determines, in turn, the reactions transmitted to the structure. These
methods are definitely only approximations. In some cases an effort is
made to bracket the actual situation rather than to make any attempt at
actually determining the response.

This portion of the report is divided into two main sections. The
first chapters of Part II deal with the treatment and the response of the
various building components, namely, glass panes, brick panels, and roofs.
The latter chapters are concerned with the response of the various buildings
to blast loadings. These building analyses apply the reactions obtained
in the component analyses to the main frames of the various structures.

The final chapter presents a discussion of the response of buildings
3.3.5a and 3.3.5b, but the treatment of these structures does not and cannot
correspond to the analysis of the idealized models or of the other real
buildings. These buildings, of the load-bearing brick-wall dwelling type,
are by their very nature much more difficult, if not impossible, to define
analytically. Therefore, the probable response to the blast loading
situation with respect to these buildings is based upon a study of damage
survey reports and upon discussions with consultants.

CHAPTER E. 8

BUILDING COMPONENTS

E.8.1 GLAZING

Many of the buildings involved in Operation Greenhouse have fairly large window areas. This fact necessitates the devising of analytical methods designed to predict the response of glass to blast loading. Since a delay of only a few milliseconds may alter the form and magnitude of a shock entering a building, the time of break of the windowpanes, t^*, is the essential quantity to be determined.

For purposed of mathematical analysis, a windowpane will be considered as a rectangular elastic plate simply supported on all sides and subjected to a uniformly distributed pressure that can vary with time. Stretching of the middle surface of the plate, elasticity of the supporting mullions, and rotational restraint of the putty and window clips will all be ignored in order to avoid undue complexity.

E.8.1.1 Strength Considerations

In order to present a numerical solution for the time of break, a representative pane will be taken from the upper outside corner on the front face of the first monitor on building 3.3.3.[1]

---

[1] See Drawing No. 100-252-1, Dept of Air Force, Hq AMC, Office of Air Installation, Wright-Patterson Air Force Base, Dayton, Ohio.

The various dimensions[2] and physical constants,[3] of this pane, are as follows:

length, b	= 20 in.
width, a	= 14 in.
thickness, h	= 1/8 in.
modulus of elasticity, E =	10×10^6 psi
density, γ	= 150 lb/ft^3
Poissons ratio, ν	= 0.23

Unfortunately, from the analytical viewpoint the ultimate strength of glass under load is not a constant, but is inversely proportional to the length of time the load has been acting and directly proportional to the rate of load increase. No data relating the strength of glass to instantaneously applied loads were found in the literature; therefore, a curve of strength versus time duration of load has been computed from several sources of information. This curve is admittedly based upon a rather liberal extrapolation and interpretation of the available data, but nevertheless, the results, because of their uniformity, lend credibility to the use of the strengths, thus derived, in the present analysis.

The curve, which is shown here as Fig. E.8.1, was constructed by plotting the breaking strengths of glass (as a percentage of the strength for a 10-sec duration) versus the time of load duration.

---

[2] Ibid.

[3] Correspondence to W. E. Lauterbach, Armour Research Foundation, Feb. 21, 1949.

Strength as Percent of Strength f
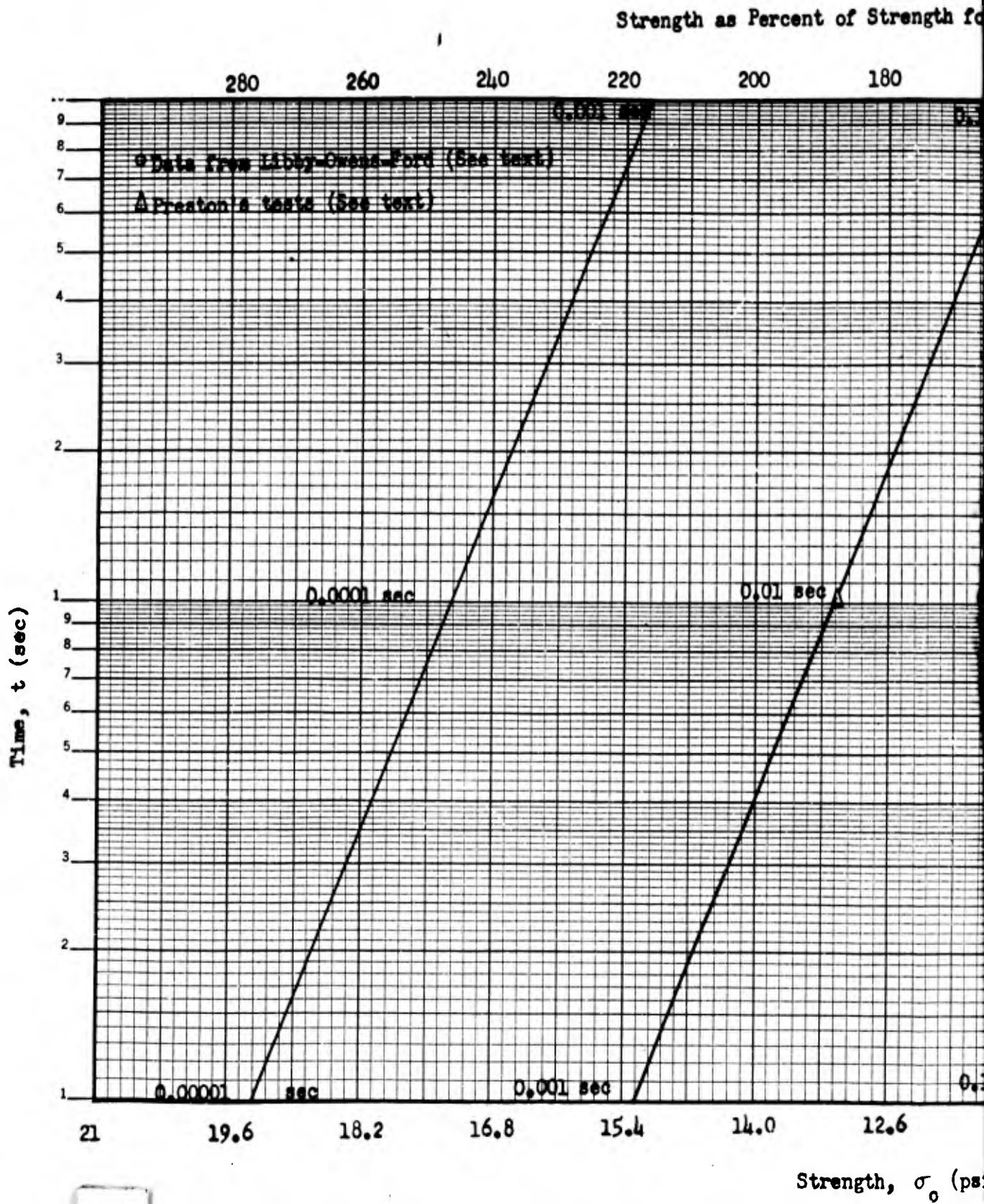
Fig. E.8.1   Ultimate Strength Vs Time

rcent of Strength for 10 sec Loadings, %

Strength, σ_o (psi x 10^{-3})
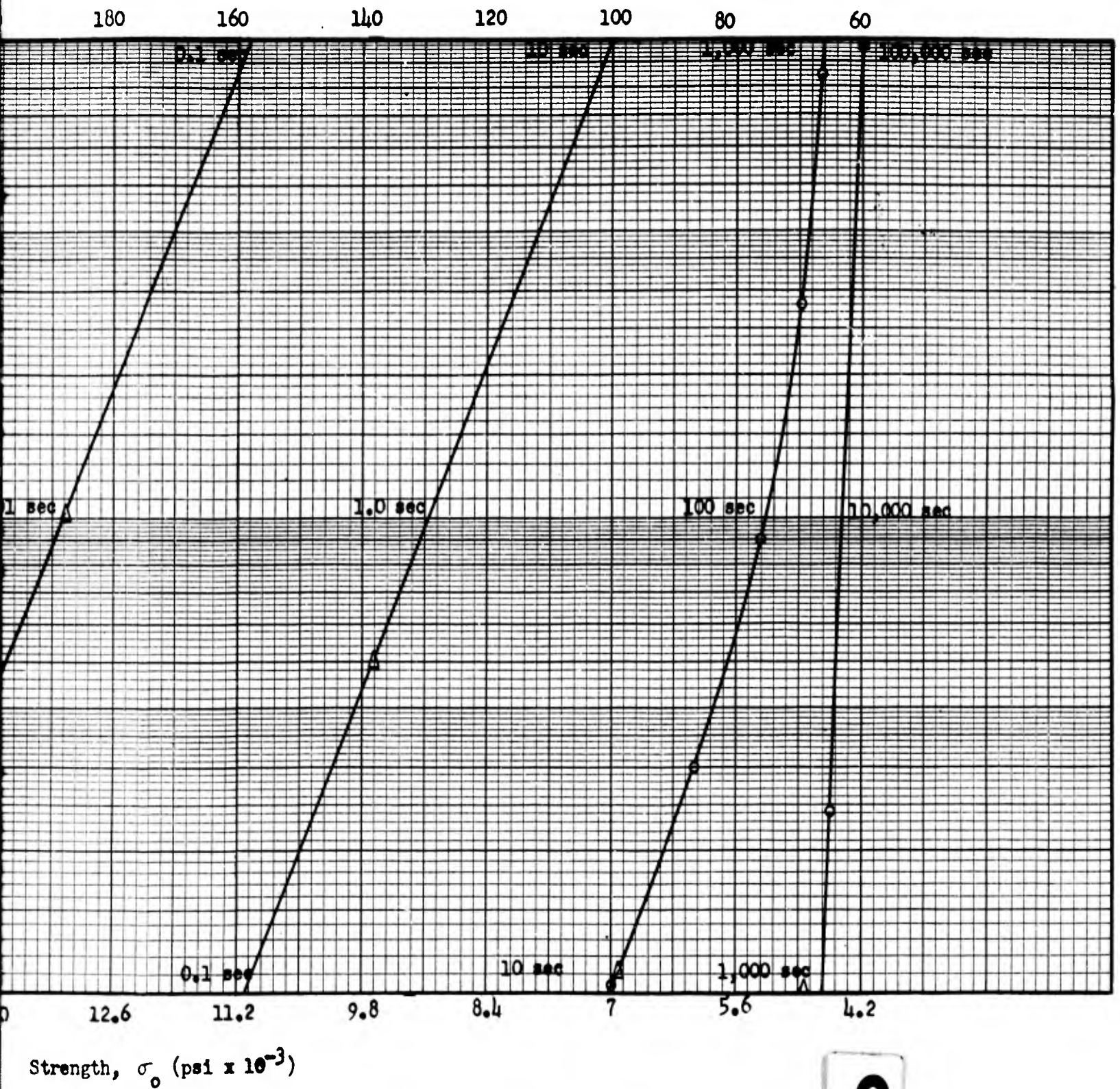
te Strength Vs Time of Load Duration for Glass

The points from 100 sec to 2400 sec were obtained from the Libby-Owens-Ford data[4] and the points, shown as Δ, covering the range from 0.1 to 100,000 sec, were obtained from Preston's tests.[5] That this reduction in strength with time is known to apply to long time periods is shown by the statement of L. Grenet, who wrote, "... this delay in fracturing is known to the Champagne makers, who never fill their bottles a second time. ... explosions of bottles of Seltzer water ... long after (they) are placed in service may be connected with this phenomenon."[6]

The decrease of strength with time duration for short times is verified by Thompson and Cousins[7] who tested commercial 14 in. by 19 in. panes under blast loadings where the load build-up was of the order of 400 psi per sec.

The static strength, if such a term may be permitted, of ordinary commercial window glass will be taken as 7000 psi and will also be taken to correspond to the 100 per cent or 10-sec load duration point on Fig. E.8.1. This value of ultimate strength, which will hereinafter be designated symbolically as σ_0, is based on 5000 samples tested by A. E. Williams.[8]

---

[4] Ibid.

[5] F. W. Preston, Jr, "The Mechanical Properties of Glass," J Applied Physics, 1948, pp 623-34.

[6] L. Grenet, in Bul Soc. Encour. Ind. Nat., IV (1899), 839. (In French; trans by F. W. Preston, Jr, J Am. Ceram Soc., XVIII (1935), 219.)

[7] N. J. Thompson and E. W. Cousins, "Explosion Tests on Glass Windows; Effect on Glass Breakage of Varying the Rate of Pressure Application," J Am. Ceram Soc., XXXII (1949), 313-15.

[8] A. E. Williams, "The Mechanical Strength of Glazing Glass," J Am. Ceram Soc., VI (1923), 980-88.

In order to develop a quantitative idea of the strength of the 14 in. by 20 in. pane of building 3.3.3, the static strength will be determined.

Using the Watkins' formula for flat glass plates[9]

$$q_{max} = \frac{2(a^2 + b^2)h^2}{a^2 b^2 K} \sigma_o \qquad (E.8.1)$$

where $K \neq 0.6$ is a physical constant for glass and a, b, h, and σ_o have been given, the maximum uniformly distributed pressure, q_{max}, is

$$q_{max} = \frac{(2)(14^2 + 20^2)}{(20^2)(14^2)(0.6)} \sigma_o = \frac{\sigma_o}{2516}. \qquad (E.8.2)$$

For the 10-sec duration, $\sigma_o = 7000$ psi

and

$$q_{max} = \frac{7000}{2516} = 2.78 \text{ psi.} \qquad (E.8.3)$$

A check with experimental data may be made by comparing the above value with the 60-sec duration tests of Thompson and Cousins on their 14 in. by 19 in. pane.[10] Reducing our value of $q_{10 \text{ sec}}$ to $q_{60 \text{ sec}}$ by means of Fig. E.8.1 gives

---

[9] G. B. Watkins and R. W. Wampler, "The Strength of Flat Glass Under Load," Bul Am. Ceram Soc., XV (1936), 243-45. The exact solution for a simply supported plate with $\nu = 0.23$ can be obtained from Eq. E.8.47 letting cos p(t) = 0. This result will give K = 1.2. Watkins' formula using K = 0.6 actually takes into account the edge restraint of the mullions and clips and doubles the load carrying capacity.

[10] Thompson and Cousins, loc. cit.

$$q_{60 \text{ sec}} = q_{10 \text{ sec}} \times 0.81 = 2.78 \times 0.81 = 2.2 \text{ psi}$$

Thompson gives q_{60} psi for a linearly built-up load. This value should be reduced to account for the build-up. Probably by using $t = 30$ sec for the analytical data the same result can be accomplished. Effectively, this change is the same as taking the average time over the linear build-up.

Then analytically,

$$q_{30 \text{ sec}} = q_{10 \text{ sec}} \times 0.9 = 2.78 \times 0.9$$

$$\text{or} \quad q_{max} = 2.5 \text{ psi}$$

and experimentally

$$q_{max} = 2.5 \text{ psi}$$

Notwithstanding the fact that one pane is 20 in. long and the other is 19 in. long, these results indicate at least that the strength-time curve is fairly good in the range just considered.

E.8.1.2 Dynamic Response

Let a and b denote the lengths of the sides of the pane and let the axes be taken as shown in Fig. E.8.2. Whatever function of the coordinates the deflection, v, may be, it always can be represented within the limits of the rectangle by the double series

$$v = \sum_{m=1}^{m=\infty} \sum_{n=1}^{n=\infty} q_{mn} \sin \frac{m\pi x}{b} \sin \frac{n\pi y}{a} \tag{E.8.4}$$

where q_{mn}, the coefficients, are the generalized coordinates for this case.
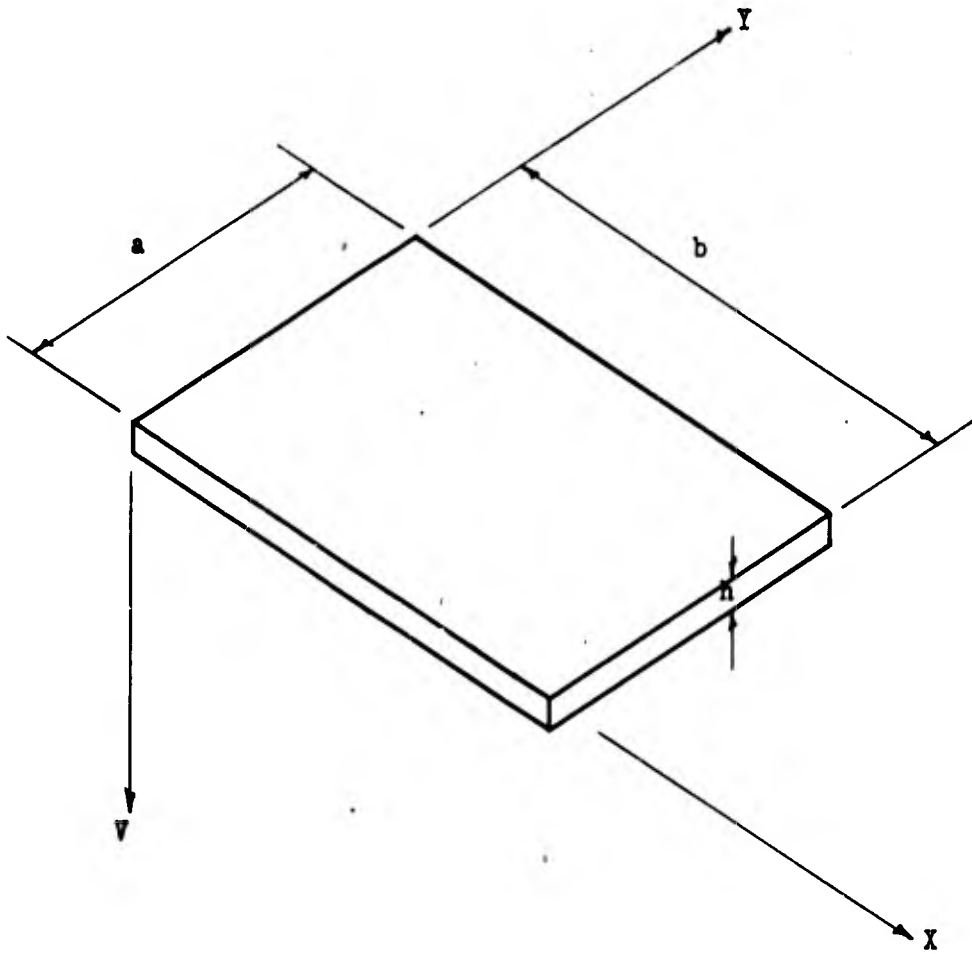
Fig. E.8.2   Axes of Pane

Lagrange's equation of motion for forced vibrations of an elastic body is, for a conservative system,

$$\frac{d}{dt}\left(\frac{\partial T}{\partial \dot{q}_{mn}}\right) + \frac{\partial V}{\partial q_{mn}} = Q_{mn} \qquad (E.8.5)$$

where the potential energy of bending and the kinetic energy are given, respectively, by

$$V = \frac{\pi^4 ab}{8} D \sum_{m=1}^{m=\infty} \sum_{n=1}^{n=\infty} q^2_{mn}\left(\frac{m^2}{b^2} + \frac{n^2}{a^2}\right)^2 \qquad (E.8.6)[11]$$

and

$$T = \frac{\gamma h}{2g} \cdot \frac{ab}{4} \sum \sum \dot{q}^2_{mn} \qquad (E.8.7)[12]$$

Substituting V and T into Eq. E.8.5 yields

$$\frac{\gamma h}{g} \cdot \frac{ab}{4} \ddot{q}_{mn} + \pi^4 \frac{ab}{4} D \, q_{mn} \left(\frac{m^2}{b^2} + \frac{n^2}{a^2}\right)^2 = Q_{mn} \qquad (E.8.8)$$

or

$$\frac{\gamma h}{g} \cdot \ddot{q}_{mn} + \pi^4 D \, q_{mn}\left(\frac{m^2}{b^2} + \frac{n^2}{a^2}\right)^2 = \frac{4}{ab} Q_{mn} \qquad (E.8.9)$$

In order to obtain the generalized force, Q_{mn}, assume that the beam is subjected to a uniformly varying load of intensity $\rho = \rho_o \cos wt$, psi. Let a small increase δq_{mn} be given to a coordinate q_{mn}. The corresponding deflection of the plate, from Eq. E.8.4, will be

$$\delta\gamma = \delta q_{mn} \sin\frac{m\pi x}{b} \sin\frac{n\pi y}{a} \qquad (E.8.10)$$

---

[11] S. Timoshenko, Vibration Problems in Engineering (2nd ed.; New York: D. Van Nostrand Co., Inc, 1937), p. 423.

[12] Ibid.

and the work done by the force intensity ρ on this displacement is

$$dU = \rho \delta q_{mn} \sin \frac{m\pi x}{b} \sin \frac{n\pi y}{a} . \tag{E.8.11}$$

The total work over the whole plate is then,

$$U = \int_0^a \int_0^b dU \, dx \, dy = \rho \delta q_{mn} \int_0^a \int_0^b \sin \frac{m\pi x}{b} \sin \frac{n\pi y}{a} \, dx \, dy \tag{E.8.12}$$

Therefore, the generalized force is the coefficient of δq_{mn} or,

$$Q_{mn} = \rho_0 \cos wt \int_0^a \int_0^b \sin \frac{m\pi x}{b} \sin \frac{n\pi y}{a} \, dx \, dy. \tag{E.8.13}$$

Integrating Eq. E.8.13 yields

$$Q_{mn} = \frac{4 \, ab}{\pi^2 mn} \rho_0 \cos wt \tag{E.8.14}$$

so that Eq. E.8.9 becomes

$$\frac{\gamma h}{g} \ddot{q}_{mn} + \pi^4 D \, q_{mn} \left(\frac{m^2}{b^2} + \frac{n^2}{a^2} \right)^2 = \frac{16}{\pi^2 mn} \rho_0 \cos wt \tag{E.8.15}$$

The complimentary solution is

$$(q_{mn})_1 = C_1 \cos pt + C_2 \cos pt \tag{E.8.16}$$

where the square of the natural frequency is

$$p^2 = \frac{\pi^4 gD}{\gamma h} \left(\frac{m^2}{b^2} + \frac{n^2}{a^2} \right)^2 \tag{E.8.17}$$

and C_1, C_2 are arbitrary constants to be determined by the initial conditions. For the particular solution put

$$(q_{mn})_2 = C_3 \cos wt + C_4 \sin wt \tag{E.8.18a}$$

so that

$$(\dot{q}_{mn})_2 = -C_3 w \sin wt + C_4 w \cos wt \qquad (E.8.18.b)$$

$$(\ddot{q}_{mn})_2 = -C_3 w^2 \cos wt - C_4 w^2 \sin wt \qquad (E.8.18.c)$$

and substitute (b) and (c) into Eq. E.8.15 after letting

$$K = \pi^4 D\left(\frac{m^2}{b^2} + \frac{n^2}{a^2}\right)^2 \qquad (E.8.19.a)$$

$$\bar{m} = \frac{\gamma h}{g} \qquad (E.8.19.b)$$

to obtain

$$C_3(K - \bar{m}w^2) \cos wt + C_4(K - \bar{m}w^2) \sin wt = \frac{16}{mn \, \pi^2} \, \rho_o \cos wt \qquad (E.8.20)$$

Equation E.8.20 is satisfied for all values of t if

$$C_3(K - \bar{m}w^2) = \frac{16}{mn \, \pi^2} \, \rho_o \qquad (E.8.21.a)$$

and

$$C_4 = 0. \qquad (E.8.21.b)$$

For the case where $K - \bar{m}w^2 \neq 0$, that is, $w \neq \sqrt{\frac{K}{\bar{m}}}$, condition of E.8.21.a yields

$$\dot{C}_3 = \frac{16}{mn \, \pi^2 (K - \bar{m}w^2)} \, \rho_o \qquad (E.8.21.c)$$

Then from Eq. E.8.18.a

$$(q_{mn})_2 = \frac{16}{mn \, \pi^2 (K - \bar{m}w^2)} \, \rho_o \cos wt \qquad (E.8.22)$$

and the complete solution is

$$q_{mn} = (q_{mn})_1 + (q_{mn})_2$$

or

$$q_{mn} = C_1 \cos pt + C_2 \sin pt + \frac{16 \rho_o}{mn \, \pi^2 (K - \bar{m}w^2)} \cos wt, \qquad (E.8.23)$$

Which when substituted into the equation for displacement, Eq. E.8.4, yields

$$v(x,y,t) = \sum_{m=1}^{m=\infty} \sum_{n=1}^{n=\infty} \left[C_1 \cos pt + C_2 \sin pt + \frac{16 \rho_0 \cos wt}{mn \, \pi^2 (K - \overline{m}w^2)} \right] \quad (E.8.24)$$

$$\sin \frac{m\pi x}{b} \sin \frac{n\pi y}{a} \, .$$

Considering the first mode of vibration only, $m = n = 1$, obtains

$$v(x,y,t) = \left[C_1 \cos pt + C_2 \sin pt + \frac{16 \rho_0 \cos wt}{\pi^2 (K - \overline{m}w^2)} \right] \sin \frac{\pi x}{b} \sin \frac{\pi y}{a} \, .$$

$$(E.8.25)$$

The initial conditions, $v(x,y,0) = 0$ and $\dot{v}(x,y,0) = 0$ yield, from Eq. E.8.25,

$$0 = \left[C_1 + \frac{16 \rho_0}{\pi^2 (K - \overline{m}w^2)} \right] \sin \frac{\pi x}{b} \sin \frac{\pi y}{a} \quad (E.8.26)$$

and

$$0 = C_2 \sin \frac{\pi x}{b} \sin \frac{\pi y}{a} \quad (E.8.27)$$

so that (since $\sin \frac{\pi x}{b} \sin \frac{\pi y}{a} \neq 0$)

$$C_1 = - \frac{16 \rho_0}{\pi^2 (K - \overline{m}w^2)}$$

$$C_2 = 0$$

Then the deflection becomes

$$v(x,y,t) = \frac{16 \rho_0}{\pi^2 (K - \overline{m}w^2)} (\cos wt - \cos pt) \sin \frac{\pi x}{b} \sin \frac{\pi y}{a} \, . \quad (E.8.28)$$

At the center of the plate, where $x = b/2$, $y = a/2$, the defelection is

$$v \left(\frac{b}{2}, \frac{a}{2}, t \right) = \frac{16 \rho_0}{\pi^2 (K - \overline{m}w^2)} (\cos wt - \cos pt) \quad (E.8.29)$$

And may be rewritten, after noting that $p^2 = \frac{K}{\overline{m}}$, so that

$$(K - \overline{m}w^2) = \overline{m}(p^2 - w^2) \quad (E.8.30)$$

And Eq. E.8.29 becomes

$$v\left(\frac{b}{2}, \frac{a}{2}, t\right) = \frac{16\rho_\ell}{\pi^2 \bar{m}(p^2 - w^2)} \ (\cos wt - \cos pt). \quad (E.8.31)$$

For the case of a constant pressure, $\rho = \rho_o \cos wt = \rho_o$ or $w = 0$,

Eq. E.8.31 becomes

$$v\left(\frac{b}{2}, \frac{a}{2}, t\right) = \frac{16\rho_\ell}{\bar{m}\ \pi^2 p^2} \ (1 - \cos pt) \quad (E.8.32)$$

or

$$v(x,y,t) = \frac{16\rho_\ell}{\bar{m}\ \pi^2 p^2} \ \sin\frac{\pi x}{b} \ \sin\frac{\pi y}{a} \ (1 - \cos pt). \quad (E.8.33)$$

The maximum deflection possible occurs when $pt = \pi$ so that

$$v\left(\frac{b}{2}, \frac{a}{2}, \frac{\pi}{p}\right) = 2 \times \frac{16\rho_o}{\bar{m}\ \pi^2 p^2} \quad (E.8.34)$$

since

$$\bar{m} = \frac{\gamma h}{g}$$

and

$$p^2 = \frac{\pi^4 g D}{\gamma h} \left(\frac{1}{a^2} + \frac{1}{b^2}\right)^2, \quad (E.8.17)$$

$$v\left(\frac{b}{2}, \frac{a}{2}, \frac{\pi}{p}\right) = 2 \times \frac{16\rho_o}{\pi^6 D \left(\frac{1}{a^2} + \frac{1}{b^2}\right)^2}. \quad (E.8.35)$$

The approximate solution for a uniformly loaded plate in the static case is

$$v_{max} = \frac{16\rho_o}{\pi^6 D \left(\frac{1}{a^2} + \frac{1}{b^2}\right)^2} \quad (E.8.36)[13]$$

which is exactly one-half of Eq. E.8.35. This comparison shows the effect of the dynamic load factor to be equal to 2, which was expected.

---

[13] S. Timoshenko, Theory of Plates and Shells (McGraw-Hill Book Co., Inc.: New York, 1940), p 119.

The stress, which is a maximum at the center, may
be obtained from the relations[14]

$$\sigma_x = \frac{Eh}{2(1 - v^2)}\left(\frac{1}{r_x} + v\,\frac{1}{r_y}\right) \tag{E.8.37}$$

$$\sigma_y = \frac{Eh}{2(1 - v^2)}\left(\frac{1}{r_y} + v\,\frac{1}{r_x}\right) \tag{E.8.38}$$

where

$$\frac{1}{r_x} = \frac{\partial^2 v}{\partial x^2} \quad ; \quad \frac{1}{r_y} = -\frac{\partial^2 v}{\partial y^2} \tag{E.8.39}$$

Rewriting Eq. E.8.28,

$$v(x,y,t) = \frac{16\rho_e}{\pi^2(K - \overline{w}^2)}\,\sin\frac{\pi x}{b}\,\sin\frac{\pi y}{a}\,(\cos wt - \cos pt),$$

as

$$v(x,y,t) = \psi\,\sin\frac{\pi x}{b}\,\sin\frac{\pi y}{a} \tag{E.8.40}$$

where, in order to save space,

$$\psi = \frac{16\rho_e\,(\cos wt - \cos pt)}{\pi^2(K - \overline{w}^2)} \tag{E.8.41}$$

we obtain for the curvatures from Eqs. E.8.39

$$\frac{1}{r_x} = \frac{\pi^2}{b^2}\,v \quad ; \quad \frac{1}{r_y} = \frac{\pi^2}{a^2}\,v \tag{E.8.42}$$

so that upon substitution of Eqs. E.8.42 into E.8.38 (since σ_y is
obviously the maximum)

$$\sigma_y = \frac{\pi^2 Eh(b^2 + v\,a^2)}{2\,a^2 b^2(1 - v^2)}\,\psi \quad . \tag{E.8.43}$$

Where, as before, we consider the suddenly applies constant uniform load
of the pseudo-steady state condition where $w \rightarrow 0$, then

---

[14] Ibid., p 40.

$$Y - Y_0 = \frac{16 \rho_0}{K \pi^2} (1 - \cos pt). \qquad (E.8.44)$$

Substituting the value of K from Eq. E.8.19.a into Eq. E.8.44 yields

$$Y_0 = \frac{16 \rho_0 (1 - \cos pt)}{\pi^6 D \left(\frac{1}{a^2} + \frac{1}{b^2}\right)^2} \qquad (E.8.45)$$

and Eq. E.8.43 becomes

$$\sigma_{yo} = \frac{96 \; a^2 b^2 (b^2 + \gamma a^2)}{\pi^4 h^2 (b^2 + a^2)^2} \quad \rho_0 \; (1 - \cos pt). \qquad (E.8.46)$$

Since $\pi^4 = 97.4$ we may, with very little error, write Eq. E.8.41 as

$$\sigma_{yo} = \frac{a^2 b^2}{h^2} \cdot \frac{b^2 + \gamma a^2}{(b^2 + a^2)^2} \cdot \rho_0 \; (1 - \cos pt). \qquad (E.8.47)$$

Using the dimensions given previously, and the pseudo-steady state
pressure from Fig. E.8.3 we obtain for Eq. (E.8.47)

$$a = 14 \text{ in.}$$

$$b = 20 \text{ in.}$$

$$h = 1/8 \text{ in.}$$

$$\gamma = 0.23$$

$$\rho_0 = 3.56 \text{ psi}$$

$$\sigma_{yo} = \frac{(14)^2 (20)^2}{(1/8)^2} \cdot \frac{20^2 + 0.23 \cdot 14^2}{(14^2 + 20^2)^2} \cdot 3.56 \; (1 - \cos \; pt)$$

or

$$\sigma_{yo} = 22,300(1 - \cos pt). \qquad (E.8.48)$$

Evaluating p, the natural frequency, from Eq. E.8.17

$$p = \pi^2 \left(\frac{1}{a^2} + \frac{1}{b^2}\right) \quad h \quad \sqrt{\frac{Eg}{12(1 - \gamma^2)\gamma}} \; ,$$

we obtain

$$p = \pi^2 \left(\frac{1}{14^2} + \frac{1}{20^2}\right)\left(\frac{1}{8}\right) \sqrt{\frac{10 \times 10^6 \times 386 \times 1728}{12(1 - 0.23^2)(150)}}$$

or

$$p = 585 \text{ rad/sec}$$

so that Eq. E.8.48 becomes

$$\sigma_{yo} = 22,300(1 - \cos 585t). \tag{E.8.49}$$

Equation E.8.49 is plotted as σ_{act} on Fig. E.8.5 and the ultimate strengths taken from Fig. E.8.1 are included on the same plot. The intersection of the two curves shows the time at which the actual stress starts to exceed the ultimate stress and may, therefore, be taken as the time of break, t^*. The value of time is seen to be $t^* = 0.0021$ sec. The loading calculations of Part I were made on the assumption that $t^* = 0.002$ sec.

Taking into account the probable increased carrying capacity of the plate caused by edge restraint, as was done in Watkins' formula for the static strength previously mentioned, and plotting one-half the actual stress vs time, the value of t^* is increased only to $t_1^* = 0.0031$. The probable limit of the time of break is, therefore, $0.0021 \leq t^* \leq 0.0031$ sec. The loadings based on $t^* = 0.002$ sec. will not change perceptibly, so far as the building response is concerned, for any t^* within the probable range.

In order to find the force transmitted to the mullions and thence to the building, the reactions of the glass panes will be calculated assuming, as before, that the supports do not yield. This condition

is on the safe side since deflection of the mullions will actually cusion the reactive forces transmitted to the building. The maximum stress, given by Eq. E.8.49, may be written as, since ρ_0 = 3.56 psi,

$$\sigma_{max} = 6630 \, \rho_0 \, (1 - \cos 585t). \qquad (E.8.50)$$

The curve of Fig. E.8.5 shows that breaking occured at $t^* = 0.0021$ sec and

$$\sigma = 14,750 \text{ psi}$$

Transposing Eq. E.8.50 to read

$$\rho_0^* = \frac{\sigma_{max}}{6630(1 - \cos 585t)},$$

and substituting the breaking values into it yields

$$\rho_0^* = \frac{14750}{6630(1 - \cos 585 \times .0021)} = \frac{14750}{(6630)(0.6658)}$$

= 3.34 psi at breaking. The force build-up transmitted to the mullions may be given, therefore, by the expression,

$$F = \frac{14750 \, nab}{6630(1 - \cos 585t)} = \frac{623 \, n}{1 - \cos 585t}, \text{ lb} \quad (E.8.51)$$

where n is the number of panes per window.

The use of the pseudo-steady state pressure to determine glazing response and the ignoring of the first declining pressure peak is based on the fact that a declining pressure will in all cases result in a lower stress factor than occurs under maintained pressure.[15] Figure E.8.3 shows that the time of decline to zero pressure of the initial pulse is 0.00275 sec. The natural period of the pane is from

---

[15] A. M. Roberts, "Elastic Structures Under Rapidly Applied Loading," Mech World, XCIX (1936), 441-504
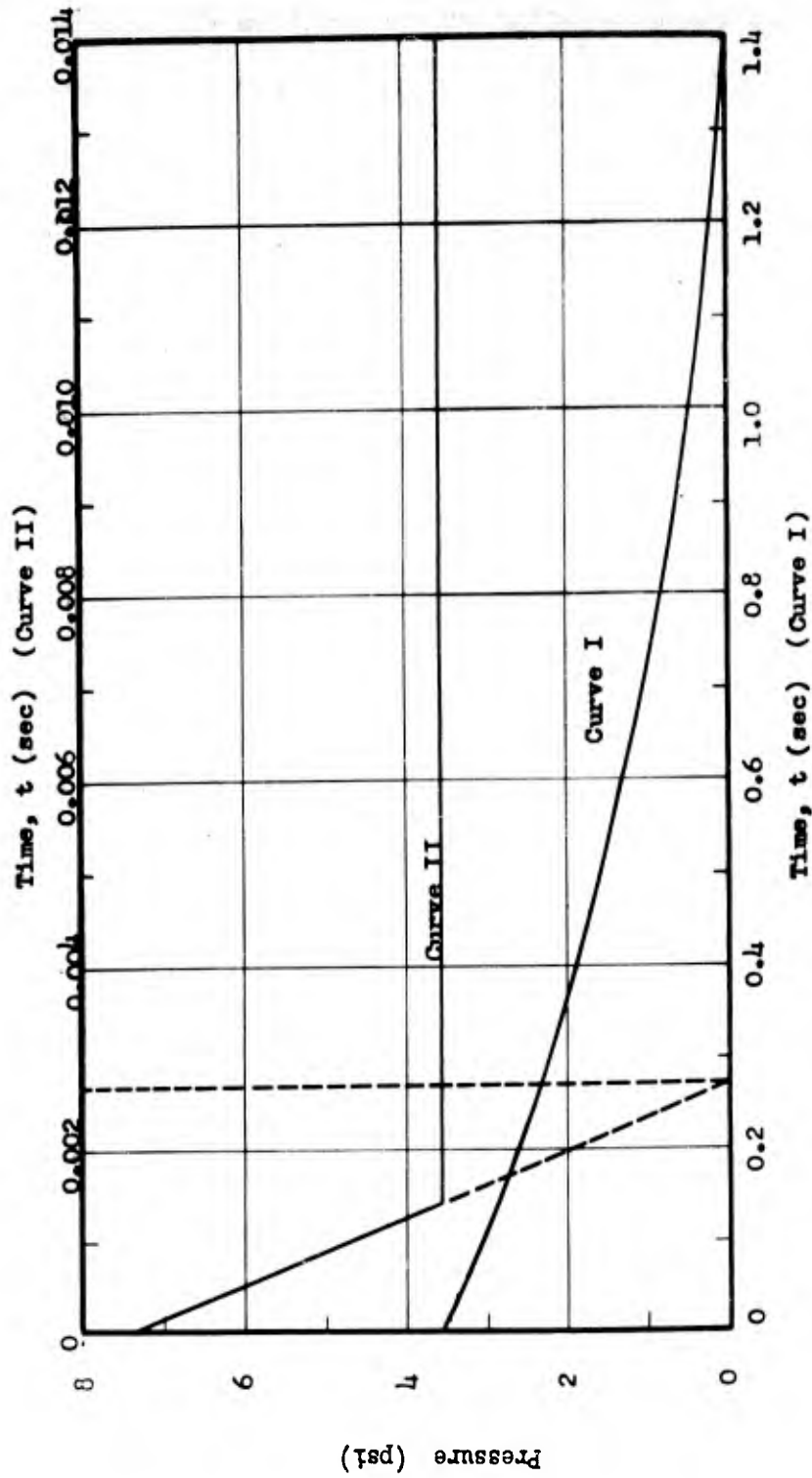
Fig. E.8.3   Pressure Vs Time on an Upper Corner of First Monitor Window Pane of
Building 3.3.3 (Reference Table E.2.17)(Curve I, 0 < t < 0.00146 sec,
Curve II, 0.00146 < t < 1.4 sec)

GLASS PANE BEING CONSIDERED
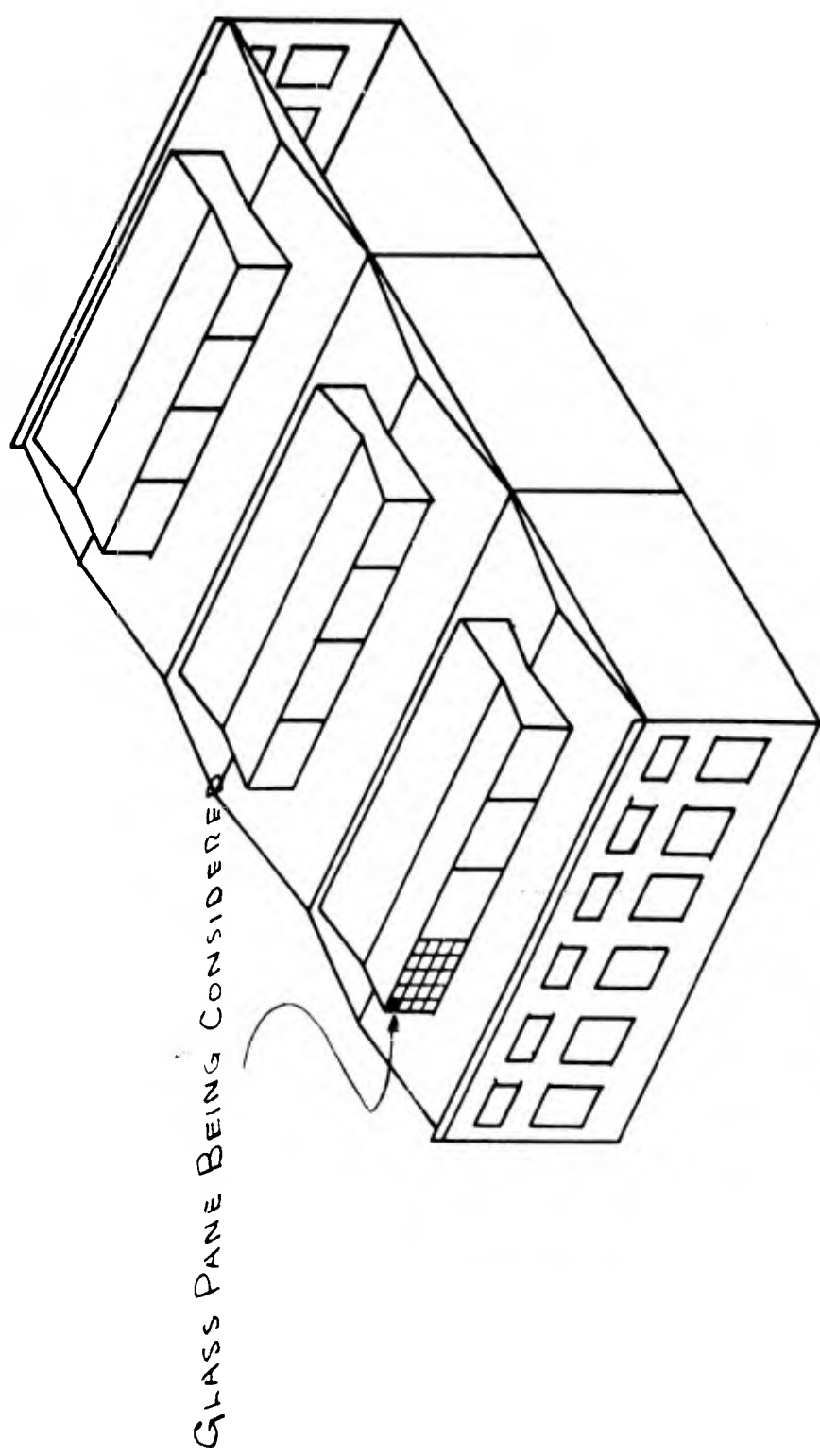
Fig. E.8.4   Glass Pane Location in Building 3.3.3
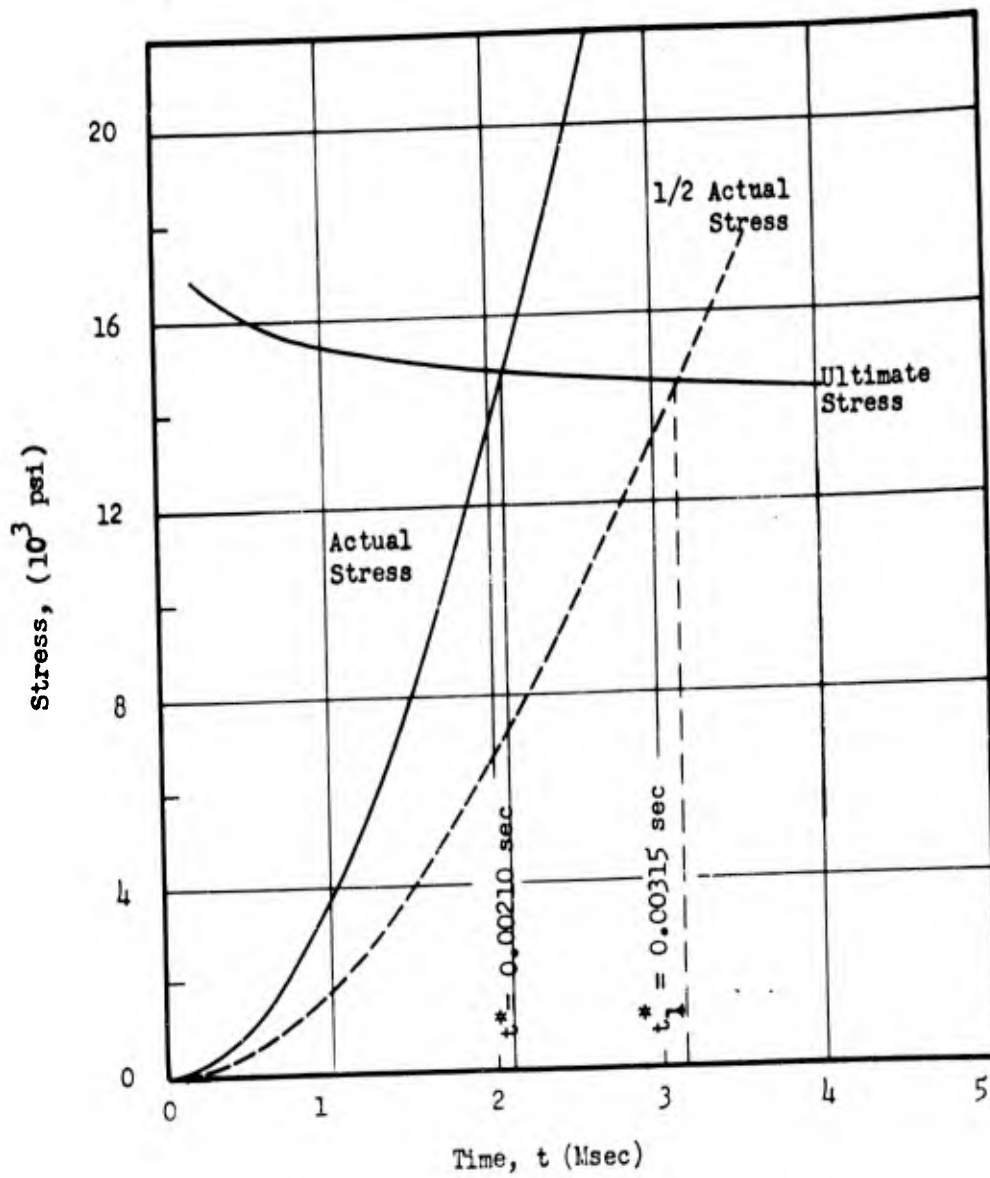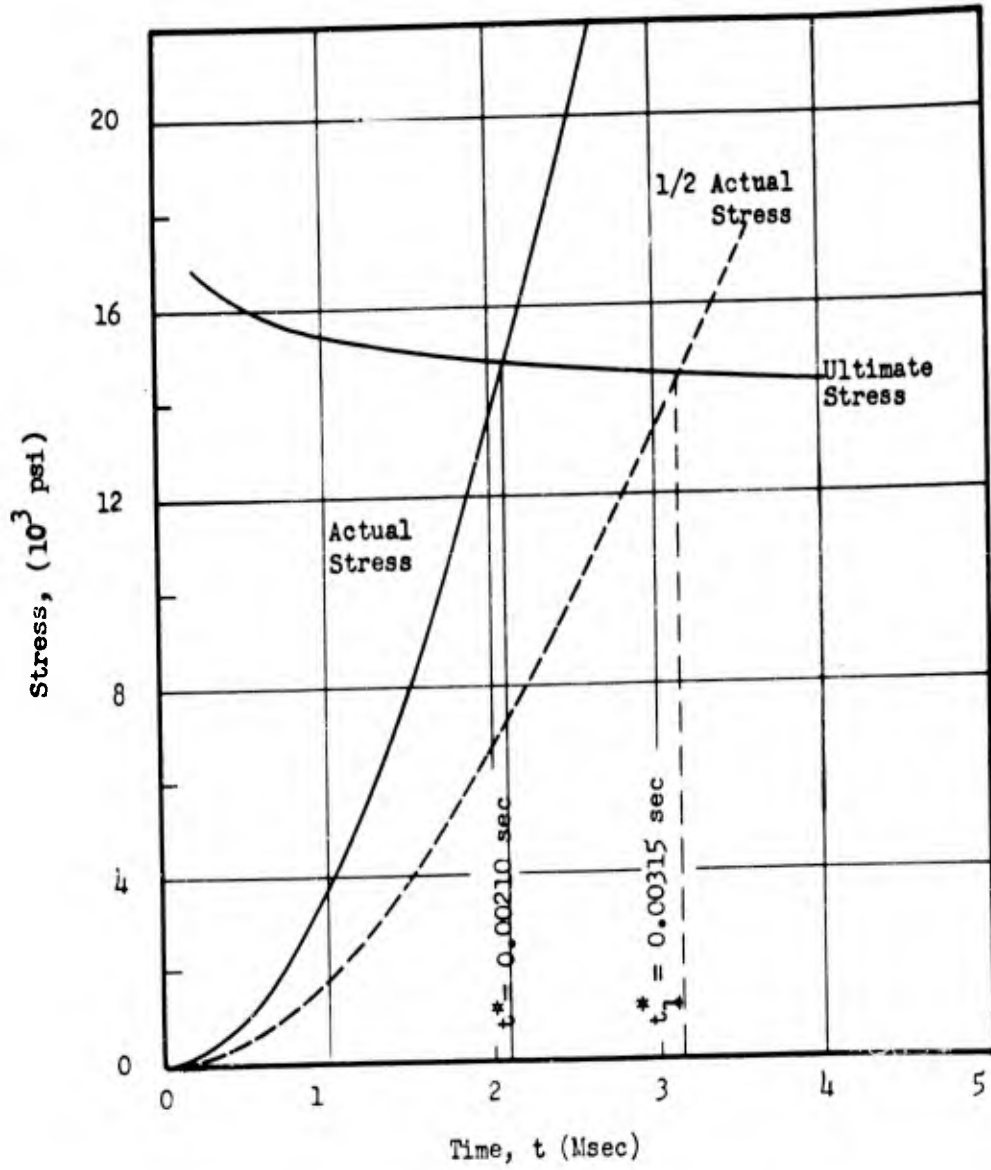
Fig. E.8.5   Actual Vs. Ultimate Stress (t^*= time of break)

Fig. E.8.5   Actual Vs. Ultimate Stress (t^* = time of break)

Eq. E.8.17,

$$\tau_n = \frac{2\pi}{p} = \frac{2\pi}{585} = 0.0107 \text{ sec}$$

The ratio of decline time to τ_n is

$$\varphi = \frac{0.00275}{0.0107} = 0.257.$$

Figure 18, from Roberts' article gives, for this ratio, a dynamic load factor of 0.65. The use of the pseudo-steady state pressure is, therefore, apparently justified.

E.8.2 WALLS

The walls of buildings 3.3.3, 3.3.4 and 3.3.8h are constructed of masonry between columns. In analyzing the response of the structures to blast loading, the walls play a double role. So long as the walls remain intact, they prevent the blast wave from entering the interior of the structure. The degree of damage to the wall thus affects the strength of the interior shock wave. The wall also has a cushioning effect in transmitting blast wave forces to the structural frame. The sharply peaked reflected pressures applied to the wall are smoothed out into a gradually applied load on the frame, with a peak of about 40 per cent of the reflected pressure peak. In order to obtain information about these two phenomena, the following theory on the action of masonry walls was developed. It is believed that this theory is qualitatively correct and will give results which are sufficiently accurate quantitatively to be of use in predicting the response of the structure to blast loading.

E.8.2.1 Assumptions of Structural Action

Experience indicates that a masonry wall is inherently stronger than can be justified by normal beam action. Planes of weakness exist at the mortar joints due to the relatively low tensile properties of the mortar and the low brick-to-mortar bond. Consequently, when a transverse load is applied to a masonry beam, cracking will occur in the tension regions for very small deflections. However, the beam is still capable of sustaining loads if the ends are restrained against longitudinal movement. This may be explained by the ability of the beam to resist compressive stresses. It is believed that after the initial failure in tension occurs, the beam becomes essentially a very flat arch with a rise approximately equal to one-half the thickness of the beam. Based on the above assumptions, the various steps in the analysis are shown in Figs. E.8.6, 7, 8, and 9. The notations on these figures are used in subsequent calculations.

When the blast wave strikes the part of the wall under consideration (Fig. E.8.6), it will be subjected to a uniformly distributed time-dependent force. The masonry wall may be considered as a beam fixed at both ends. Maximum moments will build up at the ends and cracking will occur, allowing the beam to rotate at the supports. At this time the beam-arch becomes essentially hinge ended. If failure in shear does not occur at the supports, the moment at the center reaches a maximum and cracking then occurs at this point, as shown in Fig. E.8.7. From then on, the motion of the beam is considered to be a rotation of

the two halves which is resisted by eccentric compression in much the same manner as a three-hinged arch. This arching action is shown in Fig. E.8.8. In the analysis it is assumed that normal beam action ceases when all the tension fibers have reached the ultimate stress, or presumably when cracking has occurred to the neutral axis. The beam then consists of two masses hinged at A and A' moving under the influence of the external forces and resisted by direct compressive stresses. Complete failure will occur if the total deflection reaches a value equal to approximately two-thirds the thickness of the beam, as shown in Fig. E.8.9.

E.8.2.2 Response In The Elastic Range

Considering a vertical strip of unit width, the equation of motion of the wall may be written

$$EI \frac{\partial^4 w}{\partial x^4} + m \frac{\partial^2 w}{\partial t^2} = F(t).$$

Assuming clamped end conditions, it can be shown that the resulting first mode shape is given by

$$y(x) = 0.883 \cos kx + 0.117 \cosh kx \qquad (E.8.52)[16]$$

for standard initial conditions, where

$$k\ell = 4.730 \qquad (E.8.53)[17]$$

---

[16] Timoshenko, Vibration Problems, pp 333-43.

[17] Ibid., p 344.
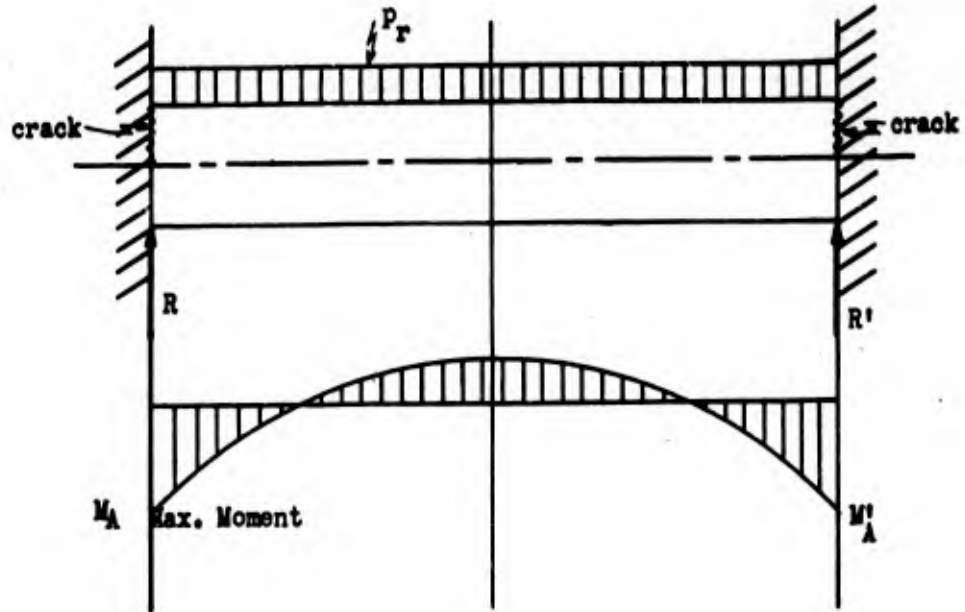
Fig. E.8.6   Beam with Fixed Ends
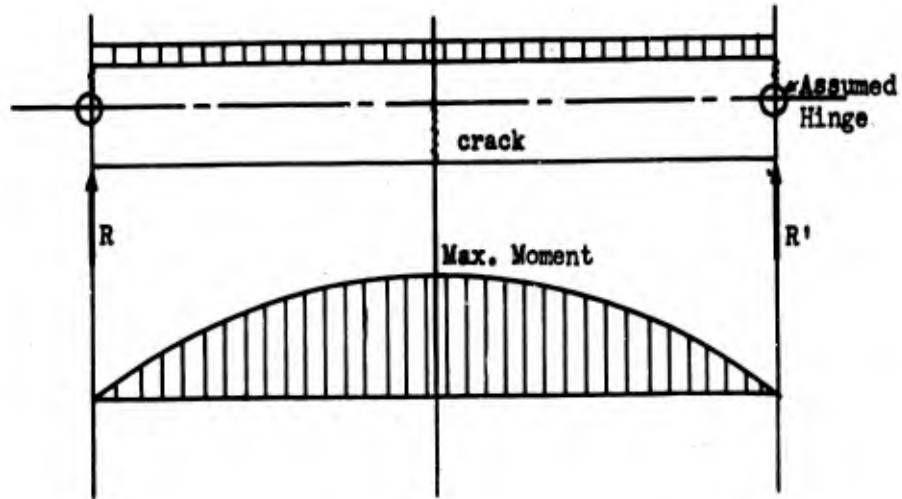
Fig. E.8.7   Beam with Hinged Ends
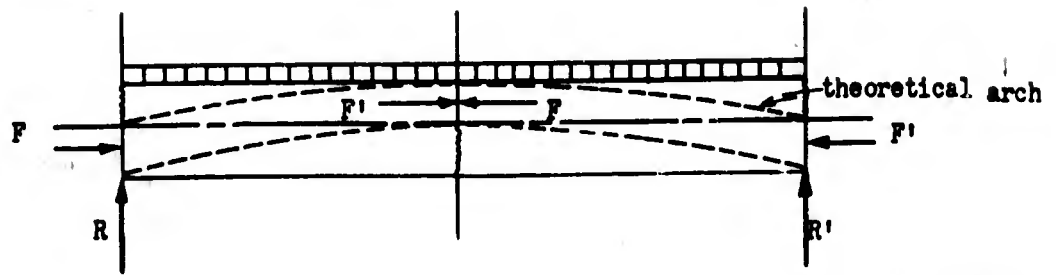
Fig. E.8.8   Arch Action
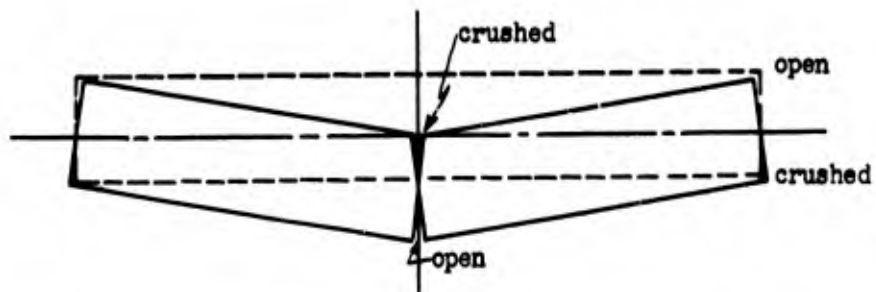
Fig. E.8.9   Arch at Failure

Having found the mode shape and corresponding frequency, one may apply a technique similar to the one employed in the case of a glass pane to determine the response of the wall panel to blast loading.

The kinetic energy is given by

$$T = \int_{-\frac{\ell}{2}}^{\frac{\ell}{2}} \frac{1}{2} m \dot{y}^2(x,t) \, dx = \frac{1}{2} m \dot{y}_0(t) \int_{-\frac{\ell}{2}}^{\frac{\ell}{2}} y^2(x) \, dx = \qquad (E.8.54)[18]$$

$$= \frac{1}{2} m \dot{y}_0^2(t) \int_{-\frac{\ell}{2}}^{\frac{\ell}{2}} (0.883 \cos kx + 0.117 \cosh kx) \, dx = \frac{0.792}{4} m \ell \dot{y}_0^2 .$$

and the potential energy by

$$U = \frac{EI}{2} \int_{-\frac{\ell}{2}}^{\frac{\ell}{2}} \left(\frac{\partial^2 y}{\partial x^2}\right)^2 dx \qquad\qquad (E.8.55)[18]$$

$$= \frac{1}{2} EI \, k^4 \, y_0^2(t) \int_{-\frac{\ell}{2}}^{\frac{\ell}{2}} \left[(0.883)^2 \cos^2 kx - (2)(0.883)(0.117) \right.$$

$$\left. (\cos kx \cosh kx) + (0.117) \cosh^2 kx \right] dx$$

$$= \frac{0.792}{4} \ell \, EI \, k^4 \, y_0^2(t) .$$

The total power of all acting forces is given by

$$P = \int_{-\frac{\ell}{2}}^{\frac{\ell}{2}} \frac{F(t)}{\ell} \dot{y} \, dx = \int_{-\frac{\ell}{2}}^{\frac{\ell}{2}} \frac{F(t)}{\ell} \dot{y}_0 (0.883 \cos kx$$

$$+ 0.117 \cosh kx) \, dx$$

$$= 0.525 \, F \dot{y}_0$$

so that

$$P = Q\dot{y}_0 = 0.525 \, F \dot{y}_0$$

---

[18] _Ibid._, p 334

and the generalized force becomes

$$Q = 0.525 \ F(t). \tag{E.8.57}$$

Substitution into Lagrange's equation $\left[\dfrac{d}{dt}\left(\dfrac{\partial T}{\partial \dot{y}_o}\right) + \dfrac{\partial U}{\partial y_o} = Q\right]$ results

in the differential equation of motion of the chosen generalized
coordinate

$$\ddot{y}_o + \Omega^2 y_o = \Gamma \ F(t) \tag{E.8.58}$$

where

$$\Omega^2 = \frac{EI(4.73)^4}{m \ell^4}$$

and
$$\Gamma = \frac{1.33}{m \ell} \ .$$

Equation E.8.58 is the equation of motion of a beam
in the fixed-end condition. This motion will continue until the
moments are large enough to induce cracking at the ends, which occurs
for a deflection

$$y^* = \frac{12}{384} \quad \frac{\sigma_{max} \ell^2}{Ec} \ . \tag{E.8.59}$$

Following failure in the clamped condition, the beam
acts as a simply supported beam until cracking occurs at the center. The
equations governing this motion have been developed by Timoshenko.[19]

E.8.2.3 Non-Flexual Action of Beam

At a certain stage of the deformation, (as outlined
previously), rational analysis indicates that flexural action ceases.
Cracking takes place both at the center and at the ends of the beam. A

---

[19] Ibid., Art. 56

reasonable approximation of the free body of the beam is shown in Fig. E.8.10. It is assumed that the beam halves are rotating about the fixed points, (at the mid-depth of the beam, "0 and 0'," under the influence of the applies blast load, $p_r(t)$. At the same time arching action will cause linearly distributed stresses A_1, A_2, A_3, and A_4, acting along $\overline{OD}$, $\overline{OB}$, and $\overline{OF}$, respectively, $(A_2 = -A_3)$.

Considering the left half of the beam, it is seen that there is no acceleration of its center of gravity in the x-direction as long as α is small. The net force in the x-direction is thus zero:

$$0 = M\ddot{x} = \frac{s_1 bd}{4} - \frac{s_2 bd}{4} , \qquad (E.8.60)$$

where s_1 and s_2 are the extreme fiber stresses, b is the width, and d is the depth of the beam. Since the stresses are equal, (from Eq. E.8.60) they produce a couple, M_c, of magnitude

$$M_c = \frac{sbd^2}{6} . \qquad (E.8.61)$$

The strain in the outer fiber will be proportional to the angular rotation, α, of the half beam and the distance, $\frac{d}{2}$, from the hinge to the outer fiber, and inversely proportional to the length of the beam. The compressive stress is therefore

$$s = \frac{E \alpha d}{\ell} . \qquad (E.8.62)$$

Substituting Eq. E.8.62 in Eq. E.8.61 yields

$$M_c = \frac{Eb}{6} \frac{d^3}{\ell} \alpha . \qquad (E.8.63)$$

The moment, M_p, about point 0, of the uniformly distributed blast pressure, p_r, is given by

$$M_p = b \frac{p_r \ell^2}{8} \tag{E.8.64}$$

The equation of motion of the half beam rotating about point 0 is

$$M_p - M_c = I \frac{d^2 \alpha}{dt^2} \tag{E.8.65}$$

where I is the moment of inertia of the half beam about point 0 (equal to $\frac{bM\ell^2}{12}$) and M is the mass per unit width of the half beam.

Substituting Eqs. E.8.63 and E.8.64 into Eq. E.8.65 yields

$$\frac{bp_r \ell^2}{8} - \frac{Ebd^3}{6\ell} \alpha = \frac{bM\ell^2}{12} \frac{d^2 \alpha}{dt^2}$$

$$\frac{M\ell^2 b}{12} \ddot{\alpha} + \frac{Ebd^3}{6\ell} \alpha = \frac{bp_r \ell^2}{8}$$

$$\ddot{\alpha} + \frac{2Ed^3}{M\ell^3} \alpha = \frac{3}{2} \frac{p_r}{M}$$

$$\ddot{\alpha} + \Omega^2 \alpha = \Gamma p_r \tag{E.8.66}$$

where

$$\Omega^2 = \frac{2Ed^3}{M\ell^3} \quad ,$$

which shall be defined as the elastic hinge frequency, and

$$\Gamma = \frac{3}{2M} \quad .$$

The equation of motion in the y-direction is

$$\frac{p_r \ell b}{2} - Rb = \frac{Mb\ell}{4} \ddot{\alpha} \tag{E.8.67}$$

ARMOUR RESEARCH FOUNDATION OF ILLINOIS INSTITUTE OF TECHNOLOGY

where R is the reaction force per unit width.

Solving for R,

$$R = \frac{P_r l}{2} - \frac{M l}{4} \ddot{\alpha} \, . \qquad \text{(E.8.68)}$$

Equation E.8.68 is used to compute the reaction force transmitted to the structure.

A complete computation according to the above scheme has been performed for the wall of building 3.3.4. From this calculation it may be seen that the flexural phase is so short as to be of no consequence; it is not considered in the computations for the other buildings. For building 3.3.3 the duration of the loading is so much less than the natural frequency of the wall that the shape of the pulse is not important in determing the response. Only the impulse of the wave is significant. Therefore a simplified shape has been adopted for the blast pulse.

It has been found (calculations not included) that the reaction force has the same period as the natural period of the wall and has a sinusoidal shape with an amplitude determined by the impulse in the wave. After the first half cycle of the reaction, when it has reached the same intensity as the drag force, the drag force is taken as the force applied to the frame.

One sample computation, which is included in this report in Section E.8.4.4, has been performed for building 3.3.4 to determine failure of the wall. The wall element chosen was the brickwork between two windows, since this appeared to be the weakest section of the wall. According to the proposed theory, this section should be relatively

undamaged by the blast, suffering a total deflection of only 0.1 in.
at its center. Because of this result, no further questions of wall
failure shall be investigated.

E.8.3   ROOF

The roofs of buildings 3.3.3, 3.3.4, and 3.3.8h consist of timber
roofing attached to nailers which are bolted to the purlins. The roof
planks of building 3.3.4 are perpendicular to the direction of the flow,
and the roof planks of building 3.3.3 and its model, building 3.3.8h,
are parallel to the flow. The information desired is whether or not the
roof will fail and, if so, the time at which it will fail.

To answer this question, the applied force is multiplied by an
appropriate dynamic load factor, and a static computation is made. If
failure is indicated, a complete dynamic analysis is made to find the
time of rupture. At the inside rear of the building, where the shock
is reflected from the back wall, the possibility of the roof pushing out
has been investigated by comparing the reaction at the ends of the roof
decking with the pulling force of the nails. Data on the resistance of
nails were taken from the Forest Products Handbook.

E.8.4   COMPONENTS OF BUILDING 3.3.4

E.8.4.1   Introduction

Building 3.3.4 is a single-story, concrete frame with
four course brick masonry curtain walls 16 1/2 in. thick. The brick is
laid with one course extending outside of the face of the columns to
present the appearance of a uniform brick masonry wall surface. The

ARMOUR RESEARCH FOUNDATION OF ILLINOIS INSTITUTE OF TECHNOLOGY

arrangement of windows and doors is shown in Fig. E.8.11.

In order to analyze the response of the walls to blast loading, the walls are divided into parts that may be considered as independent structural elements. These are designated by Roman numerals in Fig. E.8.12. It is assumed that the weakest element of the wall is the vertical portion between the windows, marked (I). If this part of the wall should collapse then it seems probable that all of the brick work above this point will also fail, since its main support has been removed. This action leaves only the portion of wall below the windows to be analyzed. If, on the other hand, this weak element should prove capable of resisting the applied forces then it would seem probable that the wall will remain intact.

E.8.4.2 Roof

The roof of building 3.3.4 (decking perpendicular to the direction of flow) is a 6-in. thick laminated timber deck made up of two-by-six boards on edge and is supported on 18 ft - 8 in. centers. The equation of motion is

$$\ddot{y}_o + \Omega^2 y_o = \Gamma F(t) \qquad\qquad (E.8.69)$$

where

$$\Omega = 55.221 \text{ rad/sec}$$
$$\Gamma = 10.367$$

and

$$y_{omax} = 13.3 \text{ in. (ultimate)}$$
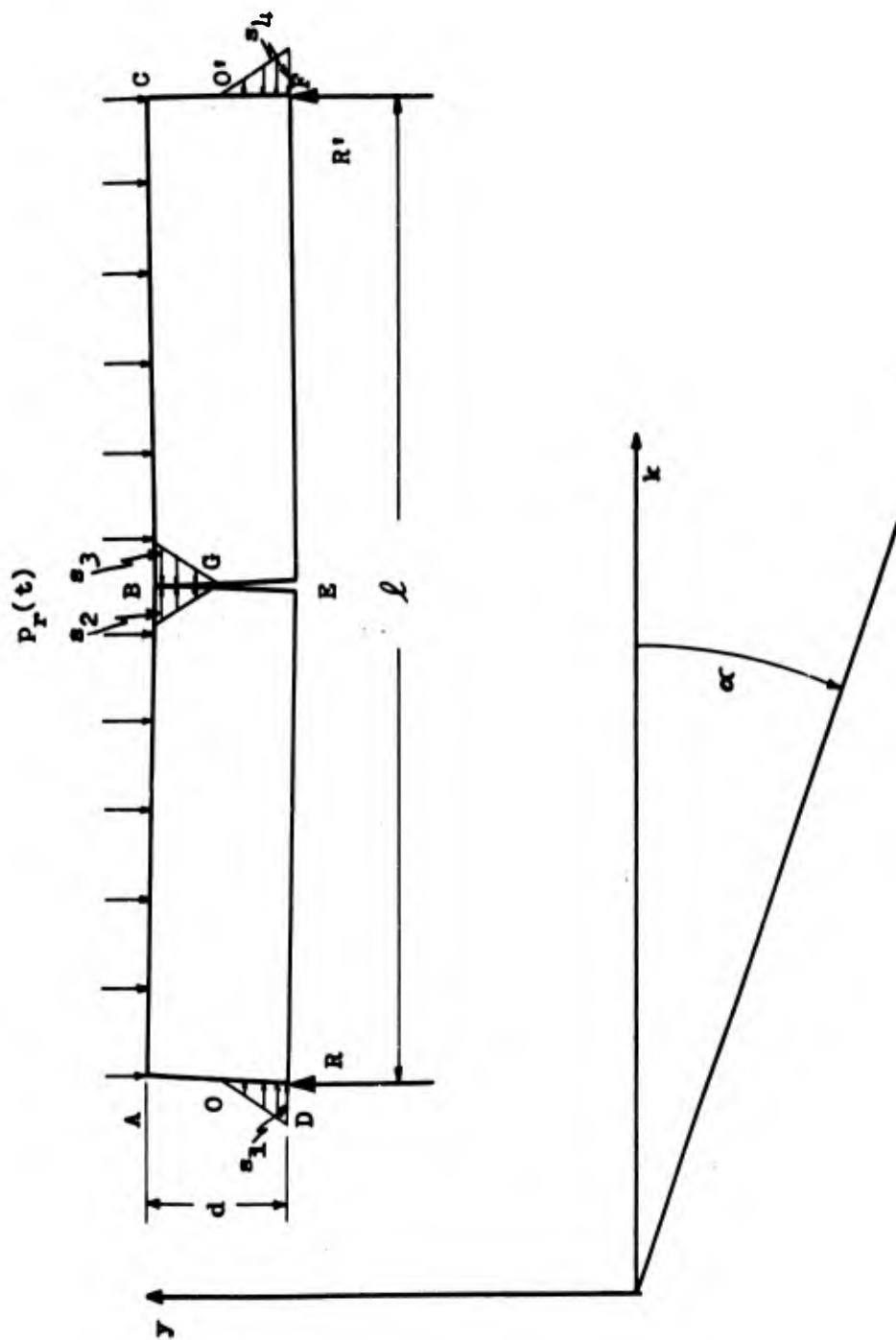
Fig. E.8.10   Free Body of Arch Beam
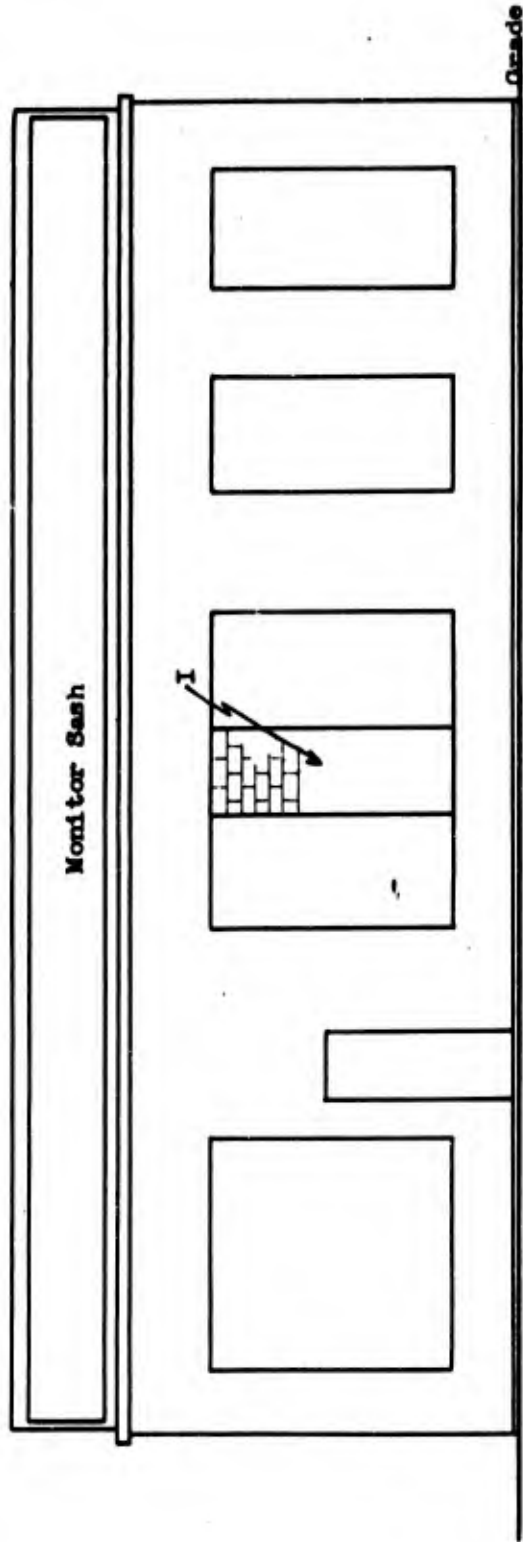
Fig. E.8.11   Front Elevation of Building 9.3.4

The maximum net external applied force is 1,110 lb/in. Using a dynamic load factor of 2, which is the maximum for a linear impulsive load,

$$y_{max} = 7.4 \text{ in.}$$

Hence, the roof will remain intact under external pressure,

E.8.4.3 Back Slope

The back slope considered is at the rear of the building, near the wall. The internal net pressure has a peak of 4.25 lb (see Part I for loadings) and a duration of 0.009 sec. Since the period of vibration of the roof is 0.11 sec,[20] the dynamic load factor is 1/2.[21] Therefore, the deflection produced will be 1/2 the static deflection for a static load of 4.25 psi. The static deflection is

$$y_s = \frac{5}{384} \frac{w \ell^4}{EI} ,$$

and when multiplied by the dynamic load factor becomes

$$y_{omax} = \left(\frac{1}{2}\right)\left(\frac{5}{384}\right) \frac{w \ell^4}{EI} . \tag{E.8.70}$$

The reaction is given by

$$R = EI \frac{\pi^3}{\ell^3} y_{omax} \tag{E.8.71}$$

Combining Eqs. E.8.70 and E.8.71

$$R = \left(EI \frac{\pi^3}{\ell^3}\right)\left(\frac{1}{2} \frac{5}{384} \frac{w \ell^4}{EI}\right) \tag{E.8.72}$$

$$= \frac{\pi^3 5 w \ell}{2 \times 384} = \frac{(3.14)^3 \times 5 \times 4.25 \times 219}{2 \times 384}$$

$$= 185 \text{ lb/in.}$$

---

[20] Timoshenko, Vibration Problems, p 339. For a simple beam the natural period is $t_n = \frac{2\ell^2}{\pi} \sqrt{\frac{A\gamma}{EIg}}$.

[21] Roberts, Loc. cit.

ARMOUR RESEARCH FOUNDATION OF ILLINOIS INSTITUTE OF TECHNOLOGY

Assuming one 30d toe nail every other board, the pulling resistance is estimated as 170 lb/in. Add to this 30 lb/in. dead weight and the total vertical resistance is 200 lb/in. The roof, therefore, will remain in place.

E.8.4.4 Analysis of Masonry Beam Between Windows

The following values are taken as the parameters for this section: (See Fig. E.8.11)

$$b = 1 \text{ in.}$$
$$d = 16.5 \text{ in.}$$
$$\ell = 151 \text{ in.}$$
$$E = 2.5 \times 10^6 \text{ lb/in.}^2$$
$$\text{density of brick} = 120 \text{ lb/ft}^3$$
$$\sigma_{max} = 90 \text{ lb/in.}^2$$

Substituting these values in Eqs. E.8.58 and E.8.59,

$$y_o = \left(\frac{12}{384}\right) \frac{90(151)^2}{2.5 \times 10^6 \times 8.25}$$

$$= 0.003 \text{ in.}$$

to produce cracking at the supports and

$$\Gamma = 2.98$$
$$\Omega^2 = (540)^2 \text{ rad}^2/\text{sec}^2$$

The value of $F(t)$ may be expressed analytically by

$$F(t) = 151(7.8 - 500t) \text{ lb.} \tag{E.8.73}$$

Substitution of Eq. E.8.73 into Eq. E.8.69 results in the equation of motion

$$\ddot{y}(t) + (540)^2 y = 2.98 \times 151(7.8 - 500t), \quad (E.8.74)$$

the solution of which is

$$y = \frac{2.98 \times 151.2}{(540)^2} \left[7.8(1 - \cos 540t) + \frac{500}{540} (\sin 540t - 540t) \right],$$

which can be approximated by expanding in Taylor's series as

$$y = 1730t^2,$$

and therefore, @ t = 0.002 sec

$$y = 0.007 \text{ in.}$$

At time t = 0.002 sec the wall cracks at the ends and begins the simply-supported phase of its motion.

Using Eq. E.8.58 and the parameters for the brick beam under consideration,

$$y_{cracking} = 0.02 \text{ in. for cracking at the center}$$

$$\Omega^2 = (240)^2 \text{ rad}^2/\text{sec}^2$$

$$\Gamma = 2.85 \quad \text{and}$$

$$F(t) = 2.85 \times 151(8.1 - 650t) \qquad 0.002 \leqslant t \leqslant 0.008.$$

The equation of motion is

$$\ddot{y} + (240)^2 y = 2.85 \times 151(8.1 - 650t), \ 0.002 \leqslant t \leqslant 0.008$$
$$(E.8.75)$$

which has the solution

$$y = - 0.062 \cos 240t + 0.023 \sin 240t +$$

$$+ \frac{151.2 \times 285}{(240)^2} \; (8.1 - 650t).$$

For

$$t = 0.0035 \text{ sec,}$$

$$y = 0.02 \text{ in.}$$

cracking occurs at the center and the flexural action ceases.

At this point, the beam enters the non-flexural stage of its action and is governed by the equation of motion of a representative wall strip of unit width, (see Section E.8.5.3),

$$\ddot{\alpha} + \Omega^2 \alpha = \Gamma \, p(t) \tag{E.8.76}$$

where

$$\Omega^2 = \frac{Ed^3}{M \ell^3} = \frac{2.5 \times (10)^6}{0.225} \times \left(\frac{16.5}{151.2}\right)^3$$

$$= (116)^2 \text{ rad}^2/\text{sec}^2,$$

$$\Gamma = \frac{3}{2M} = \frac{3}{2 \times 0.225} = 6.67 \text{ and}$$

$$M = \frac{120 \times 1 \times 16.5 \times 75.6}{386 \times 1728} = 0.225 \text{ slugs.}$$

With these values the equation of motion is

$$\ddot{\alpha} + (116)^2 \alpha = 6.7 \left[6.75 - 715(t - 0.002) \right], \; 0.002 \leq t \leq 0.008.$$

$$\tag{E.8.77}$$

The initial values obtained from the simply-supported phase of the motion are

$$\alpha(0.0035) = 0.00024 \text{ rad}$$

$$\dot{\alpha}(0.0035) = 0.127 \text{ rad/sec.}$$

The solution for α is

$$\alpha = -0.0031 \cos 116(t - 0.002) + 0.0041 \sin 116(t - 0.002) +$$

$$+ \frac{6.7\left[6.75 - 715(t - 0.002)\right]}{(116)^2} \tag{E.8.78}$$

$$\alpha(0.008) = 0.00156 \text{ rad}$$

$$\dot{\alpha}(0.008) = 0.240 \text{ rad/sec.}$$

The equation for the next interval is

$$\ddot{\alpha} + (116)^2\alpha = 6.7 \quad \left[2.46 - 223(t - 0.008)\right] \quad 0.008 \le t \le 0.014$$

$$\alpha = 0.00034 \cos 116(t - 0.008) + 0.00302 \sin 116(t - 0.008) +$$

$$+ \frac{6.7\left[2.46 - 223(t - 0.008)\right]}{(116)^2} \tag{E.8.79}$$

$$\alpha(0.014) = 0.00224 \text{ rad}$$

$$\dot{\alpha}(0.014) = 0.00058 \text{ rad/sec.}$$

In the interval $0.014 \le t \le 0.057$

$$\ddot{\alpha} + (116)^2\alpha = 6.7\left[1.13 - 20.5(t - 0.014)\right] \tag{E.8.80}$$

$$\alpha = 0.00168 \cos 116(t - 0.014) + 0.0001 \sin 116(t - 0.014) +$$

$$+ \frac{6.7\left[1.13 - 20.5(t - 0.014)\right]}{(116)^2}$$

$$\dot{\alpha}(0.015) \le 0.$$

Hence the forward motion ceases between 14 and 15 msec after the blast hits the wall and reaches a maximum deflection of

$$(15.6 \times 0.00156) = 0.12 \text{ in.,}$$

indicating that the wall remains intact.

ARMOUR RESEARCH FOUNDATION OF ILLINOIS INSTITUTE OF TECHNOLOGY

In order to compute the reactions, the same analysis is made for a brick beam which covers the entire height of the building. This analysis is identical with the preceding with the exception that l = 223 in.

The results are

$$y_o = 214 t^2$$

in the clamped phase (which ends when t = 0.002 sec).

The reaction is equal to the shear at the roof end of the beam

$$R = V(l,t) = \frac{EI \partial^3 y}{\partial x^3} = \frac{EId^3 y(x)}{dx^2} \ y(t), \tag{E.8.81}$$

$$y(x) = 0.8227 \cos(0.0212x) + 0.1173 \cosh(0.0212x)$$

from Eq. E.8.81, and

$$y'''(l) = (0.0212)^3 \left[0.8827 \sinh 0.365 + 0.1173 \sinh 0.365) \right]$$

$$= 11.6 \times 10^{-6}$$

For a unit width (1-ft) beam the shear is (from Eq. E.8.81)

$$V(l,t) = 2.5 \times 10^6 \times \frac{12(16.5)^3}{12} \times 11.6 \times 10^{-6}$$

$$= 125,000 \ y_o(t) \ lb$$

and

$$y(0.002) = 0.007 \ in.$$

$$\dot{y}(0.002) = 0.610 \ in./sec.$$

For the simply-supported phase, a similar computation on a one-foot wide strip yields

$$R(t) = 34,000 \ y_o \ lb.$$

The equation of motion is

$$\ddot{y} + 232y = 4282\left[8.18 - 715t\right].\qquad(\text{E}.8.82)$$

Solving,

$$y = -0.530 \cos 232(t - 0.002) + 0.274 \sin 232(t - 0.002) +$$

$$+ \frac{4282\,(8.18 - 715t)}{(232)^2}\,,$$

$$y_{rupture} = 0.022 \text{ in. (cracking at center)}$$

Therefore, at $t = 0.0023$ sec,

$$y = 0.022 \text{ in., and cracking occurs.}$$

The beam then enters the arching phase governed by

the equation

$$\ddot{\alpha} + \Omega^2 \alpha = \Gamma_{P_r}.\qquad(\text{E}.8.83)$$

The reaction will be computed as

$$R(t) = F(t) = M\ddot{\alpha}.\qquad(\text{E}.8.84)$$

The following values are obtained:

$$\Omega^2 = \frac{E}{M}\left(\frac{d}{\ell}\right)^3 = \frac{2.5 \times 10^6}{0.333} \times (0.109)^3$$

$$= 9722 \text{ (rad/sec)}^2$$

$$\Omega = 99 \text{ rad/sec}$$

$$\Gamma = \frac{3}{0.332} = 4.5.$$

Substituting the above values in Eq. E.8.83 yields

$$\ddot{\alpha} + (99)^2 \alpha = 4.5 \, p(t)$$

$$p(t) \begin{cases} 8.18 - 715t, & 0.002 \leqslant t \leqslant 0.008 \\ 4.24 - 223t, & 0.008 \leqslant t \leqslant 0.014 \\ 1.42 - 20.5t, & 0.014 \leqslant t \leqslant 0.057. \end{cases}$$

The above equations yield values for α (t) and are used to solve for $\ddot{\alpha}$ in Table E.8.1. The reaction is then computed in pounds per foot of length from Eq. E.8.84.

Equations E.8.83 and E.8.84 yield the values

R(0) = 0, and

R(0.002) = 975 lb/ft.

The total reaction force is found by multiplying the reactions of Table E.8.1 by the effective length of the building. The effective length is the true length times the ratio of the gross wall area minus the window area to the gross wall area. This is 35 ft for the walls of building 3.3.4. Figure E.8.12 shows the total reaction force on the front wall.

The force applied to the front wall of building 3.3.4 is given in Table E.8.2 and plotted in Fig. E.8.13. The force on the back wall is given in Table E.8.3 and plotted in Fig. E.8.14.

E.8.5 BUILDING 3.3.3

E.8.5.1 Roof

The roof, parallel to the flow, consists of 2-in. timber decking on 6 ft 6in. centers. If the roof is assumed to be
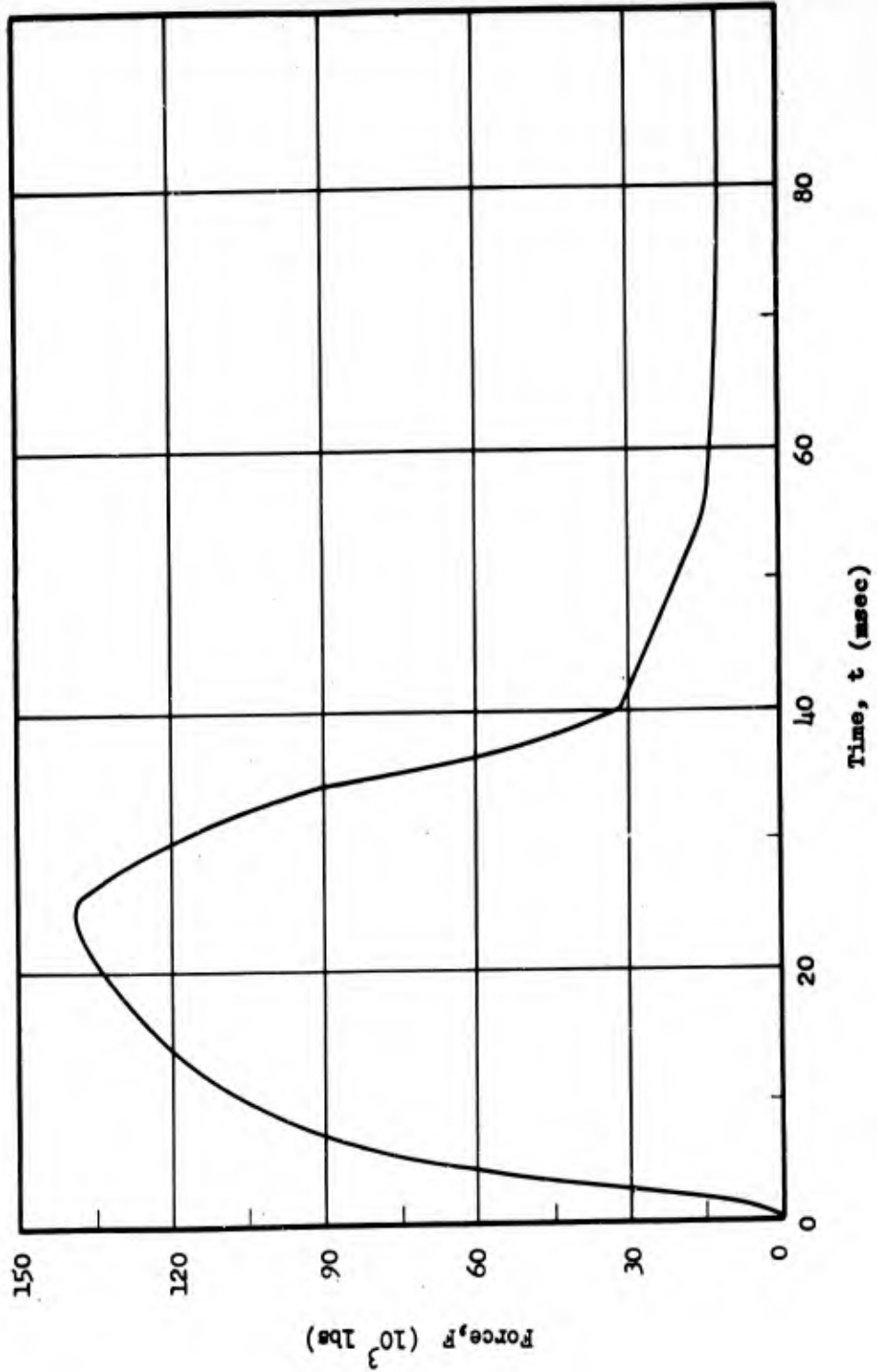
Fig. E.8.12 Reaction Forces on Front Wall of Building 3.3.4

303
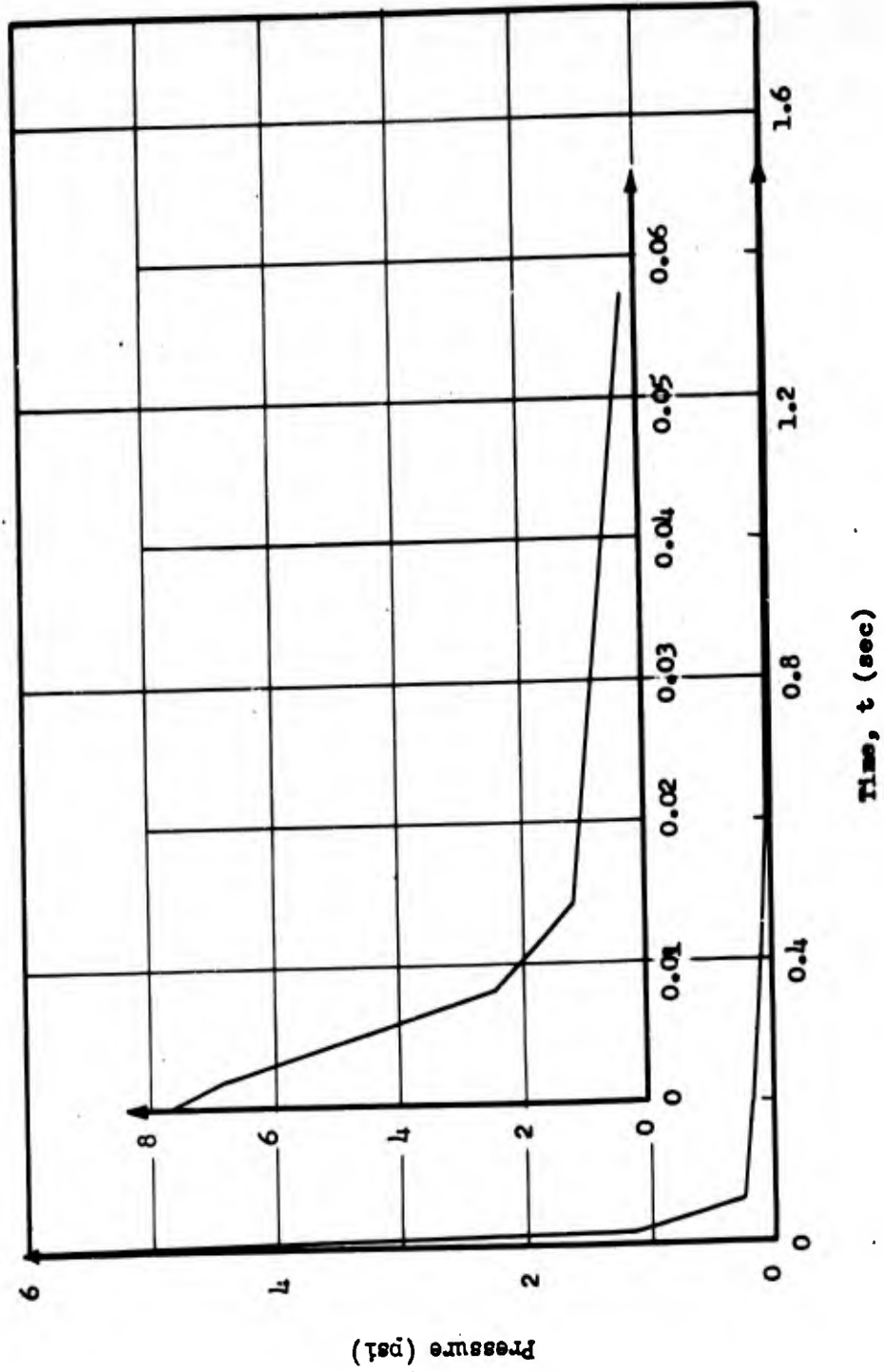
Fig. E.8.13 Pressure on Front Wall of Building 3.3.4
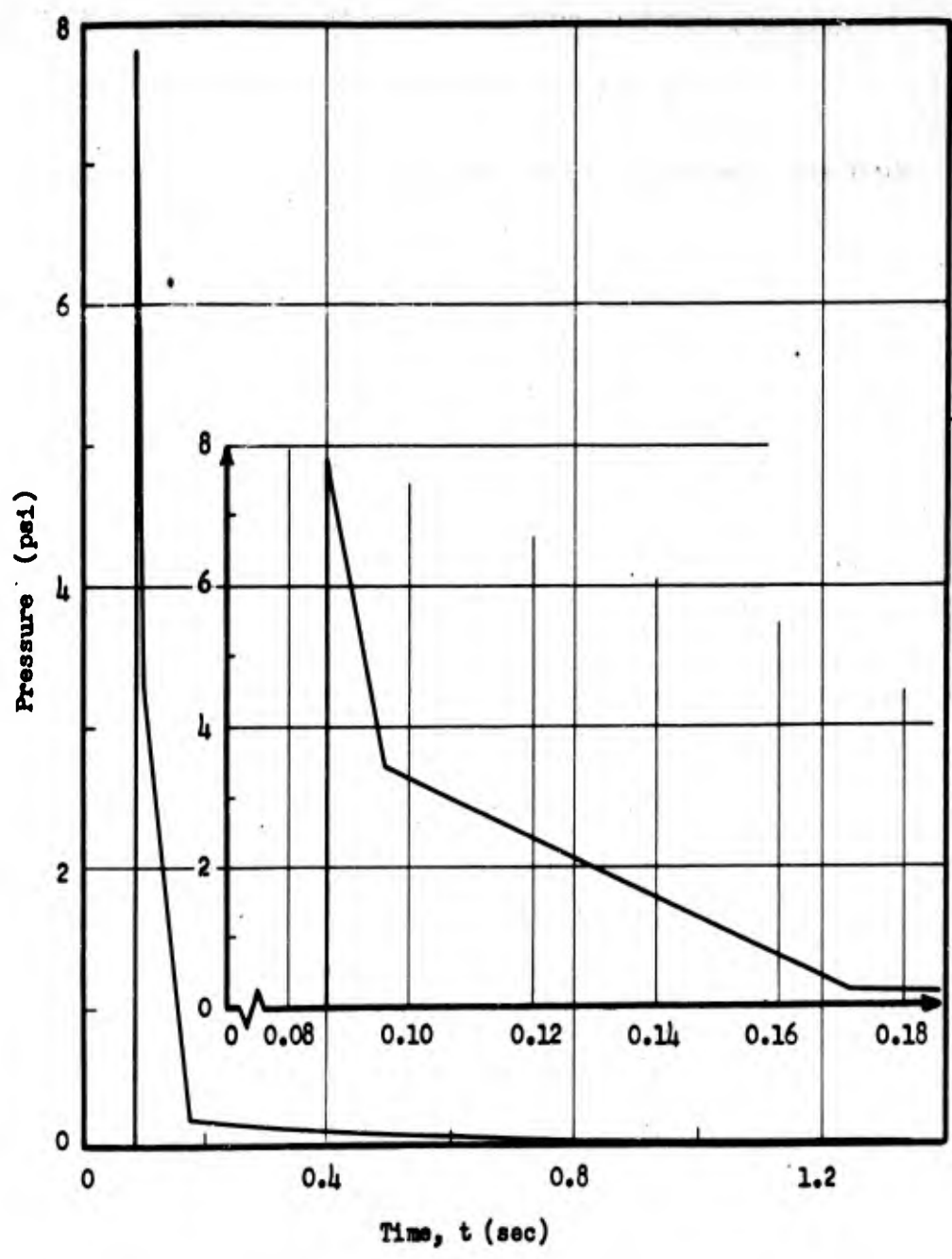
Fig. E.8.14   Pressure on Back Wall of Building 3.3.4 (3.55 psi Overpressure)

305

simply supported and the moments transmitted from adjacent sections
are neglected, then the equation of motion from Lagrange's equation is

$$\ddot{y}_o + \Omega^2 y_o = \Gamma F(t) \tag{E.8.85}$$

where again the beam is assumed to deflect in the first mode only, and

$$\Omega^2 = \frac{EI\pi^4}{m\ell^4} \tag{E.8.86}$$

$$\Gamma = \frac{4}{\pi m \ell} \tag{E.8.87}$$

and

$$F(t) = \text{total load on the beam.}$$

The deflection at rupture is given by

$$y_{o\ \text{rupture}} = \frac{40}{384} \ \frac{\sigma_{max}\ell^2}{Ec} \tag{E.8.88}$$

where

$$E = 1.5 \times 10^6 \text{ psi}$$

$$I = \frac{1}{12}(2)^3 \text{ in.}^4/\text{in.}$$

$$M = \frac{2.6}{12 \times 6 \times 386} \text{ slugs/in.}^2$$

$$\ell = 78 \text{ in.}$$

$$\sigma_{max} = 12{,}000 \text{ psi}$$

$$c = 1 \text{ in.}$$

Substituting these values into Eqs. E.8.86, E.8.87, E.8.88

$$\Omega = 168 \text{ rad/sec}$$

$$\Gamma = 174 \text{ in./slug}$$

and

$$y_{o\ \text{rupture}} = 5.06 \text{ in.}$$

ARMOUR RESEARCH FOUNDATION OF ILLINOIS INSTITUTE OF TECHNOLOGY

If, instead of using F(t), the constant value of maximum F(t) (4.31 x 78 lb) is applied instantaneously, one gets larger deflections than for the actual loading. Hence, if the roof does not break under this loading, it will not break under the actual loading. The maximum deflection under constant loading is given by

$$y_{0\,max} = \frac{2 \times \Gamma \times F(t)max}{\Omega^2} \qquad (E.8.89)$$

$$= \frac{2 \times 182 \times 4.31 \times 78}{(119)^2} =$$

$$y_{0\,max} = 4.33 .$$

The value, $y_{0\,max} = 4.33$, is smaller than that necessary to break the beam, $y_{0\,breaking} = 5.06$. Therefore it is concluded that the roof does not fail.

E.8.5.2 Back Slope

Assuming one 30d nail every 2 in., the pulling resistance will be 350 lb/in. (the pulling force of a 30d nail is about 700 lb). The shear at the end of the beam is given by

$$R = EI \frac{\pi^3}{\ell^3} y_{0\,max} \qquad (E.8.90)$$

which gives

$$1.5 \times 10^6 \times \frac{1}{12} (0.62)^3 \times \frac{(3.14)^3}{(78)^3} \times 4.5 = 250 \text{ lb/in.}$$

Hence the back slope will not fail, even if loaded as severely as the front slope.

E.8.5.3 Walls

Building 3.3.3 is of construction similar to building

3.3.4, except that the walls are constructed of concrete block instead of brick. The treatment of the walls is the same as that for building 3.3.4; however, simplifications were made in the computations as a result of the experience gained on building 3.3.4. The period of vibration of the wall in the elastic hinged arch phase is much longer than the time of clearing of the blast. Under these conditions it is possible to substitute a triangular pulse with the same impulse as the actual blast pulse with a resulting error of only a few per cent. Since the flexural action of the wall is of so little importance, it was neglected completely. Under these assumptions, the equation of motion of a representative wall strip of unit width is (from Eq. E.8.58)

$$\ddot{\alpha} + \Omega^2 \alpha = \Gamma p_r(t) \qquad (E.8.91)$$

where

$$\Omega^2 = \frac{Ed^3}{M\ell^3}$$

$$\Gamma = \frac{3}{2M}$$

and

$$P(t) = P\left(1 - \frac{t}{T}\right).$$

The elastic frequencies for the front and back walls of building 3.3.3 are

$$\Omega^2 = \frac{Ed^3}{M\ell^3} = \frac{2.5 \times 10^6 \times (16.5)^3}{2 \times 0.6768} \qquad (E.8.92)$$

$$= 700 \ (rad/sec)^2$$

$$\Omega = 26 \ rad/sec$$

$$\Gamma = \frac{3}{2M} = \frac{3}{2 \times 0.6768} = 2.22. \qquad (E.8.93)$$

The peak value of the blast impulse is used for P, that is, 7.5 psi for both front and back walls. The quantity T is obtained so that there is equality between the impulse under the blast and the triangular pulse. This choice gives T a value of 0.025 sec for the front wall and 0.018 sec for the rear wall. The graphs of the blast impulse and the assumed triangular pulse are shown in Fig. E.8.15.

Using Eqs. E.8.83 and E.8.84, the values of the reactions are computed in Tables E.8.4, E.8.5, and E.8.6.

The pressure on the front and back walls is given in Table E.8.7. Table E.8.8 gives the loading on building 3.3.3.

Where P is the peak of the triangular pulse, and T is the duration, the impulse equals 1/2 PT. The solution for this condition is:

$$\alpha = \frac{P\Gamma}{\Omega^2}(1 - \cos \Omega t) + \frac{P\Gamma}{\Omega^3 T}(\sin \Omega t - \Omega t) \quad t \leq T \quad (E.8.94)$$

$$\alpha = \frac{PMT^2}{3}\cos \Omega (t - T) + \frac{PMT}{2\Omega}\sin \Omega (t - T). \quad T \leq t \quad (E.8.95)$$

To compute the reactions, $\ddot{\alpha}$ is needed which is given by

$$\ddot{\alpha} = P\Gamma(\cos \Omega t) - \frac{P\Gamma}{\Omega t}(\sin \Omega t) \quad (E.8.96)$$

$$\ddot{\alpha} = -\Omega^2 \alpha = \frac{PT^2}{2\Gamma}\left[\cos \Omega (t - T) + \frac{3}{2\Omega T}\sin \Omega (t - T)\right] \quad (E.8.97)$$

To compute the reaction it is necessary to subtract the mass of the wall times its average acceleration, the inertial force, from the applied blast load. The inertial force must be proportional to $\ddot{\alpha}$, computed above, and the constant of proportionality is evaluated

from the condition that the reaction at time zero is zero.

E.8.6   BUILDING 3.3.8h

Building 3.3.8h is a quarter-scale model of building 3.3.3.
The computation for the walls is carried on in the same manner as for
building 3.3.3 (Section E.8.53), except that the solution for $\ddot{\alpha}$
from the equation

$$\ddot{\alpha} + \Omega^2 \alpha = \Gamma p_r(t) \tag{E.8.98}$$

is carried out with the actual loading curve instead of with the
equivalent triangular pulse as was done for building 3.3.3.

The values of $p_r(t)$ on the front wall are

$$p_r(t) = \begin{cases} 8.13 - 1070t, & 0 \leq t \leq 0.001 \\ 8.49 - 1433t, & 0.001 \leq t \leq 0.004 \\ 3.88 - 373t, & 0.004 \leq t \leq 0.007 \\ 2.69 - 149t, & 0.007 \leq t \leq 0.016 \\ 0.31 - 0.595t, & 0.016 \leq t \leq 0.100 \end{cases}$$

Since d/ℓ for building 3.3.8h is the same as d/ℓ for building
3.3.3, and since M for building 3.3.8h is 1/4 the value of M for building
3.3.3, then the frequency, Ω, for building 3.3.8h from the equation

$$\Omega = \frac{Ed^3}{M}$$

is 104, or 4 times as large as Ω for building 3.3.3 (See Eq. E.8.91).

With these values the acceleration for the front wall is given by
the following expressions:

$$-\frac{\ddot{\alpha}}{\Omega^2\Gamma} = \begin{cases} -0.726 \cos 10^4 t + 0.918 \sin 10^4 t & 0 \leqslant t \leqslant 0.001 \\ -0.758 \cos 10^4 t + 1.228 \sin 10^4 t & 0.001 \leqslant t \leqslant 0.004 \\ -0.391 \cos 10^4 t + 0.397 \sin 10^4 t & 0.004 \leqslant t \leqslant 0.007 \\ -0.263 \cos 10^4 t + 0.257 \sin 10^4 t & 0.007 \leqslant t \leqslant 0.016 \\ -0.136 \cos 10^4 t + 0.269 \sin 10^4 t & 0.016 \leqslant t \leqslant 0.100. \end{cases}$$

The factor $\dfrac{1}{\Omega^2\Gamma}$ is unimportant since the reaction will be determined by

$$R(t) = F(t) - k\ddot{\alpha} \qquad (E.8.99)$$

when

$$k = \frac{F(0)}{\ddot{\alpha}(0)}.$$

to compute the reaction it is only necessary to know the shape of $\ddot{\alpha}$ and not its absolute magnitude.

The corresponding values for the rear wall are: (t = 0 occurs 49 msec after the shock has struck the front wall,)

$$p_r(t) \begin{cases} 8.13 - 1775t, & 0 \leqslant t \leqslant 0.004 \\ 3.87 - 710t, & 0.004 \leqslant t \leqslant 0.005 \\ 0.33 - 1.55t, & 0.005 \leqslant t \leqslant 0.051 \end{cases}$$

and

$$-\frac{\ddot{\alpha}}{\Gamma\Omega^2} \begin{cases} -0.726 \cos 10^4 t + 1.524 \sin 10^4 t & 0 \leqslant t \leqslant 0.004 \\ -0.357 \cos 10^4 t + 0.688 \sin 10^4 t & 0.004 \leqslant t \leqslant 0.005 \\ -0.055 \cos 10^4 t + 0.160 \sin 10^4 t & 0.005 \leqslant t \leqslant 0.051 \end{cases}$$

From the above expression for $-\dfrac{\ddot{\alpha}}{\Gamma \Omega^2}$, the reactions are computed in Tables E.8.9 and E.8.10.

The total force used is again computed by taking the gross area of the wall minus the window area times one-half the average pressure. The area is 59,000 in.^{2}. The pressures are given in Table E.8.11 and plotted in Fig. E.8.16 for the front wall, and Fig. E.8.17 for the back wall.
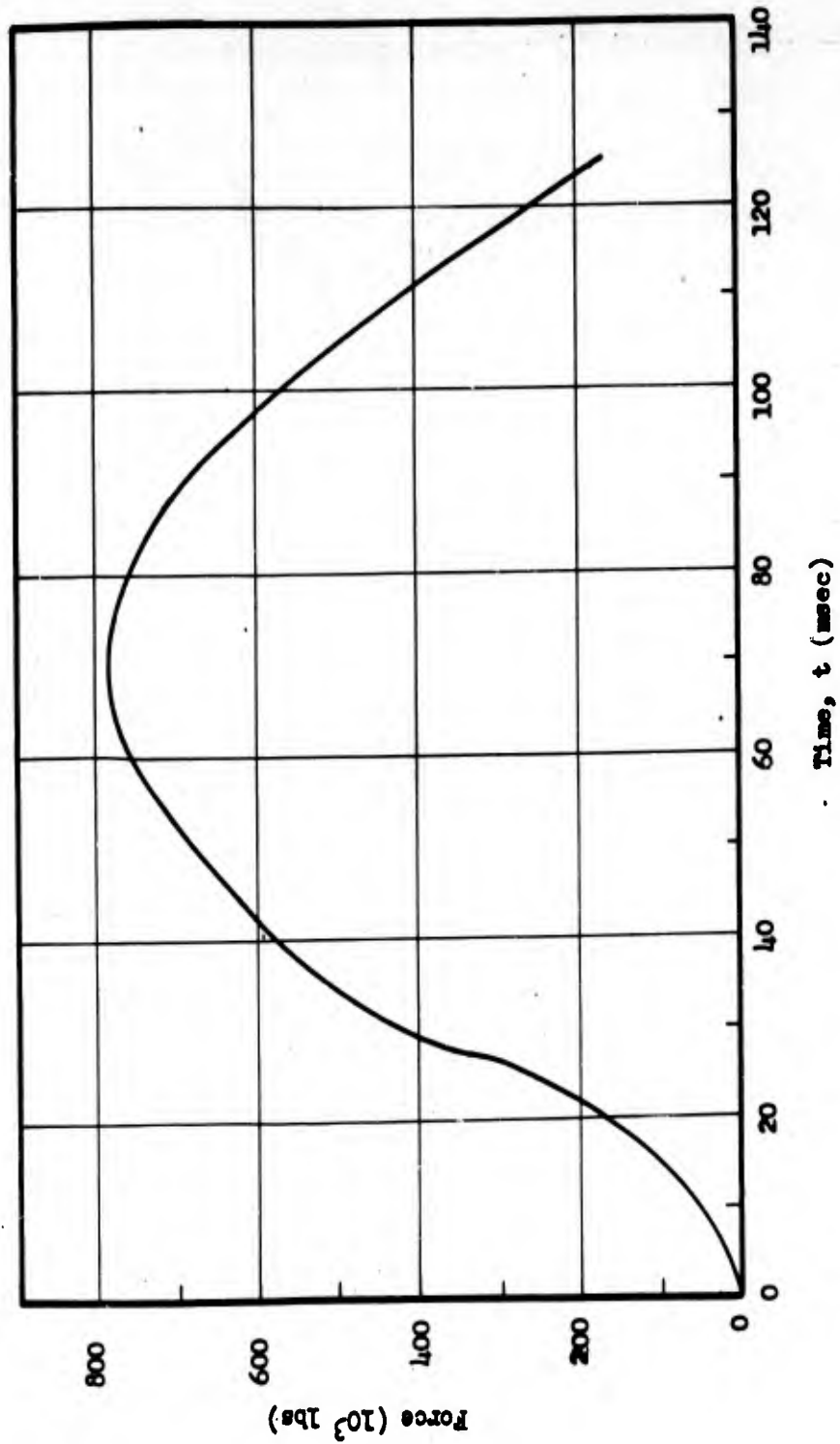
Fig. E.8.15   Rear Wall Reaction Force on Building 3.3.3
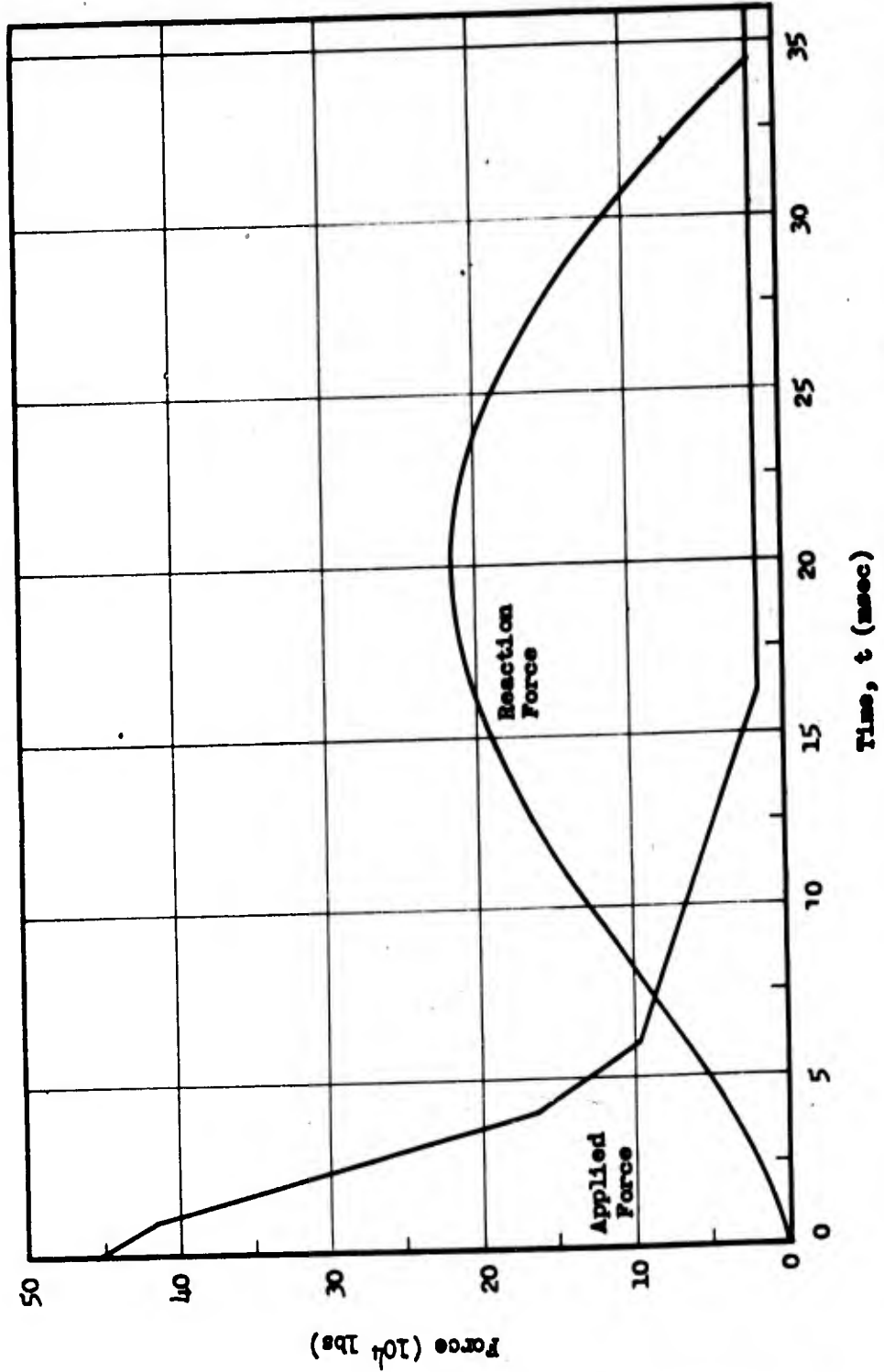
Fig. E.8.16   Applied and Reaction Forces on Front Wall of Building 3.3.8h
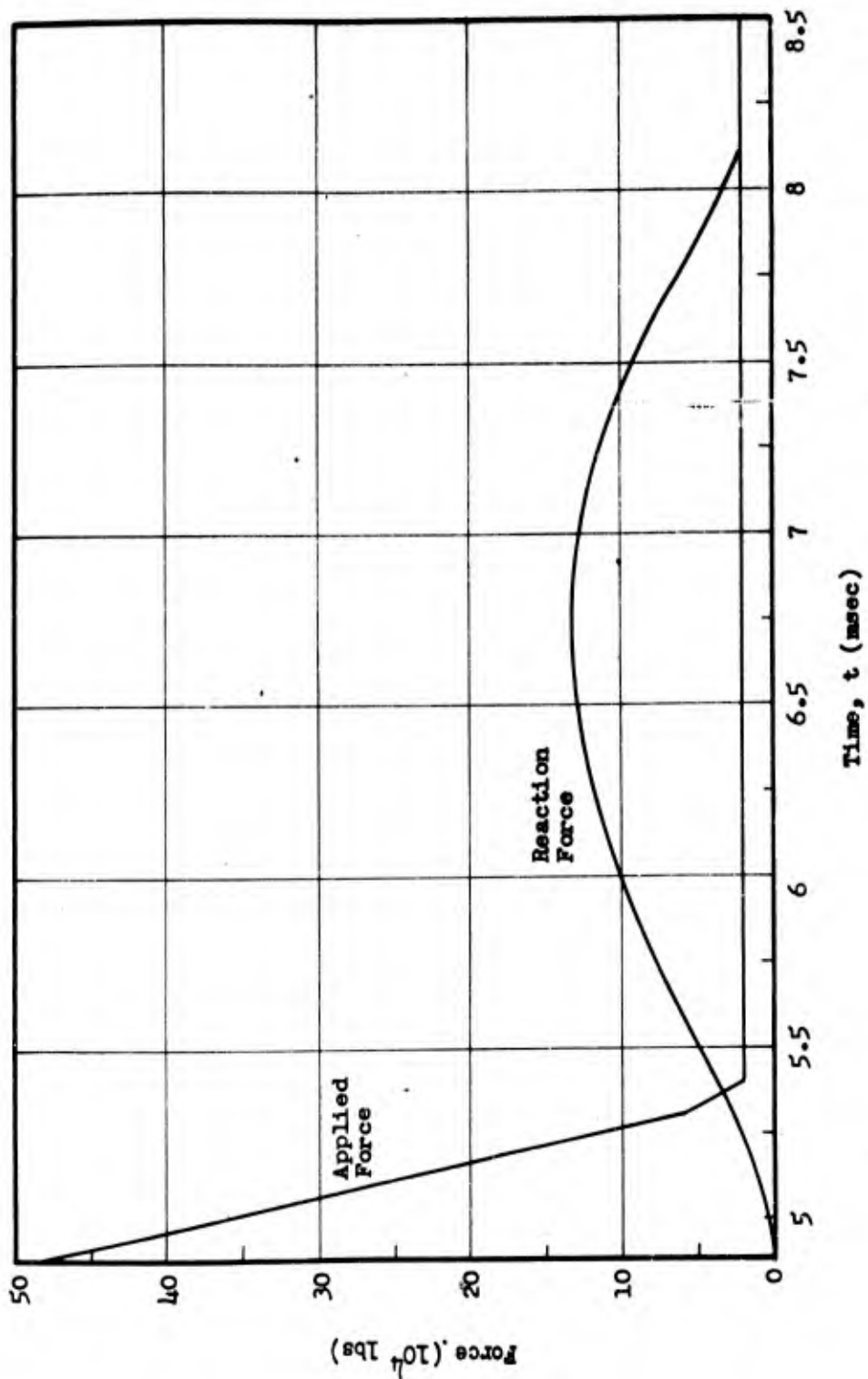
Fig. E.8.17 Applied and Reaction Forces on Back Wall of Building 3.3.8h

TABLE E.8.1

Computation of Front Wall Reaction Fo

Time, t (sec)	Pressure, $p_r(t)$ (psi)	$\Gamma p_r(t)$ $= 4.5\, p_r(t)$ (rad/sec^2)	Displacement, α (rad)	$\Omega^2 \alpha$ $= 9801\alpha$ (rad/sec^2)	A
0.008	2.46	11.1	3.4×10^{-4}	3.3	
0.021	1.00	4.5	1.8×10^{-3}	17.9	
0.024	0.93	4.2	1.9×10^{-3}	19.0	
0.030	0.79	3.6	1.79×10^{-3}	17.6	

1

TABLE E.8.1

n of Front Wall Reaction Forces for Building 3.3.4

lacement, α (rad)	$\Omega^2 \alpha$ = 9801α (rad/sec^2)	Accel, $\ddot{\alpha}_2$ (rad/sec^2)	Inertia Force $M l \ddot{\alpha}$ =1.49 (lb/ft)	External Force (lb/ft)	Reaction Force, R (lb/ft)	Total Reaction (10^3 lb)
x 10^{-4}	3.3	7.8	1163	3898	2735	97
x 10^{-3}	17.9	-13.4	-1997	1882	3879	139
x 10^{-3}	19.0	-14.8	-2206	1747	3953	140
x 10^{-3}	17.6	-14.0	-2087	1486	3473	124

2

CONFIDENTIAL
SECURITY INFORMATION

TABLE E.8.2

Loading on Front Wall of Building 3.3.4

Time, t (sec)	Pressure, p (psi)	Force, F (10^3 lb)
0	7.82	758
0.002	6.75	655
0.008	2.46	239
0.0143	1.13	110
0.057	0.25	24.3
0.1	0.22	21.4
0.2	0.16	15.5
0.4	0.08	7.7
0.6	0.04	3.9
0.8	0.02	1.9
1.0	0.01	1.0
1.2		
1.41	0	0

$$A_f = 673 \text{ ft}^2 = 96,912 \text{ in}^2$$

TABLE E.8.3

Pressures on Back Wall of Building 3.3.4
(3.55 psi Overpressure)

Time, t (sec)	Pressure, p (psi)	Force, F (10^3 lb)
0	0	0
0.0865⁻	0	0
0.0865⁺	7.82	758
0.0885	7.00	680
0.0959	3.45	334
0.1710	0.22	21.3
0.2	0.20	19.4
0.4	0.10	9.7
0.6	0.06	5.8
0.8	0.03	2.9
1.0		
1.2		
1.5	0	0
$A = 673 \text{ ft}^2 = 96,912 \text{ in}^2$		

TABLE E.8.4a

Computation for Acceleration, α̈, and Reaction Force, R, for Front Wall of Building 3.3.3 for t > T

1	2	3	4	5	6	7	8	9	10
Time, t (sec)	Ωt	cos Ωt	$\frac{\sin \Omega t}{\Omega t}$	$\frac{3}{2}\frac{\sin \Omega t}{\Omega t}$	$\cos \Omega t - \frac{3}{2\Omega t}\sin \Omega t$ (3) − (5)	$PT \times (6)$ $= 16.785\,(6)$ $= \ddot{\alpha}$ (rad/sec²)	$M\ddot{\alpha}$ $= 113.772\ddot{\alpha}$ (10³ lb)	Total Applied Force (10³ lb)	Reaction Force, R (9)−(8) (10³ lb)
0	0	1.0000	0	0	1.0000	16.7	1,900	1,900	0
0.005	0.130	0.9916	0.1296	0.1994	0.7922	13.2	1,501	1,520	18
0.010	0.260	0.9664	0.2571	0.3955	0.5709	9.53	1,084	1,140	56
0.015	0.390	0.9249	0.3802	0.5849	0.3400	5.68	646	760	94
0.020	0.520	0.8678	0.4969	0.7645	0.1033	1.73	197	380	180
0.025	0.650	0.7961	0.6052	0.9311	−0.1350	−2.25	256	0	256

TABLE E.8.4b

Computation for Acceleration, $\ddot{\alpha}$, and Reaction Force, R, for Back Wall of Building 3.3.3 for t > τ

1	2	3	4	5	6	7	8	9	10
Time, t (sec)	Ωt	cos Ωt	$\frac{\sin Ωt}{Ωt}$	$\frac{3}{2}\frac{\sin Ωt}{Ωt}$	cos Ωt − $\frac{3}{2}\frac{\sin Ωt}{Ωt}$ = (3) − (5)	P Γx (6) = 16.785 (6) = $\ddot{\alpha}$ (rad/sec²)	M $\ddot{\alpha}$ = 113.7723 (10³ lb)	Total Applied Force (10³ lb)	Reaction Force R (9)−(8) (10³ lb)
0	0	1.0000	0	0	1.0000	16.7	1,900	1,900	0
0.006	0.156	0.9879	0.1553	0.3323	0.6556	10.9	1,290	1,260	20
0.012	0.312	0.9517	0.3070	0.6570	0.2947	4.92	560	646	86
0.018	0.468	0.8925	0.4511	0.9654	−0.0729	−1.22	−139	60	200

TABLE E.8.5

Drag Calculations for Front Wall of Building 3.3.3 t>T

1	2	3	4	5	6	7	8
t - T (sec)	$2\beta(t-T)$	$\cos 2\beta(t-T)$	$\sin 2\beta(t-T)$	$\frac{3}{2\beta T}\sin 2\beta(t-T)$	$\cos 2\beta(t-T) + \frac{3}{2\beta T}\sin 2\beta(t-T)$ $(3) + (5)$	Drag Force $282.x$ (6) $(10^3$ lb)	Reaction Force R $75 \div (7)$ $(10^3$ lb)
0	0	1	0	0	1	282	256
0.005	0.13	0.9915	0.1296	0.2981	1.2896	364	439
0.010	0.26	0.9664	0.2571	0.5913	1.5577	439	514
0.020	0.52	0.8678	0.4969	1.1429	2.0107	569	642
0.030	0.78	0.7109	0.7032	1.6174	2.3283	655	720
0.040	1.04	0.5062	0.8624	1.9835	2.4897	702	777
0.050	1.30	0.2675	0.9636	2.2163	2.4838	700	775
0.060	1.56	0.0208	1.0000	2.3	2.3208	656	731
0.070	1.82	-0.2466	0.9691	2.2289	1.9823	559	634
0.080	2.08	-0.4875	0.8731	2.0081	1.5206	429	504
0.090	2.34	-0.6955	0.7185	1.6526	0.9571	270	345
0.100	2.60	-0.8569	0.5155	1.1857	0.3288	93	168

TABLE E.8.6

Drag Calculations for Rear Wall of Building 3.3.3 for t > T

1	2	3	4	5	6	7	8
t - T (sec)	26(t-T)	cos 26(t-T)	sin 26(t-T)	$\frac{3}{2\Omega T}$ sin 26(t-T)	cos 26(t-T) + $\frac{3}{2\Omega T}$ sin 26(t-T) (3) + (5)	Drag Force 145 x (6) (10³ lb)	Reaction Force 55 + (7) (10³ lb)
0	0	1.0000	0.0000	0.0000	1.0000	145	200
0.005	0.13	0.9915	0.1296	0.4160	1.4075	203	258
0.010	0.26	0.9664	0.2571	0.8253	1.7917	260	315
0.020	0.52	0.8678	0.4969	1.5872	2.4550	360	415
0.030	0.78	0.7109	0.7032	2.2573	2.9682	430	485
0.040	1.04	0.5062	0.8624	2.7683	3.2745	475	530
0.050	1.30	0.2675	0.9636	3.0932	3.3607	487	542
0.060	1.56	0.0208	1.0000	3.2100	3.2308	470	525
0.070	1.82	-0.2466	0.9691	3.1108	2.8642	415	470
0.080	2.08	-0.4875	0.8731	2.8027	2.3152	336	391
0.090	2.34	-0.6956	0.7184	2.3061	1.6005	232	287
0.100	2.60	-0.8569	0.5155	1.6548	0.7979	116	271
0.110	2.86	-0.9606	0.2779	0.8921	-0.0685	-10	45
0.120	3.12	-1.000	0.0165	0.0530	-0.9470		

ARMOUR RESEARCH FOUNDATION OF ILLINOIS INSTITUTE OF TECHNOLOGY

TABLE E.8.7

Pressures on Front and Back Walls of Building 3.3.3
(3.4 psi Overpressure)

Front Wall		Back Wall	
Time, t (sec)	Pressure, p (psi)	Time, t (sec)	Pressure, p (psi)
0	7.5	0	0
0.002	7.1	0.198⁻	0
0.013	2.5	0.198⁺	7.5
0.025	1.4	0.212	1.4
0.066	0.3	0.219	0.2⁺
0.1	0.2⁺	0.4	0.2
0.2	0.2	0.6	0.1
0.4	0.1	0.8	
0.6		1.0	
0.8		1.2	
1.0		1.4	
1.2		1.618	0
1.42	0		

t = 0 when wave strikes front wall of building

TABLE E.8.8

Loadings on Building 3.3.3 (Horizontal Components)

Front Wall		Back Wall		Horizontal Force on Trusswork	
Time, t (sec)	Pressure (psi)	Time, t (sec)	Pressure (psi)	Time, t (sec)	Force (10^3 lb)
0	7.45	0	0	0	0
0.002	7.12	0.198[a]	0	0.198	225
0.013	2.50	0.198[a]	7.45	0.30	169
0.025	1.35	0.212	1.35	0.50	90
0.066	0.25	0.219	0.23	0.70	45
0.10	0.20	0.40	0.15	0.90	22.5
0.20	0.15	0.60	0.08	1.10	11.2
0.40	0.08	0.80	0.04	1.30	
0.60	0.04	1.00	0.02	1.50	
0.80	0.02	1.20	0.01	1.618	0
1.00	0.01	1.40			
1.20		1.618	0		
1.42	0				

t = 0 when wave strikes front wall

(a) Instantaneous rise in pressure at t = 0.198 sec.

TABLE E.8.9

Calculation of Front Wall Reaction Forces for Building 3.3.A

Time t (sec)	Ωt	sin Ωt	cos Ωt	Boundary Constant A	Boundary Constant B	A cos Ωt + B sin Ωt	Inertia Force Kẍ/rΩ² (F = -641) (10³ lb)	Total Blast Force (10³ lb)	Reaction Time (10³ lbs)
0	0	0	1.0000	-0.726	0.918	-0.726	480	480	0
0.001	0.104	0.1038	0.9946	-0.758	1.228	-0.626	414	417	3
0.004	0.416	0.4041	0.9147	-0.391	0.397	-0.197	130	163	33
0.007	0.728	0.6654	0.7465	-0.263	0.257	-0.025	17	97	80
0.010	1.040	0.8624	0.5062	-0.263	0.257	0.088	-58	65	123
0.016	1.664	0.9955	-0.0930	-0.136	0.269	0.280	-185	18	203
0.018	1.872	0.9550	-0.2967	-0.136	0.269	0.297	-196.3	17.928	214
0.020	2.080	0.8731	-0.4875	-0.136	0.269	0.301	-198.9	17.857	216.8
0.022	2.288	0.7536	-0.6573	-0.136	0.269	0.292	-193	17.785	211
0.024	2.496	0.6017	-0.7987	-0.136	0.269	0.270	-178.5	17.924	196.2
0.026	2.704	0.4238	-0.9058	-0.136	0.269	0.237	-156.7	17.642	174.3
0.028	2.912	0.2276	-0.9738	-0.136	0.269	0.193	-127.6	17.571	145.2
0.030	3.120	0.0216	-0.9998	-0.136	0.269	0.142	-93.9	17.500	111.4
0.032	3.328	-0.1853	-0.9826	-0.136	0.269	0.083	-54.9	17.428	72.3
0.034	3.536	-0.3842	-0.9232	-0.136	0.269	0.022	-14.5	17.357	31.9
0.036	3.744	-0.5666	-0.8240	-0.136	0.269			17.286	17.286

ARMOUR RESEARCH FOUNDATION OF ILLINOIS INSTITUTE OF TECHNOLOGY

TABLE E.8.10

Calculation of Rear Wall Reaction Forces for Building 3.3.5a

Time t (sec)	Ωt	sin Ωt	cos Ωt	Boundary Constant A	Boundary Constant B	A cos Ωt + B sin Ωt	Inertia Force Kä/πΩ² (ä = -611)(10³ lb)	Total Blast Force (10³ lb)	Reaction Force (10³ lbs)
0	0	0	1.0000	-0.726	1.524	-0.726	480	480	0
0.001	0.416	0.4041	0.9147	-0.357	0.688	-0.048	31.728	61	29
0.005	0.520	0.4969	0.8703	-0.055	0.160	0.032	21.152	19	40
0.007	0.728	0.6654	0.7465	-0.055	0.160	0.065	43	18.826	62
0.009	0.936	0.8052	0.5930	-0.055	0.160	0.096	63.5	18.652	82
0.011	1.144	0.9103	0.4140	-0.055	0.160	0.123	81.3	18.478	100
0.013	1.352	0.9762	0.2171	-0.055	0.160	0.144	95.2	18.304	113
0.015	1.560	0.9999	0.0108	-0.055	0.160	0.159	105	18.130	123
0.017	1.768	0.9806	-0.1959	-0.055	0.160	0.167	110	17.956	128
0.019	1.976	0.9190	-0.3942	-0.055	0.160	0.169	112	17.782	129
0.021	2.184	0.8178	-0.5755	-0.055	0.160	0.163	107.7	17.608	125
0.023	2.392	0.6813	-0.7320	-0.055	0.160	0.149	98.5	17.434	111
0.025	2.600	0.5155	-0.8569	-0.055	0.160	0.130	85.9	17.261	102
0.027	2.808	0.3274	-0.9449	-0.055	0.160	0.104	68.7	17.086	86
0.029	3.106	0.0356	-0.9994	-0.055	0.160	0.061	40.3	16.913	57
0.031	3.314	-0.1710	-0.9852	-0.055	0.160	0.028	18.5	16.739	35
0.033	3.522	-0.3712	-0.9285	-0.055	0.160			16.565	16.6
0.035	3.730	-0.5550	-0.8318	-0.055	0.160				
0.037	3.938	-0.7148	-0.6993	-0.055	0.160				
0.039	4.146	-0.8449	-0.5349	-0.055	0.160				

ARMOUR RESEARCH FOUNDATION OF ILLINOIS INSTITUTE OF TECHNOLOGY

CONFIDENTIAL
SECURITY INFORMATION

TABLE E.8.11

Net Pressures on Walls of Building 3.3.8h

Time, t (sec)	Pressure on Front Wall, p(t) (psi)	Force, 59 p(t) (10³ lb)	Time, t (sec)	Pressure on Back Wall, p(t) (psi)	Force 59 p(t) (10³ lb)
0	8.13	480	0.049	8.13	480
0.001	7.06	417	0.053	1.03	61
0.004	2.76	163	0.054	0.32	19
0.007	1.64	97	0.10	0.25	15
0.016	0.30	18	0.20	0.20	12
0.1	0.25	15	0.40	0.15	9
0.2	0.20	12	0.60	0.12	7
0.4	0.15	9	0.30	0.10	6
0.6	0.12	7	1.0		
0.8	0.10	6	1.2		
1.0			1.44	0	0
1.2					
1.39	0	0			

t = 0 when shock reaches front wall

$$A_f = A_b = 59 \times 10^3 \text{ in.}^2$$

ARMOUR RESEARCH FOUNDATION OF ILLINOIS INSTITUTE OF TECHNOLOGY

CONFIDENTIAL
Security Information

CHAPTER E.9

BUILDING 3.3.3

E.9.1 DESCRIPTION OF STRUCTURE

Building 3.3.3 is a single-story, long span, three-aisle, six-bay, light steel frame, industrial type structure approximately 120 ft by 240 ft by 54 ft. Steel roof trusses cover the three aisles. Over one aisle the truss trusswork is supported at one end by steel columns and at the other end by carrier trusses. Over the other two aisles they are supported entirely be carrier trusses, each spanning three bays. The front wall of the structure is extended (in effect) by free-standing wing walls. The purpose of these walls is to insure that the test behavior of the structure closely simulates an intermediate section of a long building under real blast conditions.

The roof is composed of 3-ply roofing over timber sheathing which is supported by steel purlins spanning the roof trusses. All columns are built-up H-sections and rest upon individual, rectangular, reinforced-concrete footings.

Front and rear walls are 16 1/2 in. thick and are constructed of standard, cellular, concrete blocks. Along the edge of each wall, from the corner to the first window, standard 16-in. brick masonry is used. The walls are supported on a continuous concrete foundation, and the sides of the building are open. Monitor ends, and those portions of the monitor sides above the windows, are covered with corrugated steel

siding. Glased steel sash is used for all windows in the building walls and monitors. Sketches of building 3.3.3 are shown in Figs. E.9.1, E.9.2, and E.9.3.

E.9.2 ASSUMPTIONS OF STRUCTURAL ACTION AND METHOD ANALYSIS

The purpose of this section is to explain briefly the simplifying assumptions that have been made in order to obtain an analytical solution to the problem under consideration.

A cursory examination of the structural frame will reveal that the heavy roof structure is very stiff compared to the long and relatively flexible columns on which it is supported. Under these conditions, as has been pointed out in Vol II, "lumping" of the various structural parameters is justified. Therefore the subsequent analysis will attempt to construct a reasonable mathematical model of building 3.3.3 for purposes of dynamic response calculations. An approximation to such a model will be a single equivalent mass attached to the top of an equivalent column.

The mass, which will move under the action of externally applied forces, consists primarily of the roof and roof framing. However, if it is assumed that the walls and columns rotate about their base as the building deflects, a portion of their mass must be added to the mass of the roof. To make allowances for this, one-third of the mass of the walls and columns will be considered concentrated at the roof level.

It is further assumed that the roof structure will move as a rigid body, i.e., the tops of all columns will deflect the same distance
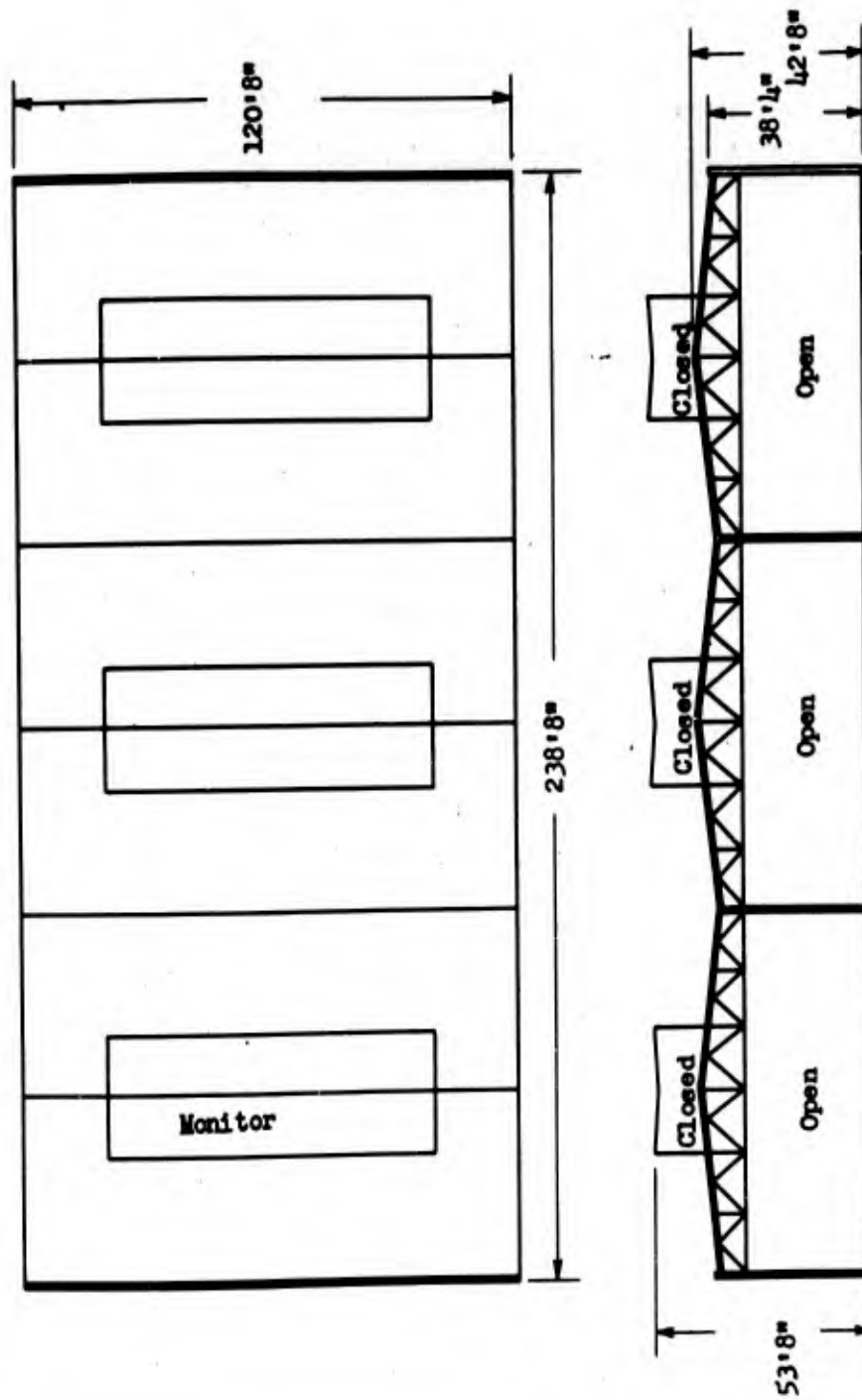
Fig. 2.9.1 - Plan and Side Elevation of Building 3434
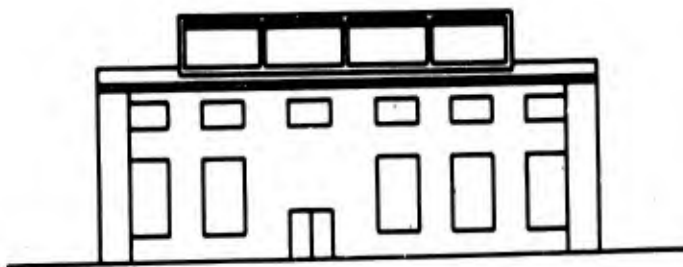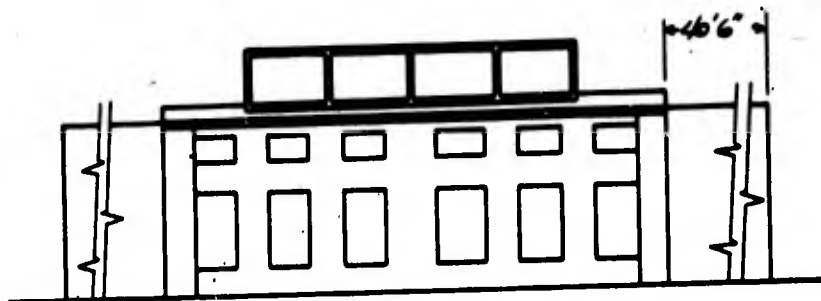
Fig. E.9.2 Front Elevation and Rear Elevation of
Building 3.3.3
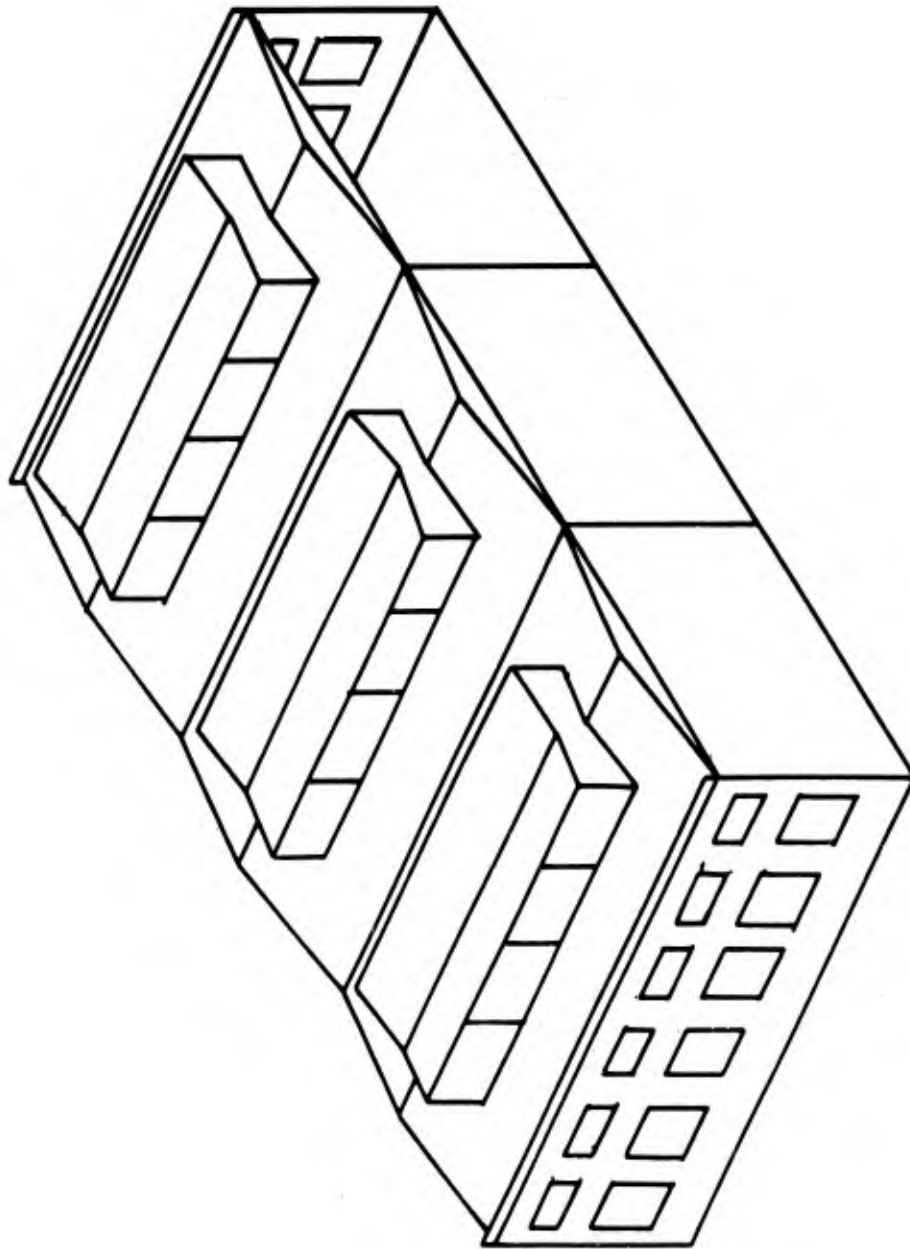
Fig. E.9.3 Isometric of Building 3.3.3 (Wing Walls not Shown)

at any instant of time. Also, a line through the upper and lower chord connection at each column will be assumed to remain vertical throughout the motion.

In determining the resistance of the structure to sidesway certain assumptions were made concerning the structural integrity of the columns and their connections to the roof trusses and footings. Structural members are oftentimes analysed as either pin-connected or fully restrained against rotation, according to the judgment of the analyst. An examination of the end conditions in this case will reveal that the anchor bolts connecting the columns to the footings are inadequate to develop an appreciable moment at the base of the columns. Furthermore, the isolated footings are likely to rotate under an applied couple. Consequently, the assumption of pin ends at the base rather than fixed ends seemed to be the most reasonable. The top and bottom chord connections of the trusses to the columns have also been considered as pin-connected since this type of connection is not designed to resist moment.

On the basis of the above assumptions, a typical column in the deflected position will appear as shown in Fig. E.9.4. It is apparent that the maximum moment in the column will occur at point B, where the bottom chord connects to the column, and that this moment will be a function of the horizontal displacement. In order to evaluate this displacement of the properties of the columns must be known and their resistance to flexure must be determined.

During the initial part of the motion of the structural frame, the columns will act elastically and the moment in the columns will be
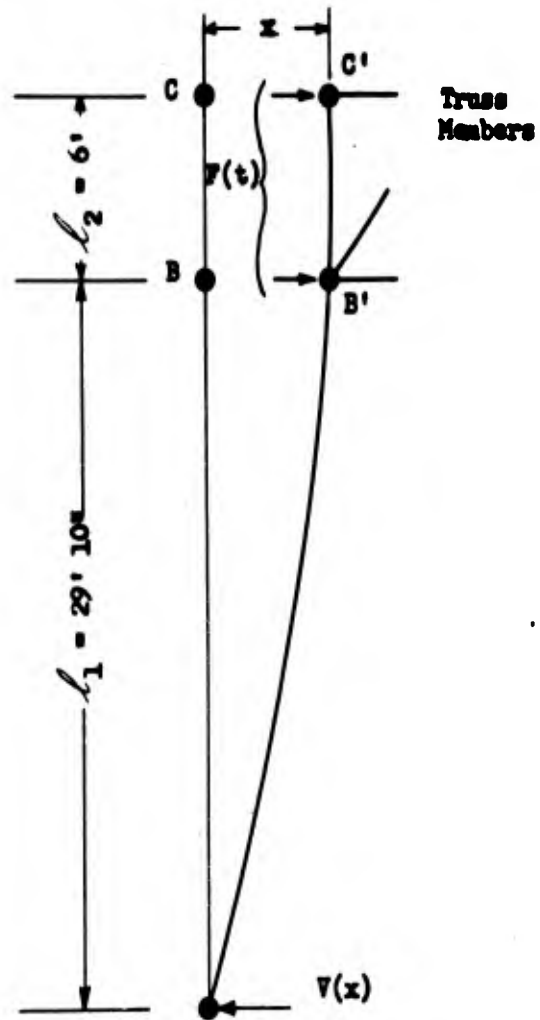
Fig. E.9.4   Deflection of Typical Column of Building 3.3.3

directly proportional to the deflection until the extreme fibers begin
to yield. Thereafter, the deformation will be of an elasto-plastic
nature, i.e., the column ends will deform partly elastically and partly
plastically until all fibers in the cross section have yielded. At this
point a plastic hinge will form at B (see Fig. E.9.4) which will offer a
constant resisting moment to further deformation. The stress distribu-
tion on the cross section at the end of a typical column is shown graphi-
cally in Fig. E.9.5b for each of the aforementioned stages of deformation.
The elasto-plastic behavior of a fiber is idealized and shown graphically
in Fig. E.9.5a.

Maximum elastic and plastic resisting moments have been computed
on the basis of a yield point stress of 40,000 psi. The selection of this
value for structural steel was based on evidence that the yield point is
increased for high rates of loading. The modulus of elasticity of steel
was taken as 30×10^6 psi for deflections in the elastic range. In addi-
tion, it was assumed that the deflection at the end of the elasto-plastic
range is equal to twice the yield point deflection. This assumption
represents merely an attempt to approximate the true shape of the resis-
tance curve.

Because all of the columns of the structure are not of equal
size nor of similar orientation with respect to their principal axes, it
is obvious that for a given lateral deflection different moments will be
developed by the various columns. Some will reach the yield point stress
earlier than others so that in order to determine the total resistance

of the structure to sidesway it is necessary to add the individual resistances throughout the entire range of deflections until all columns are plastic.

E.9.3 LOADING

It is not intended at this point to give a complete discussion of the loading phenomena on building 3.3.3, but rather only a brief qualitative description of blast action. For a complete analysis of blast loads on this building reference is made to Chapter E.2 of this volume.

A shock wave, traveling in the longitudinal direction of the building (i.e., perpendicular to the front and rear walls), will cause an initial peak load on the wall as the impinging shock wave is reflected, thereby raising the local front wall pressure. The immediate effect of this initial front wall load is to cause an acceleration of the front wall masonry since the masonry is not a fixed, rigid body. Thus, with the wall itself taking on an acceleration, it does not transmit to the building foundation and structural frame the entire load imposed by the shock wave.

Since the glass windows in the front wall shatter soon after reflection of the shock wave, a weaker shock wave re-forms within the building and travels toward the rear wall. Simultaneously, with this action, the main shock wave outside of the building is also moving toward the rear wall, but somewhat ahead of the interior wave and reflects on the sloped roof surface, resulting in an outer roof pressure that is

greater than the side-on pressure. As far as net pressure forces on the roof are concerned, the difference of advancement between the two wave fronts is not of too great importance. The difference in pressure behind each wave front adjacent to the roof is, however, the reason for a net force on the roof. This net force can be resolved into horizontal and vertical components and in such a manner be considered separately as part of the loads applied to the structure. When the interior shock wave, reinforced by the exterior shock wave enveloping the building interior through the open sides, finally strikes the rear wall, it is reflected and a second peak load is applied to the building.

While the loads due to the shock diffraction effects are of extremely short duration, there follows a high velocity air flow which endures for a considerable time after passage of the shock front. This air blast causes drag forces on the structure. Such drag loads are particularly significant in the case of the interior structural members since all such members are exposed to the interior air flow.

Drag loads resulting from air blast are also characteristic, for the most part, of the loads on the monitors. This follows from the fact the shock wave, striking the monitors and having an immediate reflection, shatters the monitor glass which makes up most of the monitor's area normal to the blast. The shock wave then enters into a rather complex situation within the monitor itself. At this point an occlusion develops between the interior monitor shock wave and the re-formed shock wave within the main part of the building. However, all monitor glass can be expected to fail. Since the mass of the glazing is relatively small

compared to the mass of the structure, the force (and energy expenditure) needed to accelerate it is small and is neglected.

It is to be noted here that the horizontal and vertical forces on the roof surface were neglected in the response analysis of building 3.3.3.

Figure E.9.6 shows the total applied horizontal load on the building as a function of time. A tabulation of these same loads will be found in Table E.9.4.

E.9.4 EQUIVALENT MASS

The determination of the building mass may be divided into two parts: the roof structure proper, and the walls and columns.

The roof structure weight was obtained by taking the sum of the weights of the component parts. In the case of the trusses, no consideration was given to the weight of gusset plates, rivet heads, or similar structural details. The working point length of truss members used in the calculations should suffice to compensate for this simplification.

Only one-third of the wall and column structure was considered as effective in contributing to the equivalent mass.

A summary of the weight calculations is shown in Tables E.9.1 and E.9.2. Since the total mass of the building is to be considered as "lumped", the following figure for the final mass of the building includes the roof mass plus one-third of the mass of the brick walls and columns. Then we have,

Weight of roof, lb   = 512,800

1/3 weight of walls, columns, etc.
1/3(597,655) , lb   = 199,200

Total   = 712,000

Final equivalent mass = $\dfrac{712,000 \text{ lb}}{32.2 \text{ ft/sec}^2}$

        = 22,100 slugs.

E.9.5   RESISTANCE TO SIDESWAY

In a previous paragraph, the reasons for the assumptions concerning the end conditions for the columns were outlined. Since the resistance of a column to bending, whether elastic, elastic-plastic, or plastic, is a function of the column's structural properties, these properties were found and are given in Table E.9.3.

A typical column deflection curve is shown in Fig. E.9.4 with the roof trusses moving as a rigid unit such that points B and C have an equal horizontal deflection of Δ to B' and C' respectively. Point A is assumed pin-connected.

Taking column B as a typical column, the fixed end moment at B is found, again referring to Fig. E.9.4,

$$M^F_{BA} = \frac{3EI\,\Delta}{\ell^2}$$

$$M^F_{BC} = 0$$

where

$$I = I_{X-X} = 481 \text{ in.}^4$$
$$\ell = 29.8 \text{ ft}$$
$$E = 30 \times 10^6 \text{ psi}$$

Hence, for $\Delta = 0.01$ ft, (arbitrarily)

$$M_{BC}^F = 0; \quad M_{BA}^F = \frac{3(30 \times 10^6)(481)(0.01)}{(29.8)^2 (12)^2} = 3.375 \text{ kip-ft}$$

The moment distribution factor for each span is:

Span AB, $\quad f_1 = \frac{6.00}{29.8 + 6.00} = 0.167$

Span BC, $\quad f_2 = \frac{29.8}{29.8 + 6.00} = 0.833$

The moment distribution for column B is as follows:

A	B		C
	.167	.833	
0	+3.375	0	0
0	−0.564	−2.81	0
0	+2.81	−2.81	0

In a similar manner, the moment at point B is found for all columns for $\Delta = 0.01$ ft and the results of this computation are shown in Table E.9.3.

The bending moment M_{yp} at the instant of yielding at point B is found as follows. Assuming a yield point stress σ_{yp} of 40,000 psi,

$$M_{yp} = \sigma_{yp} \frac{I}{c} = 40,000 \text{ (S)}$$

where $S = \frac{I}{c}$ is the section modulus. Table E.9.3 gives the yield moment for all columns of the building. Having the yield point bending moment and unit elastic deflection of point B, the yield point deflection at B is found and shown in Table E.9.3. The maximum plastic bending moment of each column is found by integrating the uniform yield stress of
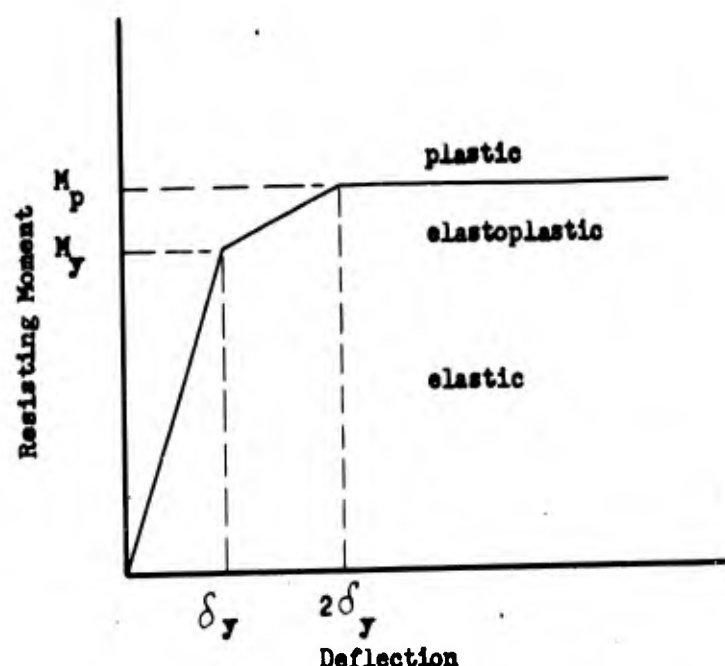
Fig. E.9.5a   Idealised Elasto-plastic Fiber Behavior
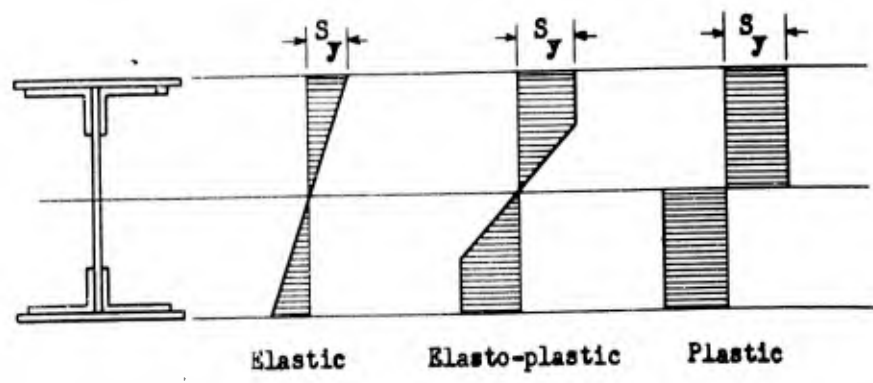
Fig. E.9.5b   Typical Column End Stress Distribution of Building 3.3.3
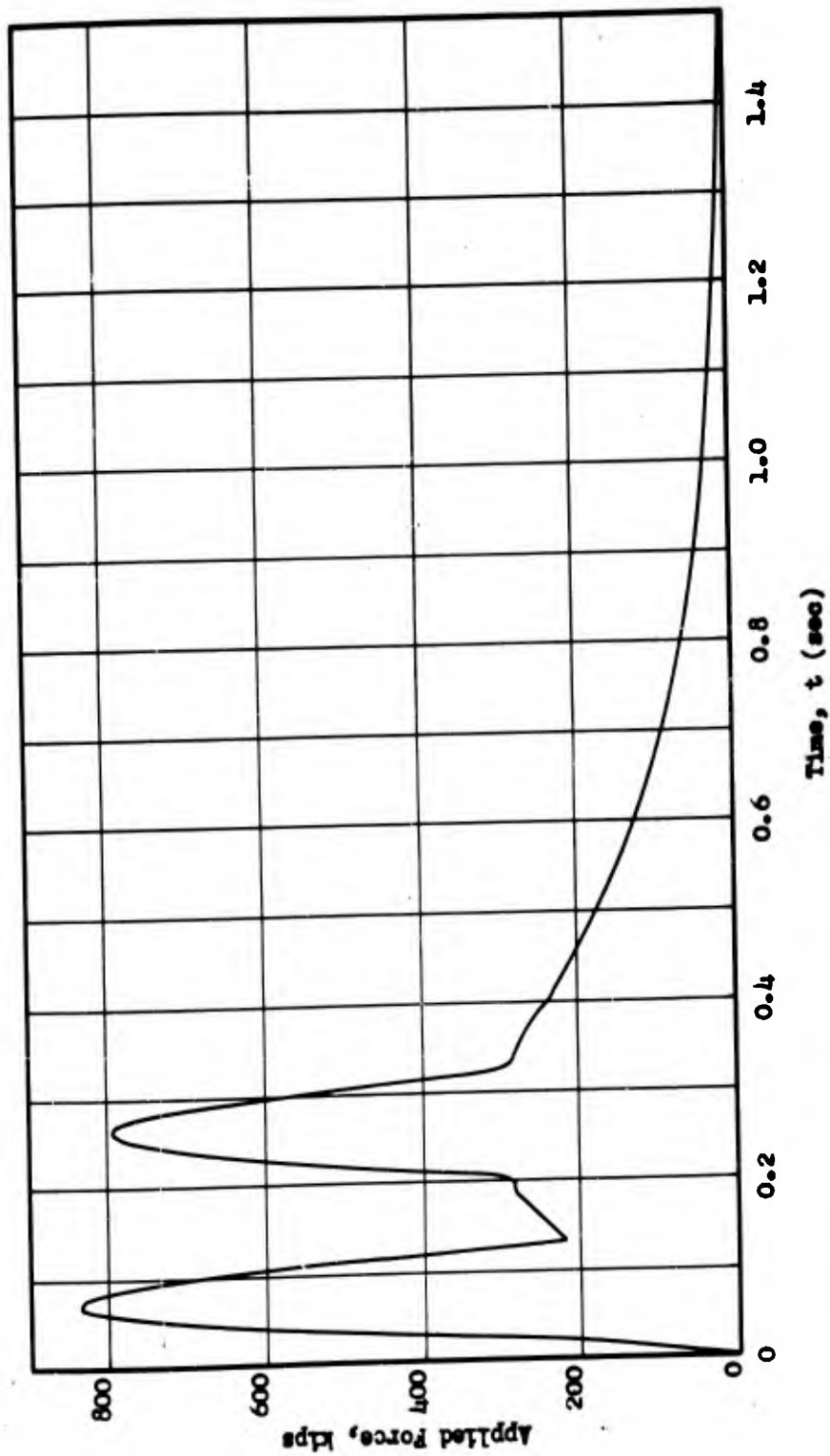
Fig. E.9.6 Total Applied Horizontal Load on Building 3.3.3

TABLE E.9.1

Summary of Roof Weight for Building 3.3.3

Item	Quantity	Wt of Each (lb)	Total Wt (lb)
Truss T-1	15	7,194	107,900
Truss T-2	4	11,734	46,900
Truss T-3	2	6,494	13,000
Truss T-4	6	3,884	23,300
Purlins	All		67,700
Planking	All		145,600
Roofing	All		28,100
Bracing	All		20,500
Nailers & Blocking	All		20,100
Girts	All		9,400
Mullions	All		10,000
Siding	All		4,100
Sash	All		16,200
		Total Roof Wt =	512,800

TABLE E.9.2

Summary of Building Weight Other Than Roof

Item	Quantity	Wt of Each (lb)	Total Wt (lb)
Column A	2	5020	10,040
Column B	4	2890	11,560
Column C	1	4140	4,140
Columns D & E	9	2370	21,330
Lintel L_1	11	645	7,095
Lintel L_{1A}	12	482	5,780
Lintel L_2	1	610	610
Window Type A[a]	24	90	2,160
Window Type B[a]	22	120	2,640
Window Type C[a]	22	150	3,300
Walls	All		343,000
Brickwork	All		186,500
Total Bldg Wt Other Than Roof			= 597,655

[a] Weight of window does not include weight of glass.

TABLE E.9.3

Column Characteristics for Building 3.3.3
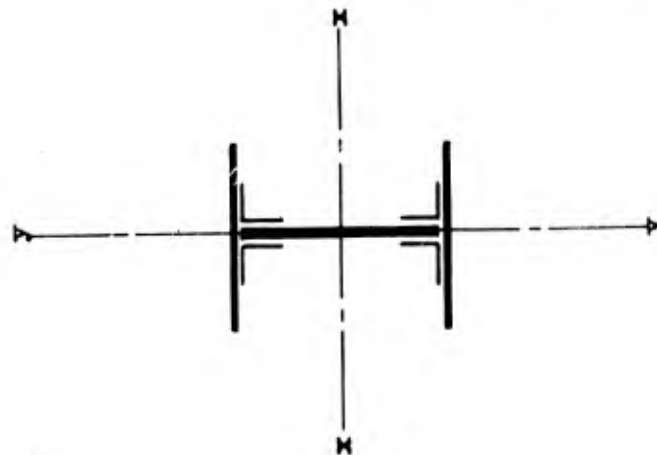
I = Moment of inertia about axis of bending, in.^{4}

S = Section modulus about axis of bending, in.^{3}

M_{u_B} = Elastic moment in kip-ft for unit deflection of point B of 0.01 ft

Δyp_B = Yield point deflection at point B, ft

Note:
Column length ℓ_i is shown in Fig. E.9.4

M_{yp_B} = Yield point bending moment at point B, kip-ft

V_{yp_B} = Yield point shear at point B, kips
$= M_{yp_B} \div \ell_i$

$V_{p\ell_B}$ = Shear at total plasticity
$= M_{p\ell_B} \div \ell_i$

$M_{p\ell_B}$ = Plastic bending moment at point B, kip ft

$\Delta p\ell_B$ = Deflection of point B at beginning of total plasticity, ft

ARMOUR RESEARCH FOUNDATION OF ILLINOIS INSTITUTE OF TECHNOLOGY

TABLE E.9.3 (Cont)

Column Characteristics for Building 3.3.3

Column	No. Cols required for Bldg	I	S	M_{u_B}	M_{yp_B}	Δ_{yp_B}	V_{yp_B}	$M_{p\ell_B}$	$\Delta_{p\ell_B}$	$V_{p\ell_B}$	Axis of Bending
A	2	347	53.3	2.03	178.0	0.876	5.96	289.4	1.752	9.70	y-y
B	4	191	29.3	1.12	97.6	0.872	3.27	157.0	1.744	5.26	y-y
C	1	957	146.0	5.60	486.0	0.868	16.30	283.5	1.736	19.00	x-x
D & E	9	481	77.0	2.81	257.0	0.914	8.61	301.0	1.828	10.10	x-x

40,000 psi over the column cross-sectional area and then taking the summation of statical moments of the resulting forces on elemental areas about the axis of bending. The values of the plastic bending moment for various columns is shown in Table E.9.3.

Figure E.9.7 gives a graphic picture of the resistance of building 3.3.3 to horizontal sideway. In this graph the shear forces corresponding to the horizontal applied load on the structure are shown as a function of the roof deflection. The lower truss chord-column attachment was taken as the point of reference at the roof level.

Since the contribution of each column is accounted for, and since, therefore, the linearity of the force-deflection curve changes every time a column yields or develops a complete plastic hinge, there are a number of characteristic points at which the force-deflection curve exhibits changes in slope until a constant resistance to deformation is attained.

E.9.6 ACTION OF MASONRY WALLS

A complete and detailed analysis of the response of the masonry walls of this structure to blast is given in Section E.8.5.3 of this report. It is intended to discuss here only the physically important aspects of that analysis, and to exhibit the final force-time curves arising from the action of the walls on the structure.

As a shock wave impinges on the wall, the wall, in general, will undergo deflections of both elastic and non-elastic natures. At the same time it will transmit time-dependent forces to the structural frame. Calculations have shown that the nature of the transmitted forces is
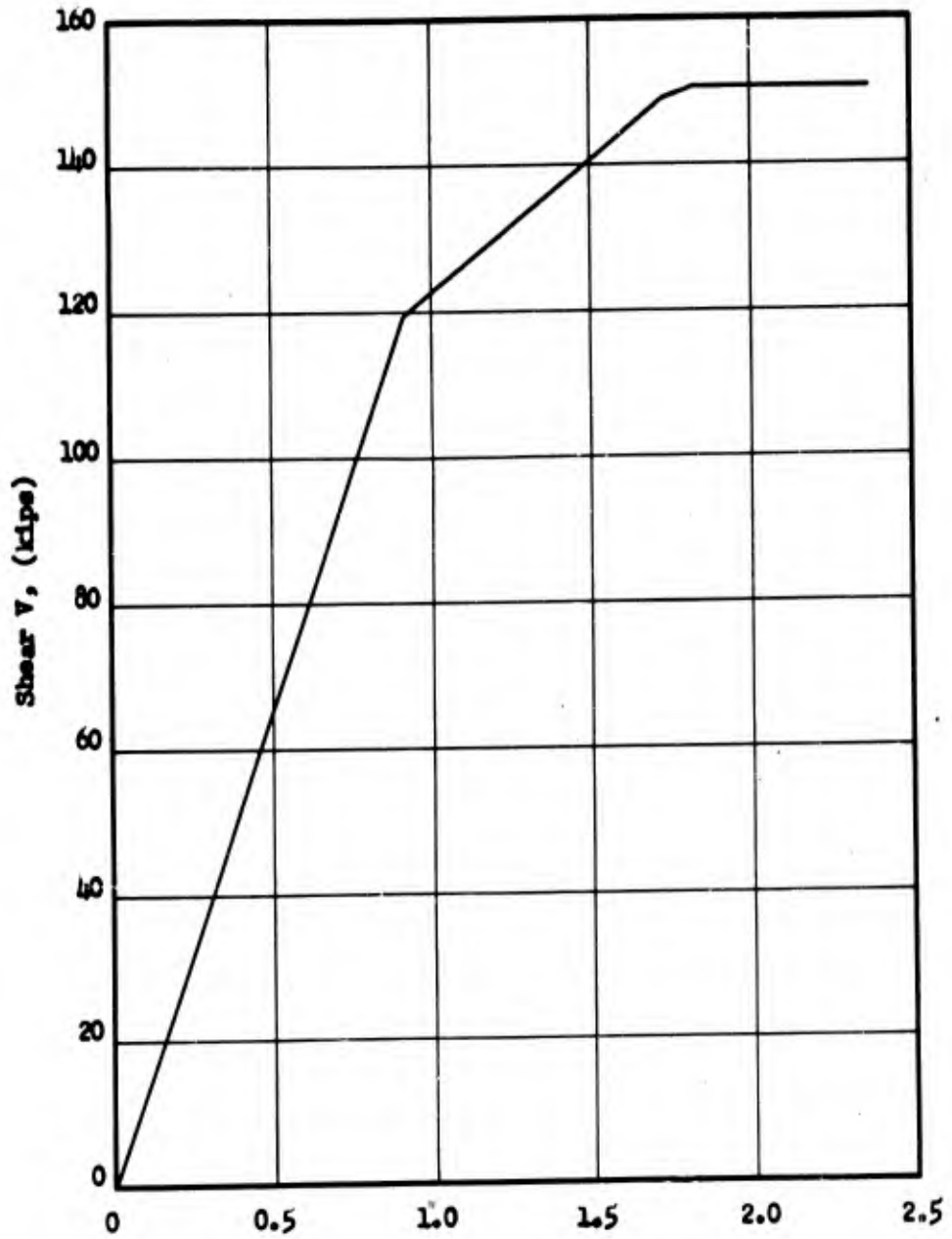
Fig. E.9.7   Resistance of Building J.3.3 to Horizontal
Sideway

different from that of the applied loads and the action of the wall is essentially that of a cushion. Initially the blast loads are high but the transmitted forces are low. As the time progresses there will be a decrease in applied loads but an increase in transmitted load. Finally the wall will fail completely and the transmitted loads will drop to zero.

The loads transmitted by the brick walls will be added to the drag forces acting on the structural frame and roof for purposes of calculating the response of the entire structure.

E.9.7 DYNAMIC RESPONSE OF STRUCTURE

It is now possible to apply the blast loadings to the entire structure and to study its time-dependent behavior. It must be pointed out that the relative phasing of the forces transmitted to the structure through its components must be considered, i.e., all applied forcing functions must be referred to a common time base. A graph showing the composite forcing function thus obtained is shown in Fig. E.9.6. It is obtained by the addition, ordinate for ordinate, of the forcing functions resulting from the front and rear wall reactions and the drag forces on the frame.

The equation of motion of the structure may be written,

$$M\ddot{x} = H(t) - R\left[x(t)\right] \tag{E.9.1}$$

where

M = mass of body

t = time, sec

$H(t)$ = forcing function, a function of time t

$R\left[x(t)\right]$ = resistance function, a function of displacement

$x = x(t)$ = displacement, a function of time t

$\ddot{x} = x(t)$ = rectilinear acceleration in direction of x.

Because of the non-analytic character of the functions $H(t)$ and $R\left[x(t)\right]$ it is necessary to solve the above equation by a numerical procedure.

If $R\left[x(t)\right]$ is replaced by $R(x)$ in Eq. E.9.1, it is understood that $x = x(t)$. Then,

$$M\ddot{x} = H(t) - R(x). \tag{E.9.2}$$

Consider now, any equation for acceleration where the acceleration $\ddot{x}$ is a function of a time parameter r. Then, $\ddot{x} = \ddot{x}(r)$ and after some elapsed time s, the velocity is

$$\int_{0}^{s} \ddot{x}\,(r)\; dr = \dot{x}(s) - \dot{x}(0). \tag{E.9.3}$$

But $x(0) = 0^{*}$ if the initial velocity $v_{0} = 0$. Then,

$$\dot{x}(s) = \int_{0}^{s} \ddot{x}\,(r)\; dr \tag{E.9.4}$$

If Eq. E.9.4 is again integrated, another expression of the displacement x as a function of time will be obtained. Considering $x = f(t)$, then,

$$\int_{0}^{t} \dot{x}(s)\; ds = x(t) - x(0) \tag{E.9.5}$$

---

* These initial conditions are arbitrary but are so chosen now to fit the conditions of the real problem of building 3.3.3.

But $x(0) = 0^*$ if the initial displacement is zero. Then,

$$x(t) = \int_0^t \dot{x}(s) \, ds \qquad (E.9.6)$$

Substituting into Eq. E.9.6 for $\dot{x}(s)$ as expressed by the integral of Eq. E.9.4,

$$x(t) = \int_0^t \int_0^s \ddot{x}(r) \, dr \, ds \qquad (E.9.7)$$

Changing the limits of the definite integral and the order of integration of Eq. E.9.7,

$$x(t) = \int_0^t \int_r^t \ddot{x}(r) \, ds \, dr \qquad (E.9.8)$$

Integrating Eq. E.9.8 with respect to ds,

$$x(t) = \int_0^t (t - r) \ddot{x}(r) \, dr \qquad (E.9.9)$$

If into Eq. E.9.9, $x(t + 2h)$ is substituted for $x(t)$,

$$x(t + 2h) = \int_0^{(t + 2h)} (t + 2h - r) \ddot{x}(r) \, dr \qquad (E.9.10)$$

Equation E.9.9 can be rewritten in the following form by introducing the term 2h. Thus,

$$x(t) = \int_0^t (t + 2h - r) \ddot{x}(r) \, dr - \int_0^t 2h \, \ddot{x}(r) \, dr. \qquad (E.9.11)$$

Subtracting Eq. E.9.11 from Eq. E.9.10,

$$x(t + 2h) - x(t) = \int_t^{(t + 2h)} (t + 2h - r) \ddot{x}(r) \, dr$$

$$+ 2h \int_0^t \ddot{x}(r) \, dr \qquad (E.9.12)$$

Now Simpson's rule, which will be applied to Eq. E.9.12 for the approximate evaluation of the first integral term, is

$$\int_{t}^{t+2h} f(x)dx = \frac{h}{3} \left[f(t) + 4f(t+h) + f(t+2h) \right]$$

Then from Eq. E.9.12,

$$x(t+2h) - x(t) = \frac{h}{3} \left[2h\ \ddot{x}(t) + 4h\ \ddot{x}(t+h) \right] + 2h\ \dot{x}(t) \quad (E.9.13)$$

Equation E.9.13 is in a form that can be numerically integrated.

Applying Eq. E.9.13 to the real case of building 3.3.3, it is seen that $\ddot{x}$ and $\dot{x}$ can be evaluated and the numerical integration of the equation can proceed.

Knowing the forcing function $H(t)$ of the blast, and the resistance function $R(x)$ and mass M of the building, Eq. E.9.2 gives:

$$\ddot{x} = \frac{H(t) - R(x)}{M}$$

From the standard expression for numerical differentiation shown below, $\dot{x}$ is obtained:

$$\dot{x}(t+h) = \dot{x}(t) + \frac{h}{2} \left[\ddot{x}(t) + \ddot{x}(t+h) \right] \quad .$$

Reference is made to Table E.9.5 where the numerical integration of the response equation E.9.13 is performed. This table gives the deflection and acceleration of the equivalent building mass corresponding to the elapsed time. The deflection and acceleration are given in Figures E.9.8 and E.9.9, respectively, both plotted as functions of time.

E.9.8 DISCUSSION OF RESULTS

This investigation was predicated on the assumption that the
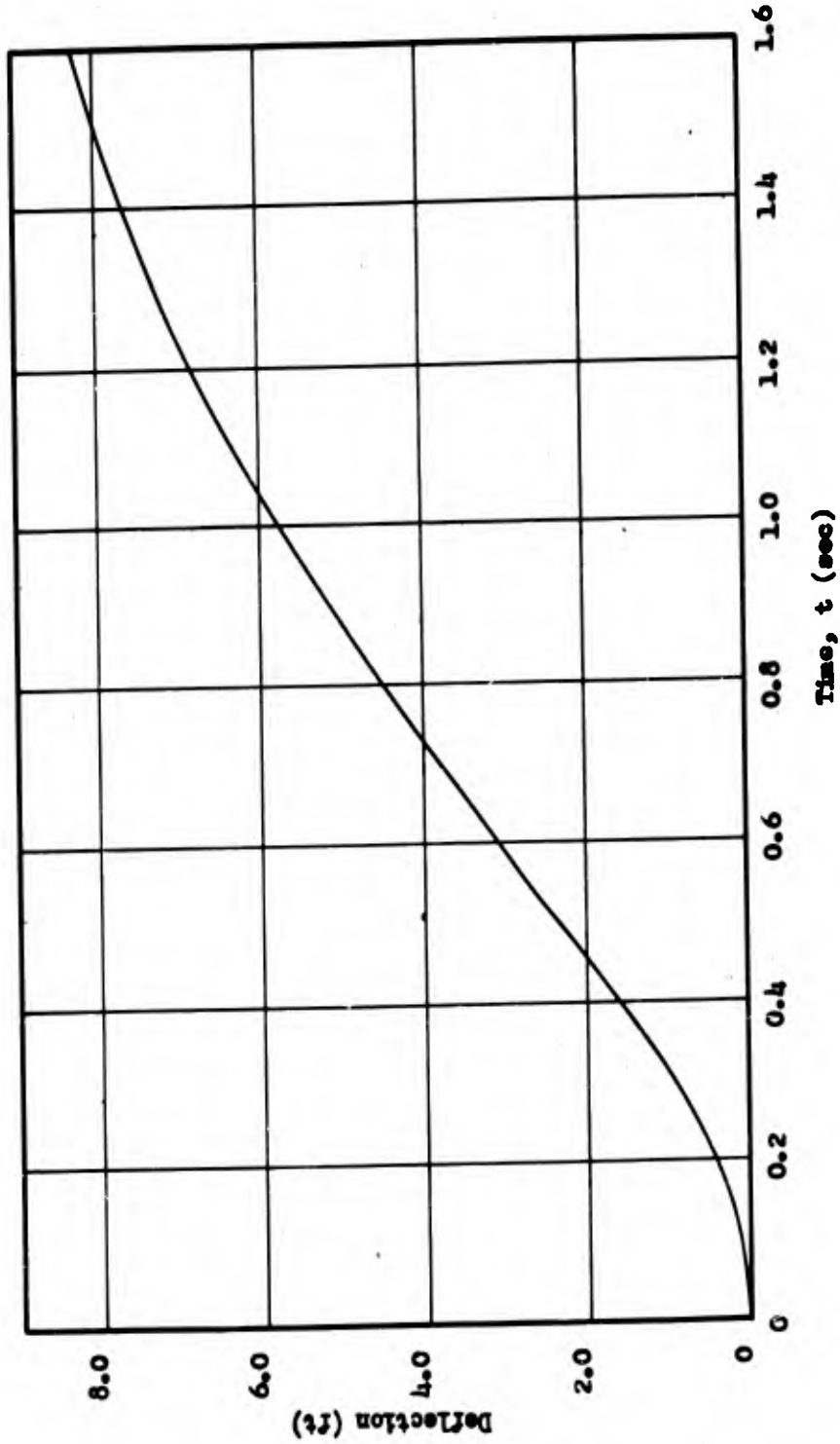
Fig. E.9.8   Deflection vs Time of Equivalent Building Mass for Building 3.3.3
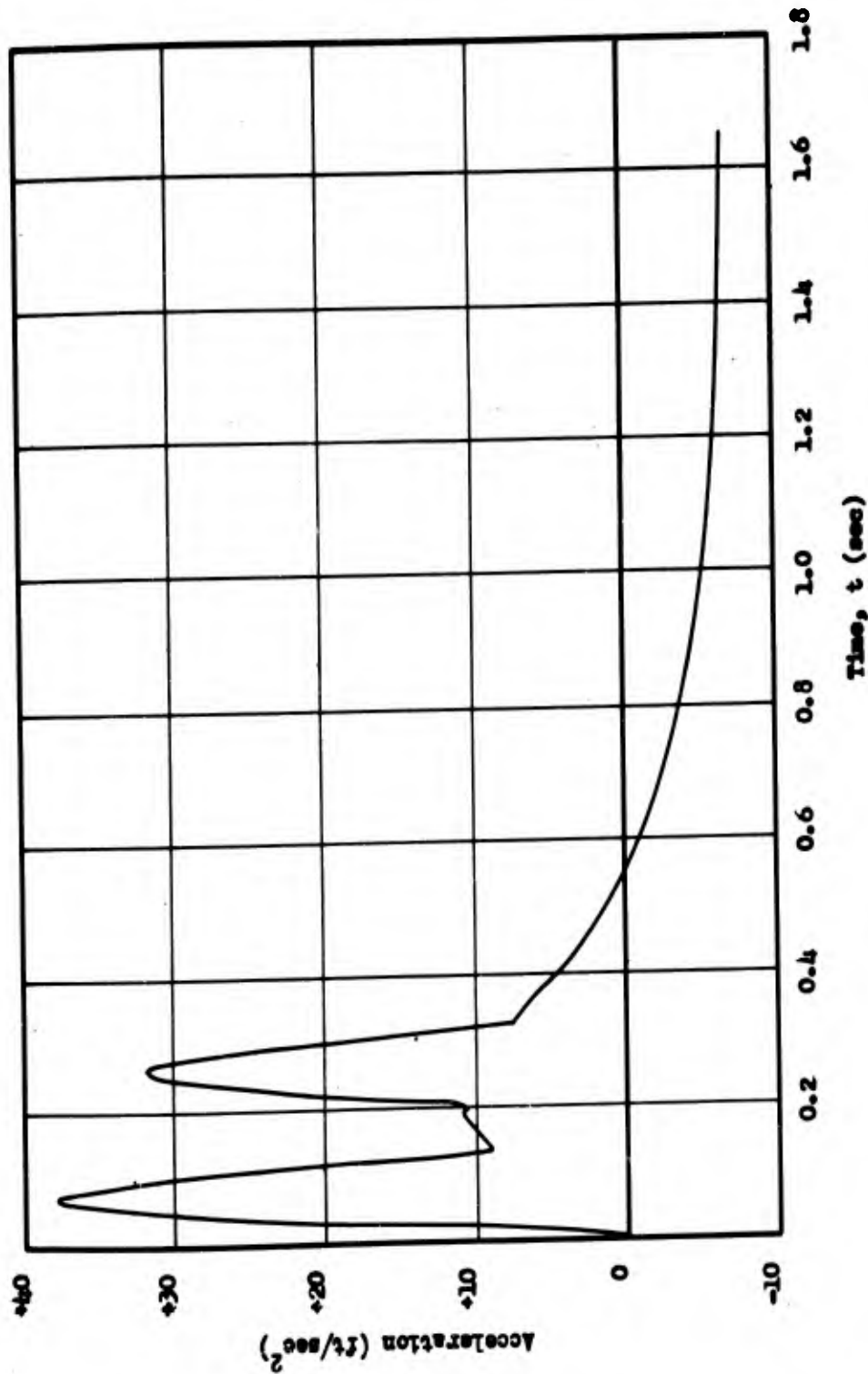
Fig. E.9.9   Acceleration vs Time of Equivalent Building Mass for Building 3.3.3

dynamic response of the building under study would be sufficiently defined by considering only the horizontal forces on the structure resulting from a shock wave. If the application of such horizontal forces alone can result in deflecting the structure sufficiently so that it is carried into a state of static instability, then structural collapse will be impending. The consideration of any other forces that would act to increase the degree of instability would reveal nothing concerning the dynamic response of the structure.

In the case of building 3.3.3, the response calculations of Table E.9.5, which are based on the horizontal forces alone, show that after 1.618 sec the equivalent building mass was deflected 8.324 ft and still had a velocity of 1.772 ft/sec. (After elapsed time of 1.618 sec, the applied force goes to zero). At a deflection of 8.324 ft, a comparison between the resisting moment (the product of the shear resistance and column length) and the overturning moment shows an unbalanced moment equal to approximately 1,442 ft-kips acting in the direction of increasing deflection. It should be noted that after a certain deflection (1.912 ft in the case of building 3.3.3), the resisting moment to deflection remains constant as explained in Section E.9.6. Since the overturning moment acts against the resisting moment and increases with deflection, the net moment tending to collapse the building also increases with the deflection after the resisting moment becomes constant. This instability will carry the building to complete structural collapse. Furthermore, the equivalent building mass has a velocity in the direction

of increasing deflection, even after the applied load goes to zero. This velocity will serve only to add to the already unstable condition.

The foregoing remarks are justification for the original assumption made that the building would be unable to sustain the entire blast load and would fail even when subjected to the horizontal forces alone due to blast. It should be noted that if the analysis indicated that the building would not collapse under the aforementioned loading conditions it would then be necessary to include the effects of the vertical forces resulting from the blast in order to get a complete analysis of the dynamic response.

TABLE E.9.4

Horizontal Loads on Building 3.3.3

Time t (sec)	Force on Trusswork (10³ lb)	Force on Frame from Front Wall (10³ lb)	Force on Frame from Back Wall (10³ lb)	N(t) (10³ lb)
0.000	0	0	0	0
0.006	6.819	21	0	28
0.012	13.638	62	0	75
0.018	20.457	140	0	160
0.024	27.276	243	0	270
0.030	34.095	430	0	465
0.036	40.914	516	0	557
0.042	47.733	586	0	632
0.048	54.552	646	0	695
0.054	61.371	690	0	750
0.060	68.19	731	0	800
0.066	75.009	760	0	835
0.072	81.828	760	0	840
0.078	88.647	730	0	820
0.084	95.466	700	0	795
0.090	102.385	650	0	750
0.096	109.204	600	0	710
0.102	116.023	545	0	660
0.108	122.842	440	0	565
0.114	129.661	340	0	470
0.120	136.48	240	0	375
0.126	143.299	140	0	280
0.132	150	70	0	220

TABLE E.9.4 (CONTD)

Horisontal Loads on Building 3.3.3

Time t (sec)	Force on Trusswork (10^3 lb)	Force on Frame From Front Wall (10^3 lb)	Force on Frame From Back Wall (10^3 lb)	H(t) (10^3 lb)
0.138	157	70	0	227
0.144	164	70	0	234
0.150	170	70	0	240
0.156	177	70	0	247
0.162	184	70	0	254
0.168	191	70	0	261
0.174	198	70	0	268
0.180	205	70	0	275
0.186	212	70	0	288
0.198	225	60	0	285
0.204	221.694	60	19	301
0.210	218.4	60	86	364
0.216	215.116	60	201	476
0.222	211.822	60	272	544
0.228	208.528	60	337	606
0.234	205.234	60	397	662
0.240	201.940	60	447	709
0.246	198.646	60	488	747
0.252	195.352	60	518	773
0.258	192.058	60	536	788
0.264	188.764	60	545	794
0.270	185.470	60	544	789
0.276	182.176	60	531	773
0.282	178.882	60	502	741
0.288	175.588	60	459	695

ARMOUR RESEARCH FOUNDATION OF ILLINOIS INSTITUTE OF TECHNOLOGY

TABLE E.9.4 (CONTD)

Horizontal Loads on Building 3.3.3

Time t (sec)	Force on Trusswork (10³ lb)	Force on Frame From Front Wall (10³ lb)	Force on Frame From Back Wall (10³ lb)	H(t) (10³ lb)
0.294	172.294	60	412	644
0.300	169	45	355	569
0.306	166.43	45	287	498
0.312	164.16	45	218	427
0.318	161.79	45	148	355
0.324	159.42	45	97	301
0.330	157.05	45	86	288
0.336	154.78	45	85	285
0.342	152.41	45	83	280
0.348	150.04	45	82	277
0.354	147.67	45	81	274
0.360	145.3	45	80	270
0.372	140.6	45	77	263
0.384	135.8	45	75	256
0.396	131.1	39	72	242
0.408	126.3	37	70	233
0.420	121.6	36	68	226
0.432	116.9	35	66	218
0.444	112.1	34	64	210
0.456	107.4	33	62	202
0.468	102.6	32	60	195
0.480	97.9	30	58	186
0.492	93.2	29	56	178
0.504	89	28	54	171
0.516	86	27	52	165

TABLE E.9.4 (CONTD)

Horizontal Loads on Building 3.3.3

Time t (sec)	Force on Trusswork (10^3 lb)	Force on Frame From Front Wall (10^3 lb)	Force on Frame From Back Wall (10^3 lb)	H(t) (10^3 lb)
0.528	84	26	50	160
0.540	81	25	48	154
0.552	78	24	46	148
0.564	76	22	44	142
0.576	73	21	42	136
0.588	70	20	40	130
0.600	68	19	38	125
0.624	62	18	36	116
0.648	57	17	33	107
0.672	51	16	31	98
0.696	46	14	29	89
0.720	43	13	27	83
0.744	40	12	24	76
0.768	37	11	22	70
0.792	35	10	20	65
0.840	29	9	17	55
0.888	24	7	15	46
0.936	21	6	13	40
0.984	18	5	10	33
1.032	15	4	9	28
1.080	12	4	8	24
1.128	11	3	6	20
1.176	10	3	5	18
1.224	9	2	4	15

TABLE E.9.4 (CONTD)

Horizontal Loads on Building 3.3.3

Time t (sec)	Force on Trusswork (10^3 lb)	Force on Frame From Front Wall (10^3 lb)	Force on Frame From Back Wall (10^3 lb)	H(t) (10^3 lb)
1.272	8	2	4	14
1.320	7	1	3	11
1.368	6	1	3	10
1.416	4	-0.045	2	6
1.464	3	0	2	5
1.512	2	0	1	3
1.560	1	0	1	2
1.608	0.3	0	0.1	0.4

TABLE E.9.5

Numerical Integration of Response Equation

t (sec)	H(t) (10³ lb)	R[x(t)] (10³ lb)	ẍ (ft/sec²)	ẋ (ft/sec)	η* (10³ ft)	x (10³ ft)
0.000	0	0	0	0	0	0
0.003	13	0	0.588	0.00088	0	0
0.006	28	0.001	1.267	0.00116	0.007	0.007
0.012	75	0.008	3.393	0.01514	0.061	0.061
0.018	160	0.028	7.239	0.04674	0.193	0.214
0.024	270	0.088	12.213	0.10510	0.429	0.672
0.030	465	0.201	21.032	0.20484	0.760	1.535
0.036	557	0.424	25.184	0.34349	1.303	3.236
0.042	632	0.747	28.563	0.50473	1.714	5.707
0.048	695	1.222	31.393	0.68460	1.975	9.333
0.054	750	1.827	33.854	0.88034	2.192	13.956
0.060	800	2.608	36.081	1.0901	2.378	19.926
0.066	835	3.542	37.623	1.3112	2.544	27.064
0.072	840	4.670	37.798	1.5375	2.672	35.679
0.078	820	5.957	36.835	1.7614	2.717	45.515
0.084	795	7.435	35.636	1.9788	2.675	56.804
0.090	750	9.063	33.527	2.1863	2.595	69.247
0.096	710	10.866	31.635	2.3818	2.465	83.015
0.102	660	12.801	29.285	2.5646	2.323	97.806
0.108	565	14.890	24.892	2.7271	2.165	113.762
0.114	470	17.078	20.494	2.8633	1.898	130.479

* η represents the numerical evaluation of the term

$$\frac{h}{3}\left[2h\,\ddot{x}(t) + 4h\,\ddot{x}(t+h)\right]$$

in the response equation.

TABLE E.9.5 (CONTD)

Numerical Integration of Response Equation

t (sec)	H(t) (10³lb)	R x(t) (10³ lb)	$\ddot{x}$ (ft/sec²)	$\dot{x}$ (ft/sec)	η (10⁻³ ft)	x (10³ ft)
0.120	375	19.380	16.091	2.9731	1.581	148.068
0.126	280	21.741	11.686	3.0564	1.264	166.103
0.132	220	24.174	8.861	3.1180	0.947	184.692
0.138	227	26.634	9.066	3.1718	0.706	203.486
0.144	234	29.156	9.269	3.2268	0.648	222.756
0.150	240	31.702	9.425	3.2829	0.662	242.210
0.156	247	34.312	9.624	3.3400	0.675	262.153
0.162	254	36.948	9.821	3.3983	0.688	282.293
0.168	261	39.650	10.016	3.4578	0.702	302.935
0.174	268	42.380	10.209	3.5185	0.716	323.789
0.180	275	45.177	10.399	3.5803	0.730	345.159
0.186	282	48.003	10.588	3.6433	0.744	366.755
0.192	288	50.899	10.729	3.7073	0.758	388.881
0.198	285	53,826	10.460	3.7709	0.769	411.244
0.204	301	56.821	11.049	3.8354	0.760	434.129
0.210	364	59.851	13.762	3.9098	0.781	457.276
0.216	476	62.967	18.689	4.0072	0.926	481.080
0.222	544	66.153	21.622	4.1281	1.227	505.421
0.228	606	69.455	24.278	4.2658	1.486	530.652
0.234	662	72.857	26.658	4.4186	1.684	556.642
0.240	709	76.399	28.624	4.5844	1.862	583.704
0.246	747	80.060	30.178	4.7608	2.015	611.680
0.252	773	83,879	31.182	4.9449	2.136	640.853
0.258	788	87.829	31.682	5.1335	2.221	671.031
0.264	794	91.942	31.767	5.3238	2.269	702.461
0.270	789	96.191	31.349	5.5131	2.285	734.918

TABLE E.9.5 (CONTD)

Numerical Integration of Response Equation

t (sec)	H(t) (10^3 lb)	R x(t) (10^3 lb)	$\ddot{x}$ (ft/sec^2)	$\dot{x}$ (ft/sec)	η (10^3 ft)	x (10^3 ft)
0.276	773	100.601	30.425	5.6984	2.267	768.614
0.282	741	105.139	28.772	5.8760	2.213	803.288
0.288	695	109.827	26.478	6.0418	2.111	839.106
0.294	644	114.625	23.954	6.1931	1.961	875.761
0.300	569	119.551	20.337	6.3260	1.785	913.393
0.306	498	120.960	17.061	6.4382	1.551	951.629
0.312	427	122.338	13.786	6.5307	1.307	990.612
0.318	355	123.729	10.465	6.6035	1.071	1,029.958
0.324	301	125.139	7.958	6.6588	0.833	1,069.813
0.330	288	126.554	7.305	6.7046	0.633	1,109.833
0.336	285	127.983	7.105	6.7478	0.542	1,150.261
0.348	277	130.864	6.612	6.8299	0.498	1,231.733
0.360	270	133.779	6.164	6.9066	1.952	1,314.16
0.372	263	136,725	5.714	6.9779	1.818	1,397.47
0.384	256	139.700	5.262	7.0438	1.689	1,481.61
0.396	242	142,701	4.493	7.1023	1.559	1,566.5
0.408	233	145.725	3.949	7.1530	1.368	1,652
0.420	226	148.766	3.495	7.198	1.19	1,738
0.432	218	150.293	3.064	7.237	1.05	1,825
0.444	210	150.34	2.700	7.273	0.932	1,912
0.456	202	150.34	2.338	7.303	0.817	2,000
0.468	195	150.34	2.021	7.329	0.708	2,087
0.480	186	150.34	1.614	7.351	0.612	2,176
0.492	178	150.34	1.252	7.368	0.504	2,263
0.504	171	150.34	0.935	7.381	0.395	2,353
0.516	165	150.34	0.663	7.391	0.3	2,440

TABLE E.9.5 (CONTD)

Numerical Integration of Response Equation

t (sec)	H(t) $(10^3$ lb)	R x(t) $(10^3$ lb)	$\ddot{x}$ (ft/sec^2)	$\dot{x}$ (ft/sec)	η $(10^3$ ft)	x $(10^3$ ft)
0.528	160	150.34	0.437	7.398	0.217	2,530
0.540	154	150.34	0.166	7.402	0.148	2,618
0.552	148	150.34	-0.106	7.402	0.074	2,708
0.564	142	150.34	-0.377	7.400	-0.004	2,796
0.576	136	150.34	-0.649	7.394	-0.046	2,886
0.588	130	150.34	-0.920	7.385	-0.098	2,974
0.600	125	150.34	-1.147	7.373	-0.151	3,063
0.624	116	150.34	-1.554	7.341	-1.13	3,240
0.648	107	150.34	-1.961	7.299	-1.634	3,415
0.672	98	150.34	-2.368	7.247	-2.103	3,590
0.696	89	150.34	-2.776	7.185	-2.572	3,763
0.720	83	150.34	-3.047	7.115	-3.041	3,935
0.744	76	150.34	-3.364	7.035	-3.406	4,104
0.768	70	150.34	-3.635	6.951	-3.754	4,273
0.792	65	150.34	-3.862	6.861	-4.083	4,438
0.840	55	150.34	-4.314	6.665	-17.031	4,762
0.888	46	150.34	-4.721	6.448	-19.185	5,077
0.936	40	150.34	-4.993	6.215	-21.129	5,381
0.984	33	150.34	-5.310	5.968	-22.59	5,673
1.032	28	150.34	-5.536	5.708	-23.982	5,954
1.080	24	150.34	-5.717	5.438	-25.163	6,221
1.128	20	150.34	-5.898	5.158	-26.066	6,476
1.176	18	150.34	-5.988	4.868	-26.9	6,716
1.224	15	150.340	-6.124	4.578	-27.454	6,944
1.272	14	150.34	-6.169	4.278	-28.01	7,155

TABLE E.9.5 (CONTD)

Numerical Integration of Response Equation

t (sec)	H(t) (10^3 lb)	R x(t) (10^3 lb)	$\ddot{x}$ (ft/sec^2)	$\dot{x}$ (ft/sec)	η (10^3 ft)	x (10^3 ft)
1.320	11	150.34	-6.305	3.978	-28.358	7,355
1.368	10	150.34	-6.350	3.678	-28.845	7,537
1.416	6	150.34	-6.531	3.368	-29.192	7,708
1.464	5	150.34	-6.576	3.058	-29.817	7,860
1.512	3	150.34	-6.667	2.738	-30.233	8,001
1.560	2	150.34	-6.712	2.418	-30.582	8,123
1.608	0.04	150.34	-6.785	2.098	-30.860	8,233
1.618	0	150.34	-6.803	1.772	-31.208	8,324

Chapter E. 10

BUILDING 3.3.8h

This structure represents a one-quarter scale model of building 3.3.3 discussed and analyzed in Chapter E.9. The scaling was accomplished, however, along geometrical lines only, and it should be noted here that this method will not scale the dynamic response of the structure, which requires dimensional scaling of all parameters. Detailed information may be obtained from the Air Force construction drawings.[1]

Since this model structure is geometrically similar in every respect to the prototype, building 3.3.3, the predicted evaluation of its behavior proceeds along lines which are identical to those described in detail in Chapter E.9. Since this chapter represents essentially a repetition of previous work, only the final numerical results of the computations and their physical significance will be discussed below.

Using the same idealized mathematical model as before, the analysis leads to the following equation of motion in the horizontal direction:

$$m \, l \, \ddot{\theta} - \left[mg + V(t) \right] \, \theta = H(t) - Q(\theta) \qquad (E.10.1)$$

---

[1] See Drawing No. 100-252-1, Dept. of Air Force, Hq. AMC, Office of Air Installation, Wright-Patterson Air Force Base, Dayton, Ohio

TABLE E.9.5 (CONTD)

Numerical Integration of Response Equation

t (sec)	H(t) (10³ lb)	R x(t) (10³ lb)	$\ddot{x}$ (ft/sec²)	$\dot{x}$ (ft/sec)	η (10³ ft)	z (10³ ft)
1.320	11	150.34	-6.305	3.978	-28.358	7,355
1.368	10	150.34	-6.350	3.678	-28.845	7,537
1.416	6	150.34	-6.531	3.368	-29.192	7,708
1.464	5	150.34	-6.576	3.058	-29.817	7,860
1.512	3	150.34	-6.667	2.738	-30.233	8,001
1.560	2	150.34	-6.712	2.418	-30.582	8,123
1.608	0.04	150.34	-6.785	2.098	-30.860	8,233
1.618	0	150.34	-6.803	1.772	-31.208	8,324

Chapter E. 10

BUILDING 3.3.8h

This structure represents a one-quarter scale model of building 3.3.3 discussed and analyzed in Chapter E.9. The scaling was accomplished, however, along geometrical lines only, and it should be noted here that this method will not scale the dynamic response of the structure, which requires dimensional scaling of all parameters. Detailed information may be obtained from the Air Force construction drawings.[1]

Since this model structure is geometrically similar in every respect to the prototype, building 3.3.3, the predicted evaluation of its behavior proceeds along lines which are identical to those described in detail in Chapter E.9. Since this chapter represents essentially a repetition of previous work, only the final numerical results of the computations and their physical significance will be discussed below.

Using the same idealized mathematical model as before, the analysis leads to the following equation of motion in the horizontal direction:

$$m \ell \ddot{\theta} - \left[mg + V(t) \right] \theta = H(t) - Q(\theta) \qquad (E.10.1)$$

---

[1] See Drawing No. 100-252-1, Dept. of Air Force, Hq. AMC, Office of Air Installation, Wright-Patterson Air Force Base, Dayton, Ohio

where

m = equivalent moving mass

ℓ = effective length of the building columns

$\ell\theta$ = horizontal displacement at the roof level

H(t) = time-dependent horizontal force

V(t) = time-dependent vertical force

Q(θ) = shear resistance of structure to deformation

This equation is identical in structure to Eq. E.8.30 derived in Vol II of this appendix for the purpose of predicting the response of the model structures.

Detailed calculations recorded in Project Logbook No. C1646 show that the numerical parameters are as follows:

m = 709 lb-sec^2/ft

ℓ = 89 in.

g = 32.2 ft/sec^2

and the functions V(t), H(t), and Q(θ) are shown in graphical form in Figs. E.10.1 - E.10.3.

Substituting the above values into the differential equation, E.10.1, one obtains

$$\ddot{\theta} - \left[4.29 + \frac{V(t)}{5250}\right]\theta = \frac{H(t)}{5250} - \frac{Q(\theta)}{5250}$$

The integration of this equation proceeds along numerical lines shown in detail in Vol II, Table E.9.3. The results of the numerical integration of the above equation are shown as accelerations in Fig. E.10.4 and as displacements in Fig. E.10.5.

The above results indicate that building 3.3.8h will suffer severe structural damage, if not total collapse, along with its prototype, building 3.3.3.
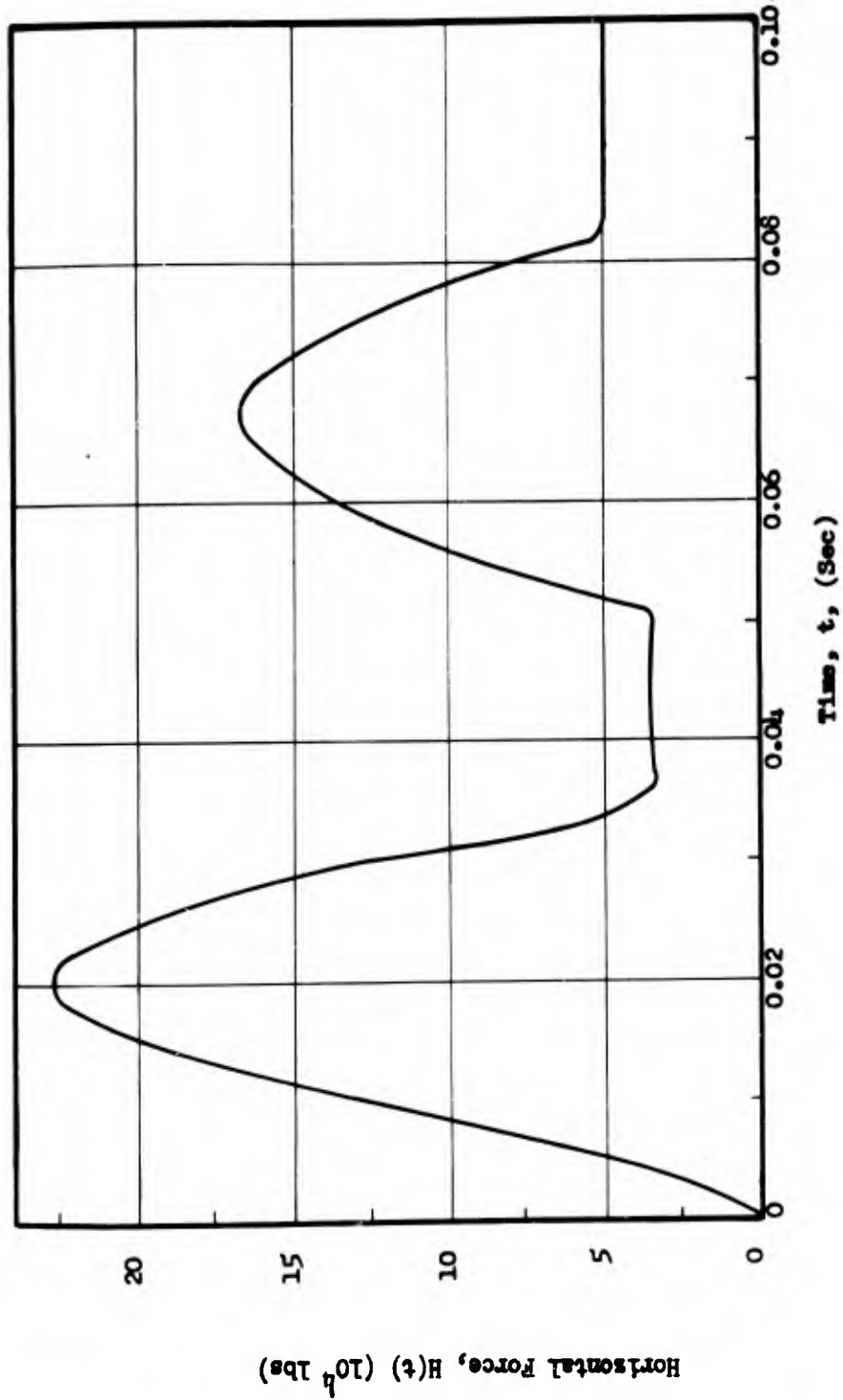
Fig. E.10.1 Horizontal Force on Building 3.3.8n (Note: For $0.1 \leq t \leq 1.5$, H decreases almost linearly. $(0 \leq t \leq 0.1)$. H(t) from analytical data)
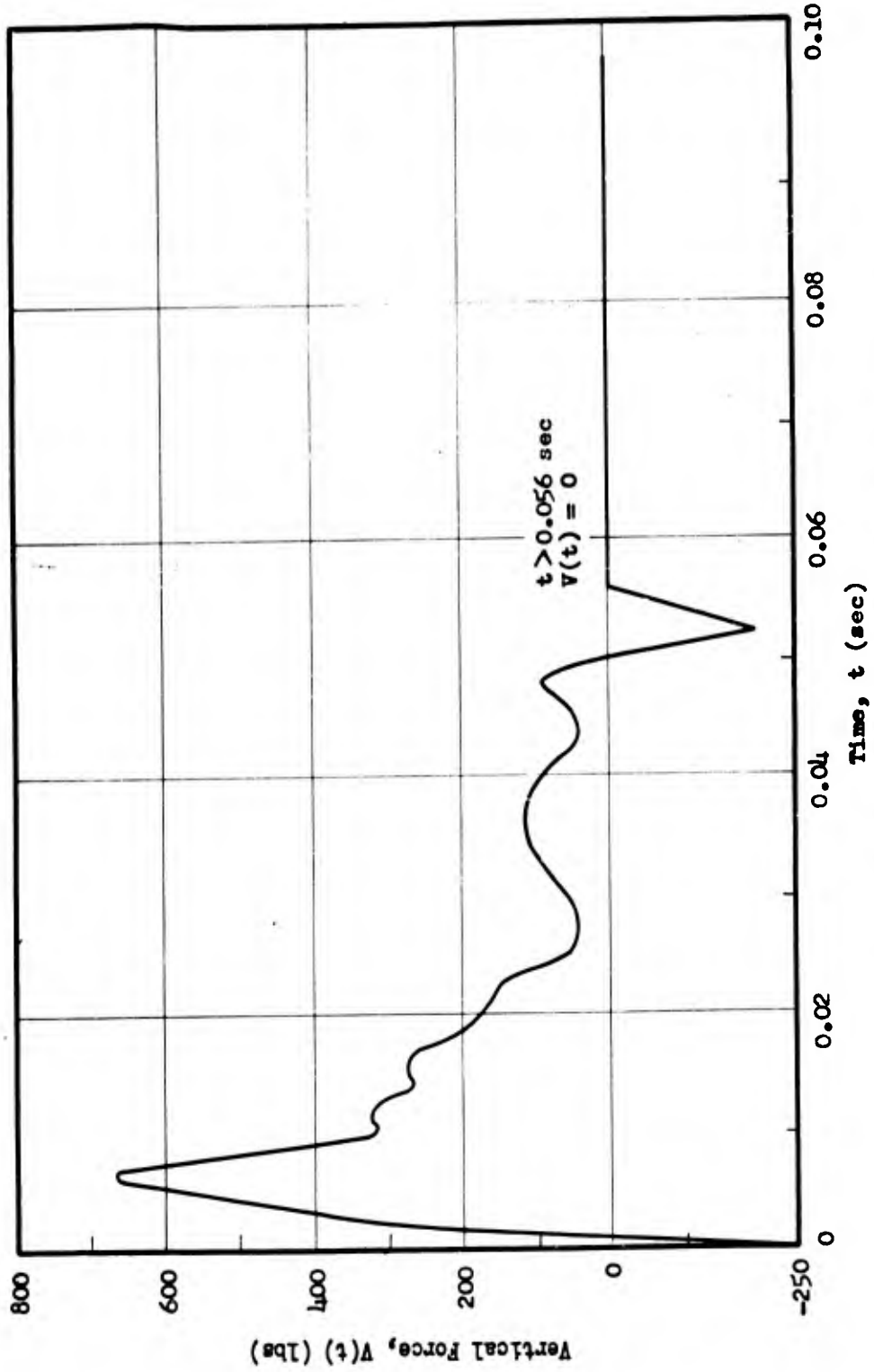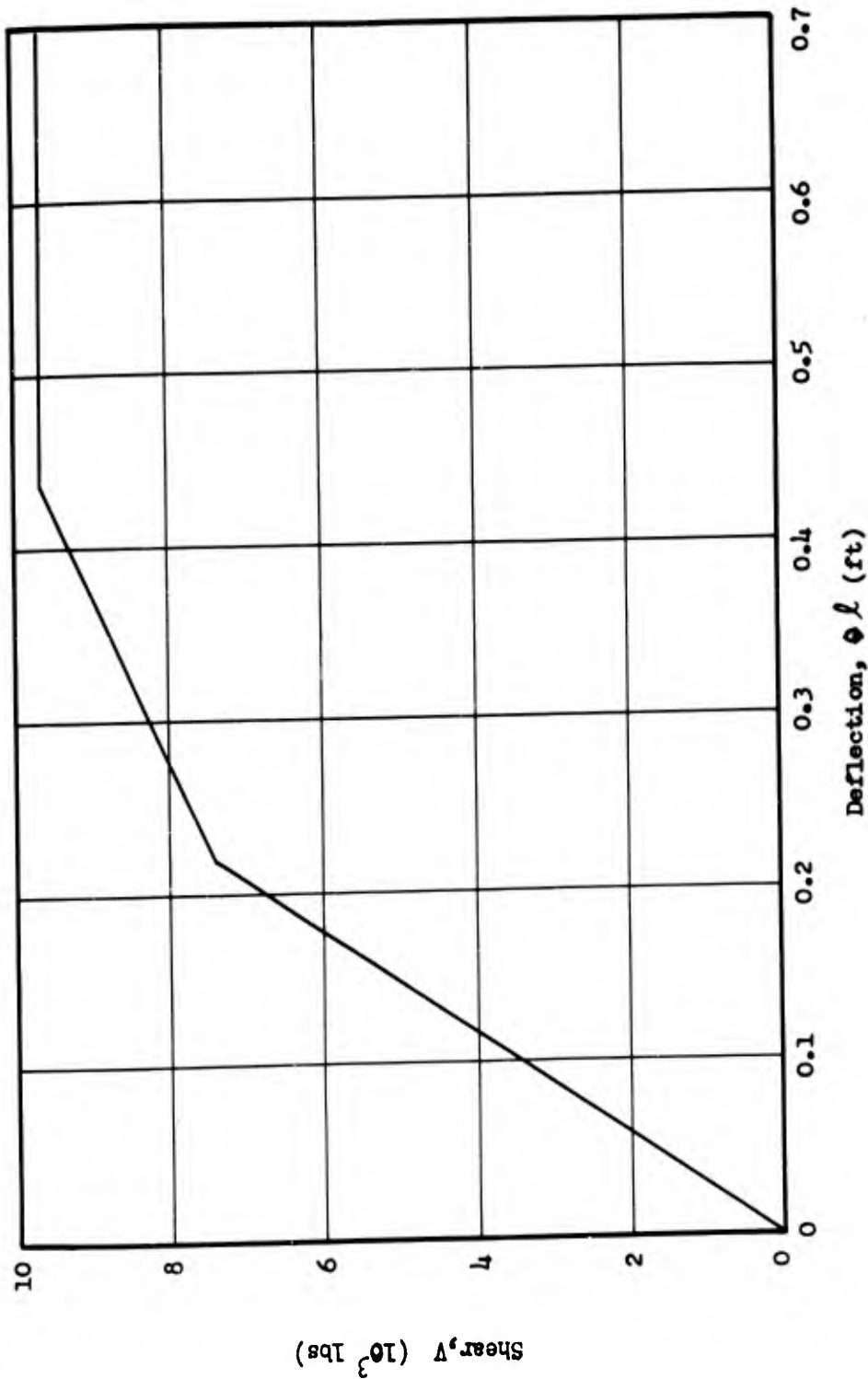
Fig. E.10.2 Vertical Force on Building 3.3.8h

Fig. E.10.3 Resistance of Building 3.3.8h
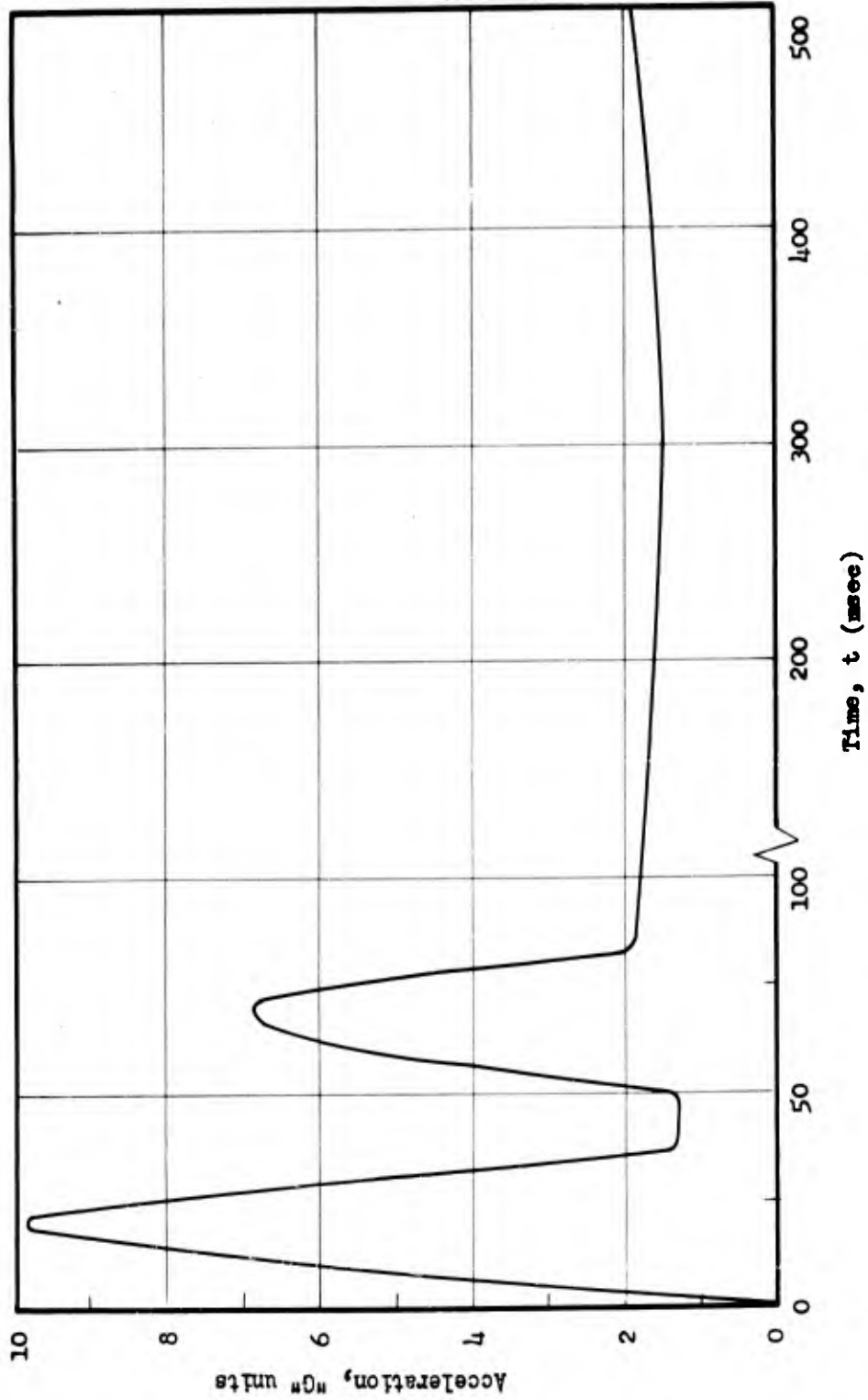
Fig. E.10.4   Acceleration on Building 3.3.8h

Time, t (Milliseconds)
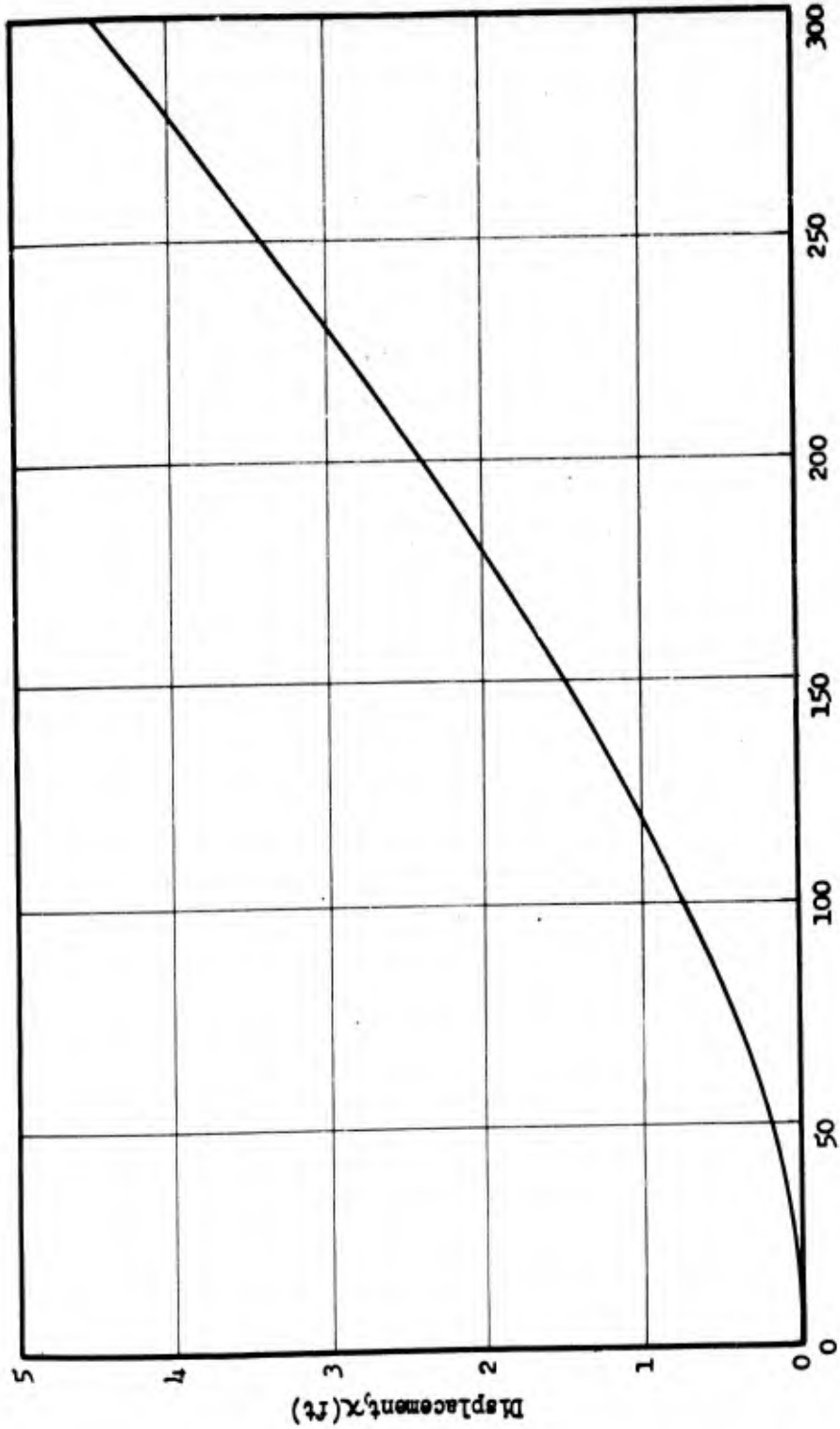
Fig. B.10.5 Displacement of Building 3.3.8h

CHAPTER E.11

BUILDING 3.3.4

E.11.1   DESCRIPTION OF STRUCTURE

Building 3.3.4 is a single-story, industrial type, reinforced concrete structure three bays wide and four bays long. The general dimensions of the building and the details of construction are as shown in Figs. E.11.1 and E.11.2.

The basic structural frame of the building consists of eight 2-column bents and four T-shaped beam and column sections. These are arranged in four rows consisting of two bents flanking a T-shaped member. The connecting beams of the two column bents extend from the outside wall, and cantilever over the inside column to the edge of the monitor. The beam portion of the T-shaped member supports the inner edges of the monitors.

The bents in the outside rows are connected by precast concrete struts along lines a-a and b-b in Fig. E.11.1b. These struts are essentially pin-connected to the beams at points a and b. All of the beams and columns are monolithically precast. The lower ends of the columns fit into sockets provided in the individual footings. The connection is completed by filling the annular space between the column and footing with a sand-cement grout.

The front and rear walls are made of four-course standard brick masonry with a number of doors and windows. Three courses of brick are

placed between the columns. The fourth course extends outside the face of the columns to present the appearance of a uniform masonry wall. The other two sides of the building are open.

The roof is a laminated deck made of 2-by-6-in. boards laid on edge and nailed to each other and to a nailing strip bolted to the top of the concrete beams. The span between bents is 18 ft 8 in. and every other laminate is spliced at the center line of the bents to provide uniform stiffness at the supports and at the center of the span. This continuous deck is broken by two lines of monitors extending the width of the building. One monitor is located in each of the two center bays of the four bays forming the length of the building. The monitors have sloping glass sides and a wooden roof. The structural framing of the monitors consists of eight steel trusses which are spaced at one-third of the column spacing.

E.11.2 ASSUMPTIONS OF STRUCTURAL ACTION AND METHOD OF ANALYSIS

In order to simplify the dynamic analysis of the building, several assumptions have been made regarding the mass and stiffness of the various components of the structure. The assumptions concerning the amount of the structure displaced and the rigidity of the displaced portions will be discussed in this section. In addition, the methods of analysis will be briefly outlined.

The mass which will be moved under the action of the forces consists primarily of the roof and monitors. However, if it is assumed that the walls and columns are, in effect, rotated about their bases, a
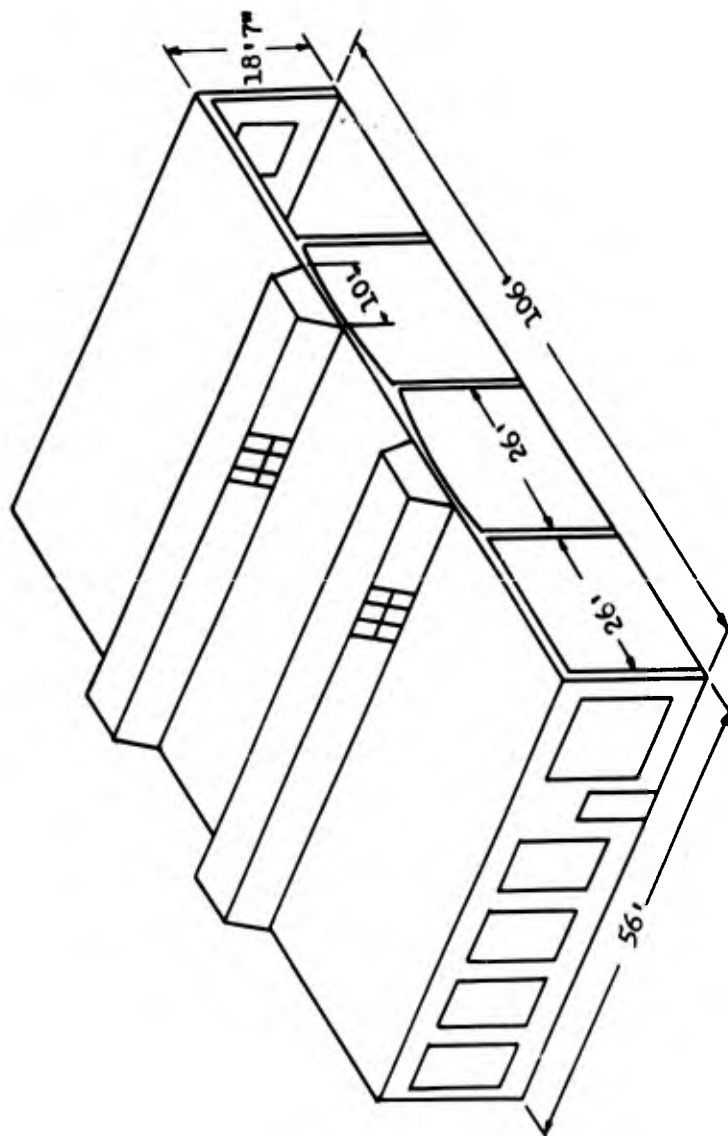
Fig. E.11.1a   Building 3.3.4
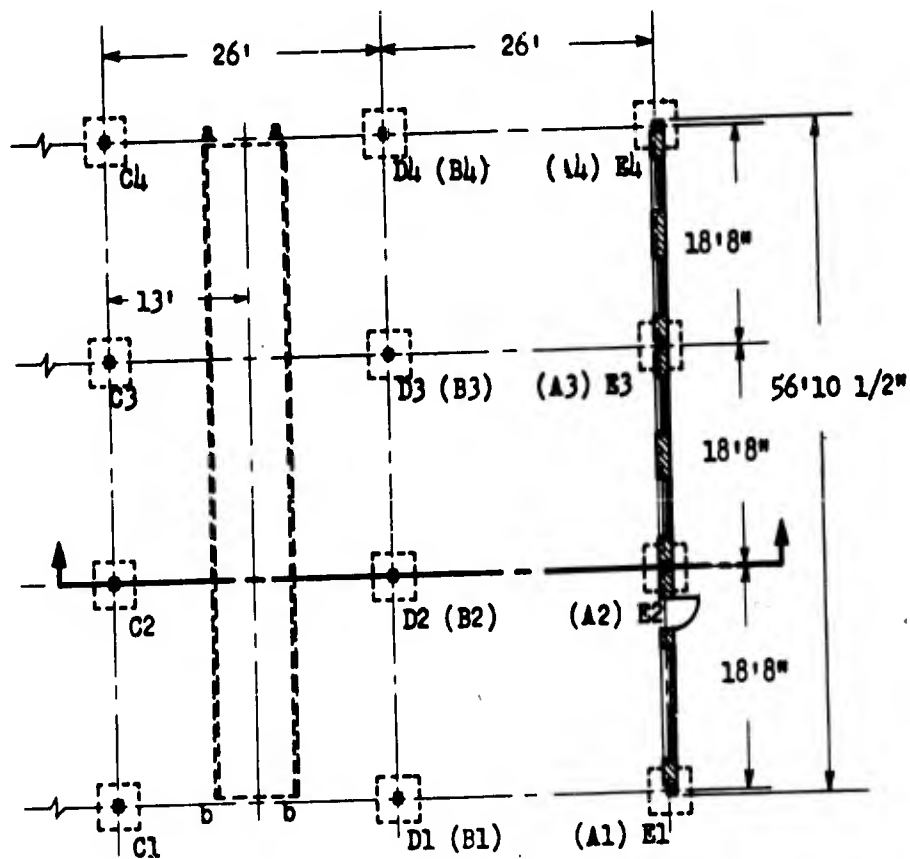
Fig. E.11.1b   Column Location and Footing Plan of Building
3.3.4 (Overall Dimensions: 56'10 1/2" x 106')
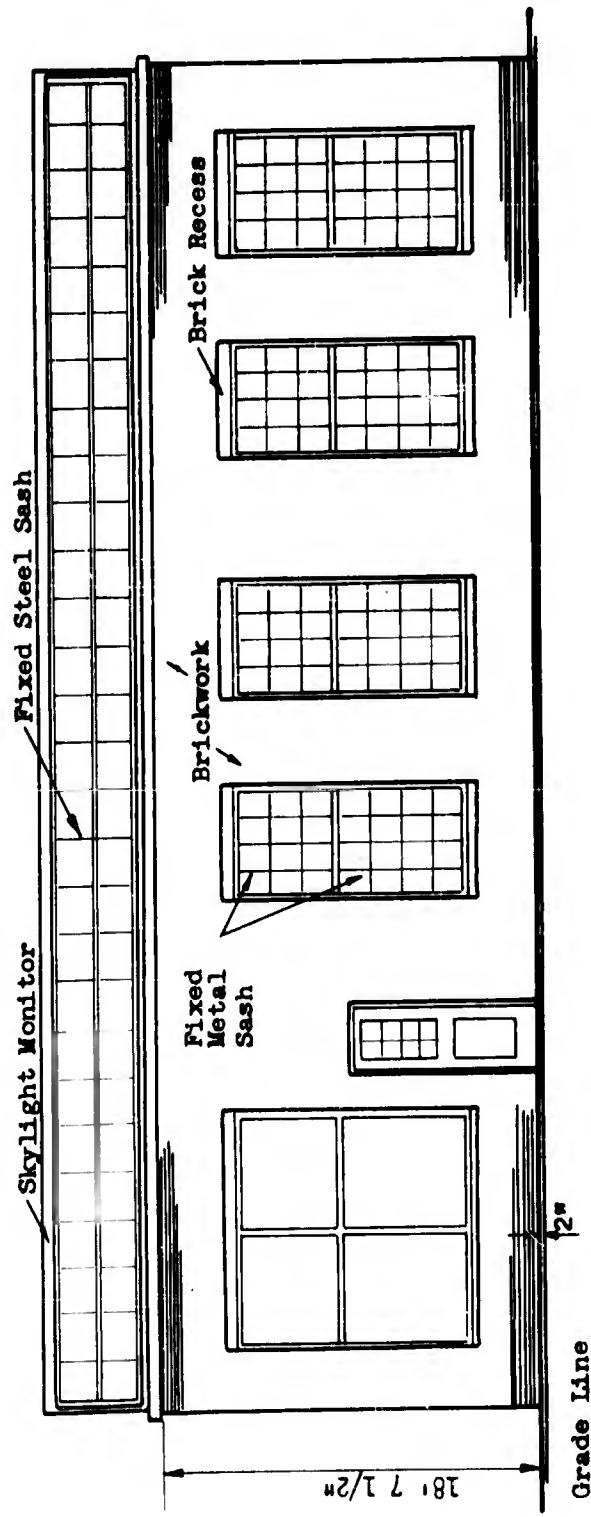
Fig. E.11.2a   End Elevation of Building 3.3.4
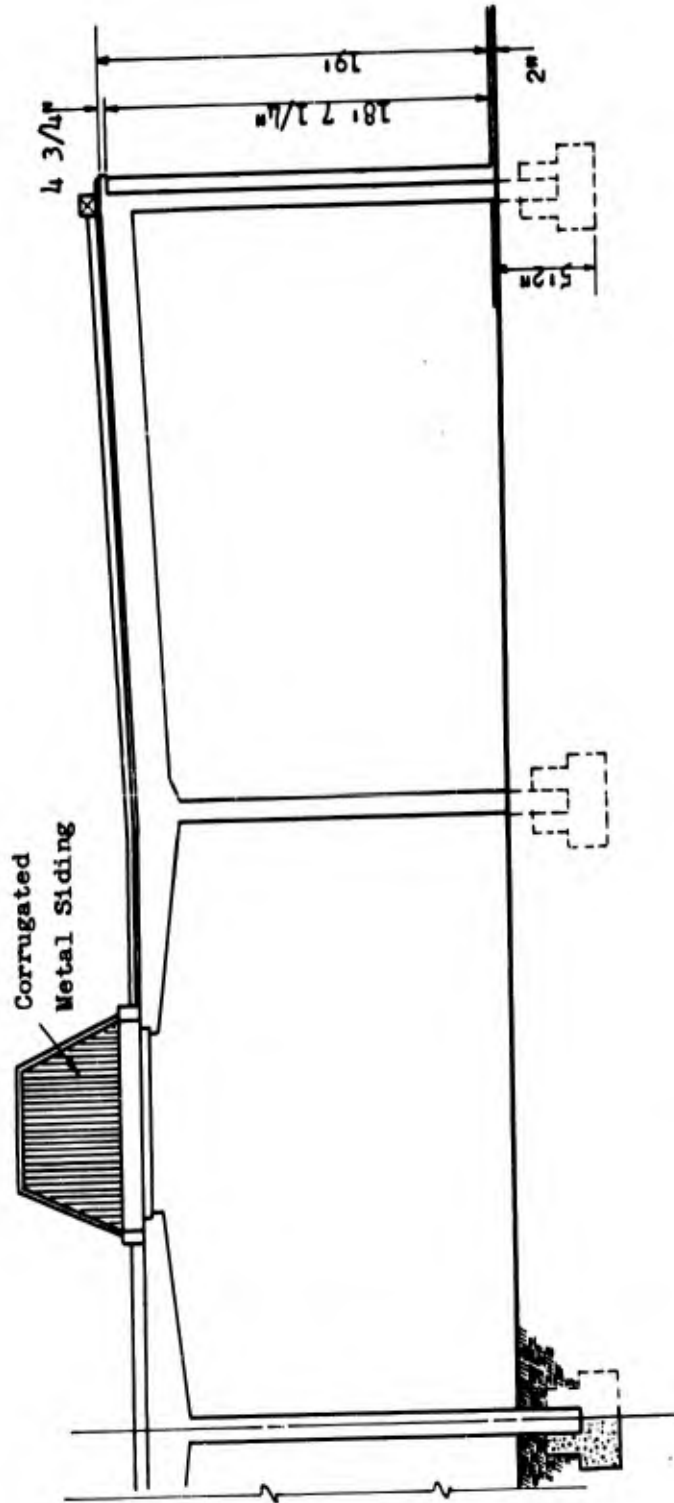
Fig. B.11.2b   Half Elevation of Building 3.3.4

portion of their mass may be considered to move with the roof. In order to take this into account, one-third of the mass of the walls and columns is taken as concentrated at the level of the roof mass. Thus the structure as a whole has been considered as a single mass on a set of elastic-plastic columns subjected to a lateral time-dependent force.

It is further assumed that the mass is rigid in the plane of the roof. That is, the horizontal displacement of all points in the mass are equal. In particular, the deflections of the upper ends of all the columns, in the direction of the forces, are assumed equal at any given time.

It should be emphasized that the roof is considered rigid only in its own plane and not in directions normal to this plane. On this supposition a number of assumptions regarding the action of the structure under the applied lateral loads have been made to substantiate this viewpoint.

From a study of Figs. E.11.1b and E.11.2b it should be apparent that the bents along column lines 1 and 4 have greater stiffness than the interior bents, due to the fact that they are connected by struts, whereas the interior bents are not. Therefore, for equal applied loads the deflection of the interior columns would be greater. For the assumption of equal column deflections to be valid there must be some transfer of loads through the deck to the exterior bents. To visualize this, imagine that the light construction of the trusses in the monitors make them unsuitable for the transfer of substantial loads across the openings; then the roof deck from the forward edge of the building to

the edge of the first monitor must act as a horizontal beam spanning between column lines 1 and 4. For the deck to act in this manner, it must have bending stiffness and adequate shear connections to the concrete beams.

Since the 2-by-6-in. boards forming the laminated deck are nailed to each other at reasonably close intervals, and the splices of individual pieces are staggered, the roof most certainly has a great deal of rigidity in the horizontal plane. The 2-by-6 boards are toe-nailed to nailing strips which are bolted to the top of the beams. The transfer of loads between the concrete bents and the roof deck will in all probabilty be limited by these connections. Their adequacy has not been investigated, but it seems reasonable to assume that as long as the roof remains in place, failure of this connection is remote.

To determine the resistance of the structure to sidesway, certain assumptions have been made concerning the structural integrity of the columns and their interaction with the connecting beams and footings. The ratio of the stiffness of the beams to the stiffness of the columns is relatively high, which was taken as justification for the simplifying assumption that the columns are fixed against rotation at the top. A more refined analysis may be used if it seems justified by future results

It should be noted that while the upper ends of the columns in Rows A, B, D, and E may be considered as fixed, this is not true for the columns in Row C. The upper ends of these columns are free to rotate since the monitors are, in effect, pin-connected along the lines a-b

(Fig. E.11.1b). A study of the cross section in Fig. E.11.2b will make this evident.

The lower ends of all the columns are assumed to be fixed. Whether or not this view is justified depends on the mass of the footings and the soil conditions at the building site. It is believed that the connections of the columns to the footings are adequate to develop the full resistance of the columns in bending and shear. Also, realizing that a completely fixed end condition is impossible, and that some rotation of the footings would occur, it seemed reasonable that a fixed end would more nearly approximate the true condition than any other rational assumption.

Figure E.11.4 shows both types of columns in the deflected position based on the above assumptions. It is apparent that for the columns fixed at both ends the maximum moment will occur at both ends simultaneously, if the cross section is symmetrical. For the column that is free at the top the maximum moment occurs at the base. In either case the moment is a function of the horizontal displacement. In order to evaluate this displacement the properties of the columns must be known and the bending resistance must be determined.

In addition to the bending moments and shears resulting from lateral loads, the columns are subjected to direct stresses due to the dead load of the roof and external forces applied to the roof. These axial stresses have been neglected in determining the resistance of the columns in the belief that their effect would be negligible. This allows considerable simplification in computing the section properties

of the columns, since for reinforced-concrete sections the position of the neutral axis of the cross section depends on the magnitude of the axial loads and the bending moment. If the axial stresses had not been neglected, the calculations would have been considerably complicated, with very little justification for the refinement.

The section properties of the reinforced concrete columns have been computed by the transformed area method, i. e., by replacing the steel by an "equivalent" concrete. The specifications require a concrete having an ultimate strength of 3000 psi at 28 days. For this strength concrete the modulus of elasticity has been taken as 3×10^6 psi. Intermediate grade, new-billet steel reinforcing bars are used; these have a minimum yield point of 40,000 psi and an ultimate strength of 70,000-90,000 psi. A modulus of elasticity equal to 30×10^6 psi has been used for the steel.

Consistent with standard reinforced-concrete design practice, the tensile strength of the concrete has been assumed as zero, i. e., the tensile stresses in the columns are resisted only by the steel. In order to simplify the computations, an idealized stress-strain curve has been assumed for the reinforcing steel. This consists of a straight line relationship up to the yield point stress and then a constant stress for all strains greater than the strain at the yield point. Since it is assumed that the concrete stresses will not be excessive and that the resisting moment of the section will depend entirely upon the stresses in the steel, the resistance of the columns follow the same stress-strain relationship.

ARMOUR RESEARCH FOUNDATION OF ILLINOIS INSTITUTE OF TECHNOLOGY

During the initial part of the motion of the structure, the columns will act elastically and the moment in the columns will be directly proportional to the deflection until the stress in the steel reaches the yield point. At this stage plastic hinges will occur at the points of maximum moment and the columns will offer a constant resistance to further deformation. This relationship is shown graphically in Fig. E.11.5.

Because all of the columns in the structure are not of the same size and stiffness, it is obvious that for a given deflection, different moments will occur in the various columns. Some of the columns will reach the yield point stress earlier than others and in order to determine the total resistance of the structure to sidesway it is necessary to add the individual resistances through the whole range of deflections until all columns are plastic. This has been done and the results are plotted in Fig. E.11.3 as a shear-deflection curve for the entire structure. The shear was obtained by dividing the sum of the end moments by the length of the column.

The adequacy of the columns to resist shearing stresses was not investigated.

The structural parameters having been evaluated and the time-dependent forcing function being known, it is possible to write the differential equation of motion of the equivalent structure. This equation is of the form

$$M\ddot{x} = H(t) - R(x) \tag{E.11.1}$$

where

M = mass of the structure, $\text{lb·sec}^2/\text{ft}$
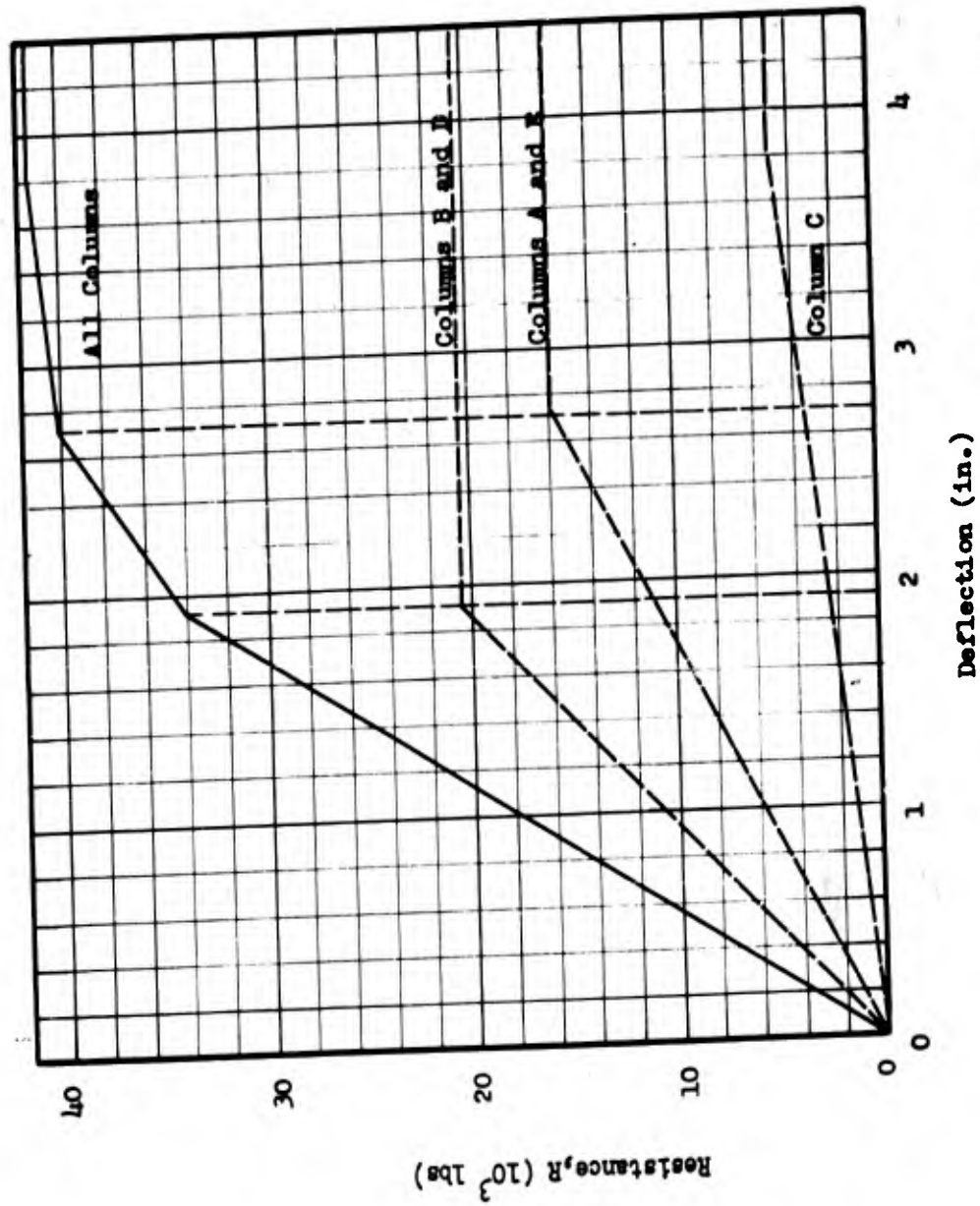
Fig. E.11.3   Shear-Deflection Curve of Columns of Building 3.3.4
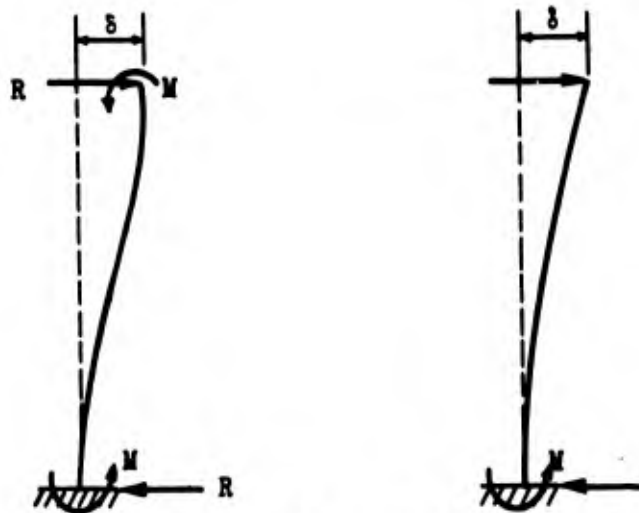
Columns in Rows A,B,D and E
(a)

Columns in Row C
(b)

Fig. E.11.4   Column Deflection Curves of Building 3.3.4
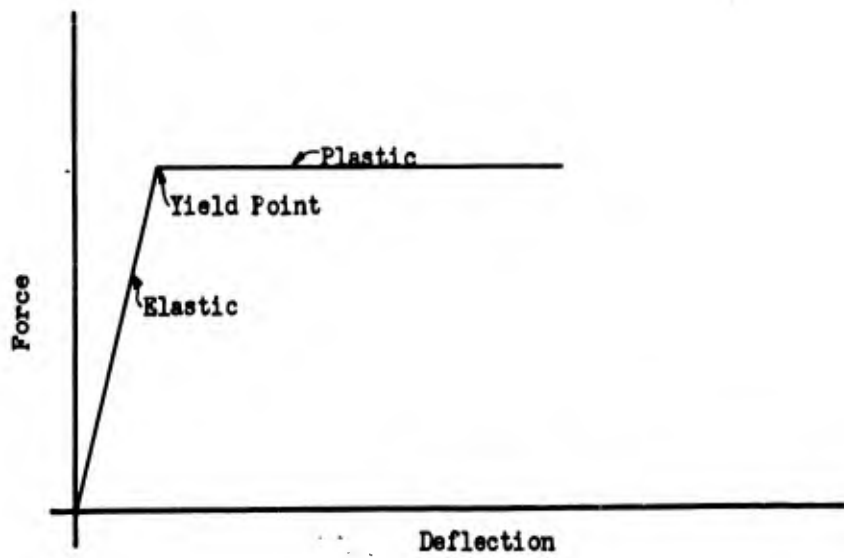
Fig. E.11.5   Column Resistance Curve of Building 3.3.4

TABLE E.11.1

Summary of Building Weight for Building 3.3.4

Weight of Roof		Weight Other Than Roof	
Item	Wt(lb)	Item	Wt(lb)
2x6 timber deck	49200	Columns	56880
Timber on top of walls	2760	Walls, etc.	224640
Timber around monitors	8950		
Nailing strips	2620		
Monitor frames	5420		
Wood covering on monitors	2760		
Window frame supports	4510		
Monitor windows	4340		
Roofing (felt, tar, etc.)	28450		
Corrugated metal siding	850		
Concrete beams and struts	71760		
Coping	9600		
Total	191,220	Total	281,520

x = acceleration of the moving mass, ft/sec^2

$F(t)$ = time-dependent force on the structure, lb

$R(x)$ = shearing resistance as a function of deflection, lb

An equation of this type may be readily solved by one of the numerical methods of successive approximations. The calculations are carried forward until the maximum deflection is determined, or until a deflection is reached where it becomes obvious that structural collapse is inevitable.

E.11.3 EQUIVALENT MASS

In the determination of the equivalent mass of the building the weight calculations are in two parts: the roof structure including the cross-beams, and the vertical structure consisting of the walls and columns. Only one-third of the weight of the walls and columns was considered in the equivalent mass of the structure.

A summary of the building weights is shown in Table E.11.1.

Since the total mass of the building is to be considered as a single equivalent mass, the following figure for the final mass includes the roof mass plus one-third of the mass of the walls and columns. Hence we have:

Weight of roof, lb = 191,220

1/3 weight of walls and columns

$\left[1/3(281,520)\right]$ = 93,840

Total   285,060

Final equivalent mass = $\dfrac{285,060}{32.2 \times 12}$

$= \dfrac{738 \text{ lb sec}^2}{\text{in.}}$

E.11.4 ELASTO-PLASTIC RESISTANCE

For the purpose of calculating the resistance of the structure to sidesway, the necessary assumptions concerning the end condition of the columns and the method of analysis of reinforced-concrete sections were given in a previous paragraph.

The computations for the plastic hinge moment and corresponding deflection for the columns in Rows B and D follow. The results for all columns are recorded in Table E.11.3.

Figure E.11.6a shows the cross section of the column and Fig. E.11.6b is the transformed section, assuming that the concrete has no tensile strength. The position of the neutral axis was determined by the static moments of the areas. Thus

$$\frac{12.0(Kd)^2}{2} + 7.95(Kd-2.00) = 8.84(10.00-Kd)$$

$$Kd = 3.00 \text{ in.}$$

The moment of inertia of the transformed area is

$$I = 1/3(12.0)(27.0) = (7.95)(1.00)^2 + (8.84)(7.00)^2$$

$$I = 549 \text{ in.}^4$$

The plastic moment is based on the tension steel being at the yield point stress

$$M_p = (\frac{f_s}{h})(\frac{I}{e_s}) = (\frac{40000}{10})(\frac{549}{7.00}) \qquad (E.11.2)$$

$$M_p = 314000 \text{ in-lb.}$$

To check the stress in the concrete

$$f_c = \frac{(314000)(3.00)}{549}$$

$$f_c = 1718 \text{ psi.}$$

To determine the yield deflection of a column fixed at both ends subjected to a lateral force at the top consider Fig. E.11.4. The deflection for this condition is:

$$\Delta = \frac{M \ell^2}{6EI} \qquad (E.11.3)$$

$$\Delta = \frac{(314,000)(245)}{(6)(3)(10^6)(545)}$$

$$\Delta = 1.903 \text{ in.}$$

The corresponding yield shear is

$$R_y = \frac{2M}{\ell} \qquad (E.11.4)$$

$$= \frac{(2)(314000)}{245}$$

$$= 2560\text{lb}$$

The yield deflection of a column fixed at the base and free at the top as shown in Fig. E.11.4 is

$$\Delta_Y = \frac{M \ell^2}{3EI} \qquad (E.11.5)$$

$$= \frac{(314,000)(245)^2}{(3)(3)(10^6)(549)}$$

$$= 3.81 \text{ in.}$$
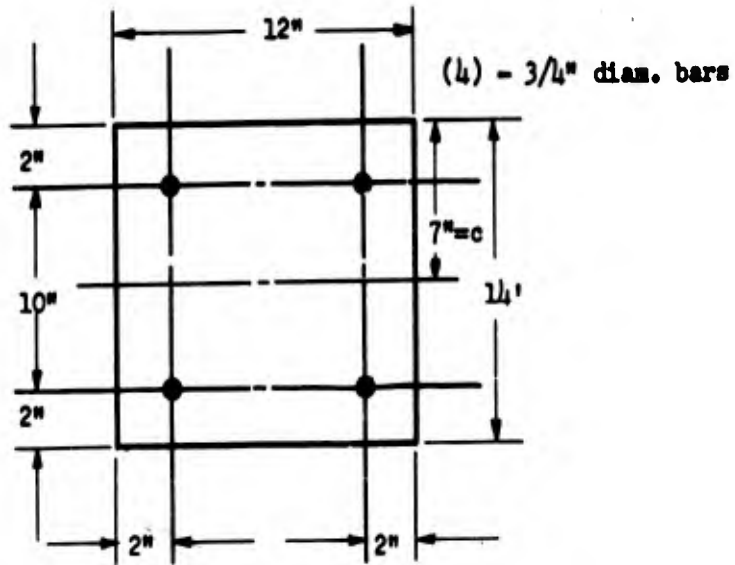
Fig. E.11.6a   Cross Section of 12" x 14" Column
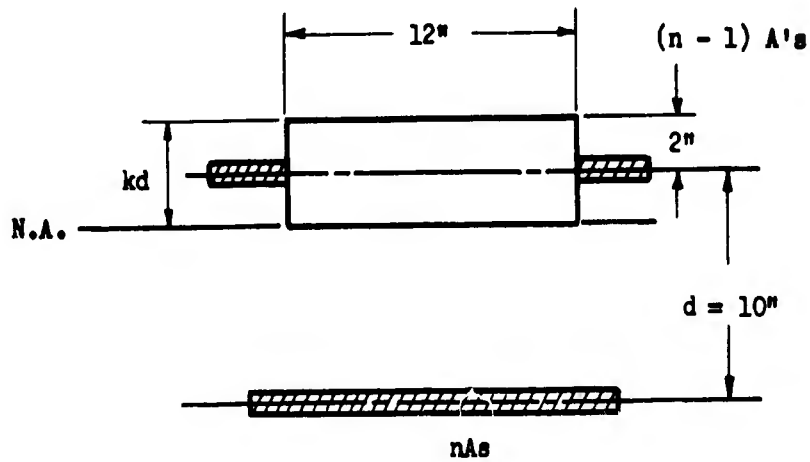
Fig. E.11.6b   Transformed Section of Column

The corresponding yield shear is

$$R_y = \frac{M}{L} = \frac{314000}{245} = 1282 \text{ lb} \qquad (E.11.6)$$

In a similar manner the data for other columns have been obtained. All of the values are recorded in Table E.11.2 and plotted as a shear-deflection curve in Fig. E.11.3. The resultant curve for all of the columns in the structure was obtained by the addition of the individual curves.

TABLE E.11.2

Physical Constants for Building 3.3.4

Row	Column size	No. n	I (in.^{4})	Stress f_c (psi)	Moment Mp (in.-lb)	Shear R (1^ycol)	Total Shear nR_y	Deflection Δy (in.)
A, E	10"x10"	8	370	2025	262,000	1992	15970	2.72
B, D	12"x14"	8	549	1718	314,000	2560	20500	1.90
C	12"x12"	4	549	1718	314,000	1282	5130	3.81

E.11.5 BLAST LOADING

It is not intended at this point to give a complete discussion of the loading phenomena , but only a brief, qualitative description of the blast action on building 3.3.4. For a complete analysis of blast loads reference is made to Chapter E.2.

A shock wave, traveling in the logitudinal direction of the

building (i.e., perpendicular to the front and rear walls) will cause an initial load on the wall as the impinging shock wave is reflected, thereby raising the front wall pressure. The immediate effect of this initial front wall load is to cause an acceleration of the wall masonry, since the wall is not a fixed, rigid body. Thus, with the wall itself taking on an acceleration, it does not transmit to the building foundation and structural frame the entire load applied to it by the shock wave.

Since the glass windows in the front wall are shattered upon the application of the shock wave, the wave re-forms within the building and travels toward the rear wall where it causes a secondary peak loading on the structure. Simultaneous with this action, the main shock wave outside of the building is also moving toward the rear wall but somewhat ahead of the interior wave. Insofar as net pressure on the roof is concerned this difference in time between the two wave fronts is not important. The difference in pressure behind each wave front, however, is the reason for a net pressure acting on the roof. The effect of these vertical forces has been neglected in the analysis of the response of building 3.3.4, since it was found that the over all movement of the structure was small. These loads are of significant magnitude only in the early stages when their effect on the horizontal movement of the structure is negligible.

While the loads due to shock effect are of extremely short time durations, there follows an air blast which endures for a considerable time after passage of the shock waves. This air blast causes drag forces

on all structural members exposed to it. Such drag loads are particularly significant in the case of those associated with the interior of the building.

Drag forces resulting from air blast are also characteristic, for the most part, of the loads applied to the monitors. This follows from the fact that the shock wave, striking the monitors, instantly shatters the glass, which makes up most of the monitor surface exposed to the shock wave.

The load versus time curve is shown in Fig. E.11.7.

E.11.6   ACTION OF BRICK WALLS

The front and rear walls of the buildings will suffer a deformation upon the application of the time dependent forces. Moreover, the character of the forces transmitted to the structural frame will change because of the cushioning effect of these walls. It was therefore necessary to calculate the individual response of the brick walls and the resulting reactions on the frame.

These calculations have been carried out in detail in Chapter E.8.

E.11.7   DYNAMIC RESPONSE OF STRUCTURE

A detailed analysis of the dynamic response of a simplified structure to blast loads is given in Vol II, Part II. It will be emphasized here that in the differential equation of motion, (See Eq. E.11.1),

$$M\ddot{x} = H(t) - R(x),$$
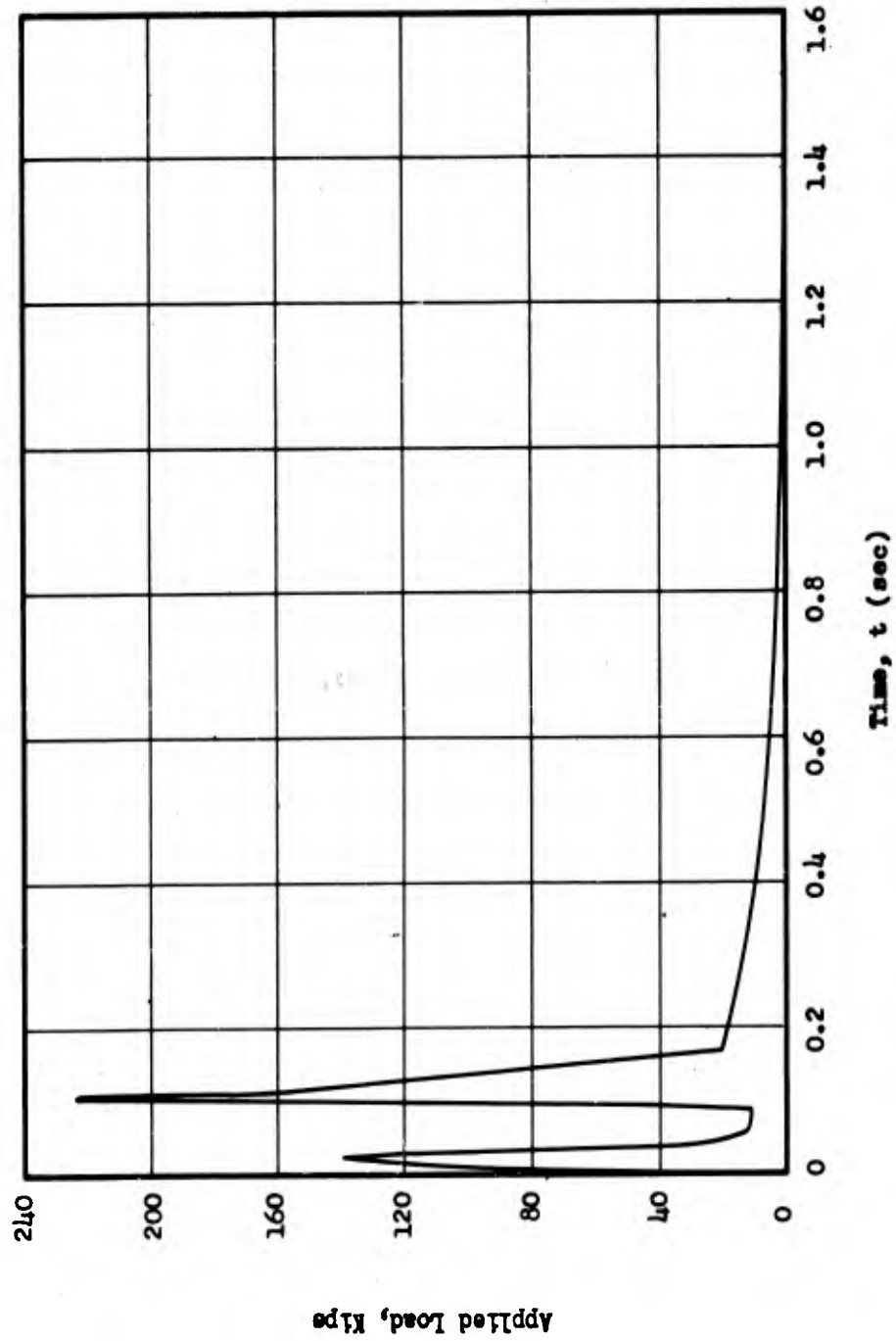
Fig. E.11.7. Applied Load on Building 3.3.4

the functions H(t) and R(x) are non-analytic and a numerical procedure must be employed to obtain a solution of the equation. In the above reference, the response equation has been reduced to a form that can be numerically integrated and is as follows:

$$x(t+2h) - x(t) = \frac{h}{3}\left[2h\ddot{x}(t) + 4h\ddot{x}(t+h)\right] + 2h\dot{x}(t) \qquad (E.11.7)$$

where h has been intorduced and is simply a time increment involved in the numerical integration of the equation.

The actual numerical procedure is carried out in Table E.11.3 where the acceleration and displacement of the building is given with respect to the corresponding elapsed time. The acceleration and displacement are plotted against time in Figs. E.11.8 and E.11.9.

E.11.8   ACTION OF ROOF

Reference is made to Section E.8.4.2 of this volume where a detailed analysis of the response of the roof of building 3.3.4 is presented.

As it will be seen from the above reference, the roof of building 3.3.4 will remain intact after the blast. This fact is, of course, of major significance.

E.11.9   DISCUSSION OF RESULTS

It is seen from the curve in Fig. E.11.9 that the maximum displacement of building 3.3.4 is 4.74 in., occuring after an elapsed time of approximately 0.57 sec. The velocity is zero at this point, which is evidenced by the zero slope of the displacement curve. The

Fig. E.11.8 Acceleration of Building 3.3.4

Fig. E.11.9   Displacement of Building 3.3.4

TABLE E.11.3

Numerical Integration of Response Equation for Building 3.3.4

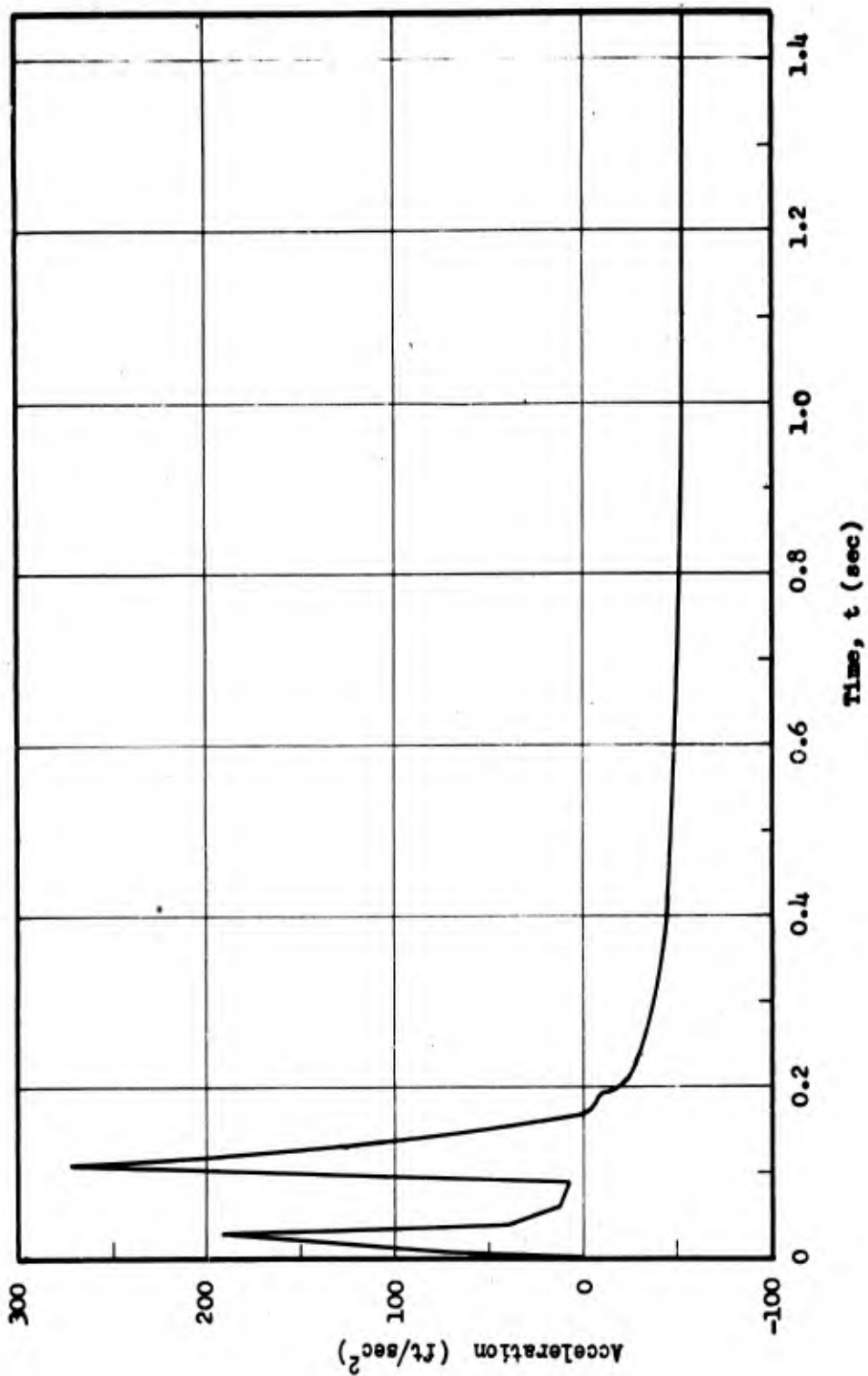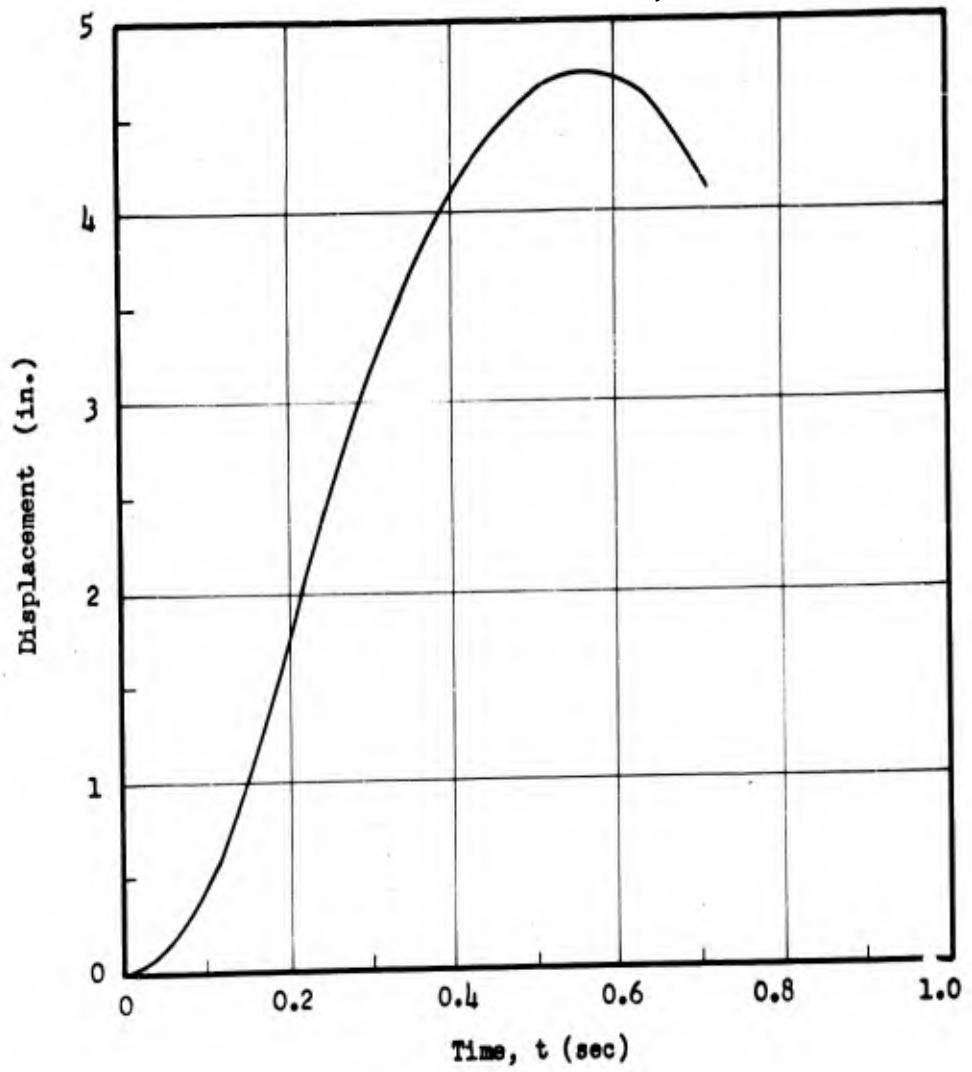| t (sec)	H(t) (10³lb)	R(x) (10³lb)	ẍ (in/sec²)	ẋ (in/sec)	η* (10⁻³ft)	x (10⁻³in.)
0	0	0	0	0	0	0
0.004	54	0.004	73.17	0.146	0	0
0.008	97	0.029	131.397	0.355	1.61	1.61
0.012	112	0.087	151.643	0.712	3.70	4.87
0.016	126	0.165	170.508	1.357	4.78	9.23
0.020	133	0.286	179.829	2.057	5.42	15.99
0.024	140	0.464	189.073	2.795	5.83	25.91
0.028	130	0.691	175.215	3.524	6.14	38.59
0.032	108	0.971	145.026	4.164	5.93	54.20
0.036	58	1.288	76.846	4.608	5.12	71.90
0.040	31	1.790	39.580	4.841	3.29	90.80
0.044	27	1.979	33.904	4.988	1.72	110.48
0.048	22	2.341	26.638	5.109	1.18	130.71
0.052	19	2.710	22.072	5.206	0.96	151.34
0.056	14.9	3.087	16.007	5.283	0.78	172.36
0.060	12.9	3.467	12.782	5.340	0.59	193.58
0.064	12.7	3.852	11.989	5.390	0.46	215.08
0.068	12.6	4.239	11.329	5.436	0.40	236.71
0.072	12.4	4.631	10.527	5.480	0.38	258.58
0.076	12.3	5.025	9.858	5.521	0.36	280.56

*η represents the numerical evaluation of the term

$$\frac{h}{3}\left[2hx(t) + 4hx(t+h)\right]$$

in the response equation.

TABLE E.11.3 (contd)

Numerical Integration of Response Equation for Building 3.3.4

t (sec)	H(t) (10³lb)	R(x) (10³lb)	$\ddot{x}$ (in/sec²)	$\dot{x}$ (in/sec)	$\ddot{z}$ (10⁻³ft)	x (10⁻³in.)
0.080	12.1	5.422	9.048	5.559	0.33	302.75
0.084	11.9	5.821	8.237	5.593	0.31	325.03
0.088	11.8	6.224	7.556	5.625	0.28	347.50
0.092	42	6.627	47.930	5.736	0.26	370.04
0.096	112	7.050	142.209	6.116	1.14	393.64
0.100	182	7.515	236.430	6.873	3.66	419.58
0.104	222	8.047	289.909	6.880	6.77	449.3
0.108	210	8.659	272.819	8.006	8.98	483.5
0.112	156	9.197	198.920	8.949	9.19	513.5
0.116	151	9.938	191.141	9.730	7.38	554.9
0.120	142	10.594	178.057	10.468	6.39	591.5
0.124	128	11.441	157.939	11.140	6.02	638.8
0.128	120	12.191	146.082	11.748	5.43	680.7
0.132	111	13.126	132.620	12.305	4.95	732.9
0.140	90.039	14.958	101.735	13.243	18.20	835.2
0.148	72.072	16.911	74.744	13.949	14.45	944.2
0.156	54.105	18.947	47.640	14.438	10.80	1,057.9
0.164	36.190	21.039	20.530	14.711	7.31	1,174.7
0.172	20.386	23.152	-3.748	14.778	3.81	1,292.7
0.180	19.871	25.264	-7.307	14.734	0.56	1,410.6
0.188	19.305	27.118	-10.586	14.662	-0.79	1,514.1
0.196	18.790	31.545	-12.755	14.475	-4.26	1,761.3
0.212	17.967	35.410	-23.635	14.184	-6.17	1,977.1
0.228	17.246	36.443	-26.012	13.610	-10.26	2,214.3
0.244	16.474	37.911	-29.047	13.169	-12.94	2,418.1
0.260	15.753	39.476	-32.146	12.919	-14.38	2,635.4
0.324	12.767	40.853	-38.057	10.673	-210.34	3,403.8

ARMOUR RESEARCH FOUNDATION OF ILLINOIS INSTITUTE OF TECHNOLOGY

TABLE E.11.3 (contd)

Numerical Integration of Response Equation for Building 3.3.4

t (sec)	H(t) (10³lb)	R(x) (10³lb)	$\ddot{x}$ (in/sec²)	$\dot{x}$ (in/sec)	x^w (10⁻³ft)	x (10⁻³in.)
0.388	9.833	41.300	-42.638	8.091	-295.55	3,993.5
0.452	8.5	41.300	-44.444	5.304	-336.70	4,433.2
0.516	7.0	41.300	-46.477	2.394	-359.20	4,669.9
0.580	5.8	41.300	-48.103	-.632	-375.23	4,737.6
0.644	4.5	41.300	-49.864	-3.767	-389.67	4,586.7
0.708	3.9	41.300			-403.73	4,253.0

continuation of the displacement curve beyond the peak value to a smaller displacement is not of too great significance since the elastic recovery will be negligible compared to the resulting permanent set. The action of the structure is not reversible and the curve was arbitrarily terminated beyond the peak value as shown.

From Table E.11.3 it is determined by summating the column moments that the maximum resisting moment of the columns is approximately 489,000 ft-lb. The maximum static overturning moment is found to be 112,600 ft-lb (the product of the equivalent building weight and the maximum displacement). From Fig. E.11.9 it is observed that at the time of maximum displacement, (0.57 sec), there still exists an applied load on the structure of approximately 5,900 lb. This load has an overturning moment of (5,900 x 245/12)=120,500 ft-lb. Hence, the total overturning moment is (112,600 ft-lb + 120,500 ft-lb)=233,100 ft-lb. This figure is less than the maximum resistance moment of 489,000 ft-lb.that can be developed. Thus, static stability exists for these conditions and the building stands.

However, it will be remembered that the vertical forces on the structure resulting from the blast were neglected in the response calculations. While these vertical forces are of significant magnitude only at the beginning of the blast application, they rapidly diminish to much smaller values. Since the building has a very small deflection during the time that the vertical forces are of significant size, their overturning moment is small.

The foregoing remarks seem to justify the assumption that the effect of the vertical forces due to the blast can be neglected in considering the dynamic response of building 3.3.4.

CHAPTER E.12

BUILDINGS 3.3.5a and 3.3.5b

•

As has been stated previously, buildings 3.3.5a and 3.3.5b
are by their very nature structurally different from any of the idealized
or real buildings with which this program is concerned. These buildings,
which are of the load-bearing, brick-wall dwelling type, defy analytical
investigation, at least at the present time. This statement is made
despite the fact that, in the analysis of the response of buildings
3.3.3, 3.3.4, and 3.3.8h, a certain analytical treatment was made of
brick panels. It is to be remembered, however, that the brick panels
in those structures had comparatively ideal mounting and response con-
ditions, that is, the support, the effective length, and the end condi-
tions of the panel could at least be reasonably well defined. For
buildings of the 3.3.5a or 3.3.5b type no such definitions of support or
boundary conditions may be made, and further, the compression loads in
the wall panels add to the general complexity.

In order to achieve some kind of a response prediction for
these structures, a study of the damage reports from Hiroshima and Nagasaki
has been undertaken and this problem has been discussed in considerable
detail with the various experts in this field. The conclusions expressed
in this chapter are based on the reading of damage reports, on discussions,
and somewhat on the meager technical information available in other litera-
ture.

On the basis of the above investigation, it is believed that building 3.3.5a will be completely demolished. "Complete demolition" in this case implies that it is difficult to see, on the basis of the Hiroshima and Nagasaki report, how anything except perhaps the few longitudinally oriented interior load-bearing partitions could be standing after the blast. This conclusion is based on the fact that, for nearly all cases reviewed in the aforementioned survey reports, load-bearing brick-walls which are subjected to blast loading in the range of 8 psi were completely demolished and reduced to rubble.

These studies and discussions have further indicated that building 3.3.5b should suffer quite severe damage. It is not expected that all of the walls will be blown down, but the Hiroshima and Nagasaki report would indicate that some of them could be blown down. All windows should be blown out. Depending upon the strength of its connection to the rest of the structure (which is almost left to the whim of the construction superintendent), the roof might very well be blown off or stripped. The final condition of this building might very well be that one or possibly two walls will collapse, the windows will be blown out, and the roof will be blown off or the roofing material will be stripped from the basic roof structure.

It is keenly appreciated that this sort of "analysis" is a crude qualitative appraisal. However, it must be pointed out and reiterated that this type of building by its very nature is extremely difficult to subject to any sort of quantitative analysis. The nature of the materials

(brick or brick panels), their definition as a structure, their response to blast loading and the effects of age, workmanship, weathering, and geographic conditions are factors which are yet only partially realized, let alone defined. This does not mean to say that all effort toward an eventual analysis of this sort of structure should be abandoned. It need hardly be pointed out that the perponderance of just this type of building in any European or American city makes it of the utmost tactical importance. It is believed, however, that only a statistical evaluation will clarify these problems.

Work going on at this time on the response of typical building components as well as subsequent tests for both scaled and prototype blast situations will do much qualitatively toward the definition of these structures for response purposes. It is recommended, therefore, that the results of all tests be continually correlated with the only single large body of information on the response of this type of building under the prototype situation, that is, the Hiroshima and Nagasaki observations. It is not known if this correlation can be actually achieved; however it is fairly obvious that such correlation should be attempted. The difficulties facing any such attempts at correlation, to list a few, are: variations of mortar joints, both in the strength of the mortar and in size of the joint; variations in the general interior structure of such buildings as a result of the traditional and geographic effects on the different techniques of construction; and variations in the size and number of openings (again traditional and geographic characteristics),

Contributing Personnel: M. S. Christensen, N. F. Eslinger, J. E. Fitsgerald, S. J. Fraenkel, K. E. Gandy, E. Ouillard, F. R. Halpern, R. L. Janes, R. J. O'Brien, M. J. Ramirez, H. Reismann, M. T. Southgate, M. P. White.

Edmund Fitsgerald, Project Engineer

BIBLIOGRAPHY

Shock Tube Model Tests, Using an Interferometer, at Princeton University

(1) Bleakney, W. The Diffraction of Shock Waves Around Obstacles and the Resulting Transient Loading of Structures. Technical Report II-3, Princeton University Physics Department; Washington, D. C.: AFSWP, Mar., 1950.

(2) Bleakney, W., Weimer, D. K., and White, D. R. The Diffraction of Shock Waves Around Obstacles and the Resulting Transient Loading of Structures. Technical Report II-6, Princeton University Physics Department; Washington, D. C.: AFSWP, Aug., 1950.

(3) Bleakney, W. The Diffraction of a Shock Wave Around a Hollow Rectangular Block—Opening Facing Shock. Tentative Report, Princeton University Physics Department; Washington, D. C.: AFSWP, Oct., 1950.

(4) Bleakney, W., White, D. R., and Griffith, W. C. Measurement of Diffraction of Shock Waves and Resulting Loading of Structures. Journal of Applied Mechanics, Vol. 17, No. 4; Dec., 1950.

(5) Princeton University Physics Department. Effects of Reynolds' Number on the Diffraction of a Shock. Technical Report II-8 Princeton University Physics Department; Washington, D. C.: AFSWP, in press, Jan., 1951.

Shock Tube Model Tests, Using Shadowgraph and Schlieren Technique, at the University of Michigan (Chronological Arrangement)

(6) Uhlenbeck, G. Diffraction of Shock Waves Around Various Obstacles. Engineering Research Institute, University of Michigan; Washington, D. C.: AFSWP, Mar., 1950.

(7) Duff, R. D. and Hollyer, R. N. The Effect of Wall Boundary Layer on the Diffraction of Shock Waves Around Cylindrical and Rectangular Obstacles. Report 50-2, Engineering Research Institute, University of Michigan; Washington, D. C.: AFSWP, June, 1950.

(8) Duff, R. E. and Hollyer, R. N. The Diffraction of Shock Waves Through Obstacles with Various Openings in Their Front and Back Surfaces. Report 50-3, Engineering Research Institute, University of Michigan; Washington, D. c.: AFSWP, Nov., 1950.

(9) Hollyer, R. N. and Dugg, R. E. Growth of the Turbulent Region at the Leading Edge of Rectangular Obstacles in Shock Wave Diffraction. Report 51-2, Engineering Research Institute, University of Michigan; Washington, D. C.: AFSWP, Jan., 1951.

Drag Information

(10) Howe, G. E. Wind Pressure on Structures. Civil Engineering, Vol. 10, No. 3: Mar., 1940.

(11) Irminger, J. O. V. and Nøkkentved, C. Wind Pressure on Buildings. Experimental Researches (Second Series); Copenhagen: Ingeniørvidenskabelige Skrifter, 1936.

(12) Lindsey, W. E. Drag of Cylinders of Simple Shapes. NACA Report 619, 1937.

(13) Rouse, H. Fluid Mechanics for Hydraulic Engineers. New York: McGraw-Hill, 1938.

(14) Subcommittee on Wind Bracing. Wind Bracing in Steel Buildings. Proceedings A.S.C.E., Vol. 62, Mar., 1936.

Shock Waves

(15) Bleakney, W. and Taub, A. H. Interaction of Shock Waves. Reviews of Modern Physics, Vol. 21, No. 4, Oct., 1949.

(16) Courant, R. and Friedrichs, K. O. Supersonic Flow and Shock Waves. Interscience, 1948.

(17) Liepmann, H. W. and Puckett, A. E. Aerodynamics of a Compressible Fluid. New York: Wiley, 1947.

(18) Los Alamos Scientific Laboratory. The Effects of Atomic Weapons. Washington, D. C.: U. S. Government Printing Office, June, 1950.

Description of Shock Tubes at Princeton and Michigan Used in Tests Reported in References 1 through 9

(19) Bleakney, W., Weimer, D. K., and Fletcher, C. H. The Shock Tube: A Facility for Investigation in Fluid Dynamics. Review of Scientific Instruments, Vol. 20, No. 11, Nov., 19

(20) Geiger, F. W. and Mautz, C. W. The Shock Tube as an Instrument for the Investigation of Transonic and Supersonic Flow. Engineering Research Institute, University of Michigan, 1949.

Compressible Flow Theory

References (16) and (17) and

(21) Binder, R. C. Fluid Mechanics, New York: Prentice-Hall,

(22) Kuethe, A. M. and Schetzer, J. D. Foundations of Aerodyna. New York: Wiley, 1950.

(23) Lampson, C. W. Resume of the Theory of Plane Shock and Ad Waves with Applications to the Theory of the Shock Tube, Princeton University Station, Div. 2, NDRC Project No. OD-03, PTM 103.

Theoretical Analysis of Diffraction of Shocks Around Corners

(24) Lighthill, M. J. The Diffraction of Blast. Proceedings of the Royal Society: Series A, Vol. 198, No. 1055, Sept. 1949, and Vol. 200, No. 1063, Feb. 22, 1950.